

# **EVALUATION OF A CLASS OF HYDRAULIC DAMPERS FOR ISOLATION OF VIBRATION AND SHOCK**

**M. Manzurul Haque**

**A Thesis  
in  
The Department  
of  
Mechanical Engineering**

**Presented in Partial Fulfillment of the Requirements  
for the Degree of Doctor of Philosophy at  
Concordia University  
Montreal, Quebec  
Canada**

**August, 1996**

**© M. Manzurul Haque, 1996**



National Library  
of Canada

Bibliothèque nationale  
du Canada

Acquisitions and  
Bibliographic Services Branch

Direction des acquisitions et  
des services bibliographiques

395 Wellington Street  
Ottawa, Ontario  
K1A 0N4

395, rue Wellington  
Ottawa (Ontario)  
K1A 0N4

*Your file    Votre référence*

*Our file    Notre référence*

**The author has granted an irrevocable non-exclusive licence allowing the National Library of Canada to reproduce, loan, distribute or sell copies of his/her thesis by any means and in any form or format, making this thesis available to interested persons.**

**L'auteur a accordé une licence irrévocable et non exclusive permettant à la Bibliothèque nationale du Canada de reproduire, prêter, distribuer ou vendre des copies de sa thèse de quelque manière et sous quelque forme que ce soit pour mettre des exemplaires de cette thèse à la disposition des personnes intéressées.**

**The author retains ownership of the copyright in his/her thesis. Neither the thesis nor substantial extracts from it may be printed or otherwise reproduced without his/her permission.**

**L'auteur conserve la propriété du droit d'auteur qui protège sa thèse. Ni la thèse ni des extraits substantiels de celle-ci ne doivent être imprimés ou autrement reproduits sans son autorisation.**

ISBN 0-612-18399-8

**Canada**

## ABSTRACT

### EVALUATION OF A CLASS OF HYDRAULIC DAMPERS FOR ISOLATION OF VIBRATION AND SHOCK

M. Manzurul Haque, Ph. D.  
Concordia University, 1996

In this dissertation, a detailed and fundamental investigation on a class of passive hydraulic dampers is carried out. Dual-phase and flexible chamber hydraulic dampers with wide ranges of orifice design are selected for detailed modeling and evaluation of performance in isolation of shock and vibration. Previous investigations on dual-phase dampers have utilized simplified damping force characterization. Models are, therefore, thoroughly redeveloped utilizing integral formulation of damping force characterization. The simulation results are compared with those of previous analytical and experimental studies. Results for displacement dependent dual-phase dampers are further obtained for evaluation of their performance. A systematic study of the flexible chambered hydraulic damper models utilizing experimental values of nonlinear compliance as well as stiffness and damping coefficient of the chamber material is also carried out. Various configurations for the orifices considered are: (i) short orifice, (ii) long orifice, (iii) long and short orifice, (iv) long orifice and short orifice with spring loaded valves. Unlike previous investigations, the models consider "oscillation effect" of the fluid within the long orifice. The model with orifice valves includes valve dynamics and variable flows requiring an iterative process for the simulations. The damper characteristics are evaluated both in time and frequency domain and presented in terms of internal variables, such as chamber pressures, flow through various orifices, damping force, transmitted force, etc. Detailed performance is evaluated

both in terms of transmissibility and shock isolation performance. An extensive parametric study is carried out for all damper configurations to demonstrate their performance potentials. The configurations utilizing long and short orifices with and without valves are proposed in this investigation in order to overcome conflicting requirements between vibration and shock isolation performance. The simulation results for dual-phase dampers show that the use of traditional approach leads to gross estimation of the damping force in comparison to the proposed integral approach. Also, the results of the integral approach show better agreement with the experimental trends. Parametric study and comparison of *low-high* and *high-low* system demonstrate the high potential of *low-high* damper for isolation of vibration in a wide frequency range. Superior shock isolation performance is, however, provided by a *high-low* configuration. Through the simulation of dampers with flexible chambers, it is shown that the effect of fluid oscillation in long orifice is highly significant both on the damper characteristics and its performance. In general, peak orifice flow is grossly overestimated when oscillation effect is not considered. The results for the combination of long and short orifice show certain improvement of both transmissibility and shock isolation performance when compared to that of the damper with long orifice only. In general, the dampers with flexible chambers are found to perform well for isolation of low amplitude (less than 1mm) vibration only. The results for the proposed concept of hydraulic damper having long orifice and short orifices with valves demonstrate significant influence of both forward and bleeder valve orifices on the dynamic characteristics and performance. A limited parametric study shows that such dampers can be tuned to provide satisfactory performance even at excitations as large as 3 mm. In this case, shock performance is also superior in comparison to other configurations with flexible chambers.



## **ACKNOWLEDGMENTS**

The author would like to express sincere gratitude to his thesis supervisor, Dr. A.K.W. Ahmed, for his constant guidance and dedication throughout the realization of this work. The author is also indebted for the guidance of Dr. S. Sankar who served as a co-supervisor until 1994, and to Dr. S. Rakheja, for his valuable advice and discussions.

The financial support provided by my supervisors from their NSERC and FCAR grants are gratefully acknowledged.

Thanks are due to the colleagues, faculty and staff of CONCAVE Research Center, Department of Mechanical Engineering, Concordia University, for their contribution to this effort.

Finally, the author would like to express his special thanks to the members of his family for their understanding and support.

## TABLE OF CONTENTS

LIST OF TABLES	xii
LIST OF FIGURES	xiv
NOMENCLATURE	xxiii
CHAPTER 1 INTRODUCTION	1
1.1 General	1
1.2 Classification of Dampers	2
1.2.1 Flexible Chambered Damper	3
1.2.2 Rigid Chambered Damper	3
1.3 State-of-the-art Survey	5
1.3.1 Passive Hydraulic Damper	7
1.3.2 Semi-active Hydraulic Damper	12
1.3.3 Active Hydraulic Damper	12
1.4 Scope of Proposed Investigation	13
1.5 Objectives of Dissertation Research	15
1.5.1 Dual-phase Viscous Damper (DPVD)	15
1.5.2 Hydraulic Dampers with Flexible Chambers (DHF)	16
1.6 Thesis Organization	17
CHAPTER 2 DISPLACEMENT SENSITIVE DUAL-PHASE VISCOUS DAMPER	19
2.1 Introduction	19
2.2 Damping Force Characterization of Displacement Sensitive Dual-phase Dampers	21

2.3	Transformation of Displacement Sensitivity to Velocity Sensitivity	24
2.3.1	Case I: Peak Relative Displacement $X$ Greater Than $\alpha A$	26
2.3.2	Case II: Peak Relative Displacement $X$ Within the Range	28
2.3.3	Case III Peak Relative Displacement $X$ Less Than $A$	29
2.4	Derivation of Damping Force Expression	29
2.5	Performance Evaluation of the Displacement Sensitive Dual-phase Damper	32
2.5.1	Model Formulation	32
2.5.2	Numerical Integration	33
2.5.3	Equivalent Linearization of the Damper	33
2.6	Results and Discussions	36
2.7	Summary	46
CHAPTER 3 ANALYSIS OF HYDRAULIC DAMPERS WITH FLEXIBLE CHAMBER		47
3.1	Introduction	47
3.2	Short Orifice Hydraulic Dampers with Flexible Chamber	48
3.2.1	Model Description	49
3.2.2	Development of Nonlinear Mathematical Model	59
3.2.2.1	Chamber Compliance Linear	53
3.2.2.2	Chamber Compliance Nonlinear	54
3.2.3	Characteristics of the Chamber Material	58
3.2.4	Static Equilibrium Equations	58
3.2.4.1	Linear Compliance	58
3.2.4.2	Nonlinear Compliance	62
3.2.5	Method of Solution	65
3.2.5.1	Linear Compliance	67

3.2.5.2	Nonlinear Compliance	67
3.3	Long Orifice Hydraulic Dampers with Flexible Chambers	68
3.3.1	Model Description	69
3.3.2	Nonlinear Mathematical Model	79
3.3.3	Method of Solution	74
3.4	Long and Short Orifice Hydraulic Damper with Flexible Chamber	74
3.4.1	Model Description	76
3.4.2	Nonlinear Mathematical Model	76
3.4.3	Method of Solution	79
3.5	Long Orifice Hydraulic Damper with Spring Loaded Valve	79
3.5.1	Model Description	81
3.5.2	Nonlinear Mathematical Model	80
3.5.2.1	Orifice Flow	82
3.5.2.2	Continuity Equation	84
3.5.2.3	Total Volume Flow	86
3.5.2.4	Fluid Flow through Valves	88
3.5.3	Method of Solution	95
3.6	Summary	96
CHAPTER 4	CHARACTERISTICS & PERFORMANCES OF DUAL-PHASE DAMPERS	98
4.1	Introduction	98
4.2	Characteristics of the Damper	99
4.2.1	Parametric Study	103
4.3	Performance of the Damper	110
4.3.1	Application of Sinusoidal Input	111
4.3.1.1	Parametric Study	112

4.4	Description of Shock Input	122
4.4.1	Characteristics of Shock Input	124
4.4.2	Shock Performance Index	126
4.5	Shock Response of Dual-phase Damper	128
4.6	Summary	134
CHAPTER 5 CHARACTERISTICS AND PERFORMANCE OF SHORT ORIFICE HYDRAULIC DAMPER		137
5.1	Introduction	137
5.2	Characteristics of the Damper	138
5.2.1	Time Domain Analysis	138
5.2.1.1	Parametric Study	148
5.2.2	Frequency Domain Analysis	152
5.2.2.1	Parametric Study	156
5.3	Performance Analysis of Hydraulic Damper	164
5.3.1	Performance Under Sinusoidal Excitation	164
5.3.1.1	Parametric Study	166
5.3.2	Performance under Shock Displacement	170
5.3.2.1	Time Domain Analysis	170
5.3.2.2	Performance Analysis in Shock Severity Domain	172
5.4	Summary	174
CHAPTER 6 CHARACTERISTICS AND PERFORMANCES OF LONG ORIFICE HYDRAULIC DAMPER		176
6.1	Introduction	176
6.2	Characteristics of the Long Orifice Hydraulic Damper	177
6.2.1	Time Domain Analysis	179
6.2.1.1	Parametric Study	185

6.2.2	Frequency Domain Analysis	190
6.2.2.1	Parametric Study	192
6.3	Performance Analysis of the Damper with Long Orifice	198
6.3.1	Performance Under Sinusoidal Excitation	199
6.3.1.1	Parametric Study	201
6.3.2	Performance under Shock Displacement	205
6.3.2.1	Time Domain Analysis	205
6.3.2.2	Shock Severity Domain Analysis	208
6.4	Characteristics of the LSDHF damper	208
6.5	Performance Analysis of the Damper	214
6.5.1	Performance Under Sinusoidal Excitation	216
6.5.2	Performance under Shock Displacement	219
6.6	Conclusion	221
CHAPTER 7	PERFORMANCES OF LONG ORIFICE DAMPER WITH SPRING LOADED VALVE	224
7.1	Introduction	224
7.2	Characteristics of the Damper	225
7.2.1	Time Domain Analysis	225
7.2.1.1	Orifice Flow	226
7.2.1.2	Transmitted Force and Top Chamber Pressure	228
7.2.1.3	Motion of the Valve	230
7.2.2	Frequency Domain Analysis	232
7.3	Performance Analysis of the Damper	235
7.3.1	Performance Under Sinusoidal Excitation	236
7.3.2	Performance under Shock Displacement	241
7.3.2.1	Time Domain Analysis	244

7.3.2.2	Performance Analysis in Shock Severity Domain	246
7.4	Summary	250
CHAPTER 8	CONCLUSION	251
8.1	General	251
8.2	Highlights of the Study	253
8.3	Conclusions of the Investigation	257
8.4	Recommendation for Further Work	262
REFERENCES		263

## LIST OF TABLES

Table 3.1	Contraction factor for different geometry of orifice	51
Table 3.2	Variation of static pressure and volume increment for different piston diameter (linear compliance)	62
Table 3.2	Variation of static pressure and volume increment for different piston diameter (nonlinear compliance)	65
Table 3.4	Flow chart for numerical solution for LDHVF dampers	97
Table 5.1	Percentage increase in some parameters with the increase in piston area based on piston diameter of 70mm.	152



## LIST OF FIGURES

	Page
Figure 1.1      Typical hydraulic dampers with: (a) flexible chambers; (b) rigid chamber.	4
Figure 2.1      A typical low-high displacement sensitive dual-phase damper.	22
Figure 2.2      A typical high-low displacement sensitive dual-phase damper.	22
Figure 2.3      Damper relative displacement and corresponding relative velocity representation for low-high damper. (a) $ X  > \alpha A$ , (b) corresponding damper characteristics; (c) $A \leq  X  \leq \alpha A$ , (d) corresponding damper characteristics; (e) $ X  < A$ , (f) corresponding damper characteristics.	25
Figure 2.4      Damper relative displacement and corresponding relative velocity representation for high-low damper. (a) $ X  > \alpha A$ , (b) corresponding damper characteristics; (c) $A \leq  X  \leq \alpha A$ , (d) corresponding damper characteristics; (e) $ X  < A$ , (f) corresponding damper characteristics.	27
Figure 2.5      A one DOF mechanical model.	32
Figure 2.6.      Comparison of energy balance method and numerical integration. For energy balance for a dual-phase damper. Energy balance: $X_1$ , ———, 40mm; - - - - -, 30mm;      , 20mm; integration: $X_1$ , $\Delta\Delta$ , 40mm; $\square\square$ , 30mm; $\circ\circ$ , 20mm.	37
Figure 2.7      Force-time history of low-high dual-phase damper for different non-linearity. ———, Integral method; - - - - -, traditional method. (a) $\beta = 2.6$ (b) $\beta = 2.0$ (c) $\beta = 1.4$ . ( $A=10\text{mm}$ , $\alpha=3$ , $\zeta=0.25$ , $X_1=40$ (mm)).	39
Figure 2.8      Force-time history of high-low type dual-phase damper for different non-linearity. ———, Integral method; - - - - -, traditional method. (a) $\beta = 2.6$ (b) $\beta = 2.0$ (c) $\beta = 1.4$ . ( $A=10\text{mm}$ , $\alpha=3$ , $\zeta=0.25$ , $X_1=40\text{mm}$ ).	40
Figure 2.9      Force-displacement plots for low-high damper. ———, Integral method; - - - - -, traditional method; (a) $\beta = 1.4$ (b) $\beta = 2.0$ (c) $\beta = 2.6$ . ( $A=10\text{mm}$ , $\alpha=3$ , $\zeta=0.25$ , $X_1=40\text{mm}$ ).	42
Figure 2.10      Force-displacement plots for high-low damper. ———, Integral method; - - - - -, traditional method; (a) $\beta = 1.4$ (b) $\beta = 2.0$ (c) $\beta = 2.6$ . ( $A=10\text{mm}$ , $\alpha=3$ , $\zeta=0.25$ , $X_1=40\text{mm}$ ).	42

Figure 2.11	Comparison of integral and traditional method using energy dissipation balance for low-high damper. ———, integral method; ·····, traditional method (a) $\beta = 2.6$ (b) $\beta = 2.0$ (c) $\beta = 1.4$ ; (A=10mm, $\zeta = 0.25$ , $\alpha = 3$ , $X_1 = 40$ mm).	44
Figure 2.12	Comparison of integral and traditional method using energy dissipation balance for high-low damper. ———, integral method; ·····, traditional method (a) $\beta = 2.6$ (b) $\beta = 2.0$ (c) $\beta = 1.4$ ; (A=10mm, $\zeta = 0.25$ , $\alpha = 3$ , $X_1 = 40$ mm).	45
Figure 3.1	Schematic diagram of an orifice type hydraulic damper (SDHF) with flexible chamber.	50
Figure 3.2	Top chamber compliance in pressure-volume increment relationship. ———, Comp_A; ·····, Comp_B; ·····, Comp_C.	56
Figure 3.3	Bottom chamber compliance in pressure-volume increment relationship. ———, Comp_D; ·····, Comp_E.	56
Figure 3.4	Dynamic characteristics of the flexible chamber material (rubber) (a) Dynamic stiffness; (b) damping coefficient.	59
Figure 3.5	Effect of static load on (a) volume increment for top chamber ———, and bottom chamber, ·····; (b) static pressure and (c) static displacement for linear compliance.	61
Figure 3.6	Effect of static load on (a) volume increment for top chamber ———, and bottom chamber, ·····; (b) static pressure and (c) static displacement for nonlinear compliance.	64
Figure 3.7	Hydraulic damper in a single degree of freedom mass-spring-damper system.	66
Figure 3.8	Schematic diagram; (a) Representation of a long orifice hydraulic damper (LDHF) with flexible chamber. (b) Lumped parameter model.	70
Figure 3.9	Schematic diagram; (a) Representation of a long and short orifice hydraulic damper (LSDHF) with flexible chamber. (b) Lumped parameter model.	77
Figure 3.10	Schematic diagram; (a) Representation of a long and short orifice hydraulic damper with spring loaded valves (LDHVF) . (b) Lumped parameter model.	82

Figure 3.11	Spring loaded valve for an orifice showing: (a) flow pattern and displacement of valve; (b) forces acting on the disk of the valve; (c) control volume for momentum balance.	90
Figure 4.1	Lissajous plots of the dual phase damper. (a) low-high damper; (b) high-low damper. ( $A = 10.0$ mm, $\alpha = 3.0$ , $\zeta = 0.25$ , and $\beta = 2.0$ ; frequency ratio 0.80).	100
Figure 4.2	Dynamic stiffness and loss angle characteristics of a low-high dual phase damper. ( $A = 10$ mm, $\alpha = 3$ , $\zeta = 0.25$ , and $\beta = 2$ ; $X_1 = 40$ mm).	102
Figure 4.3	Dynamic stiffness and loss angle characteristics of a high-low dual phase damper. ( $A = 10$ mm, $\alpha = 3.0$ , $\zeta = 0.25$ , and $\beta = 2.0$ ; $X_1 = 40$ mm).	102
Figure 4.4	Lissajous plots of a low-high dual phase damper with the variation of $\beta$ . ( $A = 10$ mm, $\alpha = 3$ , $\zeta = 0.25$ , and $X_1 = 40$ mm).	104
Figure 4.5	Lissajous plots of a high-low dual phase damper with the variation of $\beta$ . ( $A = 10$ mm, $\alpha = 3$ , $\zeta = 0.25$ , and $\beta = 2$ ; $X_1 = 40$ mm).	104
Figure 4.6	Effect of damping parameter on dynamic characteristics of a low-high damper. Transition point of damping ratio, $\beta$ , —, 1.4; ----, 2.0; , 2.6. ( $A = 10.0$ mm, $\alpha = 3.0$ , $\zeta = 0.25$ ; $X_1 = 40$ mm).	106
Figure 4.7	Effect of damping parameter on dynamic characteristics of a high-low damper. Transition point of damping ratio, $\beta$ , —, 1.4; ----, 2.0; , 2.6. ( $A = 10.0$ mm, $\alpha = 3.0$ , $\zeta = 0.25$ ; $X_1 = 40$ mm).	106
Figure 4.8	Effect of transition point of relative displacement on dynamic characteristics of a low-high damper; $\alpha$ , —, 2.0; ----, 4.0; , 6.0. ( $A = 10.0$ mm, $\alpha = 3.0$ , $\zeta = 0.25$ ; $X_1 = 40$ mm).	108
Figure 4.9	Effect of transition point of relative displacement on dynamic characteristics of a high-low damper; $\alpha$ , —, 2.0; ----, 4.0; , 6.0. ( $A = 10.0$ mm, $\alpha = 3.0$ , $\zeta = 0.25$ ; $X_1 = 40$ mm).	108
Figure 4.10	Effect of amplitude of excitation on dynamic characteristics of a low-high damper; $\alpha$ , —, 2.0; ----, 4.0; , 6.0. ( $A = 10.0$ mm, $\alpha = 3.0$ , $\zeta = 0.25$ ; $X_1 = 40$ mm).	109
Figure 4.11	Effect of amplitude of excitation on dynamic characteristics of a high-low damper; $\alpha$ , —, 2.0; ----, 4.0; , 6.0. ( $A = 10.0$ mm, $\alpha = 3.0$ , $\zeta = 0.25$ ; $X_1 = 40$ mm).	109

Figure 4.12	Performance of a low-high damper with the variation in transition point of damping ratio $\beta$ , —, 1.4; ----, 2.0 ; , 2.6; (A = 10.0 mm, $\alpha = 3.0$ ; $\zeta = 0.25$ and $X_1 = 40\text{mm}$ ).	113
Figure 4.13	Performance of a high-low damper with the variation in transition point of damping ratio $\beta$ , —, 1.4; ----, 2.0 ; , 2.6; (A = 10.0 mm, $\alpha = 3.0$ ; $\zeta = 0.25$ and $X_1 = 40\text{mm}$ ).	114
Figure 4.14	Performance of a low-high damper with the variation in transition point in relative displacement $\alpha$ ; —, 2.0; ----, 4.0 ; , 6.0; (A = 10.0 mm, $\beta = 2.0$ ; $\zeta = 0.25$ and $X_1 = 40\text{mm}$ ).	117
Figure 4.15	Performance of a high-low damper with the variation in transition point in relative displacement $\alpha$ ; —, 2.0; ----, 4.0 ; , 6.0; (A = 10.0 mm, $\beta = 2.0$ ; $\zeta = 0.25$ and $X_1 = 40\text{mm}$ ).	118
Figure 4.16	Transmissibility characteristics of a low-high damper. $X_1(\text{mm})$ , —, 10.0; ----, 20.0; , 60.0. (A = 10mm, $\alpha = 3.0$ ; $\zeta = 0.25$ and $\beta = 2.0$ ).	120
Figure 4.17	Transmissibility characteristics of a high-low damper. $X_1(\text{mm})$ , —, 10.0; ----, 20.0; , 60.0. (A = 10mm, $\alpha = 3.0$ ; $\zeta = 0.25$ and $\beta = 2.0$ ).	121
Figure 4.18	Comparison of a low-high damper with linear dampers of high and low damping value. $\alpha$ —, 4; ----, 6; $\zeta = 0.50$ (linear); $\xi = 0.25$ (linear); ( $X_1 = 40\text{mm}$ , A = 10mm, $\zeta = 0.25$ and $\beta = 2.0$ ).	123
Figure 4.19	Displacement shock characteristics under different shock severity. (a) rounded pulse displacement (b) rounded step displacement.	125
Figure 4.20	Shock response characteristics of a low-high damper. (a) acceleration ratio (b) velocity ratio (c) displacement ratio (d) relative displacement ratio. Shock severity, —, 0.10; ----, 0.20 ; , 0.50; ----, 1.0 (A = 10mm, $\alpha = 4$ , $\zeta = 0.25$ , $\beta = 2.0$ , $Y_s = 40\text{ mm}$ ).	129
Figure 4.21	Shock response characteristics of a high-low damper. (a) acceleration ratio (b) velocity ratio (c) displacement ratio (d) relative displacement ratio. Shock severity, —, 0.10; ----, 0.20 ; , 0.50; ----, 1.0 (A = 10 mm, $\alpha = 4$ , $\zeta = 0.25$ , $\beta = 2.0$ , $Y_s = 40\text{ mm}$ ).	131
Figure 4.22	Shock response characteristics of a low-high damper. (a) SAR (b) SVR (c) SDR and (d) RDR. $\beta$ , —, 1.4; ----, 2.0 ; , 2.6. (A = 10mm, $\alpha = 4$ , $\zeta = 0.25$ . $Y_s = 40\text{ mm}$ ).	133

Figure 4.23	Shock response characteristics of a high-low damper. (a) SAR (b) SVR (c) SDR and (d) RDR. $\beta$ , —, 1.4; - - - - -, 2.0 ; , 2.6. ( $A = 10\text{mm}$ , $\alpha = 4$ , $\zeta = 0.25$ . $Y_s = 40\text{ mm.}$ ).	135
Figure 5.1	Orifice flow time history of the hydraulic damper at different frequencies. ( $X_1 = 1\text{mm}$ ; piston diameter 70mm).	140
Figure 5.2	Top chamber pressure of the hydraulic damper in time domain at different frequencies. ( $X_1 = 1\text{ mm}$ ; piston diameter 70mm).	142
Figure 5.3	Bottom chamber pressure of the hydraulic damper in time domain at different frequencies. ( $X_1 = 1\text{ mm}$ ; piston diameter 70mm).	143
Figure 5.4	Damping force of the hydraulic damper in time domain at different frequencies. ( $X_1 = 1\text{ mm}$ ; piston diameter 70mm).	145
Figure 5.5	Transmitted force characteristics of the hydraulic damper at different frequencies. ( $X_1 = 1\text{ mm}$ ; piston diameter 70mm).	146
Figure 5.6	Lissajous plots of the hydraulic damper at different frequencies. ( $X_1 = 1\text{ mm}$ ; piston diameter 70mm).	147
Figure 5.7	Effect of orifice diameter on the internal variables of the damper. $X_1 = 1.0\text{ mm}$ at 10 Hz ; piston diameter 70mm; orifice diameter, —, 4.5mm; - - - - -, 6mm; , 7.5mm; .	149
Figure 5.8	Effect of piston diameter on the internal variables of the damper. $X_1 = 1.0\text{ mm}$ at 10 Hz; orifice diameter 4.5mm; piston diameter, —, 70mm; - - - - -, 80mm; , 90mm.	151
Figure 5.9	Effect of frequency of excitation on (a) dynamic stiffness and (b) loss angle. ( $X_1 = 1\text{ mm}$ ; piston diameter 70mm; orifice dia 4.5mm).	153
Figure 5.10	Effect of frequency of excitation on (a) top chamber pressure and (b) bottom chamber pressure. ( $X_1 = 1\text{ mm}$ ; piston diameter 70mm; orifice dia 4.5mm).	153
Figure 5.11	Effect of frequency of excitation on (a) orifice flow and (b) damping force. ( $X_1 = 1\text{ mm}$ ; piston diameter 70mm; orifice diameter 4.5mm).	155
Figure 5.12	Effect of orifice diameter on (a) dynamic stiffness and (b) loss angle. Amplitude 1mm; piston diameter 70mm; orifice diameter, —, 4.5mm; - - - - -, 6mm; , 7.5mm.	155

- Figure 5.13** Effect of orifice diameter on (a) top chamber pressure and (b) bottom chamber pressure. Amplitude 1mm; piston diameter 70mm. Orifice diameter; —, 4.5mm; ----, 6mm; — · — · —, 7.5mm. 157
- Figure 5.14** Effect of orifice diameter on (a) orifice flow rate and (b) peak damping force. Amplitude 1mm; piston diameter 70mm. Orifice diameter; —, 4.5mm; ----, 6mm; — · — · —, 7.5mm. 157
- Figure 5.15** Effect of piston diameter on (a) dynamic stiffness and (b) loss angle.  $X_1=1\text{mm}$  at 10 Hz; piston diameter; —, 70mm; ----, 80mm; — · — · —, 90mm. 159
- Figure 5.16** Effect of top chamber compliance on (a) dynamic stiffness and (b) loss angle.  $X_1=1\text{mm}$  at 10 Hz; orifice dia 4.5mm; piston diameter 70mm. —, Comp\_A; ----, Comp\_B; — · — · —, Comp\_C. 159
- Figure 5.17** Effect of bottom chamber compliance on (a) dynamic stiffness and (b) loss angle.  $X_1=1\text{mm}$  at 10 Hz; orifice dia 4.5mm; piston diameter 70mm. Comp\_D; ----, Comp\_E. 161
- Figure 5.18** Coefficient of discharge for various orifice opening. —, squared edge; ----, rounded edge; — · — · —, extended edge. 161
- Figure 5.19** Effect of orifice opening on (a) dynamic stiffness and (b) loss angle.  $X_1=1\text{mm}$  at 10 Hz; orifice dia 4.5mm; piston diameter 70mm. —, squared edge; ----, sharpened edge; — · — · —, extended edge. 163
- Figure 5.20** Effect of amplitude of excitation on (a) dynamic stiffness and (b) loss angle. Orifice dia 4.5mm; piston diameter 70mm. Amplitude —, 1mm; ----, 0.75mm; — · — · —, 0.50mm. 163
- Figure 5.21** Effect of amplitude of excitation on (a) acceleration transmissibility and (b) relative displacement transmissibility. Orifice dia 6mm; piston diameter 70mm. Amplitude; —, 1mm; ----, 0.75mm; — · — · —, 0.50mm. 165
- Figure 5.22** Effect of orifice diameter on (a) acceleration transmissibility and (b) relative displacement transmissibility. Amplitude 1mm; piston diameter 70mm. Orifice diameter, —, 5mm; ----, 6mm; — · — · —, 8mm; ----, 10mm. 167
- Figure 5.23** Effect of piston diameter on (a) acceleration transmissibility. Amplitude 1mm; orifice diameter 7.5mm. Piston diameter, —, 70mm; ----, 80mm; — · — · —, 90mm. 169

Figure 5.24	Effect of chamber compliance on (a) acceleration transmissibility. Amplitude 1mm; orifice diameter 7.5mm. —, Comp_A ; - - - - - , Comp_B; . . . . . , Comp_C.	169
Figure 5.25	Shock responses in time domain. Shock severity, —, 0.1; - - - - - , 0.5; . . . . . , 1.0; (a) acceleration ratio, (b) velocity ratio, (c) displacement ratio, (d) relative displacement ratio.	171
Figure 5.26	Shock responses as a function of shock severity with the variation of orifice diameter; —, 4mm; - - - - - , 6mm; . . . . . , 8mm; (a) SAR, (b) VAR, (c) SDR, (d) RDR.	173
Figure 6.1	Orifice flow characteristics in time domain at different frequencies; oscillation effect, —, considered; . . . . . , not considered; ( $X_1=1\text{mm}$ ; $L_o=50\text{mm}$ , $D_o=6\text{mm}$ ).	178
Figure 6.2	Top chamber pressure characteristic in time domain at different frequencies. ( $X_1=1\text{mm}$ ; $L_o=50\text{mm}$ , $D_o=6\text{mm}$ ).	180
Figure 6.3	Damping force characteristic in time domain at different frequencies. ( $X_1=1\text{mm}$ ; $L_o=50\text{mm}$ , $D_o=6\text{mm}$ ).	181
Figure 6.4	Transmitted force characteristic in time domain at different frequencies. ( $X_1=1\text{mm}$ ; $L_o=50\text{mm}$ , $D_o=6\text{mm}$ ).	183
Figure 6.5	Lissajous plots for the damper at different frequencies. Oscillation effect, —, considered; . . . . . , not considered; ( $X_1=1\text{mm}$ ; $L_o=50\text{mm}$ , $D_o=6\text{mm}$ ).	184
Figure 6.6	Effect of orifice diameter on the internal variables of the damper; orifice diameter —, 4.5mm; - - - - - , 6mm; . . . . . , 7.5mm; ( $X_1=1\text{mm}$ at 10 Hz; $L_o=100\text{mm}$ , $D_p=75\text{mm}$ ).	186
Figure 6.7	Effect of orifice length on the internal variables of the damper; orifice length —, 50mm; - - - - - , 100mm; . . . . . , 150mm; ( $X_1=1\text{mm}$ at 10 Hz; $D_o=6\text{mm}$ , $D_p=75\text{mm}$ ).	188
Figure 6.8	Effect of piston diameter on the internal variables of the damper; piston diameter —, 70mm; - - - - - , 80mm; . . . . . , 90mm; ( $X_1=1\text{mm}$ at 10 Hz; $D_o=6\text{mm}$ , $D_p=75\text{mm}$ ).	189
Figure 6.9	Effect of frequency of excitation on (a) dynamic stiffness and (b) loss angle (a) top chamber pressure and (b) bottom chamber pressure (e) orifice flow; ( $X_1=1\text{mm}$ , $D_o=6\text{mm}$ , $D_p=75\text{mm}$ ).	191

- Figure 6.10 Effect of orifice diameter on the (a) dynamic stiffness and (b) loss angle of the damper; oscillation effect is considered; orifice diameter —, 4mm; ·····, 6mm; ·····, 8mm; ( $X_1=1\text{mm}$ ,  $L_o=50\text{mm}$ ,  $D_p=75\text{mm}$ ). 193
- Figure 6.11 Effect of orifice diameter on the (a) dynamic stiffness and (b) loss angle of the damper; oscillation effect is not considered; orifice diameter —, 4mm; ·····, 6mm; ·····, 8mm; ( $X_1=1\text{mm}$ ,  $L_o=50\text{mm}$ ,  $D_p=75\text{mm}$ ). 193
- Figure 6.12 Effect of orifice length on the (a) dynamic stiffness and (b) loss angle of the damper; orifice length —, 50mm; ·····, 100mm; ·····, 150mm; ( $X_1=1\text{mm}$ ,  $D_o=6\text{mm}$ ,  $D_p=75\text{mm}$ ). 195
- Figure 6.13 Effect of piston diameter on the (a) dynamic stiffness and (b) loss angle of the damper; piston diameter —, 70mm; ·····, 80mm; ·····, 90mm; ( $X_1=1\text{mm}$ ,  $D_o=6\text{mm}$ ,  $L_o=50\text{mm}$ ). 195
- Figure 6.14 Effect of amplitude of excitation on the (a) dynamic stiffness and (b) loss angle of the damper.  $X_1$ ; —, 1mm; ·····, 0.75mm; ·····, 0.50mm; ( $D_o=6\text{mm}$ ,  $L_o=50\text{mm}$ ,  $D_p=70\text{mm}$ ). 197
- Figure 6.15 Effect of amplitude of excitation on (a) acceleration transmissibility and (b) relative displacement transmissibility;  $X_1$ ; —, 1mm; ·····, 0.75mm; ·····, 0.50mm; ( $D_o=9\text{mm}$ ,  $L_o=200\text{mm}$ ,  $D_p=70\text{mm}$ ). 200
- Figure 6.16 Effect of orifice length on (a) acceleration transmissibility and (b) relative displacement transmissibility; orifice length; —, 100mm; ·····, 150mm; ·····, 200mm; ( $X_1=0.75\text{mm}$ ,  $D_o=9\text{mm}$ ,  $D_p=70\text{mm}$ ). 202
- Figure 6.17 Effect of orifice diameter on (a) acceleration transmissibility and (b) relative displacement transmissibility; orifice diameter; —, 7mm; ·····, 8mm; ·····, 9mm, —, 10mm; ( $X_1=0.75\text{mm}$ ,  $L_o=150\text{mm}$ ,  $D_o=70\text{mm}$ ). 204
- Figure 6.18 Effect of piston diameter on (a) acceleration transmissibility and (b) relative displacement transmissibility; piston diameter, —, 70mm; ·····, 80mm; ·····, 90mm; —, 100mm; ( $X_1=0.75\text{mm}$ ,  $L_o=150\text{mm}$ ,  $D_o=9\text{mm}$ ). 206
- Figure 6.19 Shock responses in time domain. Shock severity, —, 0.1; ·····, 0.2; ·····, 0.5; ·····, 1mm; (a) acceleration ratio, (b) velocity ratio, (c) displacement ratio, (d) relative displacement ratio. 207



- Figure 6.20** Shock responses as a function of shock severity with the variation of orifice diameter; —, 4mm; - - - - - , 6mm;      , 8mm; (a) SAR, (b) VAR, (c) SDR, (d) RDR. 209
- Figure 6.21** Effect of bleeder orifice diameter on the (a) long orifice flow and (b) short orifice flow of the damper; short orifice diameter, —, 0.0mm (without); - - - - - , 3mm;      , 4mm - - - - - , 5mm. ( $X_1=1\text{mm}$ ,  $L_o=150\text{mm}$ ,  $D_o=7\text{mm}$ ). 211
- Figure 6.22** Effect of bleeder orifice diameter on the (a) long orifice flow and (b) short orifice flow of the damper; bleeder orifice diameter, —, 0.0mm (without); - - - - - , 3mm;      , 4mm - - - - - , 5mm. ( $X_1=5\text{mm}$ ,  $L_o=150\text{mm}$ ,  $D_o=7\text{mm}$ ). 211
- Figure 6.23** Effect of bleeder orifice diameter on the dynamic stiffness and loss angle of the damper. bleeder orifice diameter, —, 0 mm (without); - - - - - , 3mm;      , 4mm - - - - - , 5mm; (a)  $X_1=1\text{mm}$ , (b)  $X_1=2.5\text{mm}$ , (c)  $X_1=5\text{mm}$ ; ( $L_o=150\text{mm}$ ,  $D_o=7\text{mm}$ ). 213
- Figure 6.24** Effect of bleeder orifice diameter on the force-displacement characteristics of the damper. bleeder orifice diameter, —, 0.0mm (without), - - - - - , 3mm;      , 4mm; - - - - - , 5mm; (a)  $X_1=1\text{mm}$ , (b)  $X_1=2.5\text{mm}$ , (c)  $X_1=5\text{mm}$ ; ( $L_o=150\text{mm}$ ,  $D_o=7\text{mm}$ ). 215
- Figure 6.25** Effect of bleeder orifice diameter on the transmissibility performance of the damper. bleeder orifice diameter, —, 0.0mm (without); - - - - - , 3mm;      , 4mm - - - - - , 5mm; ( $X_1=0.75\text{mm}$ ,  $L_o=150\text{mm}$ ,  $D_o=7\text{mm}$ ). 217
- Figure 6.26** Effect of bleeder orifice diameter on the transmissibility performance of the damper. bleeder orifice diameter, —, 0.0 (without); - - - - - , 3.0 mm;      , 4mm - - - - - , 5mm; ( $X_1=2.5\text{mm}$ ,  $L_o=150\text{mm}$ ,  $D_o=7\text{mm}$ ). 218
- Figure 6.27** Shock responses as a function of shock severity with the variation of long orifice diameter; —, 6mm; - - - - - , 7mm;      , 8mm; (a) SAR, (b) VAR, (c) SDR, (d) RDR. ( $Y_s=20\text{mm}$ ,  $L_o=150\text{mm}$ ,  $D_{ob}=4\text{mm}$ ). 220
- Figure 6.28** Shock responses as a function of shock severity with the variation of bleeder orifice diameter; —, 3mm; - - - - - , 4.5mm;      , 6mm; (a) SAR, (b) VAR. ( $Y_s=20\text{mm}$ ,  $L_o=150\text{mm}$ ,  $D_o=8\text{mm}$ ). 222

- Figure 7.1 Long orifice flow and bleeder orifice flow of the LDVHF damper with the variation of valve short orifice —, 4mm; - - -, 6mm; . . . , 8mm; ( $X_1=5\text{mm}$ ,  $L_o=150\text{mm}$ ,  $D_o=8\text{mm}$ ,  $D_{ob}=8\text{mm}$ ). 227
- Figure 7.2 Valve short orifice flows of the LDVHF damper with the variation of its diameter; —, 4mm; - - -, 6mm; . . . , 8mm; ( $X_1=5\text{mm}$ ,  $L_o=150\text{mm}$ ,  $D_o=8\text{mm}$ ,  $D_{ob}=6\text{mm}$ ). 227
- Figure 7.3 Top chamber pressure and transmitted force (in time domain) of the LDVHF damper. Valve short orifice diameter —, 4mm; - - -, 6mm; . . . , 8mm; ( $X_1=5\text{mm}$ ,  $L_o=150\text{mm}$ ,  $D_o=8\text{mm}$ ,  $D_{ob}=6\text{mm}$ ). 229
- Figure 7.4 Top chamber pressure and transmitted force (in time domain) of the LDVHF damper. Valve short orifice diameter —, 4mm; - - -, 6mm; . . . , 8mm; ( $X_1=5\text{mm}$ ,  $L_o=150\text{mm}$ ,  $D_o=8\text{mm}$ ,  $D_{ob}=8\text{mm}$ ). 229
- Figure 7.5 Top chamber pressure and transmitted force (in time domain) of the LDVHF damper. Valve short orifice diameter —, 4mm; - - -, 6mm; . . . , 8mm; ( $X_1=5\text{mm}$ ,  $L_o=150\text{mm}$ ,  $D_o=8\text{mm}$ ,  $D_{ob}=10\text{mm}$ ). 231
- Figure 7.6 Motion of the valve orifice of the LDVHF damper. (a) orifice 1 and (b) orifice 2. Valve short orifice diameter —, 4mm; - - -, 6mm; . . . , 8mm; ( $X_1=5\text{mm}$ ,  $L_o=150\text{mm}$ ,  $D_o=8\text{mm}$ ,  $D_{ob}=6\text{mm}$ ). 231
- Figure 7.7 Effect of valve short orifice diameter on the (a) dynamic stiffness and (b) loss angle of the damper. Valve short orifice diameter —, 4mm; - - -, 6mm; . . . , 8mm; ( $X_1=5\text{mm}$ ,  $L_o=150\text{mm}$ ,  $D_o=8\text{mm}$ ,  $D_{ob}=6\text{mm}$ ). 233
- Figure 7.8 Effect of valve short orifice diameter on the (a) dynamic stiffness and (b) loss angle of the damper. Valve short orifice diameter —, 4mm; - - -, 6mm; . . . , 8mm; ( $X_1=5\text{mm}$ ,  $L_o=150\text{mm}$ ,  $D_o=8\text{mm}$ ,  $D_{ob}=8\text{mm}$ ). 233
- Figure 7.9 Effect of valve short orifice diameter on the (a) dynamic stiffness and (b) loss angle of the damper. Valve short orifice diameter —, 4mm; - - -, 6mm; . . . , 8mm; ( $X_1=5\text{mm}$ ,  $L_o=150\text{mm}$ ,  $D_o=8\text{mm}$  and  $D_{ob}=10\text{mm}$ ). 234
- Figure 7.10 Effect of valve orifice diameter on (a) acceleration transmissibility and (b) relative displacement transmissibility. Valve short orifice diameter —, 4mm; - - -, 6mm; . . . , 8mm; ( $X_1=2.5\text{mm}$ ,  $L_o=150\text{mm}$ ,  $D_o=8\text{mm}$  and  $D_{ob}=5\text{mm}$ ). 237

- Figure 7.11 Effect of valve orifice diameter on (a) acceleration transmissibility and (b) relative displacement transmissibility. Valve short orifice diameter —, 4.0 mm; ----, 6mm; — · — · —, 8mm; ( $X_1=2.5\text{mm}$ ,  $L_0=150\text{mm}$ ,  $D_o=8\text{mm}$  and  $D_{ob}=6\text{mm}$ ). 238
- Figure 7.12 Effect of valve orifice diameter on (a) acceleration transmissibility and (b) relative displacement transmissibility. Valve short orifice diameter, 4mm; ----, 6mm; — · — · —, 8mm; ( $X_1=2.5\text{mm}$ ,  $L_0=150\text{mm}$ ,  $D_o=8\text{mm}$  and  $D_{ob}=7\text{mm}$ ). 240
- Figure 7.13 Comparison of performance of hydraulic dampers.  $X_1 = 1\text{mm}$ ; —, SDHF; ----, LDHF; — · — · —, LSDHF; — · — · — · —, LDHVF. 242
- Figure 7.14 Comparison of performance of hydraulic dampers.  $X_1 = 2.5\text{mm}$ ; —, SDHF; ----, LDHF; — · — · —, LSDHF; — · — · — · —, LDHVF. 243
- Figure 7.15 Shock responses in time domain. Shock severity, —, 0.1; ----, 0.2; — · — · —, 0.5; · · · · ·, 1.0; (a) acceleration ratio, (b) velocity ratio, (c) displacement ratio and (d) relative displacement ratio. 245
- Figure 7.16 Shock responses as a function of shock severity with the variation of valve orifice diameter; —, 4mm; ----, 5mm; — · — · —, 6mm; (a) SAR, (b) SVR, (c) SDR and (d) RDR. 247
- Figure 7.17 Shock response as a function of shock severity for hydraulic dampers. —, SDHF; ----, LDHF; — · — · —, LSDHF; · · · · ·, LDHVF; (a) SAR, (b) SVR. 249

\*\*\*\*\*

## NOMENCLATURE

$A, \alpha A$	transition point of relative displacement of dual-phase damper, m
$A_l$	cross-sectional area of long orifice, $m^2$
$A_n$	coincident component of dynamic stiffness, N/mm
$A_o$	cross-sectional area of orifice, $m^2$
$A_{o1}$	cross-sectional area of orifice 1, $m^2$
$A_{o2}$	cross-sectional area of orifice 2, $m^2$
$A_{ob}$	cross-sectional area of orifice 2, $m^2$
$A_{TP}$	projected area of the top chamber acting as a piston, $m^2$
$A_v, \gamma A_v$	relative velocity corresponding to $x=A$ , and $x=\alpha A$ , m/s
$B_n$	quadrature component of dynamic stiffness, N/mm
$C$	damping coefficient, N-s/m
$C(\dot{x})$	damping coefficient as a function of relative velocity, N-S/m
$C(x)$	damping coefficient as a function of relative displacement, N-S/m
$\bar{C}$	equivalent linear damping coefficient, N-s/m
$\bar{C}_t$	trial damping coefficient, N-s/m
$C_d$	damping coefficient, N-s/m
$C_D$	discharge coefficient
$C_{D1}$	discharge coefficient for short orifice 1
$C_{D2}$	discharge coefficient for short orifice 2
$C_{Db}$	discharge coefficient for bleeder orifice
$C_v$	compliance for flexible chamber $m^5/N$
$C_{VV}$	viscous damping coefficient for valve, N-s/m
$C_{VB}$	bottom chamber compliance, $m^5/N$

$C_{VT}$	top chamber compliance, $m^5/N$
$D_b$	bleeder orifice diameter, m
$D_l$	long orifice diameter, m
$D_o$	orifice diameter, m
$D_{o1}$	diameter for short orifice 1, m
$D_{o2}$	diameter for short orifice 2, m
$D_{ob}$	bleeder orifice diameter, m
$F_d$	damping force developed by the damper, N
$F_{ST}$	force due to static load, N
$F_T$	force transmitted to the ground, N
$F_V$	force due to change in momentum, N
$f_n$	undamped natural frequency, cycle/s
$I_f$	fluid inertance, $Kg/m^4$
$I_l$	fluid inertance for long orifice, $Kg/m^4$
$I_{o1}$	fluid inertance for short orifice 1, $Kg/m^4$
$I_{o2}$	fluid inertance for short orifice 2, $Kg/m^4$
$I_{ob}$	fluid inertance for bleeder orifice, $Kg/m^4$
$K$	stiffness of the rubber element of the damper, N/mm
$K_1$	spring constant of the relief valve 1, N/mm
$K_2$	spring constant of the relief valve 2, N/mm
$K_b$	spring constant of the bleeder orifice valve 2, N/mm
$K_c$	loss due to contraction
$K_D$	dynamic stiffness of the damper, N/mm
$K_{en}$	entry loss coefficient
$K_{ex}$	exit loss coefficient
$K_s$	stiffness of the linear spring, N/mm
$L_b$	bleeder orifice length, m

$L_l$	long orifice length, m
$L_o$	orifice length, m
$L_{o1}$	length of the short orifice 1, m
$L_{o2}$	length of the short orifice 2, m
$L_{ob}$	length of the bleeder orifice, m
$m$	mass, kg
$m_v$	mass of the valve dish and the spring, Kg
$n$	number of harmonics
$P_{AT}$	atmospheric pressure, Pa
$P_B$	bottom chamber pressure of hydraulic damper with flexible chamber, Pa
$P_{set, b}$	preset pressure for the bleeder orifice to open the valve, Pa
$P_{set, i}$	preset pressure for the $i$ th orifice to open the the valve, Pa
$P_{sp}$	preload spring force, N
$P_{ST}$	static pressure, Pa
$P_T$	top chamber pressure of hydraulic damper with flexible chamber, Pa
$Q$	orifice flow, $m^3/s$
$Q_b$	flow through bleeder orifice, $m^3/s$
$Q_l$	flow through long orifice, $m^3/s$
$Q_o$	flow through short orifice, $m^3/s$
$Q_{o1}$	flow through short orifice 1, $m^3/s$
$Q_{o2}$	flow through short orifice 2, $m^3/s$
$Q_{ob}$	flow through bleeder orifice for the LDHVF damper, $m^3/s$
$r$	frequency ratio $\omega/\omega_n$
$R_e$	Reynolds number
$R_{el}$	Reynolds number due to flow through long orifice
$R_{eob}$	Reynolds number due to flow through bleeder orifice
$R_{eo1}$	Reynolds number due to flow through short orifice 1

$R_{eo2}$	Reynolds number due to flow through short orifice 2
$u$	number of cycles
$V_A$	entrapped air in the top chamber, cc
$V_o$	average fluid velocity within the orifice, m/s
$V_{TA}$	total volume of entrapped air, cc
$V_{TO}$	total volume of fluid transferred from one chamber to another, m <sup>3</sup>
$\text{sgn}(x)$	signum function; -1 when $x$ is negative and +1 when $x$ is positive.
$x$	relative displacement, m
$X$	peak relative displacement, m
$x_1$	excitation as a function of time, m
$x_2$	response as a function of time, m
$X_1$	static deflection of the damper, m
$x_s$	shock response as a function of time, m
$x_{ST}$	excitation as a function of time, m
$\dot{x}$	relative velocity, m <sup>2</sup> /s
$\dot{x}_{\text{peak}}$	peak relative velocity, m <sup>2</sup> /s
$\ddot{x}$	relative acceleration, m <sup>2</sup> /s
$y$	valve displacement, m
$y_i$	$i$ th valve displacement, m
$y_s$	shock input as a function of time, m
$Y_s$	maximum shock displacement, m
$\alpha$	transition factor for relative displacement of dual-phase damper
$\beta$	transition factor for damping coefficient of dual-phase damper
$\gamma$	transition factor for relative velocity for dual-phase damper
$\phi$	loss angle, degree
$\Delta P$	differential pressure between top and bottom chamber, Pa
$\Delta V_T$	volume increment of the top chamber, m <sup>3</sup>

$\Delta V_B$	volume increment of the bottom chamber, m <sup>3</sup>
$V_{BST}$	volume increment of bottom chamber from atmospheric pressure to static pressure change, m <sup>3</sup>
$V_{TST}$	volume increment of top chamber from atmospheric pressure to static pressure change, m <sup>3</sup>
$\rho$	density of hydraulic fluid, m <sup>3</sup> /s
$\zeta$	damping ratio
$\overline{\zeta_t}$	trial damping ratio
$\lambda_a$	correction factor for active component
$\lambda_r$	correction factor for reactive component
$\sigma$	nonlinearity index of dual-phase damper
$\tau_p$	duration for pulse displacement, sec
$\tau_s$	duration for step displacement, sec
$\mu$	absolute viscosity, N-s/m <sup>2</sup>
$\nu$	kinematic viscosity, m <sup>2</sup> /s
$\omega$	circular frequency of excitation, rad/s
$\omega_o$	undamped natural frequency, rad/s
$\omega_n$	nondimensional natural frequency
$  $	measure of absolute value
cc	cubic centimeter
Comp_A	A- type compliance
LDHF	long orifice hydraulic damper with flexible chamber
LSDHF	long and short orifice hydraulic damper with flexible chamber
LDHVF	long orifice hydraulic damper with spring loaded valves
SDHF	short orifice hydraulic damper with flexible chamber



# **CHAPTER 1**

## **INTRODUCTION**

### **1.1 General**

Damping of a system is a substantive phenomenon, indispensable for isolation of shock, vibration or noise. There are numerous applications for damping devices in mechanical systems. In vehicle design, dampers play a very important role and are being used in suspensions, seat suspensions, cab mounts, engine mounts, under carriage protection, bumpers, etc. Design of dampers for vehicle system presents a challenge as the components are subjected to excitations and shocks of wide frequency range and severity. Furthermore, the automobile suspensions pose conflicting requirements for damping and stiffness properties to enhance the vehicle ride comfort, handling or control. Low dynamic stiffness is the key property necessary for ride comfort, but it yields poor directional control and rattle space performance. On the contrary, high damping exhibits better isolation characteristics around resonance with a great reduction in relative displacement but shows very poor performance for shock and noise isolation. Thus, a damper developed for resonance control can not be effectively applied for road induced shock isolation, and a damper devised for noise isolation is inadequate for isolation of low frequency vibrations.

Currently, the most popular damping device is a hydraulic damper which can be easily designed to meet the requirements for vibration isolation for various

applications.[1-10] For example, if the orifice of the damper is made small, it develops high damping. Again, if the orifice is large, low damping is evolved, resulting in good high frequency performance as well as shock isolation. Such dampers can further be designed to produce nonlinear asymmetric characteristics with good potential for isolation of shock and vibration in a wide frequency range. Consequently, rubber dampers are being rapidly replaced by hydraulic dampers in vehicle applications, since the rubber is practically invariant with excitation amplitude and frequency over a wide range of frequency. The following section describes the typical hydraulic dampers available for various applications.

## **1.2 Classification of Dampers**

In general, classification of dampers are based on the requirement of external source of energy. Such widely known classification includes: i) Passive dampers; ii) Semi-active dampers; and iii) Active dampers. As discussed later under literature review, the semi-active and active concepts are extensively studied which are complex, expensive and have severe limitations for general applications. On the other hand, passive dampers are simple, cost effective and highly reliable.

The present study focuses on the concept of passive damping through hydraulic devices. In this respect, the hydraulic dampers are classified based on their constructional differences, such as: (a) Flexible chambered damper (DHF); and (b) Rigid chambered damper (DHR). Although these dampers have functional differences, they both provide primary damping through dissipation of energy as fluid passes from one chamber to the other. In the first case (DHF), the chambers are flexible whereas in the second case (DHR), the chambers are rigid. DHF dampers are suitable for isolation of low amplitude vibration whereas DHR dampers are mostly suitable for high amplitude low frequency vibration isolation.

### **1.2.1 Flexible Chambered Damper (DHF)**

A typical flexible chambered hydraulic (DHF) damper is shown in Figure 1.1a. It primarily consists of flexible chambers separated by an orifice plate responsible for damping generation. The flexible parts are made of rubber material. The bottom chamber is much more compliant than the upper chamber or top chamber. The function of the top chamber is of three fold; first, to support the structure resting on it, second, to act as a spring and third, to provide chamber flexibility which acts as a piston to pump the fluid from one chamber to the other. As such, it eliminates (a) the necessity of moving parts, such as piston, piston rod, etc., (b) occupies less space, as it is compact. The function of the bottom chamber is, primarily, to act as a reservoir for the fluid coming from the top chamber through the orifice. There can be a wide variation in the design of such dampers both in terms of chamber flexibility and orifices. The orifice can be designed as short, long, with and without spring loaded valves, as well as their combinations.

### **1.2.2 Rigid Chambered Damper (DHR)**

The main components of a rigid chambered damper (DHR) as shown in Figure 1.1b include a cylinder and a piston. The piston, with some orifice perforated on it moves up and down in a long narrow cylinder, sometimes surrounded by another concentric cylinder. To avoid vacuum thereby cavitation, a third chamber or a flexible chamber filled with inert Nitrogen gas, within or outside the cylinder is often included. Additional coil spring is necessary to apply such dampers in a suspension. But when it is built as a pneumatic suspension, the inert gas chamber acts as a gas spring. It can carry larger load, and isolate higher amplitude of vibration at low frequency. Such dampers have been extensively studied and developed over the years [10-11]. For vehicle suspension application, these dampers are designed with orifice valves to provide blow off and bleed control

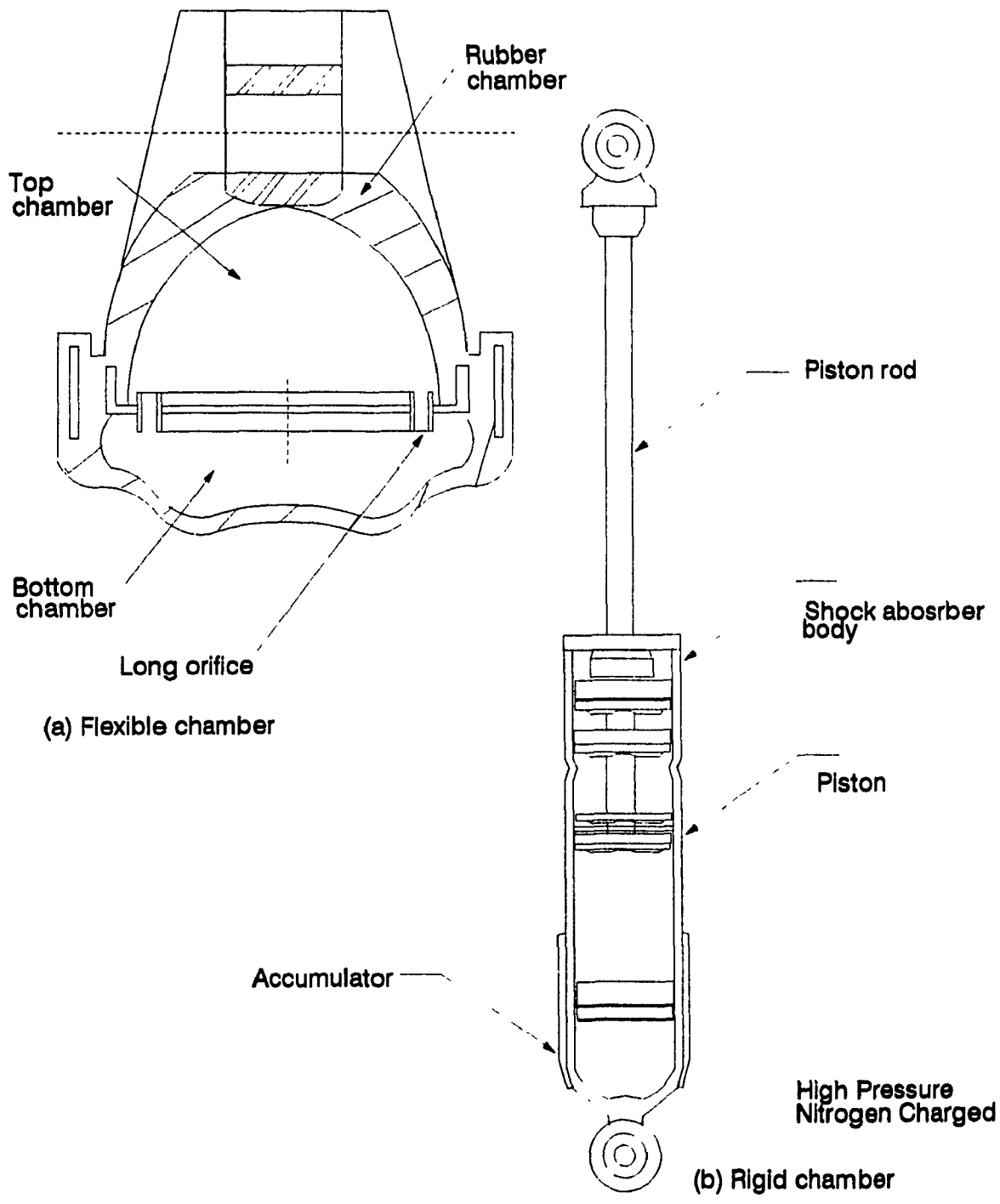


Figure 1.1 Typical hydraulic dampers with: (a) flexible chambers; (b) rigid chamber.

leading to nonlinear asymmetric characteristics. An alternative approach to obtain multi-phase damping based on relative velocity or relative position has been investigated in recent years which showed potential for improvement of both resonance and high frequency performance.

Passive hydraulic dampers with flexible and rigid chambers have proliferated into many forms in recent years due to their simplicity in construction, cost effectiveness and reliability. Significant variations in these designs are possible which may yield superior performance for specific applications. Their full potential can be evaluated by accurate and thorough modeling and analysis. This thesis presents an in-depth and detailed modeling and accurate analysis of a class of hydraulic dampers to explore their performance potential. The hydraulic dampers with flexible chambers are modeled with short orifice, without orifice, and orifice with spring loaded valve as well as their combinations. Detailed analytical models are developed to establish their dynamic characteristics and performance. The study further examines the previously reported concepts of dual-phase damper. In this case a more accurate model based on integral formulation of damping force is developed and compared with those of conventional approaches. The dynamic characteristics and performance of dual-phase damper are established via equivalent linearization and computer simulation. The performance in each case is determined for both sinusoidal excitation and shock.

The following section presents a detailed state-of-the-art survey of literature on hydraulic dampers and a brief discussion on semi-active and active dampers for completeness and to develop the scope of the present investigation.

### **1.3 State-of-the-art Survey**

Extensive research has been carried out on passive, semi-active and active suspension systems during the past few years in order to improve ride quality,

suspension rattle space, handling, roll stability, and directional control characteristics of vehicle systems [1-44]. It constitutes a variety of investigations concerning the development of improved passive element, advanced active and semi-active control systems.

Hydraulic dampers, applied, particularly to vehicle suspension and engine mounting system, are now being required to achieve better noise, shock and vibration isolation. Hydraulically damped, flexible chambered (DHF) engine mountings are a fundamental improvement over the conventional engine mountings [1-8]. Hydraulic mounts have high damping for large motion induced by engine shake and low dynamic stiffness for low amplitude caused by noise transmission [12-17]. These excellent properties cannot be achieved by conventional rubber mount. Hydraulic mounts, so far developed, are less effective in case of superimposed inputs and input in high frequency range [15]. They have demerits also in shock isolation performance [14].

Idle car shake and shock at acceleration, have conflicting requirements. When the mount is tuned to minimize idle car shake, it tends to enlarge the shock at acceleration which is obviously a drawback. In hydraulic mount, high damping is obtained by orifice effect, necessary for 5-15 Hz large amplitude vibration resulting from engine shake. Hydraulic mounts with decoupler component are best suitable for 100-200 Hz low amplitude vibration or booming noise as it produces low dynamic stiffness [15]. But, because of strong nonlinearity of the decoupler, it is not suitable for superimposed inputs such as the engine shake and booming noise acting simultaneously. Furthermore, its function is not effective for the engine combustion sound which is a problem in the range 400 to 600 Hz. This is due to increase of hydraulic stiffness resulting from liquid column resonance or rubber surging. Each of the mount is suitable for a specific purpose only. Furthermore, all of the above mentioned mounts have very poor performance in

isolating shock at acceleration. Although bush type hydraulic mount shows better performance in shock isolation [14], its performance in isolating idle car shake is like an ordinary rubber mount.

Rigid chambered hydraulic dampers (DHR), on the other hand, are widely used for shock and vibration isolation in automobile, motorcycles and aircraft landing gear. It can accommodate large relative displacement, develop high damping for vibration isolation and shows superior performances for shock isolation. These dampers with multiphase characteristics have demonstrated good potentials for improved performance over a wide frequency range. In the following subsection, a state-of-the-art survey of various damping system studied are presented in view of the present investigation.

### **1.3.1 Passive Hydraulic Damper**

The DHF dampers represent relatively recent developments in the damping technology. Although, the analysis and development of various types of passive DHF dampers have been reported in the literature, each type of damper exhibits different performance limitations and benefits.

DHF damper was first developed by Mark Bernuchon [1] having peripheral circular channel and perforated disc connecting two chambers only. Utilizing a very simplified model, under sinusoidal inputs, the study showed good performance in comparison to all rubber mounts for low frequency only. Through experimental study, an improvement in ride comfort was shown within the frequency range 2-20 Hz. It further showed substantial improvement in the acoustic levels in the order of 5 to 6 dB. Corcoran and Ticks [2] have studied hydraulic mount with spiral nozzle and clearance space. They added new technique of 'clearance space phenomenon' to overcome engine bounce, idle shake and noise inside the vehicle. By introducing clearance, dynamic stiffness was

greatly improved for high frequency of amplitude 0.20 mm with a sacrifice in loss angle. For a clearance of  $\pm 0.32$  mm, the performance was shown to be excellent for high frequencies of up to 200 Hz, but the damping in this case is almost half of the damping obtained without clearance. Test conducted with a 6 cylinder in-line gasoline engine using this hydraulic mount showed 5 dB decrease in noise level at 3300 rpm. A three degree of freedom (DOF) linear model was used by Clark [3] to describe dynamic performances (<400 Hz.) of hydraulic mount. He identified the basic principles involved in optimizing the dynamic performance of the mount. It was shown that the larger the ratio of the hydraulic mount spring stiffness, the greater the improvement in the low frequency isolation levels. To minimize the road input effects, it is, however, necessary that the mount should be tuned to "wheel hop frequency". It is true that tuning of the mount will be different for different input conditions, hence the particular vehicle influences the overall performance of hydraulic mount.

Flower [4] analyzed three types of hydraulic power train mounts, namely: hydraulic mount with simple orifice, hydraulic mount with inertia track and hydraulic mount with inertia track and decoupler. He explained in detail their performance starting from simple rubber mount using a technique known as 'bond graph' model. His results show that inertia track helps to get high damping at low frequency, while inertia track together with decoupler gives excellent performance producing low dynamic stiffness at low amplitude and retaining large loss angle at large amplitude and low frequency. Taylor [5] analyzed the same kind of hydraulic mount as Flower but without any orifice. It combines the spring and damper in one package. He showed without any mathematical solution that the mount allowed tuning of damping and stiffness independently. In application to vehicle cab suspension, Marjoram [6] investigated hydraulic mount technology in the suspension of vehicle cabs with the addition of internal pressurization. He studied



the effect of load variation on the dynamic characteristics of FAR (Fluid Air Ride) mount. The advantage of pressurization is that it provides a constant installed height independent of load. FAR mount provides a natural frequency of 2 Hz and Fluidlastic mount provides the same as low as 4 Hz.

Ushijima and Dan [12] carried out nonlinear analysis of air damping mount as well as hydraulic mount using Building Block Approach technique to analyze the frequency response of a vehicle. Their model, like others, consists of a main tube (long orifice) and a decoupler component. Using amplitude of excitation up to 1 mm, they showed, theoretically and experimentally, the characteristics and performance of the dampers. Theoretical analysis of hydroelastic engine mount carried out by Sugino & Abe [13] claims that the mount functions as a velocity amplifying dynamic damper because mass of the fluid inside the orifice is increased due to amplification of velocity and therefore damping effect is high, although the mass is small. They also investigated the influence of various parameter such as orifice length, cross-sectional area, elasticity, specific gravity, etc. on the resonant frequency. Optimization of different parameters of hydraulic mount was also carried out for application to engine mount. But the model developed by them is a mechanical model where all the process are represented by linear spring rate and different cross-sectional area. Therefore, a realistic damper model needs to be analyzed.

Hong Su, et al [7] developed a variable damping mechanism simply by limiting the pressure differential across the piston of a passive hydraulic damper using pressure relief valve. They showed the performance of the passive damping concept to be quite comparable to that of semi-active "on-off" vibration isolators. A researcher on shock isolation by hydraulic mount, Kadomatsu [14] found analytically that nonlinearity of the spring rate characteristics of the mount must be lower and/or damping rate higher in order to reduce shock at acceleration. He

developed a bush type hydraulic engine mount expecting to reduce the shock level to  $1/3$  but the dynamic stiffness is almost same as all rubber mount at idle speed. Ushijima, et al [15] reported some interesting development in hydraulic mount. In order to reduce the nonlinearity of the decoupler, they replaced it with a rubber membrane. It resulted in a low dynamic stiffness even at high frequency and superimposed input. They also applied the phenomenon called 'liquid column resonance against rubber surging' in the mount and achieved low dynamic stiffness up to 800 Hz which is a significant achievement. The performance at low frequency was, however, found to be very poor.

Very recently Singh, et. al [16] carried out a linear mathematical analysis of hydro-mechanical mount having long orifice and decoupler using continuity and momentum equation of fluid mechanics. Later, Kim and Singh [17] carried out a nonlinear analysis of a hydraulic mount having long orifice only. They considered long orifice flow and compliances of the chambers to be nonlinear. Although the model studied is quite complex, they ignored the 'oscillation effect' the long orifice encounters which may have significant effect on the dynamic performance of the damper. It might be one of the reasons for large discrepancy they obtained between the theoretical and experimental results. It is, therefore, necessary to investigate the long orifice hydraulic damper with the consideration of oscillation effect. Furthermore, the behavior of the damper under the excitation of shock input was not considered in this investigation.

A different concept for isolator damping considers multi-phase within a cycle of vibration. A number of studies have been carried out on this concept where the damper construction is same as that of conventional rigid chamber. In this case, however, damping characteristics is of dual-phase which may be based on relative position, velocity or acceleration. Venkatesan and Krishnan [8,36] described a dual-phase damping of displacement sensitive type in application to a simple

shock mount. They carried out harmonic analysis using equivalent damping ratio technique. It was shown that by using dual-phase damping, it is possible to reduce the absolute transmissibility over the whole frequency range. In fact dual phase damper is a compromise between low damping and high damping. Therefore, it has good performance near resonant frequency but poor performance in high frequency zone compared to the decoupler fitted to a hydraulic mount. This study, however, adopts a simplified approach for characterizing the damping force which is displacement sensitive. This approach may lead to under- or overestimation of the damping force to a great extent. Guntur and Sankar [37] carried out extensive research on six different kinds of dual phase damping shock mounts, namely displacement sensitive, velocity sensitive and acceleration sensitive, each with low-high and high-low form. Results are useful in the development of optimization theory in nonlinear damping. In a very recent study Sankar, et. al [38] analyzed the dual-phase damper both theoretically and experimentally showing that a displacement sensitive low-high damper has a very good potential for vibration isolation. The results show a significant reduction in the resonant transmissibility without any significant loss at high frequency when compared to a linear damper.

Following the early work of Snowdon [43] on dual-phase damping, all investigations on the subject to date have defined damping force by  $F_d = C(\dot{x})\dot{x}$ . This results from the fundamental definition  $F_d = \int_0^{\dot{x}} C(\dot{x})d\dot{x}$  when the coefficient  $C$  is a constant. In the case of dual-phase damping, however,  $C$  is a function of time response. Consequently, the traditional simplified approach used to date must have lead to under- or overestimation of the damping force in the simulation. In order to evaluate the performance of a dual-phase damper accurately, the integral approach must be used to describe the damping force characteristics.

### **1.3.2 Semi-active Hydraulic Damper**

Semi-active vibration control is based on the ability to modify the magnitude of forces transmitted through coupling devices. Low power actuators are used to induce changes in damping properties by modifying hydraulic parameters within the damper.

Graf and Shoureshi [39] analyzed semi-active hydraulic mount of two kinds; one with external bleed and the other with internal bleed having ports for pressurized fuel injection. The conclusion is that a significant improvement in transmissibility is possible in low frequency zone compared to passive hydraulic mount. But in high frequency zone it has higher transmissibility. Effect of parameter variation on mount properties were also analyzed through sensitivity analysis. West [40] utilized an external vacuum pump to control diaphragm movement in the mount, where high level of vacuum produces high damping and vice versa. Duclos [41] used five internal paths, four of which contain ER fluid valve which could be used to control the fluid flow through these paths. ER (Electro-Rheological) valve is a simple, low power consuming, low cost method of controlling tunable damper. Ushijima, et al [15] also carried out semi-active hydraulic mount analysis. They applied the principle that application of electric field strength changes the apparent viscosity of ER fluid. In their model of semi-active hydraulic mount, damping force was controlled by applying high voltage in rectangular wave. The results show that an excellent vibration isolation performance is theoretically possible when controlled by rectangular wave of half the period of sinusoidal excitation with a phase difference of 135 degrees.

### **1.3.3 Active Hydraulic Damper**

In the case of active hydraulic systems both magnitude and direction of forces applied through coupling devices are controlled. It requires high speed actuators

and fast sensors with operating bandwidths matching those of disturbance spectrum.

Mizuguchi, et al [42] developed an electric controlled engine mounting system, an active hydraulic mount, which keeps the insulator characteristics soft under normal conditions, and increases spring constant and damping force to limit engine roll when a large load change occurs. Here the two chambers are separated by a partition having fixed orifice and a valve controlled port operated by a rotary solenoid. The solenoid is controlled by a solenoid unit. This mount has a remarkably low level of shock isolation as well as reduced engine vibration at idle speed and at cruising. Hagino, et al [9] developed an active vibration control system capable of reducing vibration at acceleration by 16 dB when the control force is 32 N. Actuator, controller and power amplifier are the main component of the system to apply feed forward control method. From engine ignition pulse, engine pulsating torque is predicted and based on which the controller generates or changes the amplitude and the phase of the control signal to reduce the vibration.

#### **1.4 Scope of Proposed Investigation**

From the review of literature presented it is quite evident that significant studies have been conducted and are being carried out on advanced active and semi-active concepts for isolation of shock and vibration. As pointed out earlier, these concepts are complex, expensive, require high maintenance and are not yet viable for common applications. The present study, therefore, focuses on passive concepts utilizing hydraulic damping. A class of dampers, namely the dual-phase concept, and dampers with flexible chambers and wide ranges of orifice design are considered.

The concept of displacement sensitive dual-phase damper which can be realized via passive means has been investigated recently. Such dampers have

shown the potential for improvement in some applications. However, all investigation to date have utilized simplified approach to estimate the damping force. An accurate model must include an integral formulation to represent the damping force characteristics. This investigation, therefore, has scope to develop an accurate model for dual-phase damping, the performance of which can be compared with those of previous analytical and experimental results. The model can further be analyzed for evaluation of its performance potential for isolation of vibration and shock. Simulation of nonlinear dual-phase damper in frequency domain can be carried out utilizing a local equivalent linearization technique [45]. The technique has been successfully applied for nonlinear velocity dependent variable dampers by Rakheja [46-48] and Ahmed [49] both for symmetric and asymmetric cases. The technique, however, cannot be applied directly for the displacement sensitive dual-phase damper. In this case a velocity dependent equivalent damper characteristics has to be first established prior to application of the technique which is based on energy similarity. The study, therefore, further presents a scope for examining the effectiveness of the local equivalent linearization technique in application to displacement sensitive nonlinear damper.

For the case of hydraulic dampers with flexible chambers, several works evaluating their performance in application to engine mounts have been reported. Majority of the work considers long orifice for these dampers. Most studies, furthermore, consider simplistic approach along with the assumption of linearity which is far from the reality. Even the most comprehensive nonlinear model available [17] neglected the effect of fluid oscillation in the long orifice. In reality the fluid within the long orifice oscillates back and forth and the oscillation increases with the increase in frequency. The performance of the hydraulic dampers with flexible chambers are commonly evaluated for low amplitude sinusoidal excitations in the range of 0.1 mm to 1.0 mm. The behavior of such

dampers with long orifice are reported to be excellent for limited application. Their performance in a wide range of vibration environment and under shock are seldom reported.

The present investigation, therefore, presents a scope to carry out a detailed nonlinear modeling of hydraulic dampers with flexible chamber, which will consider all possible variables including fluid oscillation. Furthermore, models can be developed with short orifice, long orifice and their combination with and without spring loaded valve to explore their performance potentials and performance limits. In all cases, the performance can be evaluated for both isolation of vibration and shock to establish their application potentials.

## **1.5 Objectives of Dissertation Research**

Based on the scope of the study on a class of hydraulic dampers presented in the previous section, distinct objectives are outlined for each type of damper configuration considered.

### **1.5.1 Dual-phase Viscous Damper (DPVD)**

- Develop nonlinear analytical models for displacement sensitive dual-phase viscous dampers (DPVD) with low-high and high-low characteristics.
- Characterize damping force based on integral formulation as opposed to simplified approach adopted in other studies.
- Formulate local equivalent damping coefficients based on energy balance. Compare the results with direct integration to demonstrate their effectiveness.

- Establish damper properties and compare with those of other studies and available experimental results.
- Carry out simulations for isolation of simple system to establish damper performance. Examine the response to both vibration and shock of varying severity.
- Carry out a parametric study to explore their influence and performance potentials.

### **1.5.2 Hydraulic dampers with Flexible Chambers (DHF)**

- Develop nonlinear analytical models of hydraulic dampers with flexible chambers (DHF) utilizing experimental values for compliance of the chambers as well as stiffness and damping coefficients for the rubber elements.
- Formulate the models of DHF utilizing various orifice designs to explore their performance and limitations. Various configurations to be considered are:
  - Short Orifice Hydraulic Damper with Flexible Chambers (SDHF)
  - Long Orifice Hydraulic Damper with Flexible Chambers (LDHF)
  - Long and Short Orifice Hydraulic Damper with Flexible Chamber (LSDHF)
  - Long Orifice Hydraulic Damper with Spring Loaded Valve (LDHVF).
- Carry out both time and frequency domain analysis for each configuration for in-depth understanding of their performance characteristics.



- Establish performance of each configuration for isolation of both vibration and shock inputs.
- Carry out a parametric and comparative study to explore their influence, performance potentials, and limitations.

## **1.6 Thesis Organization**

Chapter 2 of the thesis presents the concept of displacement sensitive dual-phase dampers. It highlights the deficiencies of previous investigations on the concept. A detailed model is developed with low-high and high-low characteristics for the damper. For an "accurate" characterization of the damping force the displacement sensitivity is first transformed into velocity sensitivity and then the integral approach is applied for varying damping coefficient. Damping characteristics are obtained by numerical integration as well as utilizing local equivalent linearization technique. Results are compared with those of previous investigations.

The detailed model for the hydraulic damper with flexible chamber is developed in chapter 3. Nonlinear models are developed for variations in orifice configurations, namely: short orifice hydraulic damper with flexible chambers; long orifice hydraulic damper with flexible chambers; long and short orifice hydraulic dampers with flexible chambers; and long orifice hydraulic damper with spring loaded valve. Modeling considerations for each of the above cases are discussed in detail. The nonlinear equations of motion are solved to characterize the damping properties in each case.

Chapter 4 primarily deals with the performance of dual-phase dampers developed and presented in chapter 2. Here the damper characteristics are evaluated and presented along with a parametric study. The performance of the damper in isolation of vibration is presented in the form of transmissibility in

frequency domain. The system model with this damper is further exposed to shock inputs of various severity to determine their performance to shock response.

Similar to chapter 4, chapter 5 presents the performance of short orifice hydraulic damper with flexible chambers. It presents both time and frequency domain analysis along with a parametric study. The performance of the damper in isolation of vibration is presented for a range of parameters. The response to shock excitation is presented in time domain as well as in the domain of shock severity.

Chapter 6 presents the detailed performance analysis of long orifice hydraulic damper with flexible chamber, utilizing the models developed in chapter 3. The performance is evaluated following the same steps as that of short orifice system performance presented in chapter 5. Here results are presented for long orifice as well as a combination of long and short orifice.

The model developed for long orifice with spring loaded valve is analyzed in chapter 7 to evaluate its performance. A detailed time domain analysis is carried out for in-depth understanding of the damper behavior. The performance in this case is again evaluated for isolation of vibration and shock following the same steps as that of short orifice presented in chapter 5.

Chapter 8 of the thesis concludes the present investigation with highlights of the findings in each case of the damper considered. It further presents a list of recommendations for future work.

## CHAPTER 2

### DISPLACEMENT SENSITIVE DUAL-PHASE VISCOUS DAMPER

#### 2.1 INTRODUCTION

Non-linear dampers are used in isolators due to their potential in improving vibration isolation performance over a wide range of frequency. Among the different kinds of non-linear dampers, dual-phase dampers have received special attention because of simplicity in their design and good vibration isolation performance. A number of displacement, velocity and acceleration sensitive dual-phase dampers have been investigated in order to achieve better shock and vibration isolation performance [8,30,36-38,43]. In general, the dual-phase damper characteristics can be grouped under two categories, namely

- i) *low-high*, when damping coefficient increases with increase of displacement, velocity or acceleration and
- ii) *high-low*, when the damping characteristic is opposite of low-high.

Snowdon [43] studied shock isolation characteristics of a velocity dependent *low-high* dual-phase damper. The damping force  $F_d$  was defined by  $F_d = C(\dot{x}) \dot{x}$ , where  $\dot{x}$  is the relative velocity and  $C(\dot{x})$  is the velocity dependent damping coefficient. The non-linear damping coefficient was evaluated at the peak relative velocity ( i.e.  $C(\dot{x})$  at  $\dot{x} = \dot{x}_{\text{peak}}$  ) and hence the resulting damping force used in

[43] represented the peak damping force (i.e.  $F_d = C(\dot{x})|_{\dot{x} = \dot{x}_{peak}} \dot{x}$ ), for a given velocity. Venkatesan and Krisnan [8] also analyzed a velocity sensitive dual-phase damper in a landing gear of an aircraft. Like Snowdon, they also defined the damping force  $F_d = C(\dot{x}) \dot{x}$ . This approach of defining damping force, referred to here as "traditional" approach, is often used in literature. However, based on the fundamental definition, damping coefficient is given by  $C = dF_d / d\dot{x}$ . Therefore, the damping force at any given relative velocity ( $\dot{x}$ ) can only be estimated by the integral expression  $F_d = \int_0^{\dot{x}} C(\dot{x}) d\dot{x}$ . Both the integral and traditional approaches will lead to identical damping force when the damping coefficient is a constant. But when dealing with variable damping coefficient such as dual-phase damper, the "integral" approach is the "correct" approach. The "traditional approach" will either lead to under- or over-estimation of the damping force depending on the damping characteristics, i.e., high-low or low-high, respectively.

Beside velocity sensitive dampers, Venkatesan and Krishnan [36] also carried out harmonic analysis of a shock mount employing displacement dependent dual-phase damper using the damping force expression  $F_d = C(x) \dot{x}$ . The non-linear damping coefficient was evaluated at the peak relative displacement (i.e.,  $C(x)$  at  $x = x_{peak}$ ). Sankar, et. al [37] also investigated a detailed theoretical and experimental analysis on displacement sensitive dual-phase damper based on traditional approach of damping force characterization,  $F_d(x, \dot{x}, t) = C(x) \dot{x}$ . Again an integral form to represent the damping force, i.e.,  $F_d = \int C(x) dx$ , would be the correct approach to estimate the response more accurately. In addition to the two different types of dual-phase dampers described earlier, Guntur and Sankar [38] carried out investigation on the performance of an acceleration dependent dual-phase damper with rounded pulse and oscillatory step input excitations. The study concluded that *low-high* displacement sensitive damper has the best isolation

performance and its characteristics is as good as those of *high-low* velocity sensitive damper.

In fact a close examination as presented in section 2.2 will reveal that for each high-low velocity sensitive damper there is an equivalent low-high displacement sensitive damper where the performance for both should be the same. Therefore, it is quite adequate just to consider displacement sensitive dual-phase dampers to explore their performance potential. Such dampers are more attractive as they can be realized via passive means.

For the purpose of this study, both *low-high* and *high-low* displacement sensitive dampers are utilized as a vibration isolator for a single DOF system. The dynamic response of the system, for sinusoidal base excitation, is obtained using the integral formulation for the damping force. A local equivalent linearization technique based on energy similarity over a cycle is utilized for efficient simulation of the non-linear system in the convenient frequency domain. Simulation results are first validated against those obtained from direct numerical integration. Damping force-time history and frequency characteristics along with system transmissibility are compared with previous studies employing traditional non-integral approach for formulation of damping force. This simulation results are also compared with available experimental results [30,37] to demonstrate the effectiveness of the proposed simulation.

## **2.2 DAMPING FORCE CHARACTERIZATION OF DISPLACEMENT SENSITIVE DUAL-PHASE DAMPERS**

The damping characteristics of a low-high type displacement sensitive dual-phase damper are represented in Figure 2.1. The damper's characteristic is defined by four parameter  $A$ ,  $\alpha A$ ,  $C$  and  $\beta C$  where  $A$  and  $\alpha A$  are the transition points of relative displacements;  $\alpha$  and  $\beta$  ( $>1$ ) are the transition factors; and  $C$  is viscous

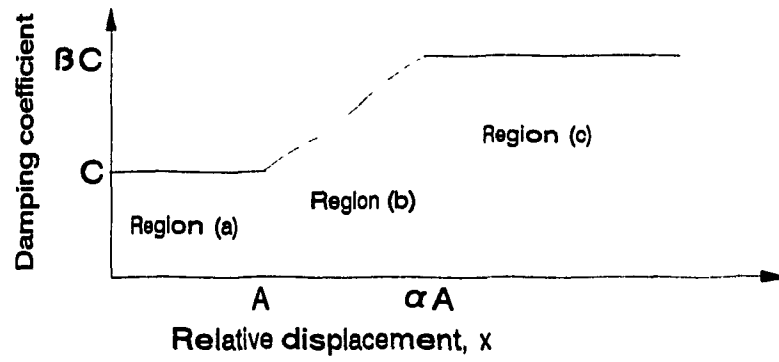


Figure 2.1 A typical low-high displacement sensitive dual-phase damper.

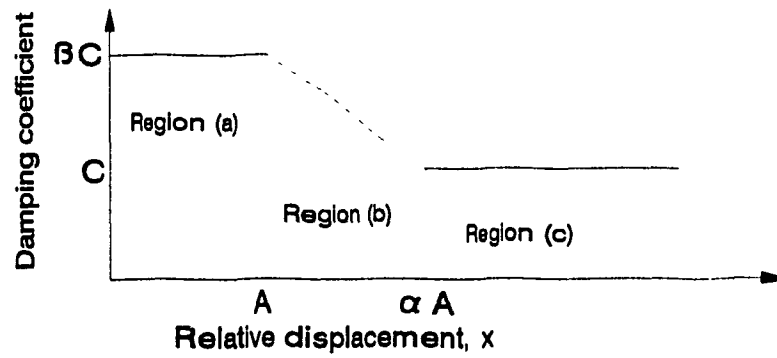


Figure 2.2 A typical high-low displacement sensitive dual-phase damper.

damping coefficient. The parameters  $\alpha$  and  $\beta$  determine the non-linearity index  $\sigma$  of the damper, where  $\sigma = \frac{\beta-1}{\alpha-1}$ . When  $\beta = 1.0$ , it implies that the non-linearity factor is zero and the resulting characteristics is that of a linear damper. When  $\alpha$  is very close to unity,  $\sigma$  tends to infinity, and will result in a sudden change in damping coefficient.

When  $\beta > 1.0$  and  $\alpha > 1.0$ , the damper is effectively either a low-high or a high-low displacement sensitive damper, where for low-high case, the damping coefficient increases with the increase of relative displacement. In this case, the dual-phase damper can be modeled as a piece-wise linear damper for the three distinct regions of relative displacement  $x$  and is given as follows:

$$\text{For } |x| > \alpha A, \text{ damping coefficient } C_d = \beta C \quad (2.1a)$$

$$\text{For } A \leq |x| \leq \alpha A \text{ damping coefficient } C_d = \beta C - \sigma C (\alpha A - x)/A \quad (2.1b)$$

$$\text{For } |x| < A, \text{ damping coefficient } C_d = C \quad (2.1c)$$

The typical characteristics of the high-low displacement sensitive damper is shown in Figure 2.2. Here the damping coefficient decreases with the increase in relative displacement. Like low-high damper, the high-low damper can be expressed as a piece-wise linear damper for the three regions of relative displacement as follows:

$$\text{For } |x| > \alpha A, \text{ damping coefficient } C_d = C \quad (2.2a)$$

$$\text{For } A \leq |x| \leq \alpha A \text{ damping coefficient } C_d = C + \sigma C (\alpha A - x)/A \quad (2.2b)$$

$$\text{For } |x| < A, \text{ damping coefficient } C_d = \beta C \quad (2.2c)$$

Based on the fundamental definition of damping coefficient, the damping force for the displacement sensitive damper is obtained from:

$$F_d = \int_0^{\dot{x}} C_d(x) d\dot{x} \quad (2.3)$$

In equation (2.3), it is necessary to transform  $C_d(x)$  into  $C_d(\dot{x})$  form in order to carry out the integration. For sinusoidal functions,  $x$  and  $\dot{x}$  can easily be interrelated by  $x = \frac{1}{\omega} \sqrt{\omega^2 X^2 - \dot{x}^2}$ , where  $\omega$  is the frequency and  $X$  is the peak relative displacement. From this expression it is evident that  $x$  is not only a function of  $\dot{x}$  and  $\omega$ , but also peak relative displacement  $X$ . Therefore, depending on the peak displacement  $X$ , and the three regions of the damper (Figure 2.1), there will be three distinctly different  $C_d(\dot{x})$  (i.e., velocity sensitive damper characteristics). For peak displacement  $X > \alpha A$ , this transformation would change, a *low-high* displacement sensitive damper into a *high-low* velocity sensitive damper and the *high-low* displacement sensitive damper, into a *low-high* velocity sensitive damper. Therefore, displacement sensitive dual-phase damper can also be viewed as an equivalent velocity sensitive dual-phase damper. That is why Guntur and Sankar [38] observed that the performance characteristics of a *low-high* displacement sensitive damper were similar to that of a *high-low* velocity sensitive damper.

### 2.3 TRANSFORMATION OF DISPLACEMENT SENSITIVITY TO VELOCITY SENSITIVITY (( $C_d(x) \rightarrow C_d(\dot{x})$ ))

With reference to Figure 2.3, the regions of the displacement sensitive dampers that will be active, depend on the peak relative displacement  $X$ . Therefore, it is necessary to find an equivalent  $C_d(\dot{x})$  for the three different cases depending on the regions that are active during a cycle. The equivalent velocity sensitive damper characteristic is established for the three cases depending on the value of peak relative displacement, illustrated for low-high (Fig. 2.3) and high-low (Fig 2.4) cases.



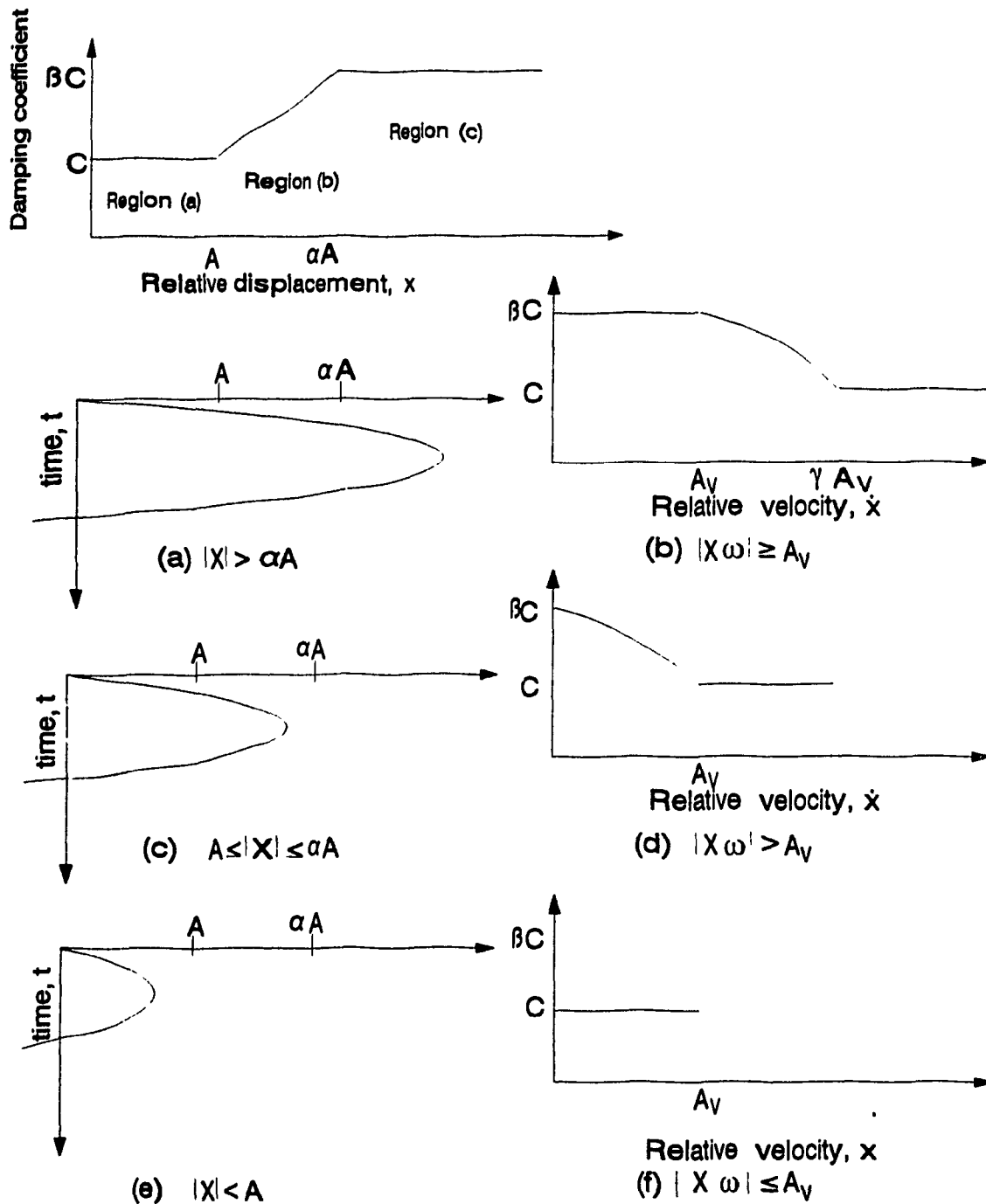


Figure 2.3 Damper relative displacement and corresponding relative velocity representation for low-high damper. (a)  $|X| > \alpha A$ , (b) corresponding damper characteristics; (c)  $A \leq |X| \leq \alpha A$ , (d) corresponding damper characteristics; (e)  $|X| < A$ , (f) corresponding damper characteristics.

### 2.3.1 Case I: Peak relative displacement $X$ greater than $\alpha A$ :

When the peak relative displacement  $X$  is greater than  $\alpha A$ , the damper passes through all the three regions (a, b and c) as shown in Figure 2.3a. The corresponding equivalent velocity sensitive damper characteristic is shown in Figure 2.3b. The transition points for the velocity are  $\gamma A_V$  and  $A_V$ .  $A_V$  is the velocity corresponding to relative displacement at  $x = A$ , i.e.,  $A_V = \omega \sqrt{X^2 - A^2}$  where  $X$  is the peak relative displacement. Similarly,  $\gamma A_V$  is the velocity corresponding to the relative displacement at  $x = \alpha A$  and can be expressed by  $\gamma A_V = \omega \sqrt{X^2 - \alpha^2 A^2}$ . A point by point transformation of the displacement sensitive damper characteristic leads to a high-low type velocity sensitive characteristics shown in Figure 2.3b. In this case, equivalent damping coefficients are as follows:

For region (a):  $|x| < A$ ,  $|\dot{x}| > A_V$ ,

$$C_d = C \quad (2.4a)$$

For region (b):  $A \leq |x| \leq \alpha A$ ,  $A_V \geq |\dot{x}| \geq \gamma A_V$ ,

$$C_d = \beta C - \frac{C}{A} \left( \frac{\beta - 1}{\alpha - 1} \right) \left( \alpha A - \frac{1}{\omega} \sqrt{\omega^2 X^2 - \dot{x}^2} \right) \quad (2.4b)$$

For region (c):  $|x| > \alpha A$ ,  $|\dot{x}| < \gamma A_V$

$$C_d = \beta C \quad (2.4c)$$

Similarly, a high-low displacement sensitive damper can be transformed into a low-high velocity sensitive damper, shown in Figure 2.4b. The equivalent damping coefficients for the low-high velocity sensitive damper is given by the following equations.

For region (a):  $|x| < A$ ,  $|\dot{x}| > A_V$ ,

$$C_d = \beta C \quad (2.5a)$$

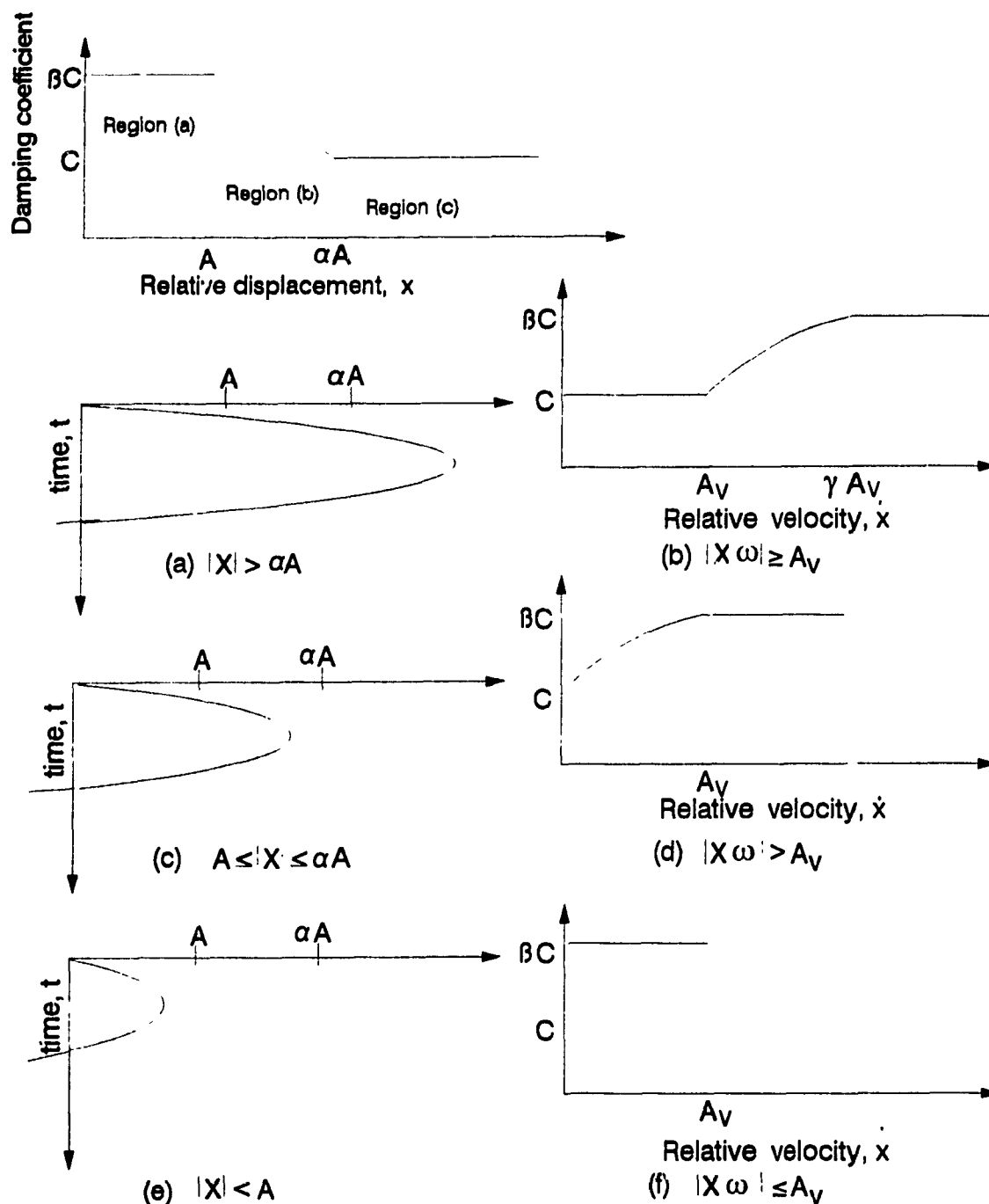


Figure 2.4 Damper relative displacement and corresponding relative velocity representation for high-low damper. (a)  $|X| > \alpha A$ , (b) corresponding damper characteristics; (c)  $A \leq |X| \leq \alpha A$ , (d) corresponding damper characteristics; (e)  $|X| < A$ , (f) corresponding damper characteristics.

For region (b):  $A \leq |x| \leq \alpha A$ ,  $A_v \geq |\dot{x}| \geq \gamma A_v$ ,

$$C_d = C + \frac{C}{A} \left( \frac{\beta-1}{\alpha-1} \right) \left( \alpha A - \frac{1}{\omega} \sqrt{\omega^2 X^2 - \dot{x}^2} \right) \quad (2.5b)$$

For region (c):  $|x| > \alpha A$ ,  $|\dot{x}| < \gamma A_v$

$$C_d = C \quad (2.5c)$$

### 2.3.2 Case II: Peak relative displacement $X$ in the range $A \leq |x| \leq \alpha A$ :

When the peak relative displacement is greater than  $A$  but less than  $\alpha A$ , the damper passes through regions (a) and (b) only as shown in Figure 2.3c. The transformation into velocity sensitivity characteristic in this case leads to a form as shown in Figure 2.3d. The equivalent velocity sensitive damping coefficient for the two regions of the damper are given by the following:

For region (a):  $|x| < A$ ,  $|\dot{x}| > A_v$ ,

$$C_d = C \quad (2.6a)$$

For region (b):  $|x| \geq \alpha A$ ,  $|\dot{x}| \leq \gamma A_v$ ,

$$C_d = \beta C - \frac{C}{A} \left( \frac{\beta-1}{\alpha-1} \right) \left( \alpha A - \frac{1}{\omega} \sqrt{\omega^2 X^2 - \dot{x}^2} \right) \quad (2.6b)$$

In the case of high-low damper (Figure 2.4c and 2.4d), the equivalent coefficients are:

For region (a):  $|x| < A$ ,  $|\dot{x}| > A_v$ ,

$$C_d = \beta C \quad (2.7a)$$

For region (b):  $|x| \geq \alpha A$ ,  $|\dot{x}| \leq \gamma A_v$ ,

$$C_d = C + \frac{C}{A} \left( \frac{\beta-1}{\alpha-1} \right) \left( \alpha A - \frac{1}{\omega} \sqrt{\omega^2 X^2 - \dot{x}^2} \right) \quad (2.7b)$$

### 2.3.3 Case III: Peak relative displacement $X$ less than $A$ :

When the peak relative displacement is less than the transition point  $A$ , the low-high damper operates only within the region (a) (Figure 2.3e,f). The corresponding equivalent damping coefficient for this is simply given by the following:

For region (a):  $|x| < A$ ,  $|\dot{x}| < A_v$ ,

$$C_d = C$$

(2.8)

In the case of the high-low damper, Figure 2.4e, 2.4f.

For region (a):  $|x| < A$ ,  $|\dot{x}| < A_v$ ,

$$C_d = \beta C$$

(2.9)

## 2.4 DERIVATION OF DAMPING FORCE EXPRESSION

For the displacement sensitive dual-phase damper with symmetric characteristics, the damping force for sinusoidal excitation can be obtained from the fundamental relationship:

$$F_d = \int_0^{\dot{x}} C_d(\dot{x}) d\dot{x} \quad (2.10)$$

where  $C_d(\dot{x})$  is the equivalent velocity sensitive damping coefficient corresponding to the given displacement sensitive damping characteristics. An expression for these damping coefficients were obtained as stated in Equations. 2.4, 2.6 or 2.8 depending on the peak relative displacement for the case of low-high damper. Performing the above integration (Equation 2.10) for each case of peak relative displacement leads to three equations for damping force

corresponding to the three regions in case I. Similarly, two equations for case II and only one equation for case III. The final expression for these damping forces for low-high damper are obtained as follows:

Case I:  $|X| > \alpha A$

when  $|x| < A$

$$F_d = \frac{\sigma C}{2A} \left\{ \omega \alpha A \sqrt{X^2 - \alpha^2 A^2} - \omega A \sqrt{X^2 - A^2} + \omega X^2 (\sin^{-1} \sqrt{X^2 - A^2} / X - \sin^{-1} \sqrt{X^2 - \alpha^2 A^2} / X) \right\} \text{sgn}(\dot{x}) + C\dot{x} \quad (2.11a)$$

when  $A \leq |x| \leq \alpha A$

$$F_d = \frac{\sigma C}{2A} \left\{ (\omega \alpha A \sqrt{X^2 - \alpha^2 A^2} - \omega X^2 \sin^{-1} \sqrt{X^2 - \alpha^2 A^2} / X) \text{sgn}(\dot{x}) + (2A \frac{\alpha - \beta}{\beta - 1} + |x|) \dot{x} + \omega X^2 \sin^{-1} \frac{\dot{x}}{\omega X} \right\} \quad (2.11b)$$

when  $|x| > \alpha A$

$$F_d = \beta C\dot{x} \quad (2.11c)$$

Case II:  $A \geq |X| \geq \alpha A$

when  $|x| \leq A$

$$F_d = \frac{\sigma C}{2A} \left\{ -\omega A \sqrt{X^2 - A^2} + \omega X^2 \sin^{-1} \sqrt{X^2 - A^2} / X \right\} \text{sgn}(\dot{x}) + C\dot{x} \quad (2.12a)$$

when  $|x| > A$

$$F_d = \frac{\sigma C}{2A} \left\{ (2A \frac{\alpha - \beta}{\beta - 1} + |x|) \dot{x} + \omega X^2 \sin^{-1} \frac{\dot{x}}{\omega X} \right\} \quad (2.12b)$$

Case III:  $|X| \leq A$

when  $|x| \leq A$

$$F_d = C\dot{x} \quad (2.13)$$

In the above expressions (Equations 2.11 to 2.13),  $\text{sgn}(\dot{x})$  has a value of either +1 or -1 for positive and negative value of velocity to ensure the phase relationship between the damping force and velocity.

Similar to above, the damping force expression for high-low displacement sensitive damper are as follows:

**Case I:**  $|X| > \alpha A$

when  $|x| < A$

$$F_d = \frac{\sigma C}{2A} \left\{ \omega A \sqrt{X^2 - A^2} - \omega \alpha A \sqrt{X^2 - \alpha^2 A^2} - \omega X^2 (\sin^{-1} \sqrt{X^2 - A^2} / X - \sin^{-1} \sqrt{X^2 - \alpha^2 A^2} / X) \right\} \text{sgn}(\dot{x}) + \beta C \dot{x} \quad (2.14a)$$

when  $A \leq |x| \leq \alpha A$

$$F_d = \frac{\sigma C}{2A} \left\{ (\omega X^2 \sin^{-1} \sqrt{X^2 - \alpha^2 A^2} / X - \omega \alpha A \sqrt{X^2 - \alpha^2 A^2}) \text{sgn}(\dot{x}) - (2A \frac{\alpha\beta - 1}{\beta - 1} + |x|) \dot{x} - \omega X^2 \sin^{-1} \frac{\dot{x}}{\omega X} \right\} \quad (2.14b)$$

when  $|x| > \alpha A$

$$F_d = C \dot{x} \quad (2.14c)$$

**Case II:**  $A \geq |X| \geq \alpha A$

when  $|x| \leq A$

$$F_d = \frac{\sigma C}{2A} \left\{ \omega A \sqrt{X^2 - A^2} - \omega X^2 \sin^{-1} \sqrt{X^2 - A^2} / X \right\} \text{sgn}(\dot{x}) + \beta C \dot{x} \quad (2.15a)$$

when  $|x| > A$

$$F_d = \frac{\sigma C}{2A} \left\{ -(2A \frac{\alpha\beta - 1}{\beta - 1} + |x|) \dot{x} - \omega X^2 \sin^{-1} \frac{\dot{x}}{\omega X} \right\} \quad (2.15b)$$

**Case III:**  $|X| \leq A$

when  $|x| \leq A$

$$F_d = \beta C \dot{x} \quad (2.16)$$

## 2.5 PERFORMANCE EVALUATION OF DISPLACEMENT SENSITIVE DUAL-PHASE DAMPERS

### 2.5.1 Model formulation

Vibration isolation performance of a low-high displacement dependent dual-phase damper in a single DOF system as shown in Figure 2.5 is carried out for base excitation of  $x_1 = X_1 \sin \omega t$ . The spring is a linear element with stiffness  $k_s$  and the damper is a displacement sensitive dual-phase damper. The equation of motion for the nonlinear system is:

$$m\ddot{x} + F_d(x, \dot{x}, t) + K_s x = -m\ddot{x}_1 \quad (2.17)$$

where  $x = x_1 - x_2$ ,  $\dot{x} = \dot{x}_1 - \dot{x}_2$ ,  $\ddot{x} = \ddot{x}_1 - \ddot{x}_2$  and  $F_d(x, \dot{x}, t)$  is the damping force given by Equations. (2.11), (2.12) and (2.13) for low-high damper or Equations (2.14), (2.15), (2.16) for high-low dampers, depending on the peak relative displacement.

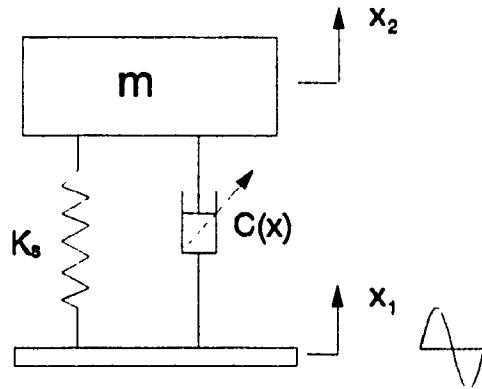


Figure 2.5 A one DOF mechanical model



### 2.5.2 Numerical Integration

The nonlinear system Equation (2.17) has been solved using the 4th order Runge-Kutta method. Initial conditions are taken as  $x(0) = \dot{x}(0) = 0$  and the time step  $\Delta t = 0.01/\omega$ . Since the instantaneous damping force depends on peak relative displacement which is yet to be determined, an iterative procedure is utilized. For a selected frequency, a peak relative displacement is assumed for each cycle, and the Equation (2.17) is solved for that cycle. The maximum value of relative displacement obtained is compared with the assumed value and if the percentage difference is less than some error tolerance (0.001% of previous value), integration is stopped for that cycle. Otherwise, the integration is carried out for that cycle again with the new value of the peak relative displacement and the integration procedure is continued until convergence is achieved. This process is continued for the next cycle with the new value of peak relative displacement. The numerical integration procedure outlined to obtain the frequency response is a highly tedious and time consuming task. Alternatively, the damping force characteristic can be obtained using a local equivalent linearization technique described in the following section.

### 2.5.3 Equivalent linearization of the dual-phase damper

The system Equation (2.17) is a non-linear differential equation due to the damping force  $F_d(x, \dot{x}, t)$ . For each excitation frequency, an equivalent damping coefficient of the non-linear damper is determined using Jacobson's equivalent damping concept [45]. The energy dissipated in one cycle by a non-linear dual-phase damper due to the harmonic excitation at a selected frequency  $\omega$ , and corresponding peak relative amplitude  $X$ , is equated to that of an equivalent linear damper at that particular frequency:

$$\int_0^{2\pi/\omega} F_d(x, \dot{x}, t) \dot{x} dt \equiv \int_0^{2\pi/\omega} \bar{C} \dot{x}^2 dt \quad (2.18)$$

where  $\bar{C}$  is the equivalent damping coefficient. The local equivalent damping coefficients are obtained by performing the above integration by parts for each of the three regions corresponding to the magnitude of the peak relative displacement. Therefore, three expressions are obtained for equivalent linear coefficient:

$$\bar{C} = C \quad \text{for } |X| < A \quad (2.19a)$$

$$\begin{aligned} \bar{C} = & \frac{2\sigma}{\pi X} (-A\sqrt{X^2 - A^2} + X^2 \sin^{-1} \sqrt{X^2 - A^2} / X) \sin \omega t_1 + \frac{C}{\pi} (2\omega t_1 + \sin 2\omega t_1) \\ & + \frac{C}{\pi} \frac{\alpha - \beta}{\alpha - 1} (\pi - 2\omega t_1 - \sin 2\omega t_1) + \frac{2\sigma X C}{3\pi A} \cos^3 \omega t_1 \\ & + \frac{2\sigma X C}{\pi A} \left\{ \cos \omega t_1 - \sin \omega t_1 \sin^{-1}(\cos \omega t_1) \right\} \\ & \text{for } A \geq |X| \geq \alpha A \end{aligned}$$

(2.19b)

$$\begin{aligned} \bar{C} = & \frac{2\sigma C}{\pi X A} \left\{ \alpha A \sqrt{X^2 - \alpha^2 A^2} + A \sqrt{X^2 - A^2} + X^2 (\sin^{-1} \sqrt{X^2 - A^2} / X - \sin^{-1} \sqrt{X^2 - \alpha^2 A^2} / X) \right\} \\ & \sin \omega t_1 + \frac{C}{\pi} (2\omega t_1 + \sin 2\omega t_1) + \frac{2\sigma C}{\pi X A} \left\{ \alpha A \sqrt{X^2 - \alpha^2 A^2} - \omega X^2 \sin^{-1} \sqrt{X^2 - \alpha^2 A^2} / X \right\} \\ & (\sin \omega t_2 - \sin \omega t_1) + \frac{C}{\pi} \frac{\alpha - \beta}{\alpha - 1} (2\omega t_2 - 2\omega t_1 + \sin 2\omega t_2 - \sin 2\omega t_1) + \\ & \frac{2\sigma X C}{3\pi A} (\cos^3 \omega t_1 - \cos^3 \omega t_2) + \frac{2\sigma X C}{\pi A} \left\{ \cos \omega t_1 - \sin \omega t_1 \sin^{-1}(\cos \omega t_1) \right. \\ & \left. - \cos \omega t_2 + \sin \omega t_2 \sin^{-1}(\cos \omega t_2) \right\} + \frac{\beta C}{\pi} (\pi - 2\omega t_2 - \sin 2\omega t_2) \\ & \text{for } |X| > \alpha A \end{aligned}$$

(2.19c)

$$\text{where } \omega t_1 = \sin^{-1} \left( \frac{A}{X} \right) \quad \omega t_2 = \sin^{-1} \left( \frac{\alpha A}{X} \right)$$

For the high-low damper, the equivalent damping coefficients are as follows:

$$\bar{C} = \beta C \quad \text{for } |X| < A \quad (2.20a)$$

$$\begin{aligned} \bar{C} = & \frac{2\sigma}{\pi X} (A\sqrt{X^2 - A^2} - X^2 \sin^{-1} \sqrt{X^2 - A^2} / X) \sin \omega t_1 + \frac{\beta C}{\pi} (2\omega t_1 + \sin 2\omega t_1) \\ & + \frac{C}{\pi} \frac{\alpha\beta - 1}{\alpha - 1} (\pi - 2\omega t_1 - \sin 2\omega t_1) - \frac{2\sigma XC}{3\pi A} \cos^3 \omega t_1 \\ & + \frac{2\sigma XC}{\pi A} \left\{ \sin \omega t_1 \sin^{-1}(\cos \omega t_1) - \cos \omega t_1 \right\} \\ & \text{for } A \geq |X| \geq \alpha A \end{aligned} \quad (2.20b)$$

$$\begin{aligned} \bar{C} = & \frac{2\sigma C}{\pi X A} \left\{ A\sqrt{X^2 - A^2} - \alpha A\sqrt{X^2 - \alpha^2 A^2} + X^2 (\sin^{-1} \sqrt{X^2 - \alpha^2 A^2} / X - \sin^{-1} \sqrt{X^2 - A^2} / X) \right\} \\ & \sin \omega t_1 + \frac{\beta C}{\pi} (2\omega t_1 + \sin 2\omega t_1) + \frac{2\sigma C}{\pi X A} \left\{ \omega X^2 \sin^{-1} \sqrt{X^2 - \alpha^2 A^2} / X - \alpha A\sqrt{X^2 - \alpha^2 A^2} \right\} \\ & (\sin \omega t_2 - \sin \omega t_1) + \frac{C}{\pi} \frac{\alpha\beta - 1}{\alpha - 1} (2\omega t_2 - 2\omega t_1 + \sin 2\omega t_2 - \sin 2\omega t_1) + \\ & \frac{2\sigma XC}{3\pi A} (\cos^3 \omega t_2 - \cos^3 \omega t_1) + \frac{2\sigma XC}{\pi A} \left\{ \cos \omega t_2 - \cos \omega t_1 + \sin \omega t_1 \sin^{-1}(\cos \omega t_1) \right. \\ & \left. - \sin \omega t_2 \sin^{-1}(\cos \omega t_2) \right\} + \frac{C}{\pi} (\pi - 2\omega t_2 - \sin 2\omega t_2) \\ & \text{for } |X| > \alpha A \end{aligned} \quad (2.20c)$$

where  $\omega t_1$  and  $\omega t_2$  are same as those defined earlier.

It should be noted that the equivalent damping coefficient corresponding to each frequency depends on the peak relative displacement  $X$  and hence are valid only for that frequency and amplitude of excitation. The damping constants, therefore, must be obtained as an array of such local constants. In view of lack of prior knowledge of the response amplitude, an iterative scheme is required. The equivalent damping coefficient  $\bar{C}_i$ , is initially selected in the range  $C \leq \bar{C}_i \leq \beta C$  and the corresponding peak relative displacement is found using the following equation:

$$|X| = |X_1| \frac{r^2}{\sqrt{(1-r^2)^2 + (2\bar{C}_i r^2)^2}} \quad (2.21)$$

where  $r$  is the frequency ratio,  $\omega / \omega_n$  and  $\bar{\xi}_t$  is the damping ratio corresponding to  $\bar{C}_t$ . Depending on the value of  $|X|$ , from Equation (2.21),  $\bar{C}_{t(new)}$  is calculated from an appropriate Equation (2.19) or (2.20). If the difference  $(\bar{C}_t - \bar{C}_{t(new)})$  is greater than a prespecified value (0.001%), Wegstein's [50] iterative method is carried out until convergence. The whole procedure is carried out for each frequency of interest to get an array of damping coefficients for all frequencies of interest.

## 2.6 RESULTS AND DISCUSSIONS

The results and discussions presented in this section pertain to the evaluation of the present formulation. Displacement dependent nonlinear dual-phase damper is linearized using a local equivalent linearization method based on energy dissipation balance. This method has been utilized to solve the nonlinear equation for constant amplitude harmonic excitations. The response characteristics of the equivalent linear system is compared with those obtained by direct numerical integration outlined in section 2.5.2. The formulation presented in this study for damping force based on integral approach is different from those of all previous investigations. Therefore, results are further obtained to compare damper characteristics and performance with those of previous investigations using traditional approach.

The 1 DOF system is selected with a sprung mass  $m=240$  kg and linear spring  $k=9475$  N/m so that the undamped natural frequency ( $f_o = \omega_o / 2\pi$ ) is 1 Hz. The dual-phase damper parameters are chosen as  $\zeta = 0.25$ ,  $\beta = 2.6$ ,  $A=10$  mm and  $\alpha = 3$  so that a moderately high nonlinearity results. Response curves in terms of absolute ( $X_2/X_1$ ) and relative  $[(X_2 / X_1) - 1]$  displacement transmissibilities using local equivalent linear model are presented in Figure 2.6 for different excitation amplitudes ( $X_1 = 20$  mm, 30 mm and 40 mm). The results obtained by direct

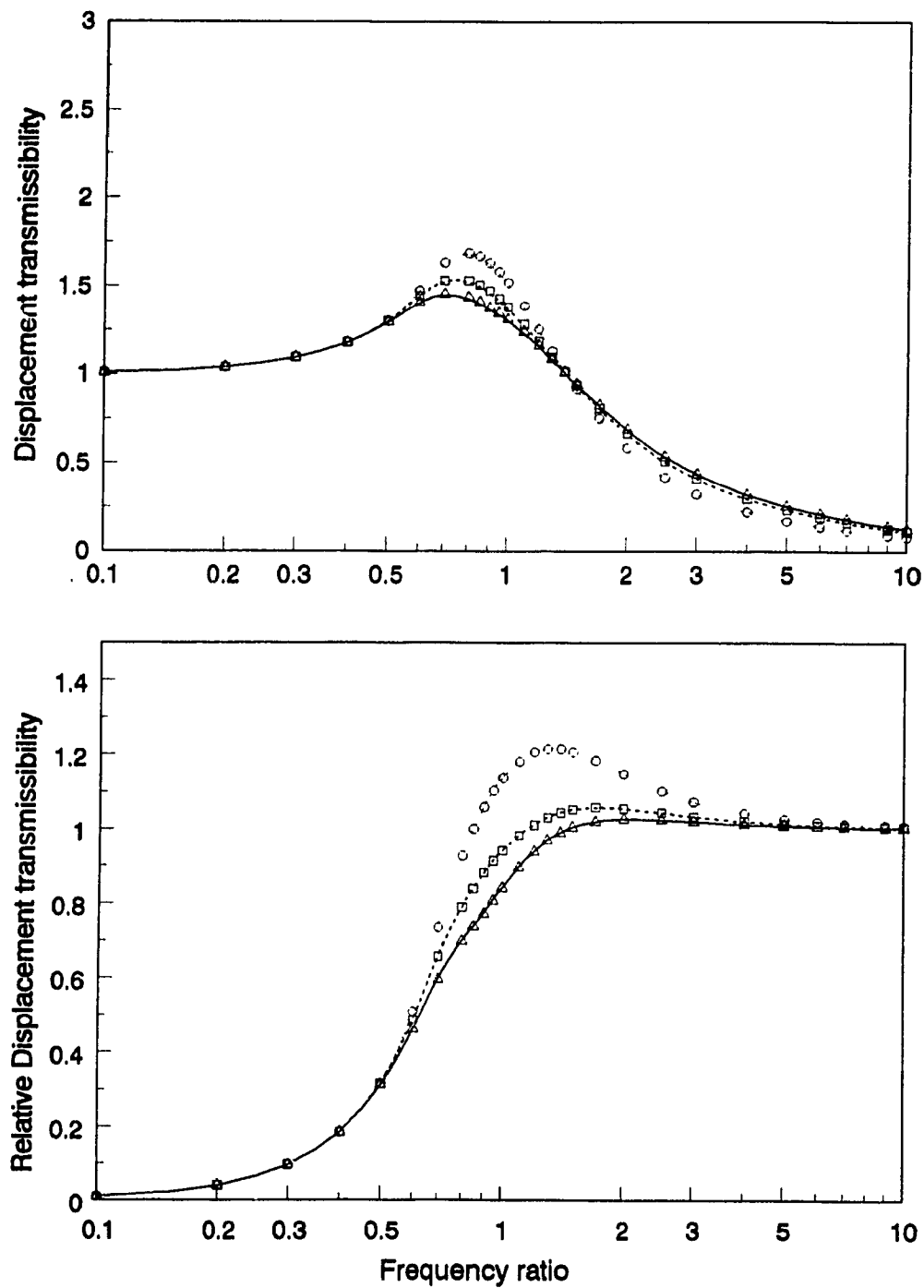


Figure 2.6. Comparison of energy balance method and numerical integration. For energy balance for a dual-phase damper. Energy balance:  $X_1$ , —, 40mm; ---, 30mm; ···, 20mm; integration:  $X_1$ ,  $\Delta\Delta$ , 40mm;  $\square\square$ , 30mm;  $\circ\circ$ , 20mm.

integration of nonlinear system are superimposed on Figure 2.6 for validation of the linearized system. It is found that maximum error occurs near resonance and is less than 0.35%, which is very negligible. These results demonstrate that the equivalent linearization method using energy dissipation balance can accurately determine the response behavior of the system for a wide variety of excitations and frequencies of interest. In order to compare the damping force characteristics obtained by the integral formulation to those of traditional, damping force time history was obtained. For this a harmonic excitation of  $X_1 = 0.04\text{m}$  at frequency ratio  $(\omega/\omega_n)$  of 0.80 is selected with three different gradually decreasing nonlinearity indices,  $\sigma$ . At the frequency ratio of 0.80, the relative displacement will be close to the maximum and thus will force the damper to operate in all three regions shown in Figure 2.1. The steady state damping forces for the low-high damper, calculated from both the integral and traditional (non-integral) formulations, are presented in Figure 2.7. The results clearly show that even for low non-linearity (small  $\beta$ ), the traditional approach produces unrealistic number of peaks. Furthermore, as the non-linearity is increased, the traditional approach grossly underestimates the peak damping force. The differences in the peak values were found to be 25%, 46% and 50% for increasing nonlinearity.

On the other hand, application of traditional approach to a high-low displacement sensitive damper may grossly overestimate the damping force, as shown in Figure 2.8. This fact is true even at very low nonlinearity. The damper considered here has the same parameter as the low-high one, except the damping ratio is interchanged to make it high-low type damper. A high-low displacement sensitive damper is basically a low-high velocity sensitive damper, therefore, for the given amplitude of excitation and given  $A$  and  $\alpha$ , the damper always remains within the lower damping coefficient region. The damping force, thus developed, is lower which is the correct estimation. With the increase in nonlinearity, the

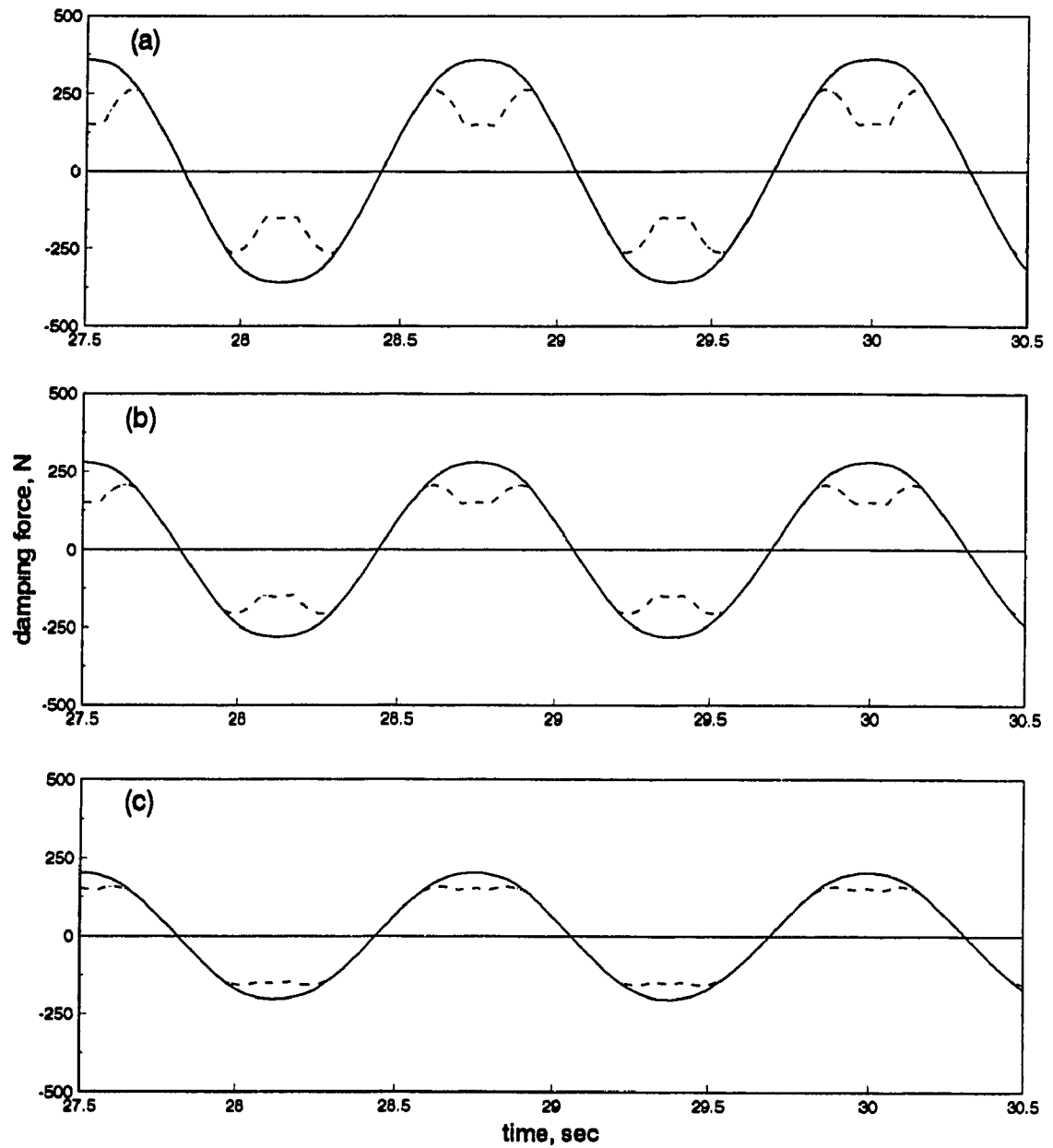


Figure 2.7 Force-time history of low-high dual-phase damper for different non-linearity. —, Integral method; ----, traditional method. (a)  $\beta = 2.6$  (b)  $\beta = 2.0$  (c)  $\beta = 1.4$ . ( $A=10\text{mm}$ ,  $\alpha=3$ ,  $\zeta=0.25$ ,  $X_1=40\text{mm}$ ).

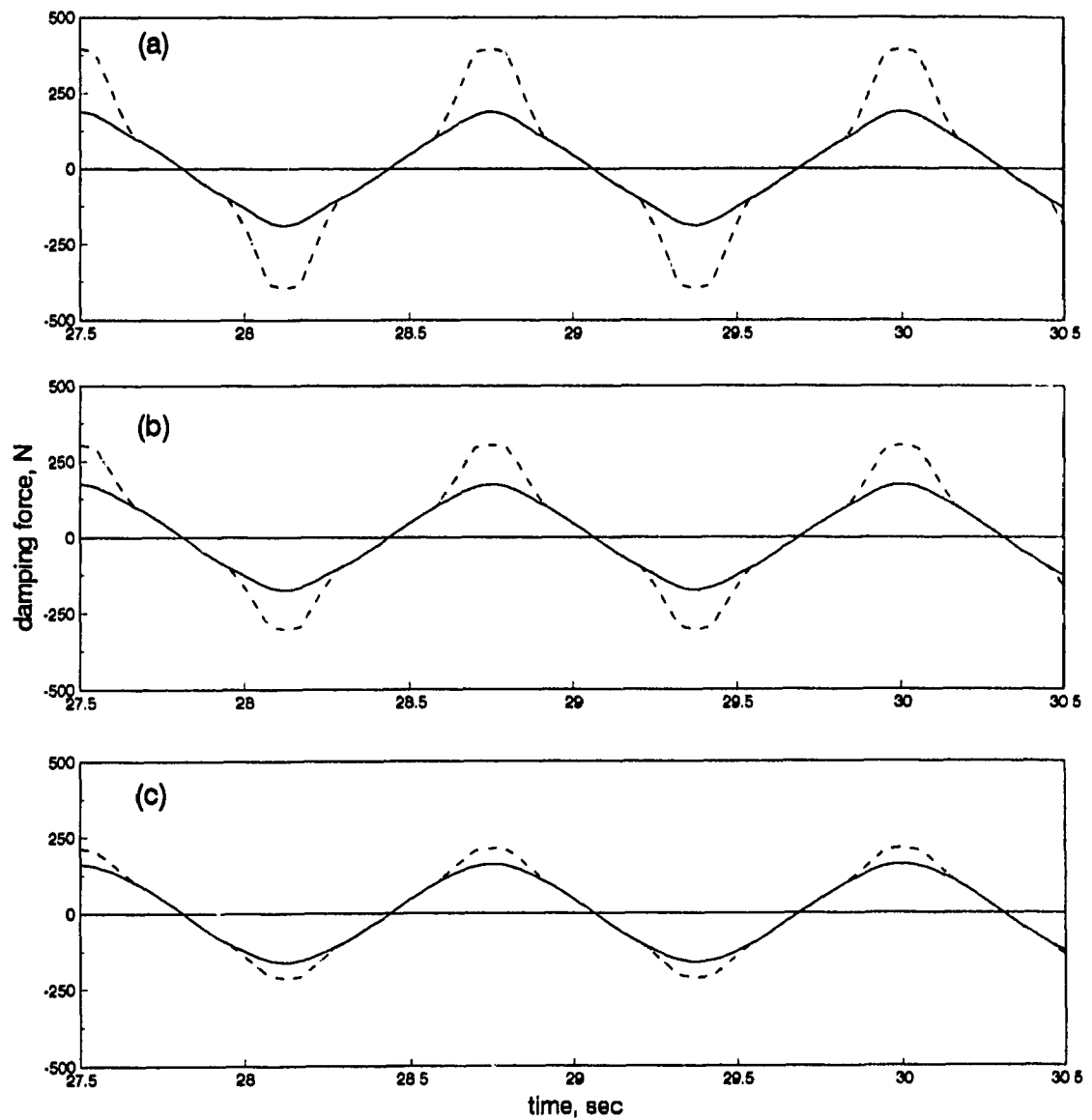


Figure 2.8 Force-time history of high-low dual-phase damper for different non-linearity. —, Integral method; ----, traditional method. (a)  $\beta = 2.6$  (b)  $\beta = 2.0$  (c)  $\beta = 1.4$ . ( $A=10\text{mm}$ ,  $\alpha=3$ ,  $\zeta=0.25$ ,  $X_1=40\text{mm}$ ).



overestimation increases, with the appearances of sudden peaks as shown in Figure 2.8.

To demonstrate that the damping force calculated using the integral method correlates well with experimental results [37], a dual-phase damper with parameters:  $A=12.5$  mm,  $\alpha=1.82$ ,  $\zeta=0.13$ , and  $\beta=1.77$  was selected to simulate an experimental set-up. The experimental set-up presented in [37] is a single DOF mass-spring-damper system with a mass of 74.9 kg and stiffness 13.66 N/mm. The damper was a displacement sensitive damper with parameter values as listed above. The experimental damping force was found to be 482.2 N with the peak relative displacement of 49.5 mm, when subjected to a 3 Hz harmonic excitation with amplitude of 25.4 mm. The simulation results based on the integral formulation of damping force gives a damping force of 476.25 N with the peak relative displacement of 44.6 mm, which are very close to the experimentally found values. Application of traditional formulation of damping force, on the other hand, results in a damping force of 322.25 N, a 33.2% lower than experimental value.

Figure 2.9 shows comparisons of transmitted force-displacement curves (Lissajous plots) under sinusoidal excitation for both integral and traditional methods for a low-high damper. The results again show underestimation of the transmitted force when traditional approach is used, and the difference in the estimated force increases with an increase in the nonlinearity. A comparison of these Lissajous plots with the experimentally obtained results in the reference [37], it reveals that the plots obtained by the integral formulation are smooth, similar to experimental results and, furthermore, that the maximum transmitted force occurs at zero displacement, as in the case of experimental results. However, the Lissajous plots for the traditional approach show kinks in the plots and also the transmitted force at zero displacement is not a maximum as it should be. Similar

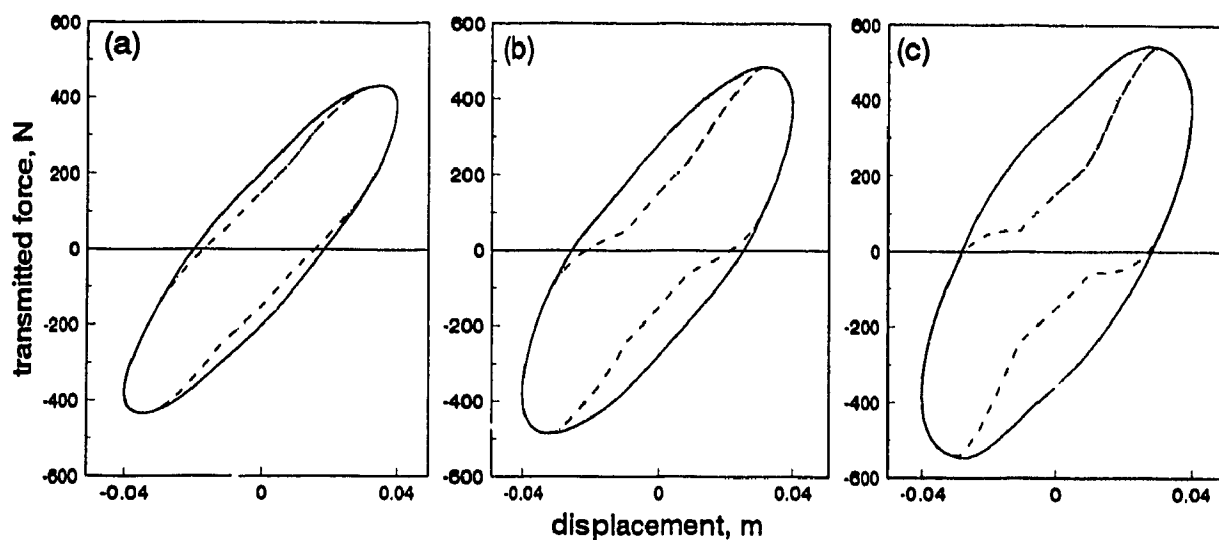


Figure 2.9 Force-displacement plots for low-high damper. —, Integral method; - - -, traditional method; (a)  $\beta = 1.4$  (b)  $\beta = 2.0$  (c)  $\beta = 2.6$ . ( $A=10\text{mm}$ ,  $\alpha=3$ ,  $\zeta=0.25$ ,  $X_1=40\text{mm}$ ).

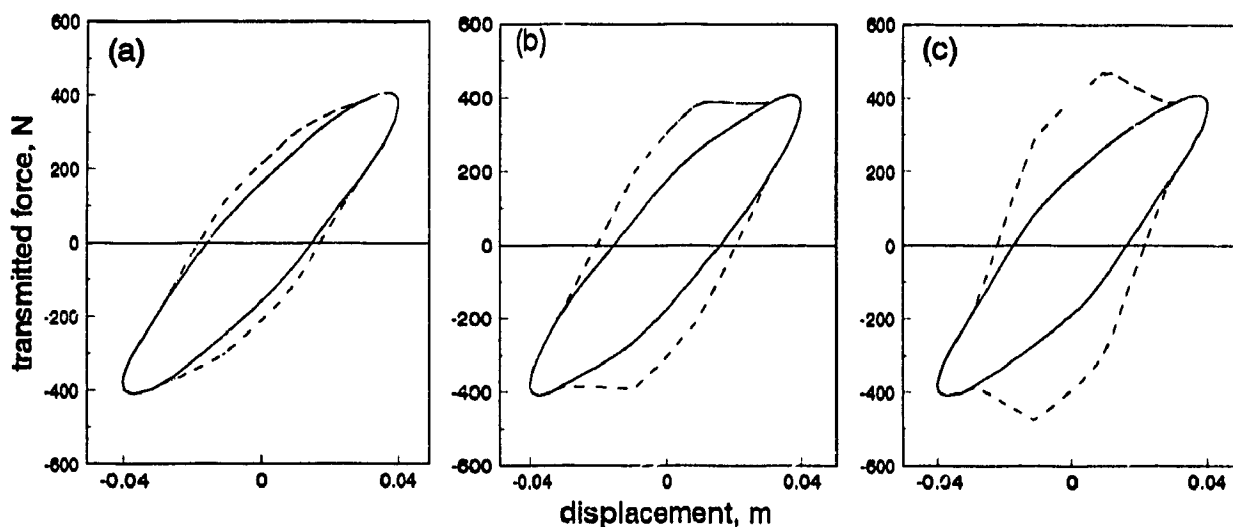


Figure 2.10 Force-displacement plots for high-low damper. —, Integral method; - - -, traditional method; (a)  $\beta = 1.4$  (b)  $\beta = 2.0$  (c)  $\beta = 2.6$ . ( $A=10\text{mm}$ ,  $\alpha=3$ ,  $\zeta=0.25$ ,  $X_1=40\text{mm}$ ).

results for a high-low type damper using integral and traditional formulation is presented in Figure 2.10. The results show that the amount of energy dissipation per cycle is grossly exaggerated for the same damper when traditional approach is utilized. This overestimation of damping increases with the increase in nonlinearity. These results clearly demonstrate that the traditional method is not accurate for characterizing a displacement sensitive dual-phase damper and the proposed integral method is the only correct method for analyzing the damper.

A further comparison of integral and traditional methods for different values of transition factor  $\beta$  are presented in Figure 2.11, in terms of equivalent damping ratio and absolute transmissibility for the whole range of frequencies of interest. It can be seen that the traditional method significantly underestimates the damping ratio of the dual-phase damper. The error in the estimation of equivalent damping ratio using the traditional method increases with increase in frequency as well as nonlinearity. At low frequencies, when relative velocity is small, the damper operates in the linear range and as a result there is no difference in the two methods. However, as the relative velocity increases with frequency, the damper operates more and more in the nonlinear regions, and hence the error increases and reaches a maximum value.

Since the traditional method underestimates the effective damping ratio, it significantly overestimates the transmissibility around the resonance zone and underestimates it around the high frequency zone as shown in the Figure 2.11. Similar trend was also found for variation of transition factor  $\alpha$ . The trend is reverse for the case of high-low damper. Figure 2.12 shows the equivalent damping ratio and corresponding transmissibility for high-low dampers with different nonlinearity parameter  $\beta$ . In all cases, traditional approach grossly overestimate the damping ratio for all range of frequency and the difference increases with the increase in nonlinearity. The effect is severe in transmissibility

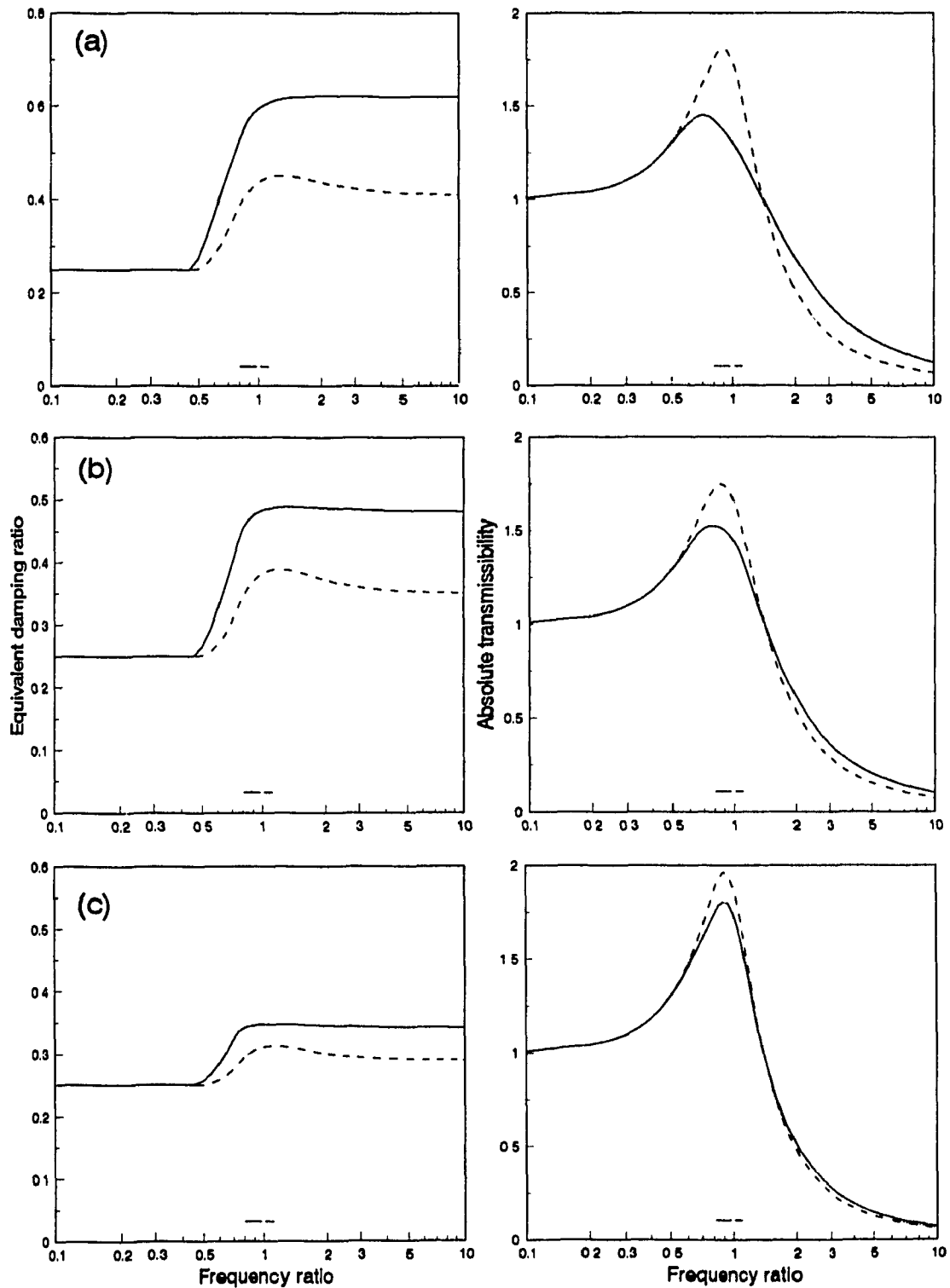


Figure 2.11 Comparison of integral and traditional method using energy dissipation balance for low-high damper. —, integral method; ---, traditional method (a)  $\beta = 2.6$  (b)  $\beta = 2.0$  (c)  $\beta = 1.4$ ; ( $A=10\text{mm}$ ,  $\zeta=0.25$ ,  $\alpha=3$ ,  $X_1=40\text{mm}$ ).

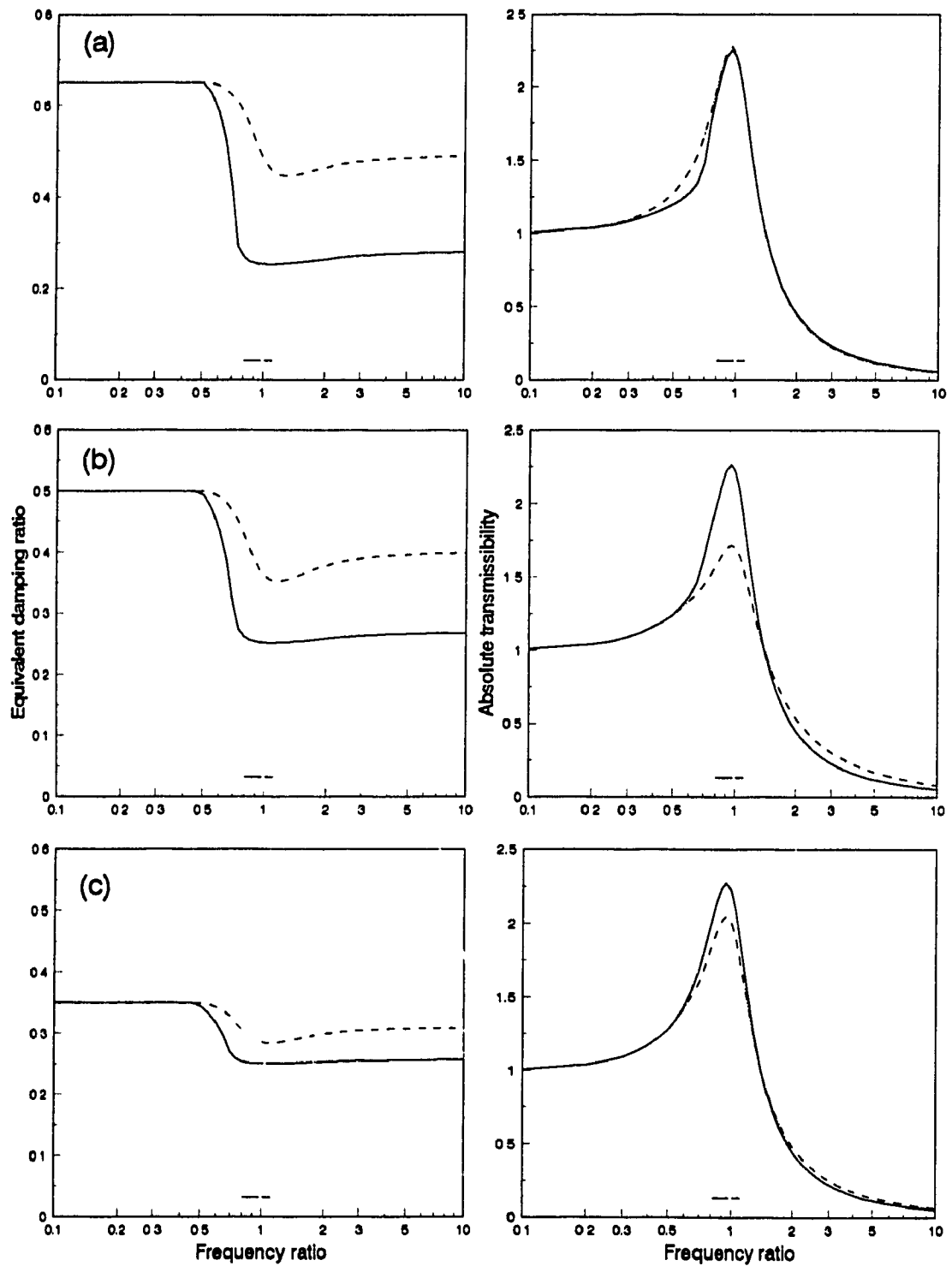


Figure 2.12 Comparison of integral and traditional method using energy dissipation balance for high-low damper. —, integral method; - - - , traditional method (a)  $\beta = 2.6$  (b)  $\beta = 2.0$  (c)  $\beta = 1.4$ ; ( $A=10\text{mm}$ ,  $\zeta=0.25$ ,  $\alpha=3$ ,  $X_1=40\text{mm}$ ).

performance of the damper. By comparing Figure 2.11 with 2.12, it is found that for the same parameters of the damper, the low-high damper produces much better transmissibility than the high-low damper.

## **2.7 SUMMARY**

An analysis of displacement sensitive dual-phase damper is carried out both in time and frequency domains using an integral formulation to characterize the damping force. A local equivalent linearization method based on energy similarity is shown to be an highly efficient tool for simulation of systems with such nonlinear elements, in frequency domain.

The results of this study are compared with those obtained from traditional formulation of damping force reported earlier in the literature and with some available experimental results. It is shown that the damping force via integral formulation correlates well with experimental values. It is further shown that for "low-high" type displacement sensitive damper, the traditional approach may lead to gross underestimation of peak damping force leading to significant overestimation of peak response and for "high-low" damper, the traditional approach may lead to gross overestimation of peak damping force. Based on the findings, it is concluded that the integral formulation of the damping force is the correct approach for simulation of displacement sensitive damper systems. The model developed here is used in chapter 4 for detailed performance evaluation under vibration and shock.

## **CHAPTER 3**

### **HYDRAULIC DAMPERS WITH FLEXIBLE CHAMBERS**

#### **3.1 Introduction**

Hydraulic dampers with flexible chambers have gained considerable popularity in recent years for their vibration isolation potential in mount application [1-6, 12-19]. These dampers are simple, reliable, compact and have no moving parts like dampers with rigid chamber. The simplest type of hydraulic damper with flexible chambers consists of two chambers filled with hydraulic fluid, connected to each other by a sharp short orifice. One of the chambers is much more flexible i.e., compliance of one chamber is very high compared to that of the other. First one acts only as a reservoir to receive fluid coming from second one during forward stroke.

Although a damper with flexible chambers has a very good potential for shock and vibration isolation, a very little attention is being directed towards the diversity of properties of the damper. A widely popular hydraulic damper utilizing long orifice has been studied and developed by a number of investigators [12-18]. The long orifice damper develops high damping to isolate idle engine vibration. Although long orifice hydraulic dampers has been investigated extensively, none of the study considered the realistic effect of fluid oscillation. Furthermore, extensive parametric study of such damper with combination of orifices have not been reported. For example, by changing the long orifice with simple short orifice

or a combination of long and short orifice or a series of orifices with spring loaded valves can make the damper useful for diversified application.

This chapter deals with the complete mathematical formulation of short orifice hydraulic damper (SDHF), long orifice hydraulic damper (LDHF), long and short orifice hydraulic damper (LSDHF) and hydraulic damper with spring loaded valve (LDHVF). Fundamental equations of continuity and momentum derived from Fluid Mechanics are used to determine fluid flow characteristics. Fluid flow through orifice  $Q_o$ , top chamber pressure  $P_T$ , bottom chamber pressure  $P_B$ , piston area  $A_{TP}$ , orifice diameter  $D_o$ , and orifice length  $L_o$  are considered as the principal variables for mathematical formulation. Experimentally obtained nonlinear compliances of the chambers in terms of pressure rise as a function of volume increments are taken from the available literature [17]. Variation of spring stiffness as well as damping coefficient as a function of exciting frequency is also considered in the model. For the long orifice model, the fluid oscillation effect is included in this study. The models developed in this section will be used for detailed analysis and parametric study both in time and frequency domain.

### **3.2 Short Orifice Hydraulic Damper with Flexible Chambers (SDHF)**

Although different types of orifices (long orifice, decoupler, inner orifice, etc. ) have been developed [1-40], the advantages of a simple orifice type hydraulic damper can not be ignored. It is very simple in construction and produces very satisfactory performances beyond resonant frequencies compared to other type of dampers. A comprehensive analytical model and analysis of such damper with flexible chambers has not been reported yet.



### **3.2.1 Model Description**

Figure 3.1 represents an orifice type hydraulic damper. In its simplest form, it has two chambers, connected to each other by a short cylindrical orifice. The opening of the orifice is a key factor in determining the discharge coefficient of the orifice. Most part of the top chamber consists of elastic material such as rubber, shaped like conical frustum. The reasons for choosing compliant rubber material and conical shape are

- i) top chamber acts as a spring, hence, additional spring is not required.
- ii) compliance of the chamber may develop stiffness in addition to its static stiffness
- iii) it also acts as a piston, so necessity of moving parts required for rigid wall orifice damper is eliminated.
- iv) it is very compact in design.

Due to the piston action of the top chamber, the bottom chamber has to be a chamber of very high compliance. This will act as a reservoir, thus eliminates the requirement of an extra reservoir. External excitation makes the top chamber oscillate back and forth, causing the fluid flow through the orifice which produces damping effect. Although compliance of the bottom chamber behaves nonlinearly for a wide range of pressure distribution [17], it is assumed linear because chamber pressure variation is very low.

### **3.2.2 Development of Nonlinear Mathematical Model**

The damping action in a hydraulic damper is purely due to the fluid flowing through the short cylindrical orifice, which is nothing but a sudden restriction of very short length. Flow through short orifice is "turbulent flow" phenomenon, not solvable from Navier-Stokes equation. However, partly theoretical and partly empirical pressure-flow relationship is available using Bernoulli's equation [51].

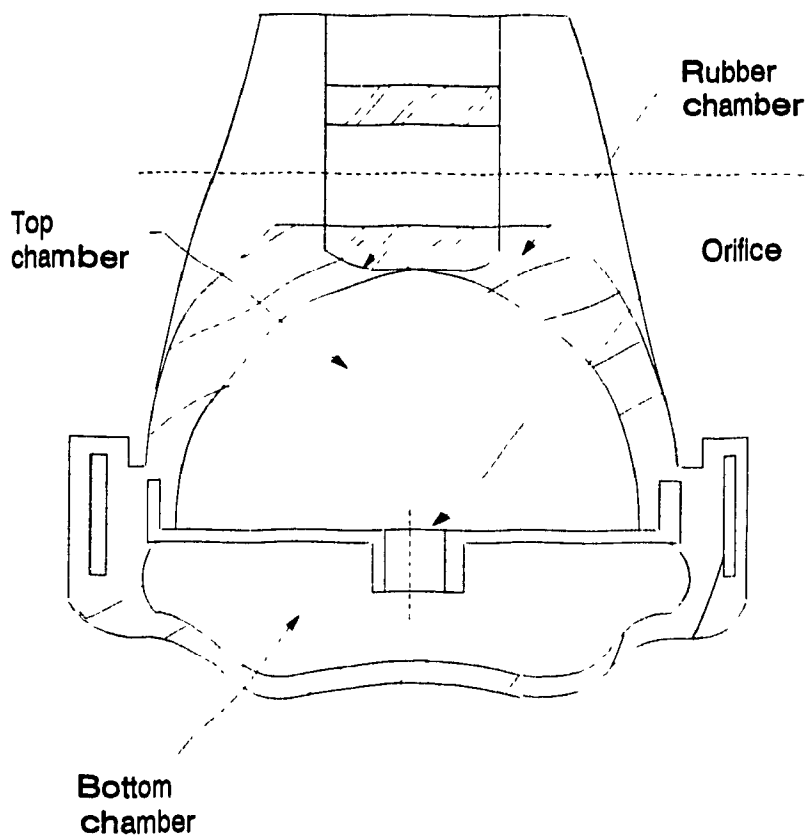


**Figure 3.1** Schematic diagram of a orifice type hydraulic damper (SDHF) with flexible chamber.

The flow  $Q_0(t)$  through orifice is given by:

$$Q_0 = A_o C_D (D_o, R_e, L_o) \sqrt{\frac{2[P_T(t) - P_B(t)]}{\rho}} \quad (3.1)$$

Where  $A_o$  is the short orifice area,  $P_T(t)$  and  $P_B(t)$  are the pressure state in the top and bottom chambers, respectively. Discharge coefficient  $C_D$ , for the short orifice is a function of diameter of the orifice  $D_o$ , Reynolds number  $R_e$ , and length of the orifice  $L_o$ . It can have value ranging from 0.13 up to 0.816 depending primarily on Reynolds number which is given by [52]:

$$R_e = \frac{\rho V D_h}{\mu} = \frac{\rho Q_o D_o}{\mu A_o} \quad (3.2)$$

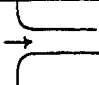
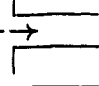
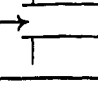
Where  $D_h$  is the hydraulic diameter of the orifice and is equal to  $D_o$  for rounded orifice.  $A_o$  is its cross-sectional area and  $\mu$  is the absolute viscosity of the fluid.

Fluid flowing from top chamber to the orifice suffers a sudden contraction leading to a loss of energy. The corresponding pressure difference is given by [52]:

$$P_T(t) - P_C(t) = K_C \frac{\rho}{2} \left( \frac{Q_o(t)}{A_o} \right)^2 \quad (3.3)$$

where  $K_C$  is the contraction loss which depends on inlet geometry of the orifice and weakly depends on Reynolds number. The following table shows the contraction factor for different geometry of the orifice [52].

Table 3.1 Contraction factor for different geometry of orifice [52]

Type	Geometry	Description	Contraction factor, $K_C$
1		well rounded entrance	$K_C = 0.05$
2		sharp-edged entrance	$K_C = 0.50$
3		inward projecting entrance	$K_C = 0.80$

When the pipe has a sudden contraction from a finite diameter  $D_1$  to a finite diameter  $D_2$ ,  $K_C$  is given by the following equation [52] :

$$K_C = \frac{1}{2} \left( 1 - \frac{D_2^2}{D_1^2} \right) \quad (3.4)$$

Similarly, when fluid is entering out of the orifice to the bottom chamber, sudden enlargement situation occurs. In this case the pressure difference is given by:

$$P_C(t) - P_B(t) = K_{ex} \frac{\rho}{2} \left( \frac{Q_0(t)}{A_0} \right)^2 \quad (3.5)$$

where  $K_{ex}$  is the exit loss coefficient, independent of Reynolds number. An abrupt exit into a large reservoir has a loss coefficient of 1, which means all the kinetic energy of the issuing fluid is lost into the turbulent mixing with the fluid in the reservoir. If the reservoir has a finite diameter  $D_2$ , the exit coefficient is given by:

$$K_{ex} = \left( 1 - \frac{D_1^2}{D_2^2} \right)^2 \quad (3.6)$$

The total energy losses associated with equation (3.1) are due to the obstruction caused by the orifice and can be expressed as a sum of losses due to flow contraction at the entrance, to flow enlargement in the orifice and to exit from orifice where the dynamic pressure is totally lost. Therefore, the pressure difference can be expressed as:

$$P_T(t) - P_B(t) = (K_C + K_{en} + K_{ex}) \frac{\rho V_o^2}{2} \quad (3.7)$$

where  $V_o$  is the average velocity in the orifice, equal to  $Q_c/A_c$ .  $K_C$  is the contraction factor,  $K_{en}$  is the enlargement loss coefficient which strongly depends on Reynolds number and  $K_{ex}$  is the exit loss coefficient which is a function of diameter ratio. The discharge coefficient  $C_D$  for a sharp edged cylindrical orifice is a function of

Reynolds number, orifice diameter and orifice length obtained by Shapiro, *et al* is available in the literature [53].

$$C_D = \frac{1}{\sqrt{(1.0 + K_C) + 13.74\sqrt{L_o / D_o R_e}}} \quad \text{for } \frac{D_o R_e}{L_o} > 50 \quad (3.8)$$

$$C_D = \frac{1}{\sqrt{(2.28 + K_C) + 64.0 L_o / D_o R_e}} \quad \text{for } \frac{D_o R_e}{L_o} < 50 \quad (3.9)$$

The changes in top chamber as well as bottom chamber pressure build up depend not only on the externally applied force or excitation but also on the compliances of the material of the chambers.

Chamber compliance may be defined as the increase in volume of the chamber per unit rise in pressure [54-55], i.e.,

$$C_v = \frac{dV}{dP} \quad (3.10)$$

Since the chamber is highly compliant compared to that of fluid, fluid is assumed incompressible and it's compliance will not be taken into consideration for derivation of damping characteristics for flexible dampers. Two cases of chamber compliance may be considered:

### 3.2.2.1 Case I: Linear Chamber Compliance

In this case continuity equation of flow from top chamber can be written as:

$$A_{TP} \dot{x}(t) - Q_o(t) = C_{VT} \dot{P}_T(t) \quad (3.11)$$

where  $A_{TP}$  is projected area of the top chamber acting as a piston,  $\dot{x}(t)$  is the relative velocity across the damper,  $C_{VT}$  is a constant for top chamber compliance, and  $\dot{P}_T(t)$  is the rate of change of top chamber pressure.

Similarly, continuity equation for bottom chamber yields:

$$Q_O(t) = C_{VB} \dot{P}_B(t) \quad (3.12)$$

where  $C_{VB}$  is the compliance of the bottom chamber,  $\dot{P}_B(t)$  is the rate of change of pressure in the bottom chamber.

Solution of Equation (3.1), (3.11) and (3.12) gives the orifice flow, top chamber pressure and bottom chamber pressure. Instantaneous damping force thus obtained is given by:

$$F_D(t) = A_{TP} [P_T(t) - P_B(t)] \quad (3.13)$$

where  $P_{AT}$  is the atmospheric pressure.

### 3.2.2.2 Case II: Chamber Compliance Nonlinear

In this case compliances are assumed to be a function of chamber pressure and chamber volume increment.

At a particular instant 't', total volume of fluid transferred from one chamber to other chamber is given by:

$$V_{TO}(t) = \int_0^t Q_O(t) dt \quad (3.14)$$

Therefore, volume increment of the top chamber is given by

$$\Delta V_T(t) = V_{TO}(t) + V_{TST} - A_{TP} x(t) \quad (3.15)$$

where  $V_{TST}$  is the volume increment from atmospheric pressure to static pressure change.  $A_{TP}$  and  $x(t)$  are projected piston area and displacement, respectively.

The top chamber pressure as a function of volume increment obtained experimentally [17], is given by:

$$P_T(t) = -32.339 \Delta V_T(t) + 15.095 \Delta V_T^{7/6}(t) + 3.904 \times 10^{-6} \Delta V_T^{2.5}(t) + P_{AT}, \quad (3.16)$$

for  $\Delta V_T(t) > 0$

Here  $P_T(t)$  is measured in Pascal and  $\Delta V_T(t)$  is measured in cubic millimeter.

For  $\Delta V_T(t) < 0$ , the chamber is in a state of vacuum and it is assumed that an amount of entrapped air  $V_A$  takes that volume increment obeying Boyle's Law [51]. Expressing total volume of entrapped air by:

$$V_{TA}(t) = V_A + |\Delta V_T(t)| \quad (3.17)$$

The pressure at the top chamber may be written as:

$$P_T(t) = P_{AT} V_A / V_{TA}(t) \quad \text{for } \Delta V_T(t) < 0 \quad (3.18)$$

The above pressure-volume relationship (Equation 3.16) for top chamber compliance is named as property for Comp\_A. Since the top chamber compliance has the significant effect on the damping property of the damper, other two types of chamber compliance are also considered, named as Comp\_B and Comp\_C. Variation in chamber compliance can easily be made by increasing or decreasing the thickness of the chamber. These are obtained by simulating the experimentally found data [17]. Comp\_B has the following pressure-volume increment relationship.

$$P_T(t) = -38.339\Delta V_T(t) + 15.095\Delta V_T^{7/6}(t) + 1.904 \times 10^{-6} \Delta V_T^{2.5}(t) + P_{AT}, \quad (3.19)$$

for  $\Delta V_T(t) > 0$

Similarly, Comp\_C may be defined as follows:

$$P_T(t) = -12.339\Delta V_T(t) + 12.095\Delta V_T^{7/6}(t) + 14.904 \times 10^{-6} \Delta V_T^{2.5}(t) + P_{AT}, \quad (3.20)$$

for  $\Delta V_T(t) > 0$

Figure 3.2 shows the pressure volume increment relationship in graphical form. Comp\_B has the higher compliance than Comp\_A and Comp\_C has the lower compliance compared to Comp\_A.

Similar to Equation 3.15, the volume increment of the bottom chamber is given by

$$\Delta V_B(t) = -V_{TO}(t) + V_{BST} \quad (3.21)$$

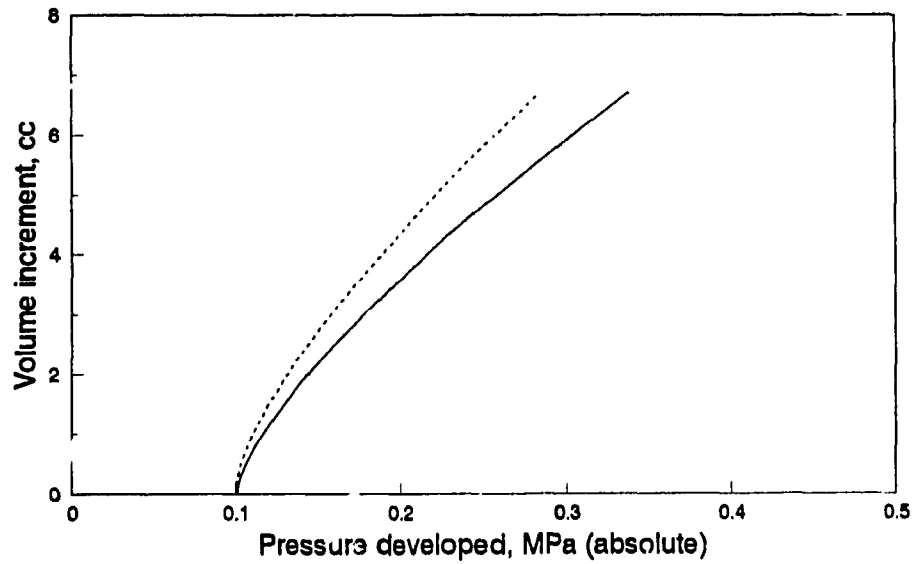


Figure 3.2 Top chamber compliance in pressure-volume increment relationship.  
 —, Comp\_A; ----, Comp\_B; ·····, Comp\_C.

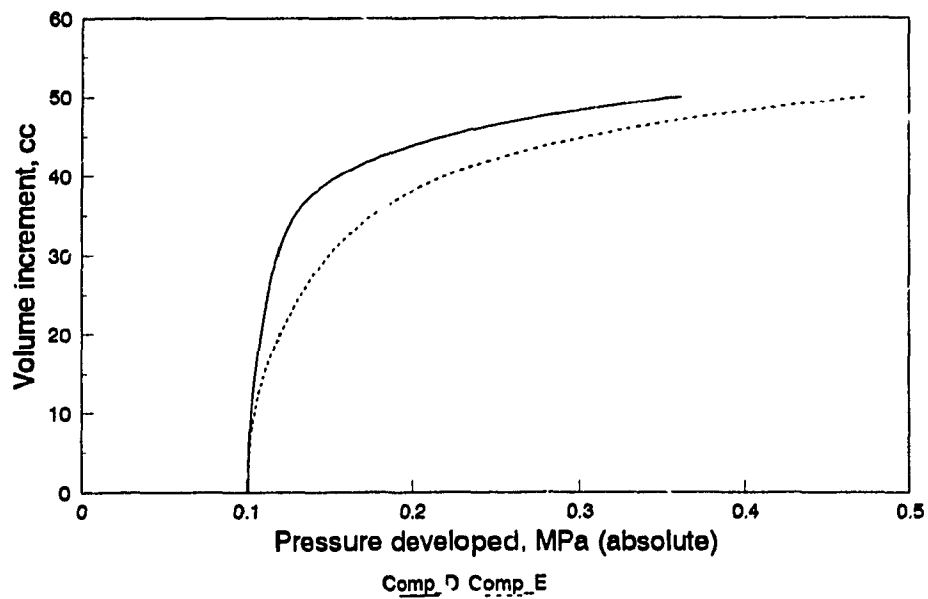


Figure 3.3 Bottom chamber compliance in pressure-volume increment relationship.  
 —, Comp\_D; ----, Comp\_E.



The measured bottom chamber pressure as a function of volume increment is [17]:

$$P_B(t) = 1.663 \times 10^8 \Delta V_B^{2.5}(t) - 8.9 \times 10^{13} \Delta V_B^6(t) + 4.459 \times 10^{14} \Delta V_T^{6.5}(t) + P_{AT} \quad (3.22)$$

where the pressure is in Pascal and volume increment is in cubic millimeter.

The type of compliance will be known as Comp\_D. To see the effect of bottom chamber compliance on the system's performance, another type of compliance, similar to the experimentally found one, Comp\_E, is introduced. Pressure -volume increment relationship is given by the following equation.

$$P_B(t) = 3.663 \times 10^8 \Delta V_B^{2.5}(t) - 8.9 \times 10^{13} \Delta V_B^6(t) + 4.459 \times 10^{14} \Delta V_T^{6.5}(t) + P_{AT} \quad (3.23)$$

Characteristics of Comp\_D and Comp\_E are shown in Figure 3.3 where Comp\_D is more compliant than Comp\_E. As the wall of the bottom chamber is highly compliant, bottom chamber pressure will never be below atmospheric. Equation (3.1), (3.16), (3.18) and (3.22) will give orifice flow, top chamber pressure and bottom chamber pressure.

The instantaneous damping force developed by the damper is again given by:

$$F_D(t) = A_{TP} [P_T(t) - P_B(t)] \quad (3.24)$$

The damper dynamic stiffness  $K_D$  for a particular frequency  $\omega$ , is defined as the ratio of rms (root mean square) dynamic force to the rms dynamic displacement at a steady state condition, which can be expressed as:

$$K_D(\omega, Y) = \frac{\text{rms}(|k(\omega)y(t) + c(\omega)\dot{y}(t) - A_{TP}[P_T(t) - P_{ST}]|)}{\text{rms}(|y(t)|)} \quad (3.25)$$

Here the force transmitted by the damper is given by the following equation:

$$F_T(t, \omega) = K(\omega)x(t) + C(\omega)\dot{x}(t) + A_{TP}[P_{ST} - P_T(t)] \quad (3.26)$$

### 3.2.3 Characteristics of the Chamber Material

Figure 3.4 shows the dynamic stiffness and damping coefficient of the rubber material used for making the chambers of the damper. The rubber has the property of gradually increasing dynamic stiffness with frequency. The damping coefficient of the damper falls sharply as the frequency is increased [22, 56].

### 3.2.4 Static Equilibrium Equations

The hydraulic pressure developed within the damper under the application of static equilibrium load depends on static mass, spring stiffness of rubber, chamber compliance and equivalent piston area of the damper. Since linear and nonlinear compliances are considered for investigation, two sets of equations will govern the static equilibrium conditions of the damper.

#### 3.2.4.1 Linear Compliance

If the chamber is considered linear, it means that pressure builds up is proportional to the increment in volume of the top or bottom chamber. Thus the top and bottom chamber pressures can be written as

$$P_T(t) = \Delta V_T(t) / C_{VT} + P_{AT} \quad (3.27)$$

$$P_B(t) = \Delta V_B(t) / C_{VB} + P_{AT} \quad (3.28)$$

Where  $\Delta V_T$  and  $\Delta V_B$  are the volume increments of the top chamber and the bottom chamber due to increase in pressure, from the conditions that  $P_T = P_B = P_{ST}$ .  $C_{VT}$  and  $C_{VB}$  are the compliances of top and bottom chambers, respectively. Bottom chamber is made much more compliant than the top chamber, therefore, the total volume increment can be assumed to be equal to the volume increment of the bottom chamber, i.e.,

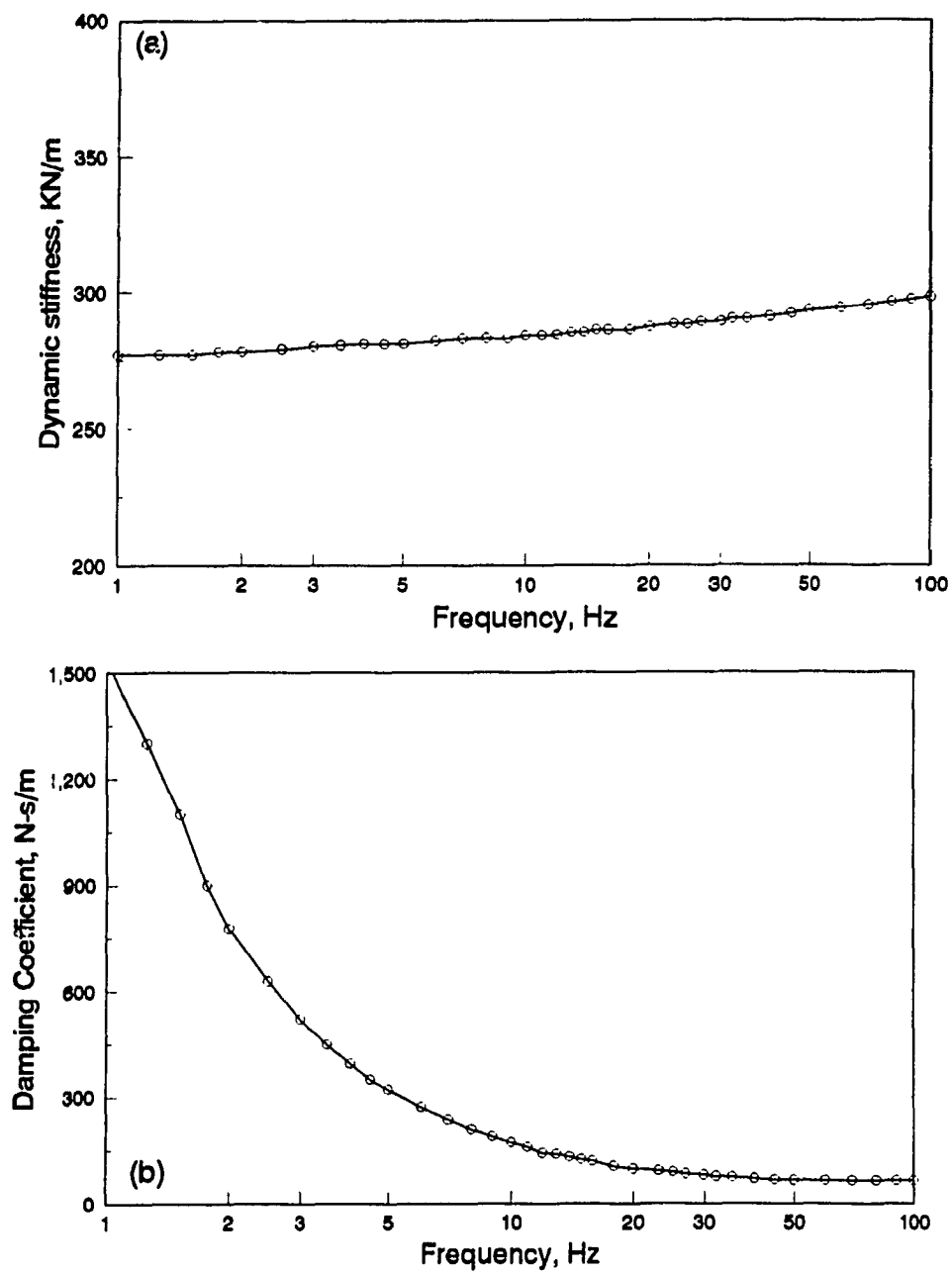


Figure 3.4 Dynamic characteristics of the flexible chamber material (rubber) (a) dynamic stiffness; (b) damping coefficient.

$$V_{TST} + V_{BST} \equiv V_{BST} \quad (3.29)$$

$$P_T = P_B = P_{ST} \quad (3.30)$$

Assuming that the projected cross-sectional area of the top and bottom chamber are equal, then the static load is given by:

$$F_{ST} = K_{ST} x_{ST} + A_{TP} (P_{AT} - P_{ST}) \quad (3.31)$$

which can also be expressed as:

$$F_{ST} = K_{ST} V_{TST} / A_{TP} + A_{TP} (V_{TST} / C_{VT}) \quad (3.32)$$

For any value of  $F_{ST}$ , the equation (3.32) is solvable for  $V_{TST}$  which upon substitution in to equation (3.27) gives  $P_{ST}$ . Equation (3.28) provides  $V_{BST}$ . Based on the change in volume under static load and projected piston area, the static deflection is obtained from:

$$x_{ST} = - (V_{TST} + V_{BST}) / A_{TP} \quad (3.33)$$

The following Figure 3.5a shows the variation of top chamber volume increment and bottom chamber volume increment as a function of static load is displayed in Figure 3.5b. The variation of static pressure and static deflection as a function of static load. The numerical values for top and bottom chamber compliance for this simulation are taken as  $1.0 \times 10^{-11} \text{ m}^5 / \text{N}$  and  $1.0 \times 10^{-10} \text{ m}^5 / \text{N}$  respectively. The result presented in Figure 3.5 using linear expressions for compliance show identical trend for top and bottom chamber with significant difference in magnitude. Table 3.2 shows the numerical values of static parameters for a constant static load of 125 kg for different piston diameters. These static parameters are required for the simulation for a given piston diameter.

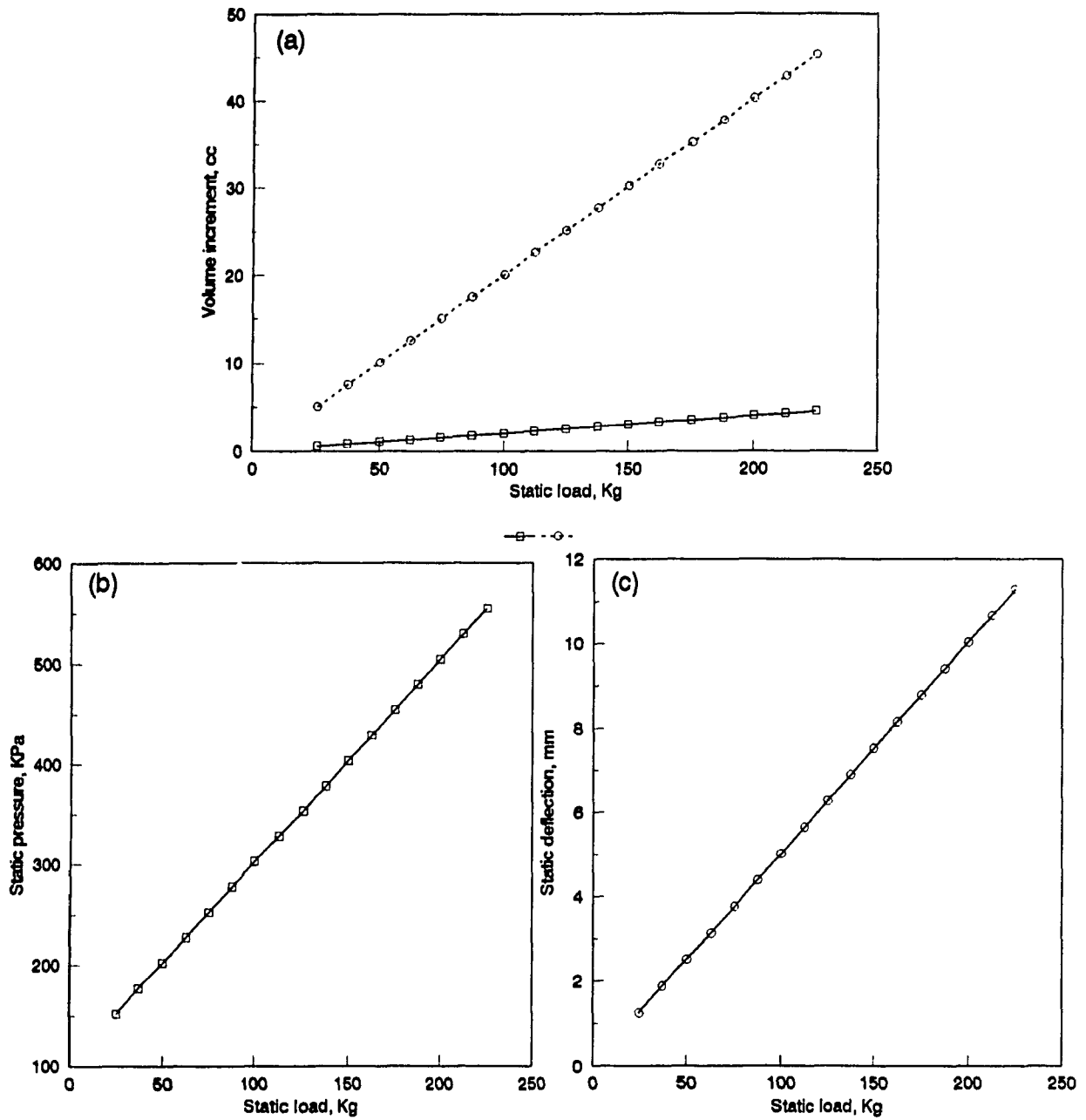


Figure 3.5 Effect of static load on (a) volume increment for top chamber —○—, and bottom chamber, -□- ;(b) static pressure and (c) static displacement for linear compliance.

Table 3.2 Variation of static pressure and volume increment for different piston diameter.

$D_o$ (mm)	$V_{TST}$ (cc)	$V_{BST}$ (cc)	$P_{ST}$ (KPa)	$x_{ST}$ (mm)
70.0	2.80726	140.362	382.12	37.202
75.0	2.51767	125.883	353.16	29.064
80.0	2.26061	113.030	327.46	22.936
85.0	2.03461	101.730	304.86	18.286

### 3.2.4.2 Nonlinear Compliance

In order to determine the static values of the pressure, volume increments and deflection for the damper having nonlinear compliances, the method described in earlier section is adopted. The chamber pressures as a function of top and bottom chamber volume increments found experimentally [17] are given by:

$$P_T(t) = -32.34\Delta V_T(t) + 47.73\Delta V_T^{7/6}(t) + 0.1234\Delta V_T^{2.5}(t) + P_{AT} \quad (3.34)$$

for  $\Delta V_T(t) > 0$

$$P_B(t) = 5.26 \times 10^{-3} \Delta V_B^{2.5}(t) - 8.9 \times 10^{-8} \Delta V_B^6(t) + 1.41 \times 10^{-8} \Delta V_B^{6.5}(t) + P_{AT} \quad (3.35)$$

where volume increment is measured in cubic centimeter and pressure in kilopascal. Applying the equation (3.33) and (3.35) to equation (3.31) one can obtain:

$$F_{ST} = A_{TP} (5.26 \times 10^{-3} V_{BST}^{2.5} - 8.9 \times 10^{-8} V_{BST}^6 + 1.41 \times 10^{-8} V_{BST}^{6.5}) + K_{ST} (V_{BST} / A_{TP}) \quad (3.36)$$

Equation (3.36) is solvable for  $V_{BST}$  for any value of  $F_{ST}$ . Once the magnitude of the static volume increment of the bottom chamber is obtained, static pressure can be derived from the following equation

$$P_{ST}(t) = 5.26 \times 10^{-3} \Delta V_{BST}^{2.5}(t) - 8.9 \times 10^{-8} \Delta V_{BST}^6(t) + 1.41 \times 10^{-8} \Delta V_{BST}^{6.5}(t) + P_{AT} \quad (3.37)$$

Since at static equilibrium  $P_T = P_B = P_{ST}$ , Equation (3.37) is nothing but other form of Equation (3.35). Similarly Equation (3.34) gives:

$$P_{ST} = -32.34V_{TST} + 47.73V_{TST}^{7/6} + 0.1234V_{TST}^{2.5} + P_{AT} \quad \text{for } V_{TST} > 0 \quad (3.38)$$

Static volume increment of the top chamber can be found from the equation by applying iteration scheme. Once static volume increments for top chamber and bottom chamber are calculated, static deflection can be obtained from Equation (3.33).

Figure 3.6 presents the effect of load on the static parameter for nonlinear compliance. For the chamber compliance relationships given by Equation (3.34) and (3.35), the effect of static load on volume increment is shown in figure 3.6a. As the figure shows, the trend for top and bottom chamber in this case is significantly different unlike the linear case shown in Figure 3.5a. Figure 3.6b presents the trend for static pressure and static deflection for a variation in the static load. These results show that the static pressure in the damper is a highly nonlinear function of static load, whereas the static deflection is a quite linear function.

The following tables represent numerical values of different parameters of the damper under static equilibrium condition with the variation in piston diameter for an operating load of 125 kg. The three compliances considered are same as those discussed in section 3.2.2.2. These static parameters are required to carry out the simulation for a given piston diameter.

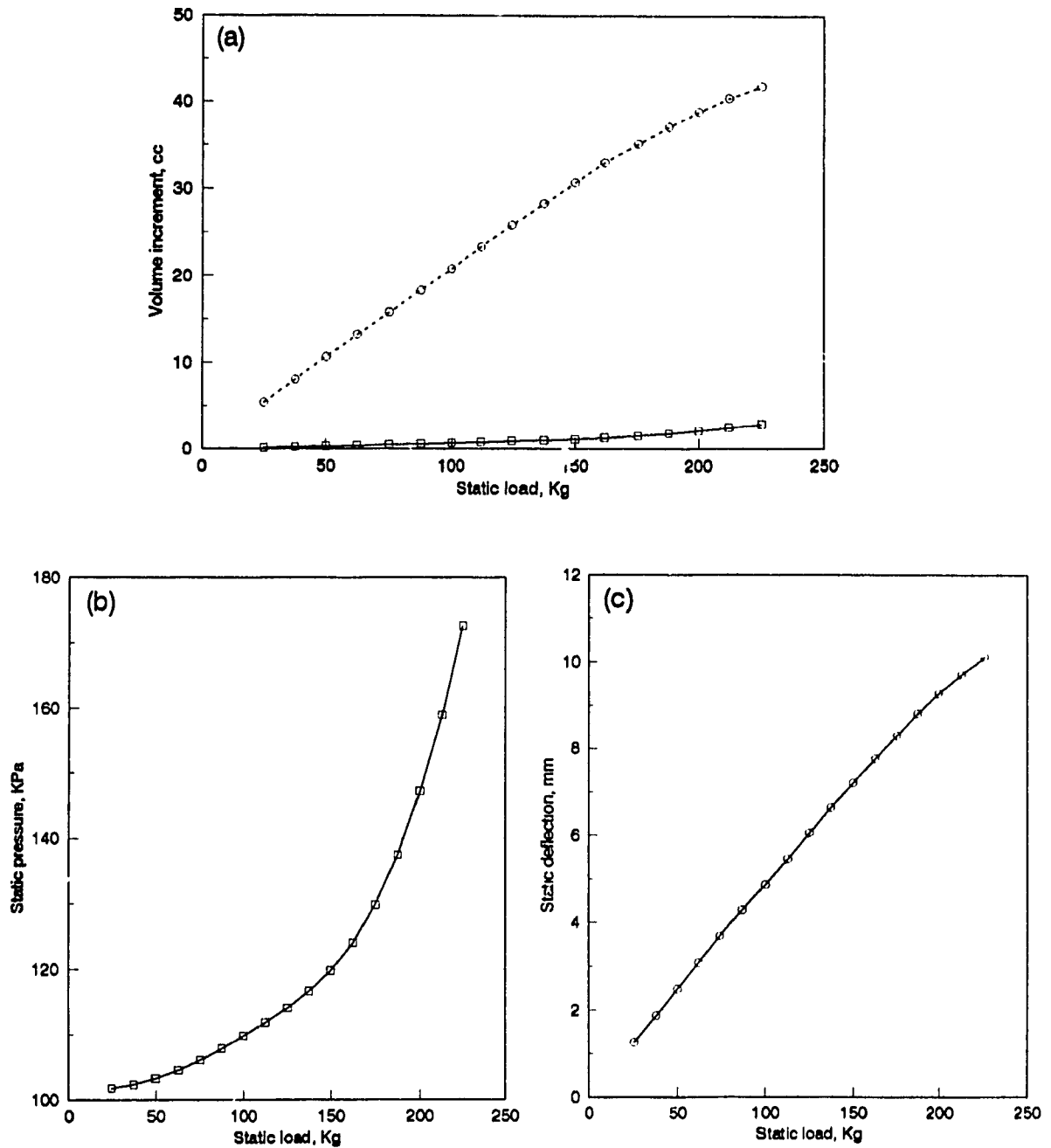


Figure 3.6 Effect of static load on (a) volume increment for top chamber ———, and bottom chamber, - - - - - ;(b) static pressure and (c) static deflection for nonlinear compliance.



**Table 3.3 Variation of static parameter under static load**

**For Comp\_A**

$D_0$ (mm)	$V_{TST}$ (cc)	$V_{BST}$ (cc)	$P_{ST}$ (KPa)	$-x_{ST}$ (mm)
70.0	0.75583	22.85139	111.452	6.13422
75.0	0.87770	25.84767	114.100	6.04939
80.0	1.01300	28.81964	117.227	5.93501
85.0	1.17597	31.59980	121.226	5.77597

**For Comp\_B**

$D_0$ (mm)	$V_{TST}$ (cc)	$V_{BST}$ (cc)	$P_{ST}$ (KPa)	$x_{ST}$ (mm)
70.0	1.03706	22.85139	111.452	6.20729
75.0	1.18147	25.84767	114.100	6.11815
80.0	1.34127	28.81964	117.227	6.00032
85.0	1.53319	31.59980	121.226	5.83892

**For Comp\_C**

$D_0$ (mm)	$V_{TST}$ (cc)	$V_{BST}$ (cc)	$P_{ST}$ (KPa)	$x_{ST}$ (mm)
70.0	0.46744	22.85139	111.452	6.05928
75.0	0.56188	25.84767	114.100	5.97796
80.0	0.66832	28.81964	117.227	5.86644
85.0	0.79832	31.59980	121.226	5.70942

### 3.2.5 Method of Solution

For the development of the mathematical model of the hydraulic damper, two types of compliances are considered, linear and nonlinear. Consequently, method of solution of nonlinear system of equation is made different to minimize computational time. The following two subsections describe the procedure in

detail for application to a single DOF system shown in Figure 3.7. As shown in the Figure, the mass to be isolated  $M_E$  is supported by a hydraulic damper only, where the stiffness is primarily provided by the top chamber wall, and the damping is due to orifice flow. The stiffness and damping property of the rubber material is considered frequency varying. Defining the relative displacement  $x(t)$ , in terms of response  $x_2(t)$  and excitation  $x_1(t)$  by:

$$x(t) = x_2(t) - x_1(t) \quad (3.39)$$

The governing equation of motion for the mass is:

$$m \ddot{x}(t) = -K(\omega)x(t) - C(\omega)\dot{x}(t) - A_{TP}[P_T(t) - P_{ST}] - m\ddot{x}_1 \quad (3.40)$$

where  $K(\omega)$  is the stiffness,  $C(\omega)$  is the damping coefficient of the rubber material and  $x_1(t) = X_1 \sin \omega t$ , a sinusoidal excitation.

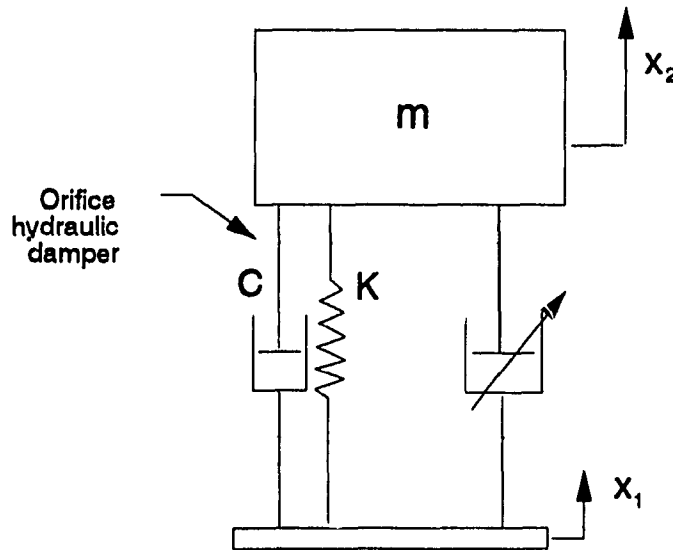


Figure 3.7 Hydraulic damper in a single degree of freedom mass-spring-damper system.

### 3.2.5.1 Linear Compliance

The system of equations for damper flow shown in equations (3.1) and (3.11-3.12) are linear except equation (3.1) which is highly nonlinear. The fluctuation of pressure is sinusoidal because of the sinusoidal excitation. Therefore it is not possible to linearize the equation, and hence numerical integration is adopted for the solution. Equations (3.1) and (3.11-3.12) applied to the one DOF system can be re-written in the following manner:

$$m\ddot{x}(t) = -k(\omega)x(t) - C(\omega)\dot{x}(t) - A_{TP}(P_{ST} - P_T(t)) - m\ddot{x}_1 \quad (3.41)$$

$$C_{VT}\dot{P}_T(t) = A_{TP}\dot{x}(t) - A_0C_D\sqrt{\frac{2[P_T(t) - P_B(t)]}{\rho}} \quad (3.42)$$

$$C_{VB}\dot{P}_B(t) = A_0C_D\sqrt{\frac{2[P_T(t) - P_B(t)]}{\rho}} \quad (3.43)$$

Equations (3.42-3.43) are very stiff differential equations because  $C_{VT}$  value is of the order of  $10^{-11}$  and  $P_T$  value can go as high as  $10^6$ . So a double precision Runge-Kutta 4th order routine was selected [57] with very small step size. The independent variables taken were absolute displacement, absolute velocity, top chamber pressure, and bottom chamber pressure. For each frequency  $\omega$ , the routine was run for sufficiently long time to ensure steady state condition in order to establish the peak values for all variables.

### 3.2.5.2 Nonlinear Compliance

Equation (3.1), (3.14-3.23) constitute the nonlinear analysis of the hydraulic damper. Here also Runge-Kutta 4th order method is applied to solve the system equation (3.40). At  $t=0$  second, static condition is maintained when  $Q_0=0.0$ ,  $V_{T0}=0.0$ ,  $\Delta V_T = \Delta V_B = 0.0$ ,  $P_T = P_B = P_{ST}$ . For an increment of excitation  $x_1(t)$ ,  $\Delta V_T$ , and  $\Delta V_B$  can be evaluated from equation (3.15) and (3.21) respectively; which in

turn gives  $P_T$  and  $P_B$  from equation (3.16) for Comp\_A and (3.22) for Comp\_D. As pressures are known, equation (3.1) can be applied to get  $Q_O$  which will give  $V_{TO}$  after integrating Equation 3.14. This procedure is repeated until steady-state condition is achieved. The simulation results and a detailed parametric study using these formulations for flexible hydraulic damper with short orifice is presented in chapter 5.

### **3.3 Long Orifice Hydraulic Damper with Flexible Chambers**

A hydraulic damper with a long orifice (LDHF) only is very common among flexible chambered hydraulic dampers. The geometric configuration of the long orifice creates additional damping due to the inertia effect of the fluid within the long orifice. This additional damping assists in reducing transmissibility at low frequency, such as engine idling frequency, although high frequency transmissibility is poor.

The analytical investigations for LDHF type dampers, reported by various researchers [12-18] did not consider oscillation effect of the fluid contained in the long orifice although it has significant effect on the characteristics of the damper. A thorough investigation carried out by Kim and Singh [17] for the LDHF damper shows complexity in the construction in spite of the fact that a simply constructed damper may produce the similar effect. Besides, the authors showed no dynamic performances; only characteristics of the damper were mentioned. A performance analysis is always desirable to conclude its superiority over the other.

The objective of this section is to develop a detailed model of long orifice hydraulic damper with flexible chamber. The models are developed with and without the consideration of fluid oscillation effect to demonstrate its influence. The models are later applied for detailed evaluation of damper characteristics and their isolation performance on a simple system.

### 3.3.1 Model Description

Figure 3.8a shows the simplest type of LDHF damper. There is much similarity in construction of LDHF with SDHF. The only difference is that instead of a short orifice, a long orifice with dimensional parameters, length and diameter, connects the chambers. These two parameters define the amount of damping and the frequency at which peak damping occurs. The operational activity of such a damper is very simple: At static equilibrium condition, the long orifice contains certain amount of fluid, therefore, has mass inertia. Due to the external excitation, fluid is forced to flow back and forth from top chamber to bottom chamber via the orifice. At low frequency, the long orifice acts like an ordinary orifice, but at higher frequency, inertia effect of the fluid within the orifice provides additional damping.

### 3.3.2 Nonlinear Mathematical Model

An accurate and complete theoretical analysis for the inertia track hydraulic damper is not possible because of the turbulent and oscillatory nature of flow within the inertia track. At present, theoretical analysis for laminar flow with small oscillation is available in the literature. However, a lump-parameter model for the analysis of the damper seems to be adequate for dynamic analysis.

Figure 3.8b shows the damper in the form of lump-parameter model. The governing equation for the inertia track of the damper is given by:

$$P_B(t) - P_T(t) = \lambda_r I_l \dot{Q}_l(t) + \frac{128\mu L_l}{\pi D_l^2} \lambda_a \left[ 1 + 0.0434 \frac{D_l}{L_l} R_{el} \right] \quad (3.44)$$

where  $P_B(t)$  and  $P_T(t)$  are the instantaneous pressures of the bottom and top chamber respectively.  $L_l$  and  $D_l$  are the length and diameter of the long orifice, respectively.  $Q_l(t)$  is the orifice flow, and  $\mu$  is the absolute viscosity of the fluid.  $R_{el}$

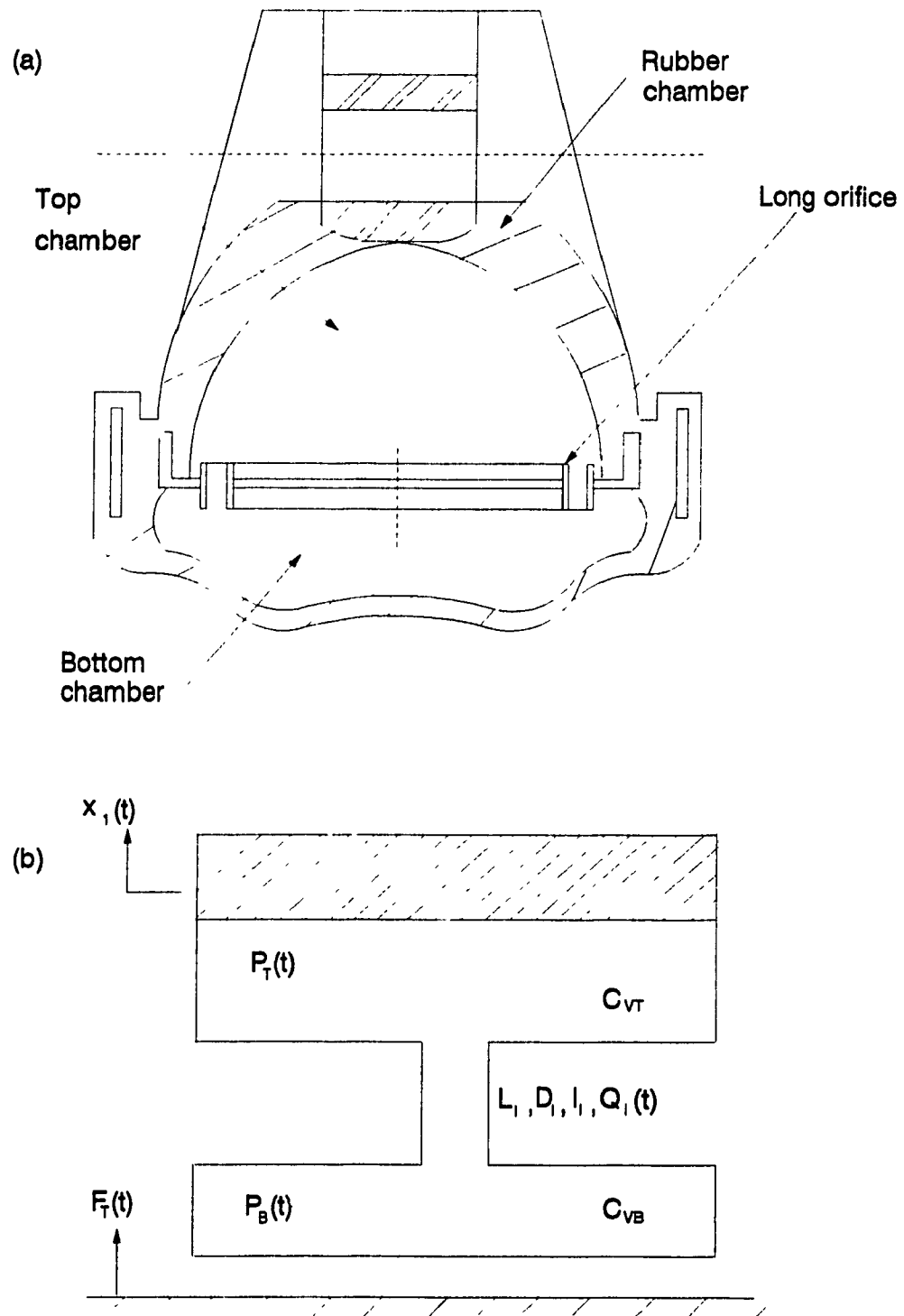


Figure 3.8 Schematic diagram; (a) Representation of a long orifice hydraulic damper (LDHF) with flexible chamber. (b) Lumped parameter model.

is the Reynolds number and is given by Equation (3.2).  $I_f$  represents the fluid inertance for the amount of fluid within the inertia track and is given by  $\rho L_f / A_f$ . Since the parameter of the orifice is time invariant, therefore, the fluid inertance is time invariant as well.

The coefficients  $\lambda_r$  and  $\lambda_a$  in the Equation (3.44) are the correction factors necessary for an oscillatory flow and for active and reactive components of hydraulic impedance, respectively. Those factors can be expressed through the non dimensional frequency of oscillation,  $\omega_n$  by the following analytical expressions [20, 31]

$$\lambda_a = \frac{\omega_n(4\omega_n - \sqrt{\omega_n})}{(2\sqrt{\omega_n} - 1)(4\omega_n - 2\sqrt{\omega_n} + 1)} \quad (3.45a)$$

$$\lambda_r = \frac{4\omega_n}{4\omega_n - 2\sqrt{\omega_n} + 1} \quad (3.45b)$$

where the non dimensional frequency of oscillation  $\omega_n$  is obtained by:

$$\omega_n = \frac{\omega D_f^2}{32\nu} \quad (3.45c)$$

Irrespective of orifice type, the continuity equation of flow from top chamber can be expressed as:

$$A_{TP} \dot{x}(t) - Q_I(t) = C_{VT} (\Delta V_T, P_T) \dot{P}_T(t) \quad (3.46)$$

where  $A_{TP}$  is the projected area of the top chamber acting as a piston,  $\dot{x}(t)$  is the relative velocity,  $C_{VT}$  is the compliance of the top chamber, and  $\dot{P}_T(t)$  is the rate of change of chamber pressure. Similarly, the continuity equation for bottom chamber yields:

$$Q_I(t) = C_{VB} (\Delta V_B, P_B) \dot{P}_B(t) \quad (3.47)$$

where  $C_{VB}$  and  $\dot{P}_B(t)$  are the compliance and rate of change of pressure for the bottom chamber.

A sample compliances of top and bottom chambers in pressure-volume increment relationship may be found from Equation (3.16) and (3.22) referred to as Comp\_A and Comp\_D.

The force transmitted to the ground by the damper can be given by the following equation:

$$F_T(t, \omega) = K(\omega)x(t) + C(\omega)\dot{x}(t) + A_{TP}[P_{ST} - P_T(t)] \quad (3.48)$$

where  $x(t)$  is the relative displacement of the mass. Equations (3.44) to (3.48) can now be solved for all variables of interest.

The principal variables which are of interest in the case of LDHF are: (a) pressure in the top chamber, (b) orifice flow, (c) transmitted force to the ground, (d) damping force generated, (e) dynamic stiffness and (f) loss angle. Because of the nonlinearity of the chamber compliances, flow restriction phenomenon in long orifice, creation of negative pressure in the top chamber during upward stroke, etc., the response of the system in terms of those variables are quite nonlinear. Therefore, under the application of pure sinusoidal excitation, the responses are nonsinusoidal and asymmetric.

In time domain, one can analyze those non sinusoidal variables both at transient state and at steady state. Responses under the application of shock input can be observed only in time domain. Under sinusoidal input, it is also of great importance to see responses in frequency domain. It is well established that in steady state, any non sinusoidal variable, such as  $K_D(t)$  can be expressed as a series of harmonics functions by employing Fourier series expansion, such as:

$$K_D(t) = K_{D0} + K_{D1} \sin(\omega t + \varphi_1) + K_{D2} \sin(\omega t + \varphi_2) + K_{D3} \sin(\omega t + \varphi_3) + \dots + K_{Dn} \sin(\omega t + \varphi_n) + \dots \quad (3.49)$$



where  $K_{D0}$  is the mean value,  $K_{D1}$ ,  $K_{D2}$ ,  $K_{D3}$ , etc., are the amplitudes of each harmonic and  $\varphi_1$ ,  $\varphi_2$ ,  $\varphi_3$ , etc., are the phase leads of each harmonics with respect of excitation.

Now,  $K_{D0}$  is given by:

$$K_{D0} = \frac{1}{uT} \int_0^{uT} K_D(t) dt \quad (3.50)$$

where  $m$  is the number of cycles with period  $T = 2\pi/\omega$ . The coincident or in-phase component  $\mathcal{A}_n(\omega)$  and the quadrature component  $\mathcal{B}_n(\omega)$  of dynamic stiffness  $K_D$  are given by the following expressions:

$$\begin{aligned} \frac{1}{uT} \int_0^{uT} \sin n\omega t \cdot K_D(t) dt &= \frac{1}{uT} \int_0^{uT} \sin n\omega t \cdot K_{Dn} \sin(n\omega t + \varphi_n) dt \\ &= \frac{K_{Dn} \cos \varphi}{2} = \mathcal{A}_n(\omega) \end{aligned} \quad (3.51)$$

$$\begin{aligned} \frac{1}{uT} \int_0^{uT} \cos n\omega t \cdot K_D(t) dt &= \frac{1}{uT} \int_0^{uT} \cos n\omega t \cdot K_{Dn} \sin(n\omega t + \varphi_n) dt \\ &= \frac{K_{Dn} \sin \varphi}{2} = \mathcal{B}_n(\omega) \end{aligned} \quad (3.52)$$

where  $n$  is the number of harmonics, and  $u$  is the number of cycles with period  $T$ .

The dynamic stiffness and loss angle in frequency domain, thus, can be obtained from Equations 3.51 and 3.52 such as:

$$K_{Dn}(\omega, X) = 2\sqrt{\mathcal{A}_n^2(\omega) + \mathcal{B}_n^2(\omega)} \quad (3.53)$$

$$\varphi_n(\omega, X) = \tan^{-1}[\mathcal{B}_n(\omega) / \mathcal{A}_n(\omega)] \quad (3.54)$$

Therefore, for a particular displacement  $X$ , dynamic stiffness and loss angle can be calculated for each frequency of interest. It may be mentioned that the above

equations are for up to  $n$  harmonics. It is found that the fundamental harmonics ( $n=1$ ) dominates the higher harmonics, therefore, in defining characteristics of the damper, only the first harmonics is retained.

The same procedure can be adopted for other variables such as, orifice flow, damping force and transmitted force to the ground. But for the top chamber pressure, display of peak chamber pressure corresponding to each frequency is more important than its amplitude spectra with regard to its fundamental harmonic. Therefore, frequency response of the top chamber pressure is based on peak top chamber pressure only.

### **3.3.3 Method of Solution**

Following the procedure outlined in article 3.2.2.2, the variables at static load are calculated using iteration scheme. Under the application of sinusoidal excitation, nonlinear governing equations are solved using 4th order Runge-Kutta method. As the differential equations are very stiff in nature, a very fine step size is applied to the numerical integration. For each frequency of excitation, sufficient time is allowed (30 cycles) to ensure that the steady state condition is reached. Then, three cycles are considered to obtain the steady state time responses of all internal variables. To furnish frequency response characteristics, these three cycles ( $u=3$ , in Equation 3.51 and 3.52) are also utilized to obtain the fundamental harmonic.

## **3.4 Long and Short Orifice Hydraulic Damper with Flexible Chamber (LSDHF)**

The hydraulic damper with long orifice, discussed in section 3.3 has some severe operating limitations. Some of the well known limitations for such dampers include:

- (a) performance is very poor for amplitude of excitation  $> 1$  mm.

(b) performance under shock input is very poor (as demonstrated in chapter 6).

(c) poor high frequency (second resonance frequency and higher) transmissibility even for low amplitude.

For high amplitude of excitation, relative displacement is even higher which makes the piston to displace larger amount of fluid. There is only one long orifice and the orifice has oscillation effect prohibiting flow at faster rate for high relative displacement. Due to compliance of the top chamber, the chamber does not increase in volume fast enough so as to keep the pressure low. The pressure rises rapidly in the top chamber which makes the damper to perform very poorly at high amplitudes. For the same reason, the performance of the LDHF damper under shock load is very poor. In the performance analysis of the LDHF damper, there always exists two peaks in the transmissibility performance. The first peak occurs due to the systems' natural frequency and the second peak occurs due to the mass of the liquid present in the long orifice. For smaller long orifice diameter, the damper performs very well to obtain reduced transmissibility but at the cost of high transmissibility around second resonance frequency.

An addition of a short orifice as bleeder orifice with the long orifice can improve the performance of the LDHF damper substantially. This new damper, referred to here as long and short orifice hydraulic damper with flexible chamber (LSDHF), can be used for higher amplitude of excitation. Inclusion of a bleeder orifice is very simple in construction. Keeping all other parameter unchanged, the mathematical model of the LSDHF damper is developed in this section for a thorough investigation of damper characteristics and performance to be presented later.

### 3.4.1 Model Description

Figure 3.9a shows the schematic diagram of the LSDHF damper. It is similar to the that of long orifice damper shown in Figure 3.8, where a bleeder orifice is added. At the middle of the orifice plate where the long orifice is placed along the circumference, the short orifice or the bleeder orifice is placed. At high frequencies when fluid can not pass through the long orifice, the bleeder orifice will allow considerable fluid to pass, thus improving the performance. At low frequencies fluid will be forced to flow back and forth from top chamber to bottom chamber through both long orifice and bleeder orifice. This effect is likely to increase the low frequency transmissibility to some extent. However, by using appropriate parameters this increase can be made insignificant compared to improved performance at high frequencies.

### 3.4.2 Nonlinear Mathematical Model

The LSDHF damper is identical to LDHF except the inclusion of a bleeder orifice. Therefore, the flow of the fluid will increase by an amount  $Q_b(t)$ , where  $Q_b(t)$  is the flow through bleeder orifice in  $m^3/s$ . The mathematical model, the lumped parameter model used in article 3.3.2 for LDHF can be adapted here with the inclusion of the bleeder orifice and  $Q_b$  as shown in Figure 3.9b.

The flow through the bleeder orifice is given by:

$$Q_b(t) = A_b C_D (D_b, R_{eb}, L_b) \sqrt{\frac{2[P_T(t) - P_B(t)]}{\rho}} \quad (3.55)$$

where  $A_b$  is the bleeder orifice area,  $D_b$  is the diameter of the bleeder orifice,  $L_b$  is the length of the bleeder orifice.  $P_T(t)$  and  $P_B(t)$  are the pressure state in the top and bottom chambers, respectively. The discharge coefficient  $C_D$  for the bleeder orifice

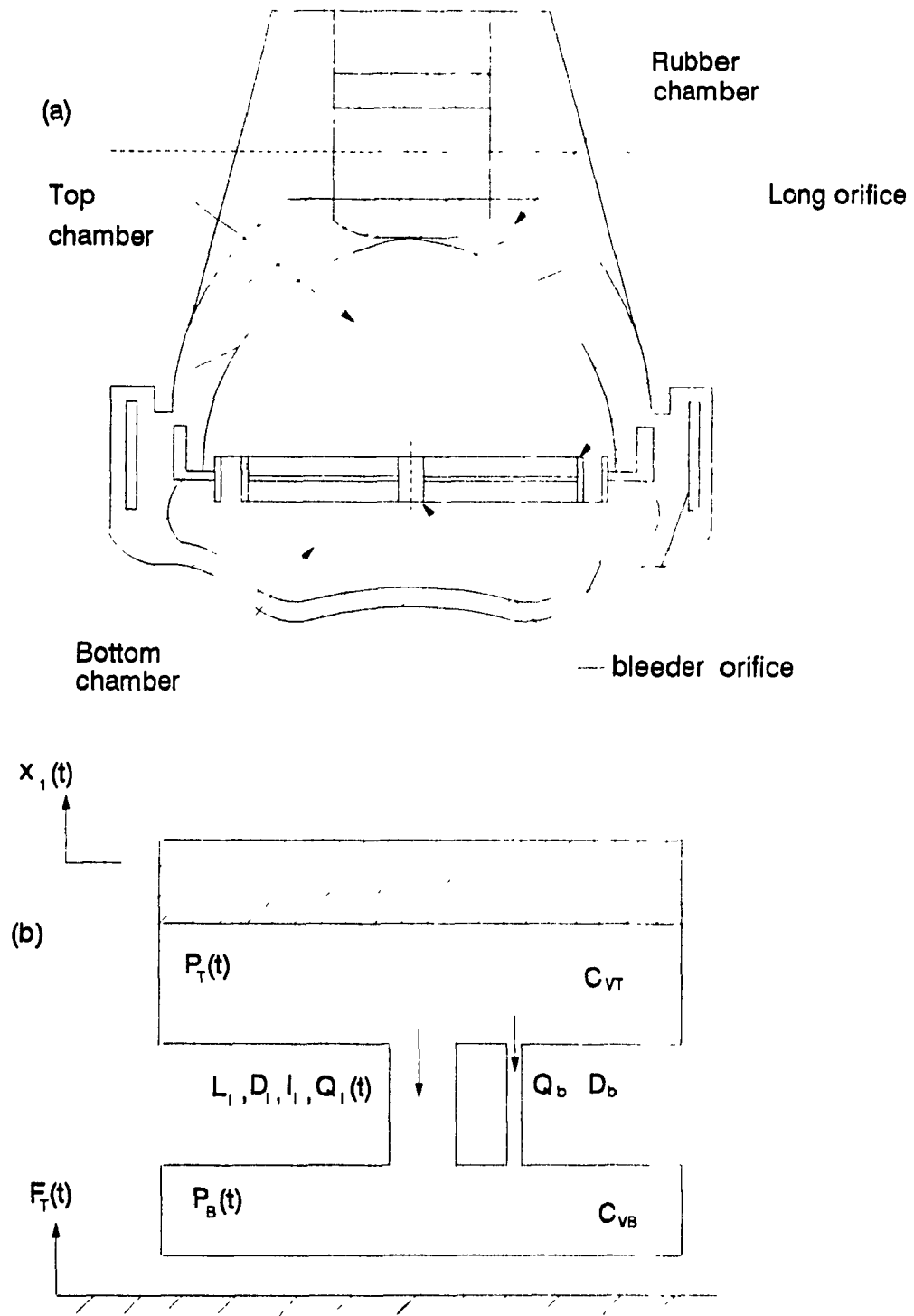


Figure 3.9 Schematic diagram; (a) Representation of a long and short orifice hydraulic damper (LSDHF) with flexible chamber. (b) Lumped parameter model.

is a function of the length and diameter of the orifice as well as the Reynolds number. Reynolds number for the bleeder orifice is given by:

$$R_{eb} = \frac{\rho V D_b}{\mu} = \frac{\rho Q_b D_b}{\mu A_b} \quad (3.56)$$

The expression for coefficient of discharge is similar to Equations (3.8-3.9) and are given as:

$$C_D = \frac{1}{\sqrt{(1.0 + K_C) + 13.74 \sqrt{L_b / D_b R_{eb}}}} \quad \text{for } \frac{D_b R_{eb}}{L_b} > 50 \quad (3.57)$$

$$C_D = \frac{1}{\sqrt{(2.28 + K_C) + 64.0 L_b / D_b R_{eb}}} \quad \text{for } \frac{D_b R_{eb}}{L_b} < 50$$

The governing equation for the long orifice inertia track of the damper presented earlier as Equation (3.44) is rewritten with different subscripts to represent the present damper:

$$P_B(t) - P_T(t) = \lambda_r I_l \dot{Q}_l(t) + \frac{128 \mu L_l}{\pi D_l^2} \lambda_a \left[ 1 + 0.0434 \frac{D_l}{L_l} R_{el} \right] \quad (3.58)$$

where  $I_l$  is the fluid inertance of the amount of fluid within the inertia track,  $L_l$  and  $D_l$  are the length and diameter of the long orifice respectively.  $R_{el}$  is the Reynolds number for the flow through the long orifice.  $\lambda_r$  and  $\lambda_a$  are the correction factors for oscillatory flow and are given by Equation (3.45).

Similar to Equation (3.46) the volumetric continuity in this case yields:

$$A_{TP} \dot{x}(t) - Q_l(t) - Q_b(t) = C_{VT} (\Delta V_T, P_T) \dot{P}_T(t) \quad (3.59)$$

where  $A_{TP}$  is the projected area of the top chamber acting as a piston,  $Q_l(t)$  and  $Q_b(t)$  are the flow through long and bleeder orifices and  $C_{VT}$  is the compliance of the top chamber. Similarly, the continuity equation for the bottom chamber yields:

$$Q_l(t) + Q_b(t) = C_{VB} (\Delta V_B, P_B) \dot{P}_B(t) \quad (3.60)$$

where  $C_{VB}$  is the compliance of the bottom chamber.

The formulations presented earlier in section 3.2.2.2 for nonlinear chamber compliance and top and bottom chamber pressure are also valid here. Except in this case the total volume of fluid transferred is given by:

$$V_{TO}(t) = \int_0^t [Q_l(t) + Q_b(t)] dt \quad (3.61)$$

where  $Q_l(t)$  and  $Q_b(t)$  are the flow through long and bleeder orifices, respectively.

The experimental pressure volume increment relationships presented in section 3.2.2.2 as Comp\_A (Equation. 3.18) and Comp\_D (Equation. 3.22) are used for top and bottom chambers, of the present nonlinear model [17].

The force transmitted to the ground given by Equation (3.48) and rest of the formulation for the long orifice damper (section 3.2.2) is also applicable to the present model.

### 3.4.3 Method of Solution

The method of solution and the internal variables of interest in the case of the damper with long and short orifice is similar to that of only long orifice presented in section 3.3.3.

## 3.5 Long Orifice Hydraulic Damper with Spring Loaded Valve (LDHVF)

The damper configuration with short and long orifices presented and modeled in the previous section may perform well for sinusoidal excitation in wide frequency range. However, hydraulic dampers with flexible chambers are known to perform poorly under shock environment. If such damper suffers sudden impulse of load, pressure in the top chamber rises suddenly. The damper, then, performs very poor

as there is no device to subside the high pressure buildup. The hydraulic damper may be redesigned to create such device as to reduce the sudden increase in pressure. For this, a number of short orifices with spring loaded valves of different spring constants can be fitted to the orifice plate. The spring may be designed such that the valve will operate (open the orifice) when there will be a sudden pressure rise exceeding a preset value. Otherwise the orifice will remain closed by the spring. When the valve is open, a quantity of fluid will be allowed to pass through the orifices, thus reducing the pressure in the top chamber of the damper. A bleeder orifice which works only during reverse stroke of excitation may also be fitted to the damper to send back excessive fluid to the top chamber. At low amplitude of excitation, the pressure build up will not be up to the limit so as to open the valve. The damper in this case will work like an ordinary damper with long orifice.

A flexible chambered hydraulic damper with spring loaded valve (LDHVF) is proposed and modeled in this section. Such damper may exhibit superior performances for both low amplitude as well as shock excitations. The detailed model for the proposed (LDHVF) damper is developed in the following subsections.

### **3.5.1 Model Description**

A schematic diagram of the proposed hydraulic damper with spring loaded valves (orifices) is shown in Figure 3.10a. The essential features of the damper is similar to the long and short orifice hydraulic damper with modifications made on orifice plate. In addition to the long orifice along the circumference of the orifice plate, there are three short orifices with sharp-edged entrance and exit. Each orifice is operated by a spring loaded valve of different spring constant. Two of those (orifice 1 and 2) are designed to release excessive pressure in the top chamber.



Both the orifices work only during forward stroke of excitation. Each orifice has different operating pressure, set by the spring constant of the valve. Third orifice (orifice 3) is called bleeder orifice which works only during reverse stroke to replace excessive fluid back to the top chamber. It is also operated by a spring loaded valve. The diameter of the orifices as well as the spring constants of the valves may be varied to study the effects on the dynamic characteristics.

### 3.5.2 Nonlinear Mathematical Model

The modeling considerations of the LDHVF damper proposed in this section is same as that of LSDHF presented in section 3.4.2. In this case however, three short orifices are used with spring loaded valves, in addition to the long orifice. The lumped parameter model used for this is shown in figure 3.10b. In this case the flow through each orifice depending on the valve position has to be expressed. The detailed model is developed in the following subsections which is used in chapter 5 for detailed analysis of its characteristics and performance.

#### 3.5.2.1 Orifice Flow

The damper proposed here contains altogether four orifices;

- i) one long orifice of length  $L_l$  and diameter  $D_l$
- ii) one short orifice of diameter  $D_{o1}$ , operated by the spring loaded valve
- iii) one short orifice of diameter  $D_{o2}$  operated by the spring loaded valve
- iv) one bleeder orifice of diameter  $D_{ob}$  operated by the spring loaded valve only in the reverse stroke.

The flow through short orifice 1,  $Q_{o1}$  is given by:

$$Q_{o1}(t) = A_{o1} C_{D1} (D_{o1}, R_{eo1}, L_{o1}) \sqrt{\frac{2[P_T(t) - P_B(t)]}{\rho}} \quad (3.62)$$

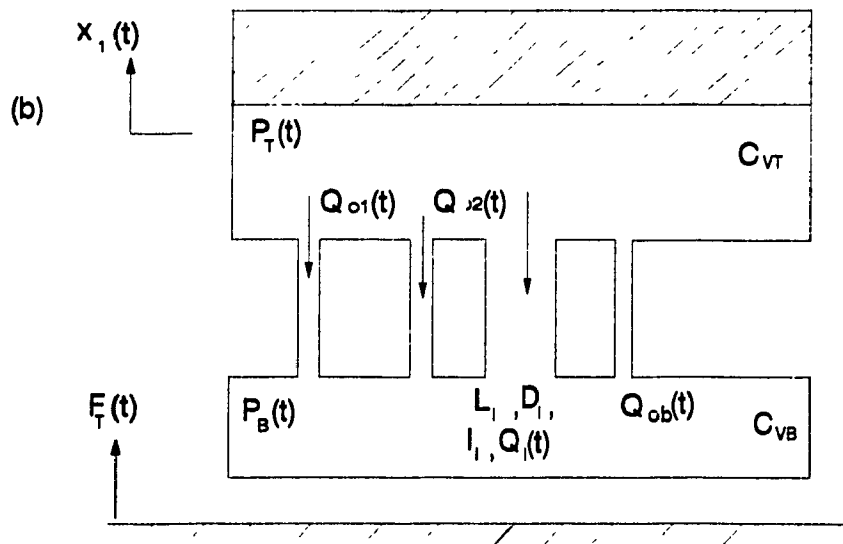
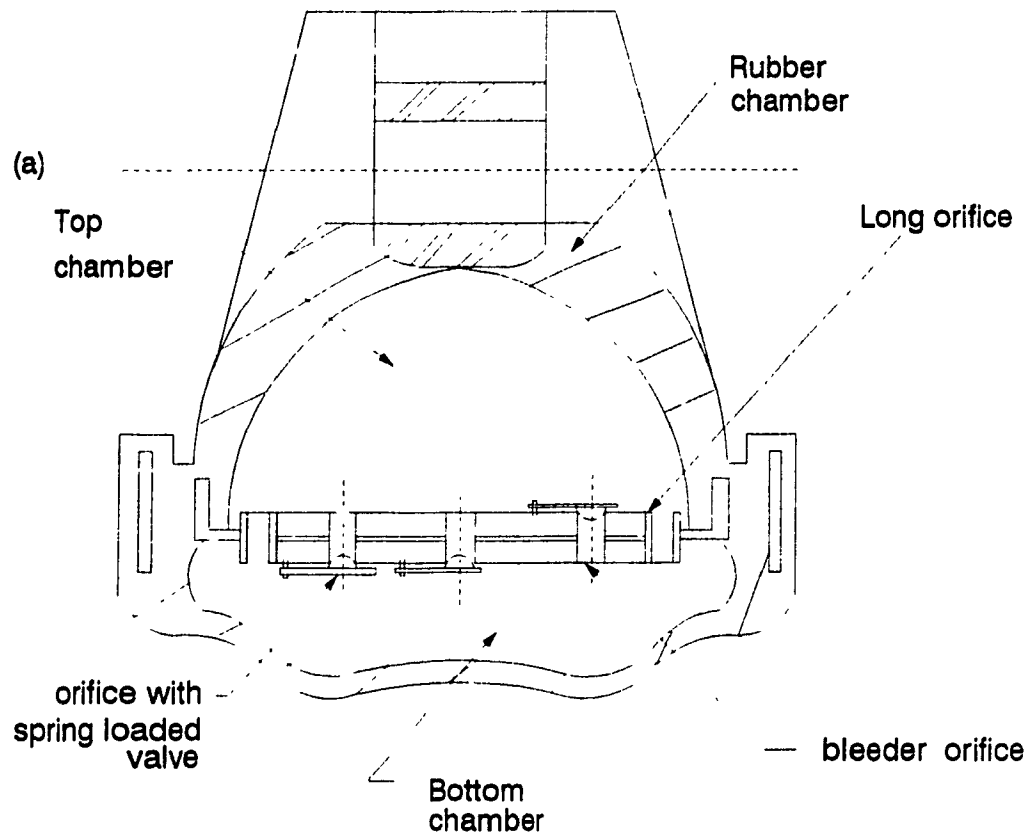


Figure 3.10 Schematic diagram; (a) Representation of a long and short orifice hydraulic damper with spring loaded valves (LDHVF) . (b) Lumped parameter model.

where  $A_{o1}$  is the orifice area;  $C_{D1}$  is the discharged coefficient for the orifice, which is a function of  $D_{o1}$ ,  $L_{o1}$  and  $R_{eo1}$  representing the diameter, length and the Reynolds number corresponding to the flow  $Q_{o1}(t)$ , respectively.

Similarly the flow through the second orifice is given as:

$$Q_{o2}(t) = A_{o2} C_{D2}(D_{o2}, R_{eo2}, L_{o2}) \sqrt{\frac{2[P_T(t) - P_B(t)]}{\rho}} \quad (3.63)$$

Equation (3.62) and (3.63) are active only during forward stroke and are subject to the condition that the valves are partially open or fully open.

The flow through orifice 3 or the bleeder orifice is:

$$Q_{ob}(t) = A_{ob} C_{Db}(D_{ob}, R_{eob}, L_{ob}) \sqrt{\frac{2[P_B(t) - P_T(t)]}{\rho}} \quad (3.64)$$

This flow is feasible only when the orifice 1 and 2 are in active and occurs during reverse stroke of excitation only.

The coefficient of discharges for orifice flow presented earlier in Equations (3.8-3.9) can be rewritten in terms of new variables for a range of Reynolds number.

The coefficient of discharge for orifice 1 is given as follows:

$$C_{D1} = \frac{1}{\sqrt{(1.0 + K_C) + 13.74 \sqrt{L_{o1} / D_{o1} R_{eo1}}}} \quad \text{for } \frac{D_{o1} R_{eo1}}{L_{o1}} > 50 \quad (3.65)$$

$$C_{D1} = \frac{1}{\sqrt{(2.28 + K_C) + 64.0 L_{o1} / D_{o1} R_{eo1}}} \quad \text{for } \frac{D_{o1} R_{eo1}}{L_{o1}} < 50$$

Similarly, the coefficient of discharge for orifice 2 is given as:

$$C_{D2} = \frac{1}{\sqrt{(1.0 + K_C) + 13.74 \sqrt{L_{o2} / D_{o2} R_{eo2}}}} \quad \text{for } \frac{D_{o2} R_{eo2}}{L_{o2}} > 50 \quad (3.66)$$

$$C_{D2} = \frac{1}{\sqrt{(2.28 + K_C) + 64.0 L_{o2} / D_{o2} R_{eo2}}} \quad \text{for } \frac{D_{o2} R_{eo2}}{L_{o2}} < 50$$

The coefficient of discharge for bleeder orifice reverse flow is given as follows:

$$C_{Db} = \frac{1}{\sqrt{(1.0 + K_C) + 13.74 \sqrt{L_{ob} / D_{ob} R_{eob}}}} \quad \text{for } \frac{D_{ob} R_{eob}}{L_{ob}} > 50 \quad (3.67)$$

$$C_{Db} = \frac{1}{\sqrt{(2.28 + K_C) + 64.0 L_{ob} / D_{ob} R_{eob}}} \quad \text{for } \frac{D_{ob} R_{eob}}{L_{ob}} < 50$$

The governing equation for the long orifice inertia track of the damper presented earlier as Equation (3.58) in section 3.4.2 which includes the oscillation effect is also valid for the present model.

### 3.5.2.2 Continuity Equation

The volumetric continuity equations for the case of LDHVF damper depends on whether the stroke is in compression or extension as different orifices are active in each case. Furthermore, the number of orifices that are active depend on the differential pressure  $\Delta P$ .

(a) Compression Stroke: Under compression, the flow through each of the short orifice with valve depends on differential pressure  $\Delta P$  across the orifice and the present pressure  $P_{set}$  assigned for each valve. Therefore, for two short orifices and a long orifice, there can be three cases for continuity equation for the top chamber under compression:

for  $\Delta P > P_{set,2}$

$$A_{TP} \dot{x}(t) - Q_i(t) - Q_{o1}(t) - Q_{o2}(t) = C_{VT} (\Delta V_T, P_T) \dot{P}_T(t) \quad (3.68)$$

for  $\Delta P > P_{set,1}$

$$A_{TP} \dot{x}(t) - Q_i(t) - Q_{o1}(t) = C_{VT} (\Delta V_T, P_T) \dot{P}_T(t) \quad (3.69)$$

for  $\Delta P \leq P_{\text{set},1}$

$$A_{\text{TP}} \dot{x}(t) - Q_I(t) = C_{\text{VT}} (\Delta V_T, P_T) \dot{P}_T(t) \quad (3.70)$$

where  $A_{\text{TP}}$  is the projected area of the top chamber acting as a piston,  $C_{\text{VT}}$  is the compliance of the top chamber and  $Q_I$  is the flow through the long orifice.  $\Delta P$  is the pressure difference between top and bottom chamber for orifice 1 and 2 respectively.  $P_{\text{set},1}$  and  $P_{\text{set},2}$  are the preset pressures required to open orifice 1 and orifice 2, respectively.

Similarly, for the highly compliant bottom chamber the continuity equation yield:

for  $\Delta P > P_{\text{set},2}$

$$Q_I(t) + Q_{o1}(t) + Q_{o2}(t) = C_{\text{VB}} (\Delta V_B, P_B) \dot{P}_B(t) \quad (3.71)$$

for  $\Delta P > P_{\text{set},1}$

$$Q_I(t) + Q_{o1}(t) = C_{\text{VB}} (\Delta V_B, P_B) \dot{P}_B(t) \quad (3.72)$$

for  $\Delta P \leq P_{\text{set},1}$

$$Q_I(t) = C_{\text{VB}} (\Delta V_B, P_B) \dot{P}_B(t) \quad (3.73)$$

where  $C_{\text{VB}}$  is the compliance of the bottom chamber.

(b) Expansion Stroke: For the case of expansion stroke the flow depends on whether the bleeder orifice valve is open or not. The two cases of continuity equation for top chamber under expansion stroke are:

for  $\Delta P > P_{\text{set},b}$

$$A_{\text{TP}} \dot{x}(t) - Q_I(t) - Q_{ob}(t) = C_{\text{VT}} (\Delta V_T, P_T) \dot{P}_T(t) \quad (3.74)$$

for  $\Delta P \leq P_{\text{set},b}$

$$A_{\text{TP}} \dot{x}(t) - Q_I(t) = C_{\text{VT}} (\Delta V_T, P_T) \dot{P}_T(t) \quad (3.75)$$

And for bottom chamber the continuity equations yield:

for  $\Delta P > P_{\text{set},b}$ ,

$$Q_i(t) + Q_{ob}(t) = C_{vB}(\Delta V_B, P_B) \dot{P}_B(t) \quad (3.76)$$

for  $\Delta P \leq P_{\text{set},b}$ ,

$$Q_i(t) = C_{vB}(\Delta V_B, P_B) \dot{P}_B(t) \quad (3.77)$$

where  $P_{\text{set},b}$  is the preset pressure required to open the bleeder orifice.

Since the compliances of the top and bottom chambers are given experimentally in terms of pressure-volume increment relationship, the following procedure is adopted to find pressures.

### 3.5.2.3 Total Volume Flow

Since the fluid flows from top chamber to bottom chamber through three different orifices, the total volume of fluid transferred from one chamber to the other for a given stroke and at a particular instant 't', is given by the following equations:

(a) Compression Stroke: During compression stroke fluid enters to the bottom chamber through three orifices depending on the pressure state of the damper. Total volume of fluid is given as:

If  $\Delta P > P_{\text{set},2}$ , then,

$$V_{TO}(t) = \int_0^t [Q_i(t) + Q_{o1}(t) + Q_{o2}(t)] dt \quad (3.78)$$

Or if  $\Delta P > P_{\text{set},1}$ , then,

$$V_{TO}(t) = \int_0^t [Q_i(t) + Q_{o1}(t)] dt \quad (3.79)$$

Otherwise only long orifice is working, therefore,

$$V_{TO}(t) = \int_0^t [Q_i(t)] dt \quad (3.80)$$

Depending on the validity of the above equations, the volume increment of the bottom chamber can now be obtained from:

$$\Delta V_B(t) = V_{TO}(t) + V_{BST} \quad (3.81)$$

where  $V_{BST}$  is the volume increment of the bottom chamber from atmospheric pressure to static pressure change.

Similarly, the volume increment of the top chamber is given by:

$$\Delta V_T(t) = -V_{TO}(t) + V_{TST} - A_{TP}x_1(t) \quad (3.82)$$

where  $V_{TO}$  is the total volume given by Equations (3.78-3.80),  $V_{TST}$  is the volume increment from atmospheric pressure to static pressure change,  $A_{TP}$  is the effective piston area, and  $x_1(t)$  is the excitation.

(b) Expansion Stroke: During expansion stroke only the long orifice or the long orifice with bleeder orifice is active depending on the pressure state of the damper.

If  $\Delta P > P_{set,b}$ , then,

$$V_{TO}(t) = \int_0^t [Q_i(t) + Q_{ob}(t)] dt \quad (3.83)$$

Otherwise only long orifice is working, therefore,

$$V_{TO}(t) = \int_0^t [Q_i(t)] dt \quad (3.84)$$

Utilizing the appropriate volume of the top chamber from above, volume increment of the top chamber can be obtained from:

$$\Delta V_T(t) = V_{TO}(t) + V_{TST} - A_{TP}x_1(t) \quad (3.85)$$

Similarly, volume increment of the bottom chamber under the expansion stroke is given by:

$$\Delta V_B(t) = -V_{TO}(t) + V_{BST} \quad (3.86)$$

Now based on the volume increment for top and bottom chambers in a given stroke, the pressure can be obtained from experimental compliance relationships presented in section 3.2.2.2. The baseline compliances used for the top and bottom chambers are given in Equations (3.18) and (3.22) respectively.

For  $\Delta V_T(t) < 0$ , the chamber is in a state of vacuum and it is assumed that an amount of entrapped air  $V_A$  takes that volume increment obeying Boyle's Law. Total volume of air is:

$$V_{TA}(t) = V_A + |\Delta V_T(t)| \quad (3.87)$$

Therefore, pressure at the top chamber may be written as

$$P_T(t) = P_{AT} V_A / V_{TA}(t) \quad \text{for } \Delta V_T(t) < 0 \quad (3.88)$$

The force transmitted by the damper to the ground, given earlier by Equation (3.48) is also valid for the present model.

#### 3.5.2.4 Fluid Flow Through Valves

The spring loaded valves typically found in shock absorbers are, essentially, puppet valves with a  $90^\circ$  seat angle. The flow leaves the orifice in the direction perpendicular to the axis of the orifice. The model of the valve may be approximated by the diagram in Figure 3.11a. Due to the presence of the leaf type spring, the area of the valve through which fluid is discharging is not uniform. However, it can be assumed uniform for the sake of simplicity of calculation



without introducing any significant error in the determination of force due to change in momentum of the fluid.

The various forces acting on the disk of the valve, shown in Figure 3.11b are:

$F_d$  represents the viscous damping force,  $F_d = C_v \dot{y}(t)$

$F_s$  denotes spring force,  $F_s(t) = P_{sp} + Ky(t)$ , and  $K$  is the spring constant

$P_{sp}$  is the spring preload, a constant value

$F_v$  is the force due to change in momentum of the fluid

$F_p$  denotes the force due to change in pressure,  $F_p(t) = [P_T(t) - P_B(t)] A_o$

Figure 3.11c represents the control volume of the valve used to determine the force due to the change in momentum. Assuming that the fluid leave the valve with velocity in the radial direction, the momentum equation in the  $y$  direction yields [26]

$$\rho v_y(t) Q_{in}(t) - \rho v_y(t) Q_{out}(t) = F_v(t) \quad (3.89)$$

where  $v_y$  denotes  $y$  component of the velocity of fluid. Since the fluid leaving the valve is in radial direction, therefore,

$$v_{y, out}(t) = 0$$

$$\text{and } v_{y, in}(t) = Q_{in}(t) / A_{in}$$

The force due to change in momentum is given by

$$F_v = \rho v_{y, in}^2(t) A_{in} = \rho \frac{Q_{in}^2(t)}{A_{in}} \quad (3.90)$$

Application of standard orifice flow equation, for example equation 3.62 into equation 3.90 yields,

$$F_v(t) = 2 \frac{A_{out}^2(t)}{A_{in}} C_d^2 [P_T(t) - P_B(t)] \quad (3.91)$$

Since

$$A_{out}(t) = y(t) \pi D_o$$

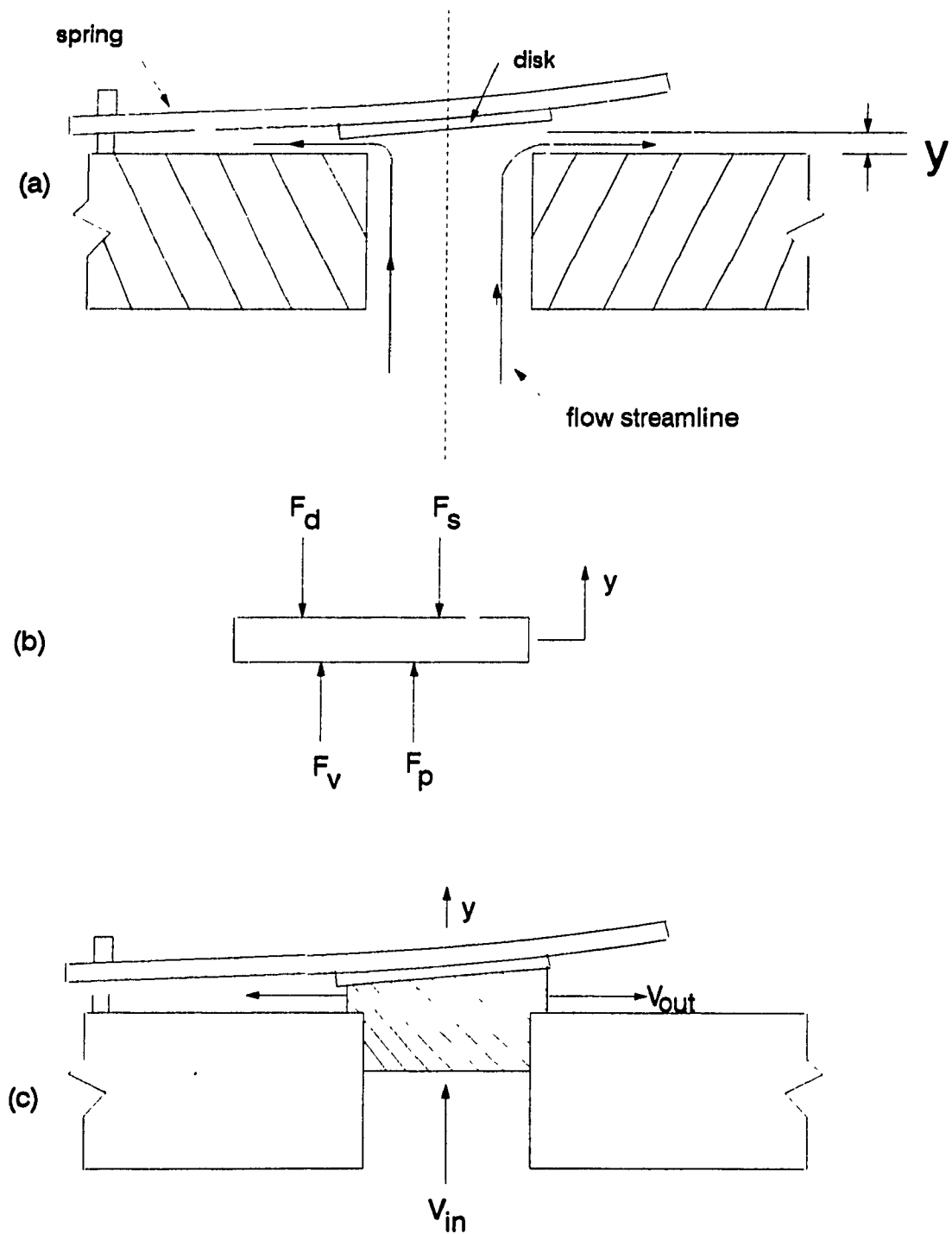


Figure 3.11 Spring loaded valve for an orifice showing: (a) flow pattern and displacement of valve; (b) forces acting on the disk of the valve; (c) control volume for momentum balance.

where  $D_0$  is the diameter of the orifice and  $y(t)$  is the valve displacement. Substitution of above into Equation (3.91) leads to:

$$F_v(t) = \frac{1}{A_{in}} 2C_d^2 \pi^2 D_o^2 [P_T(t) - P_B(t)] y(t)^2 \quad (3.92)$$

It is likely that  $v_{out}(t)$  will have a component in the  $y$  direction. However, compared to the magnitude of the velocity in the radial direction, it is neglected.

Applying Newton's Law of motion to the disk of the valve,

$$\sum F_y(t) = m_v \ddot{y}(t)$$

or

$$F_p(t) + F_v(t) - F_s(t) - F_d(t) = m_v \ddot{y}(t) \quad (3.93)$$

where  $m_v$  is the mass of valve disk and the spring.

Substituting for all the external forces, Equation 3.93 can be rewritten as follows:

$$\begin{aligned} m_v \ddot{y}(t) + C_w \dot{y}(t) + K y(t) - \frac{1}{A_{in}} 2C_d^2 \pi^2 D_o^2 [P_T(t) - P_B(t)] y(t)^2 \\ = [P_T(t) - P_B(t)] A_o - P_{sp} \end{aligned} \quad (3.94)$$

Equation (3.94) describes the motion of the valve disk in vertical direction to open the orifice after exceeding certain pressure limit.

Three equations of the form (3.94), one for each valve must be solved simultaneously with the four equations for flow through long orifice as well as three orifices with valves. The flow equations for valve orifices can be obtained in three stages [35].

- (i) *valve is closed*
- (ii) *valve is partially open*
- (iii) *valve is fully open*

(i) *Valve is closed:*

When the valves are closed there is no flow through the orifices, thus:

$$Q_{o1}(t) = Q_{o2}(t) = Q_{ob}(t) = 0$$

(3.95)

#### Orifice 1

This stage for orifice 1 occurs when  $[P_T(t) - P_B(t)] < \frac{K_1 y_{1,i}}{A_{o1}}$

where  $K_1$  is the spring constant of the relief valve

$A_{o1}$  is the area of the first orifice

$y_{1,i}$  is the preloaded displacement of the first valve spring

#### Orifice 2

This stage for orifice 2 occurs when  $[P_T(t) - P_B(t)] < \frac{K_2 y_{2,i}}{A_{o2}}$

where  $K_2$  is the spring constant of the relief valve

$A_{o2}$  is the area of the second orifice

$y_{2,i}$  is the persuaded displacement of the second valve spring

#### Orifice 3 (bleeder orifice)

This stage for orifice 3 occurs when  $[P_B(t) - P_T(t)] < \frac{K_b y_{b,i}}{A_{ob}}$

where  $K_b$  is the spring constant of the relief valve

$A_{ob}$  is the area of the bleeder orifice

$y_{b,i}$  is the preloaded displacement of the bleeder valve spring

(ii) *Valve is partially open*

The valve is considered partially open until it has reached its maximum displacement.

### Orifice 1

This stage for orifice 1 occurs when  $\frac{K_1 y_{1,i}}{A_{o1}} \leq [P_T(t) - P_B(t)] \leq \frac{K_1 (y_{1,i} + y_{1,m})}{A_{o1}}$

where  $K_1$  is the spring constant of the relief valve for first orifice

$A_{o1}$  is the area of the first orifice

$y_{1,m}$  represent the maximum displacement of the disk of the first valve.

The maximum displacement occurs when the valve flow area (in radial direction) equals that of the orifice.

$$A_{o1} = \pi D_{o1} y_{1,m}$$

where  $D_{o1}$  is the diameter of the first orifice

Since  $A_{o1} = \pi D_{o1}^2 / 4$ ,

Therefore, the maximum valve displacement can be expressed as:

$$y_{1,m} = D_{o1} / 4$$

The displacement of the partially open valve disk  $y_1(t)$  for the orifice as a function of time may be obtained from equation (3.94). The flow through orifice 1 may be expressed as:

$$Q_{o1}(t) = \pi D_{o1} y_1(t) C_{D1} (D_{o1}, R_{eo1}, L_{o1}) \sqrt{\frac{2[P_T(t) - P_B(t)]}{\rho}} \quad (3.96)$$

### Orifice 2

This stage for orifice 2 occurs when  $\frac{K_2 y_{2,i}}{A_{o2}} \leq [P_T(t) - P_B(t)] \leq \frac{K_2 (y_{2,i} + y_{2,m})}{A_{o2}}$

where  $K_2$  is the spring constant of the relief valve for second orifice.

$A_{o2}$  is the area of the second orifice

$y_{2,m}$  represent the maximum displacement of the disk of the second valve.

Similar to the orifice one, maximum displacement for the second valve can be found by:

$$y_{2,m} = D_{o2} / 4$$

The displacement of the partially open valve disk  $y_2(t)$  for the orifice as a function of time may be obtained from equation (3.94). The flow through orifice 2 may be expressed as:

$$Q_{o2}(t) = \pi D_{o2} y_2(t) C_{D2}(D_{o2}, R_{eo2}, L_{o2}) \sqrt{\frac{2[P_T(t) - P_B(t)]}{\rho}} \quad (3.97)$$

### Orifice 3 (bleeder orifice)

This stage for orifice 3 occurs when  $\frac{K_b y_{b,i}}{A_{ob}} \leq [P_B(t) - P_T(t)] \leq \frac{K_b (y_{b,i} + y_{b,m})}{A_{ob}}$

where  $y_{b,m}$  represent the maximum displacement of the disk of the bleeder valve and is given by:  $y_{b,m} = D_{ob} / 4$

The displacement of the valve disk  $y_b(t)$  for the orifice as a function of time may be obtained from equation (3.94). The flow through bleeder orifice may be expressed as:

$$Q_{ob}(t) = \pi D_{ob} y_b(t) C_{Db}(D_{ob}, R_{eob}, L_{ob}) \sqrt{\frac{2[P_B(t) - P_T(t)]}{\rho}} \quad (3.98)$$

### *(iii) Valve is fully open*

When a given valve is fully open, the respective disk has reached its maximum displacement. Therefore in this case the flow can be expressed in terms of maximum disk position.

### Orifice 1 and 2

This stage for orifice 1 occurs when  $[P_T(t) - P_B(t)] > \frac{K_j (y_{j,i} + y_{j,m})}{A_{oj}}$

And the resulting flow rate at this stage is given by:

$$Q_{oj}(t) = \pi D_{oj} y_{j,m}(t) C_{Dj}(D_{oj}, R_{eoj}, L_{oj}) \sqrt{\frac{2[P_T(t) - P_B(t)]}{\rho}} \quad (3.99)$$

where  $j=1$  for orifice 1, and  $j=2$  for orifice 2.

### Orifice 3 (bleeder orifice)

This stage for orifice 3 occurs when  $[P_B(t) - P_T(t)] > \frac{K_b(y_{b,l} + y_{b,m})}{A_{ob}}$

The flow rate at this stage is given by

$$Q_{ob}(t) = \pi D_{ob} y_{b,m}(t) C_{Db}(D_{ob}, R_{eob}, L_{ob}) \sqrt{\frac{2[P_B(t) - P_T(t)]}{\rho}} \quad (3.100)$$

### 3.5.3 Method of Solution

The mathematical modeling of long orifice hydraulic damper with spring loaded valve consists of a number of nonlinear differential equations and algebraic equations. Again the numerical integration is carried out to solve those equations. 4th order Runge Kutta method with very fine step size is proved to be sufficient to find the solution. The vertical displacement  $y_1(t)$ ,  $y_2(t)$ , and  $y_b(t)$  of disk of orifice 1, 2 and 3 respectively, are taken as independent variable. The flow  $Q_1(t)$ ,  $Q_{o1}(t)$ ,  $Q_{o2}(t)$ , and  $Q_{ob}(t)$  through long orifice, and short orifices 1, 2 and 3, respectively are also considered as independent variable. The modeling results in the following seven equations that are required to be solved simultaneously.

$$m_1 \ddot{y}_1(t) + C_w \dot{y}_1(t) + K_1 y_1(t) - \frac{1}{A_{o1}} 2C_{D1}^2 \pi^2 D_{o1}^2 [P_T(t) - P_B(t)] y_1(t)^2 = [P_T(t) - P_B(t)] A_{o1} - P_{sp} \quad (3.101)$$

$$m_2 \ddot{y}_2(t) + C_w \dot{y}_2(t) + K_2 y_2(t) - \frac{1}{A_{o2}} 2C_{D2}^2 \pi^2 D_{o2}^2 [P_T(t) - P_B(t)] y_2(t)^2 = [P_T(t) - P_B(t)] A_{o2} - P_{sp} \quad (3.102)$$

$$m_b \ddot{y}_b(t) + C_w \dot{y}_b(t) + K_b y_b(t) - \frac{1}{A_{ob}} 2C_{Db}^2 \pi^2 D_{ob}^2 [P_T(t) - P_B(t)] y_b(t)^2 = [P_T(t) - P_B(t)] A_{ob} - P_{sp} \quad (3.103)$$

$$P_B(t) - P_T(t) = \lambda_r I_l \dot{Q}_l(t) + \frac{128\mu L_l}{\pi D_l^2} \lambda_a \left[ 1 + 0.0434 \frac{D_l}{L_l} R_{el} \right] \quad (3.104)$$

$$P_B(t) - P_T(t) = I_{o1} \dot{Q}_{o1}(t) + \frac{\rho}{2\pi D_{o1} y_1(t) C_{D1} C_{D1}} Q_{o1} |Q_{o1}| \quad (3.105)$$

$$P_B(t) - P_T(t) = I_{o2} \dot{Q}_{o2}(t) + \frac{\rho}{2\pi D_{o2} y_2(t) C_{D2} C_{D2}} Q_{o2} |Q_{o2}| \quad (3.106)$$

$$P_B(t) - P_T(t) = I_{ob} \dot{Q}_{ob}(t) + \frac{\rho}{2\pi D_{ob} y_b(t) C_{Db} C_{Db}} Q_{ob} |Q_{ob}| \quad (3.107)$$

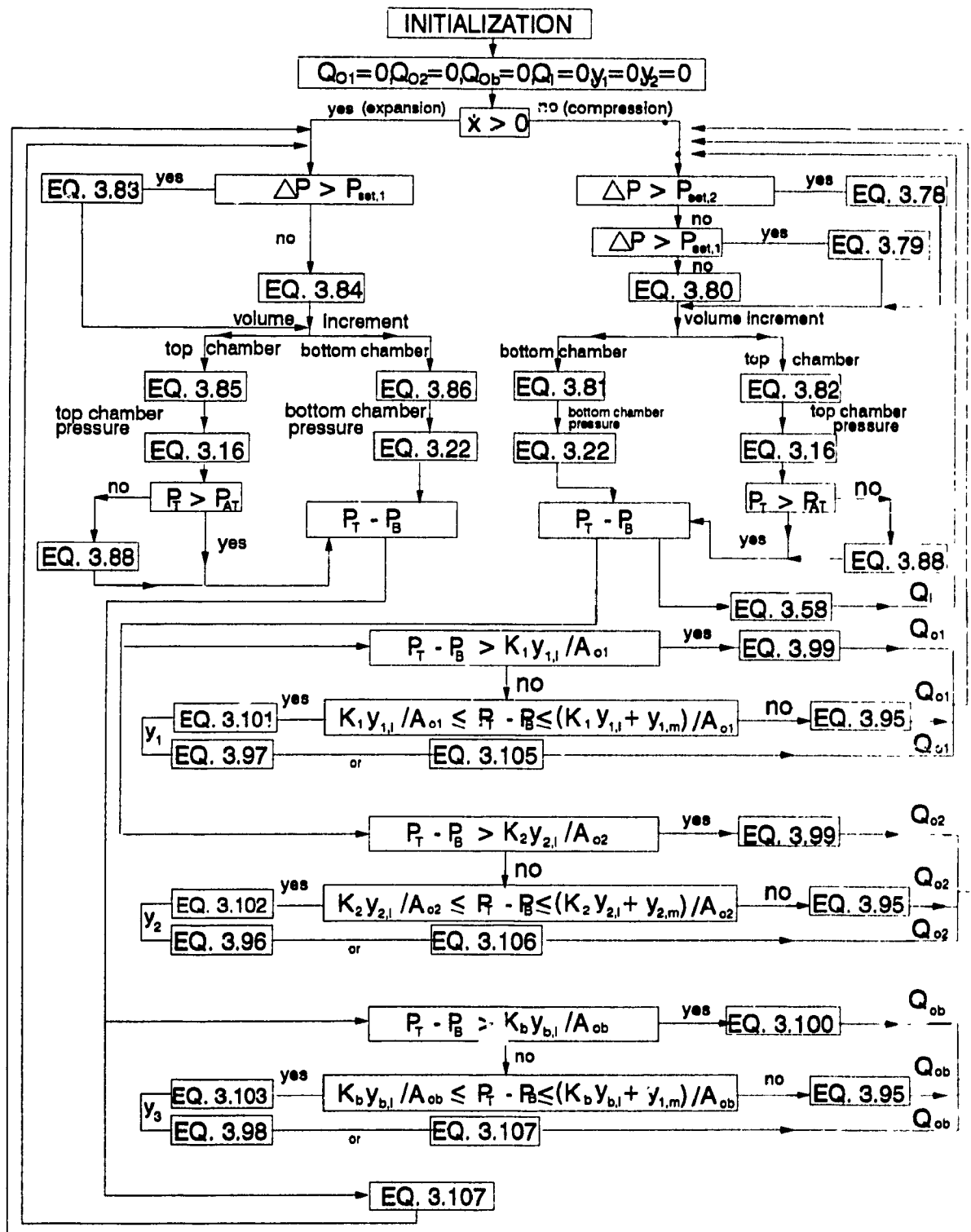
The following flow chart describes the procedure for the numerical solution that can be used to characterize the damper and evaluate its performance .

### 3.6 Summary

This chapter presents the modeling considerations for hydraulic dampers with flexible chambers. Detailed mathematical models are developed for hydraulic dampers with short orifice and long orifice. The model consider experimentally obtained nonlinear compliances for the flexible chambers along with the effects of orifice shape and fluid oscillation within the long orifice. The concept of hydraulic damper with flexible chambers is further extended to include a combination of short and long orifice due to its expected potential in improved performance over a wide frequency range. A model is developed for long orifice with a set of short orifices equipped with spring loaded valve. The detailed model further includes the valve dynamics. The four models developed in this chapter will be thoroughly investigated in time and frequency domain to establish their characteristics and performance for isolation of vibration and shock.



**Table 3.4** Flow chart for numerical solution for LDHVF dampers  
The equation numbers inside the box are taken from chapter 3.



## **CHAPTER 4**

# **CHARACTERISTICS & PERFORMANCE OF DUAL-PHASE DAMPERS**

### **4.1 Introduction**

A detailed nonlinear model of dual-phase dampers was developed as presented in chapter 2. This study only considers low-high and high-low displacement sensitive dampers as they are effectively same as high-low and low-high velocity sensitive dampers, respectively. Unlike previous investigations of such dampers, an integral formulation was used for characterizing the damping force. A local equivalent linearization technique was adopted to carry out computer simulation in the convenient frequency domain. The primary objective of this chapter is to carry out a detailed analysis of the model in terms of damper characteristics and isolation performance.

The dual-phase damper has the good potential in improving both shock and vibration isolation performance. The damper may be applied for any range of amplitude excitation, for any range of shock severity by only changing its four governing parameters, namely, transition point of displacement, transition factor for displacement, damping coefficient and transition factor for damping coefficient. Both low-high damper and high-low damper are analyzed to evaluate their characteristics under the application of sinusoidal input. The characteristics of the damper are determined by finding the transmitted force to the ground, dynamic

stiffness and loss angle. A detailed parametric study is also carried out to examine the influence of transition point and damping coefficient parameters. The response characteristics of the damper is determined by implementing the damper to a one degree of freedom (1 DOF) system. The isolation performance of the dampers is evaluated for both vibration and shock of various severity.

## 4.2 Characteristics of the Damper

The damper characteristics are primarily evaluated in terms of its force-displacement characteristics as well as dynamic stiffness and loss angle. Dynamic stiffness for the damper is defined by Equation 3.53. The loss angle, on the other hand, is obtained by Equation 3.54. The dynamic stiffness and loss angle for damping device are important characteristics often used in comparative studies. Results are obtained for baseline as well as variation of the nonlinearity parameters.

The baseline parameters for the damper are taken as:  $A = 10$  mm,  $\alpha = 3$ ,  $\zeta_1 = 0.25$  and  $\zeta_2 = 0.50$  ( $\beta = 2$ ) for both low-high and high-low dampers. A high amplitude of excitation of 40 mm is considered to ensure that the damper covers all the regions. Such amplitude is common for application of the damper to an off-road vehicle as a shock absorber. The linear spring constant that supports the mass is taken as 10 N/mm. A static mass of 75 kg is placed on the top of the damper and is excited by the application of sinusoidal input at the base. The undamped natural frequency of the system is 1.85 Hz. Therefore, the damping coefficient value of the damper is  $C = 436$  N-s/m which represents the low damping case. The high damping coefficient value as defined in chapter 2 is given by  $\beta C$ .

Figure 4.1a shows the Lissajous (force-displacement) plot of the baseline low-high dual-phase damper and Figure 4.1b shows the same for a high-low damper. The plots are obtained for the frequency ratio ( $\omega/\omega_0$ ) of 0.80. The area within the

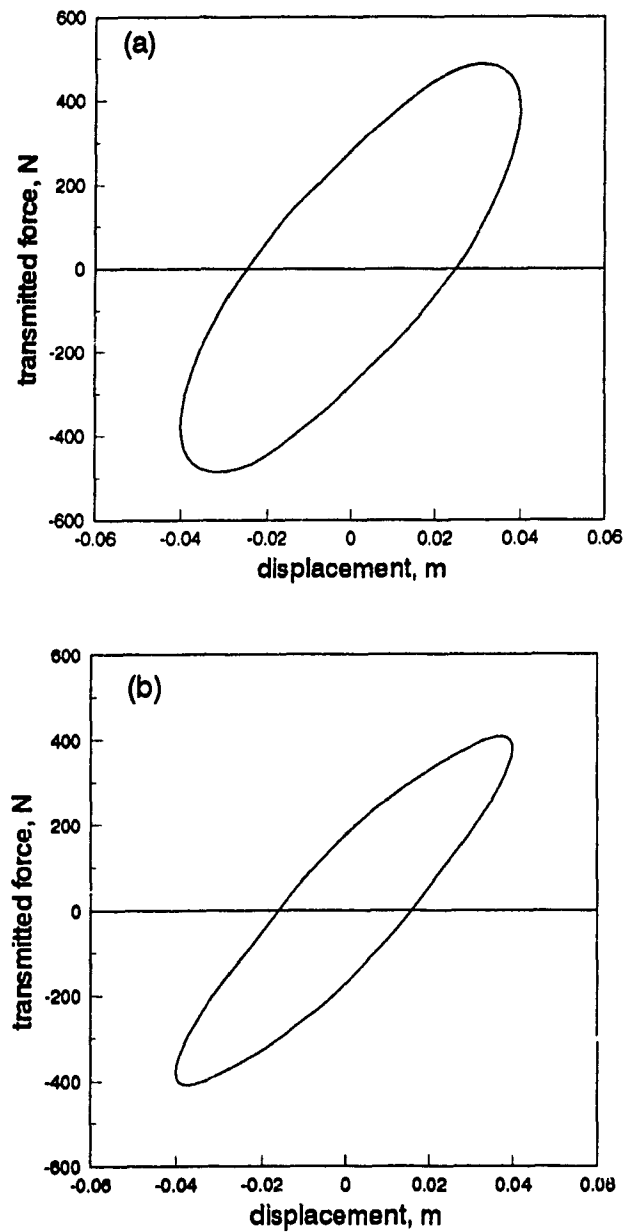


Figure 4.1 Lissajous plots of the dual phase damper. (a) low-high damper; (b) high-low damper. ( $A = 10\text{mm}$ ,  $\alpha = 3$ ,  $\zeta = 0.25$ , and  $\beta = 2$ ; frequency ratio 0.80).

loop determines the amount of energy dissipated per cycle of damper movement, which in turn, defines the damping associated with the damper. It is observed that for the same baseline parameters and an excitation amplitude of 40 mm, the low-high damper produces much higher damping than the high-low damper. For a low-high damper, damping coefficient is higher at lower velocity compared to a high-low damper where damping coefficient is lower at low velocity. That is why the low-high displacement sensitive damper produces more damping effect than that of a high-low damper. The peak damping force is also observed to be higher for a low-high damper for the high amplitude of excitation.

The dynamic stiffness and the loss angle properties as a function of frequency are shown in Figure 4.2 for the baseline low-high dual-phase damper under sinusoidal excitation of amplitude 40 mm. At low frequency, velocity is very low, therefore, the contribution to the dynamic stiffness from damper is also very low. As the results show, for frequency of up to 5 Hz, the dynamic stiffness is very low and is approximately equal to the spring stiffness. With the increase in frequency, velocity across the damper increases and hence the dynamic stiffness increases rapidly and dominates the characteristics. For the low-high damper, it reaches a value of 475 N/mm at a frequency of 100 Hz. The loss angle is also often used as a measure of damping effect of the damper. The loss angle property for the low-high damper shown in Figure 4.2b indicates a low value for loss angle at low frequency of excitation. It rises rapidly around resonance frequency zone (1 to 5 Hz). The loss angle property of the damper is almost insensitive to frequency beyond 20 Hz.

Similar to Figure 4.2, Figure 4.3 shows the dynamic stiffness and the loss angle of a high-low dual-phase damper. The parameter of the high-low damper is same as that of the low-high damper. These results confirm that for the same parameters the high-low damper produces lower dynamic stiffness throughout the frequency range. The maximum value of the dynamic stiffness is, in this case is

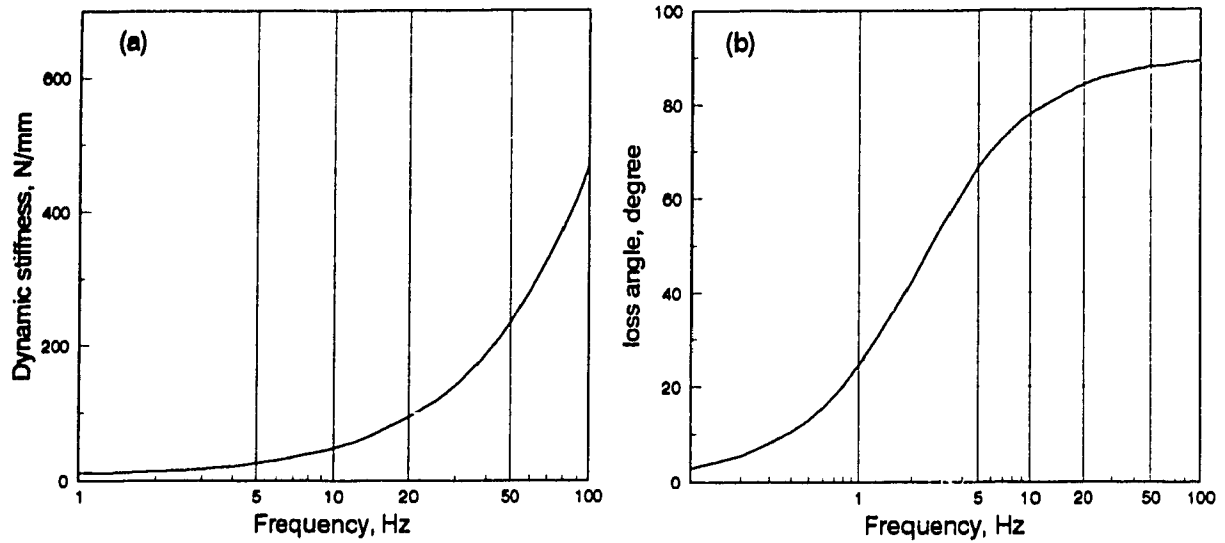


Figure 4.2 Dynamic stiffness and loss angle characteristics of a low-high dual phase damper. ( $A=10\text{mm}$ ,  $\alpha = 3$ ,  $\zeta=0.25$ , and  $\beta = 2$ ;  $X_1 = 40\text{mm}$ ).

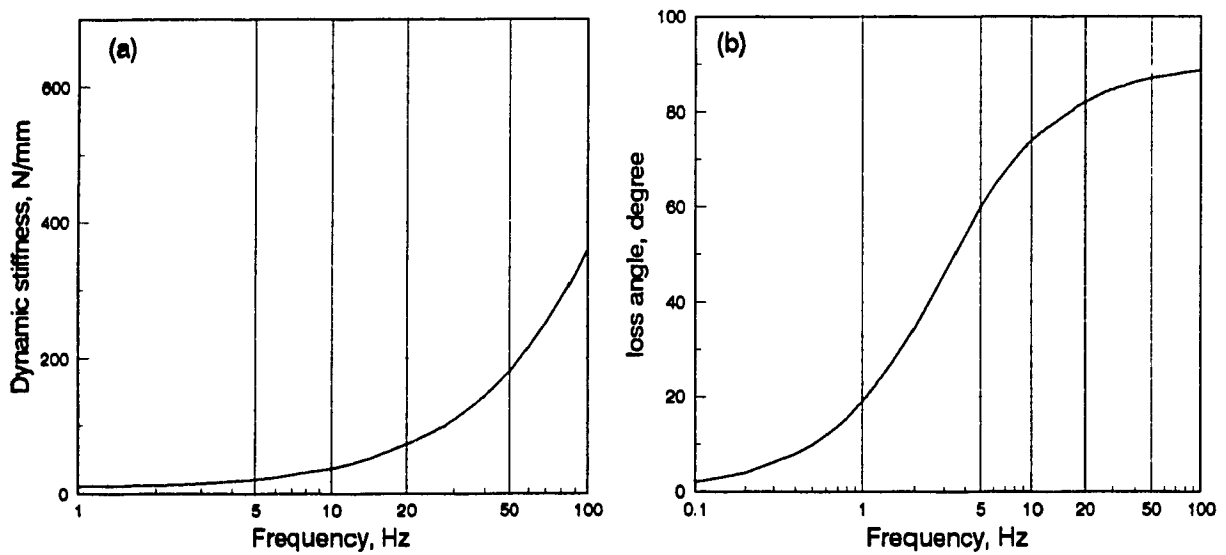


Figure 4.3 Dynamic stiffness and loss angle characteristics of a high-low dual phase damper. ( $A=10\text{mm}$ ,  $\alpha = 3.0$ ,  $\zeta=0.25$ , and  $\beta = 2$ ;  $X_1 = 40\text{mm}$ ).

found to be 375 N/mm (Figure 4.3a) at 100 Hz which is almost 25% lower than the dynamic stiffness produced by a low-high damper. Comparison of loss angle characteristics for low-high (Fig. 4.2b) and high-low (Fig. 4.3b) dampers shows identical trend where the loss angle for high-low damper is consistently lower for the entire frequency range.

#### 4.2.1 Parametric study

The objective for the parametric study here is to examine the influence of dual-phase parameters on the dynamic damping characteristics. The dual-phase parameters that are of interest include: (a) transition factor  $\beta$  for damping ratio; and (b) transition factor  $\alpha$  for displacement. A parameter further considered is the amplitude of excitation. One parameter is varied at a time while all other parameters are held constant and equal to their nominal values stated earlier.

(a) *Effect of Transition Factor  $\beta$  for Damping Ratio:* The transition factor  $\beta$  is the ratio between low and high damping of a dual-phase damper. By keeping  $\zeta_1$  constant as 0.25,  $\zeta_2$  is varied as 0.35, 0.50 and 0.65 which results in a value of  $\beta$  equal to 1.4, 2.0 and 2.6, respectively. Lissajous plots of a low-high damper for each of these  $\beta$  values are shown in Figure 4.4. The plots are obtained for a frequency ratio of 0.8 Hz. The results show that as the factor  $\beta$  is increased, the size of the loop of the Lissajous plot also increases. It is also observed that increase in damping ratio also increase the nonlinearity of the loop geometry. At low damping ratio (Figure 4.4a), the Lissajous plot shows that the system is almost linear. The results further show that there is an increase in peak transmitted force with the increase in damping factor  $\beta$ .

The effect of damping parameter  $\beta$  on the damper characteristics is also observed for a high-low damper. Figure 4.5 shows the Lissajous plots of high-low damper for three values of damping parameter  $\beta$ . The results show that for the

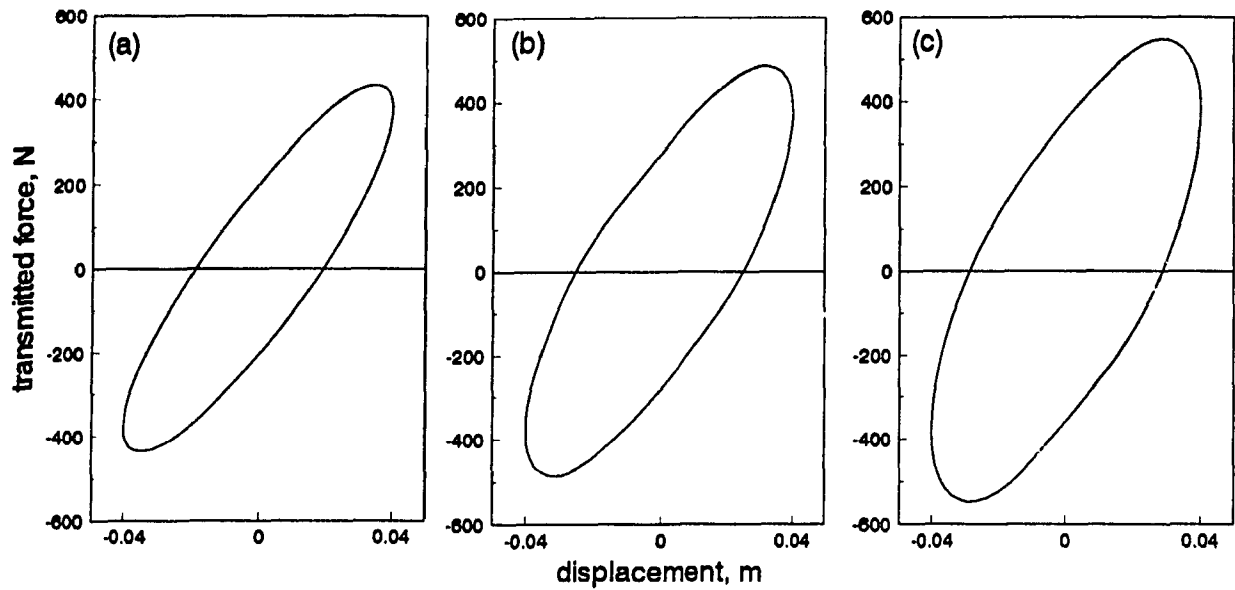


Figure 4.4 Lissajous plots of a low-high dual phase damper with the variation of  $\beta$ . ( $A=10\text{mm}$ ,  $\alpha = 3$ ,  $\zeta=0.25$ , and  $X_1 = 40\text{mm}$ )

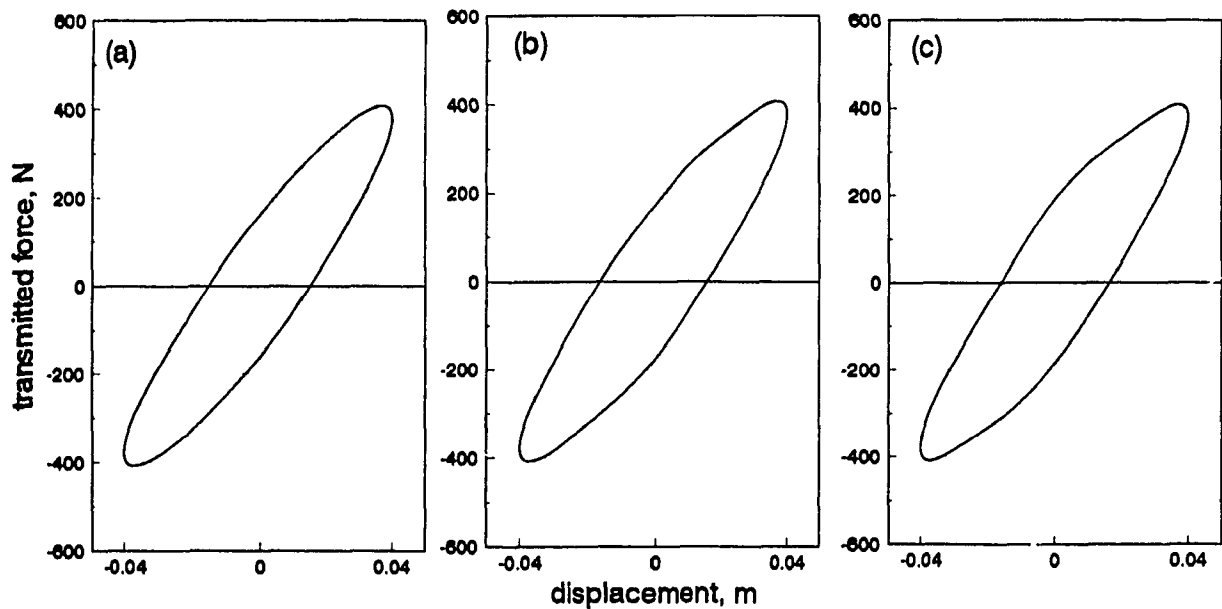


Figure 4.5 Lissajous plots of a high-low dual phase damper with the variation of  $\beta$ . ( $A=10\text{mm}$ ,  $\alpha = 3$ ,  $\zeta=0.25$ , and  $\beta = 2$ ;  $X_1 = 40\text{mm}$ )



particular geometry of damper considered here, variation of damping parameter  $\beta$  does not change the energy dissipation capacity of the damper. It has negligible effect on damping force development for the frequency and amplitude used. In this case, the amplitude of excitation and transition point of displacement are not varied, therefore, the excitation cycle passes only a small portion of the high damping region. Consequently, the damping force development does not change significantly. If the transition point of displacement is kept lower or the amplitude of excitation is kept higher, one may see the changes in the energy dissipation. With the increase in damping ratio, only the nonlinearity in the geometry of the loop is observed (Figure 4.5c).

Figure 4.6 shows the variation of dynamic stiffness and loss angle property of the low-high dual-phase damper as a function of frequency for the three values of  $\beta$ . For the case of low-high damper, it is observed that an increase in damping ratio ( $\zeta_2$ ) increases the dynamic stiffness throughout the whole range of frequency (Figure 4.6a). For damping ratio  $\zeta_2 = 0.65$ , the dynamic stiffness goes up to 600 N/mm whereas static stiffness is only 10 N/mm. Increase in damping ratio also increases the loss angle throughout the whole range of frequency until it reaches a maximum value which is close to 90 degree. The rate of increase in loss angle around resonance frequency is found to be maximum which is desirable to dampen the resonance amplitude.

Similar to Figure 4.6, Figure 4.7 shows the variation of dynamic stiffness and loss angle property of a high-low damper. As explained earlier, the excitation cycle does not pass a considerable amount through the high damping ratio region, therefore, the increase in damping ratio  $\zeta_2$  will not affect the dynamic stiffness and loss angle of the damper like low-high damper. The high-low displacement sensitive damper is a low-high velocity sensitive damper, therefore, for the same

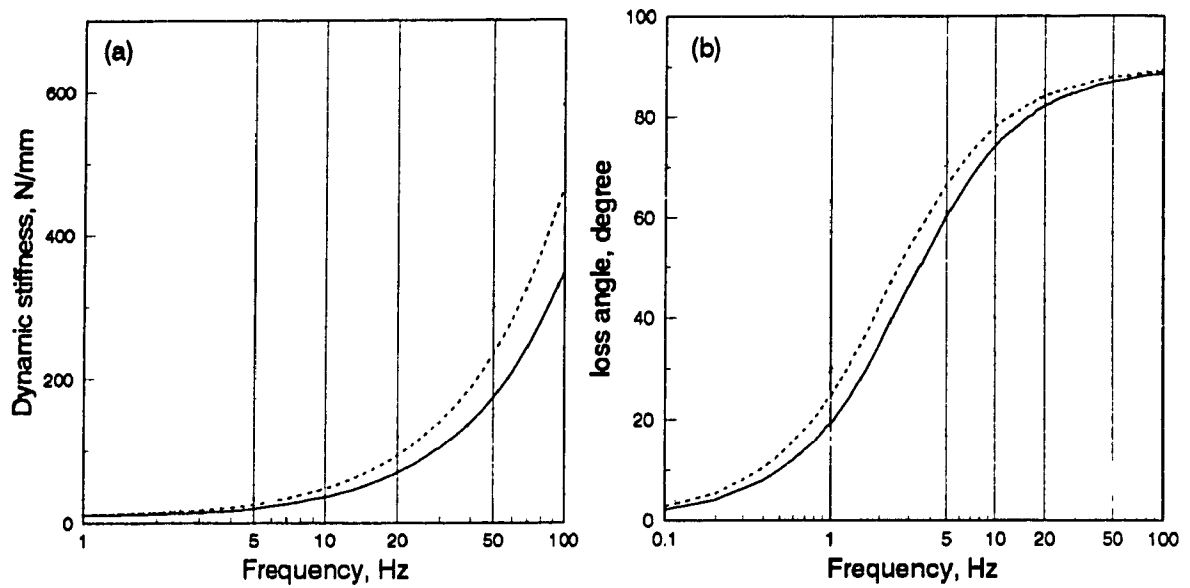


Figure 4.6 Effect of damping parameter on dynamic characteristics of a low-high damper. Transition point of damping ratio,  $\beta$ , —, 1.4; ----, 2.0; ·····, 2.6. ( $A = 10\text{mm}$ ,  $\alpha = 3.0$ ,  $\zeta = 0.25$ ;  $X_1 = 40\text{mm}$ ).

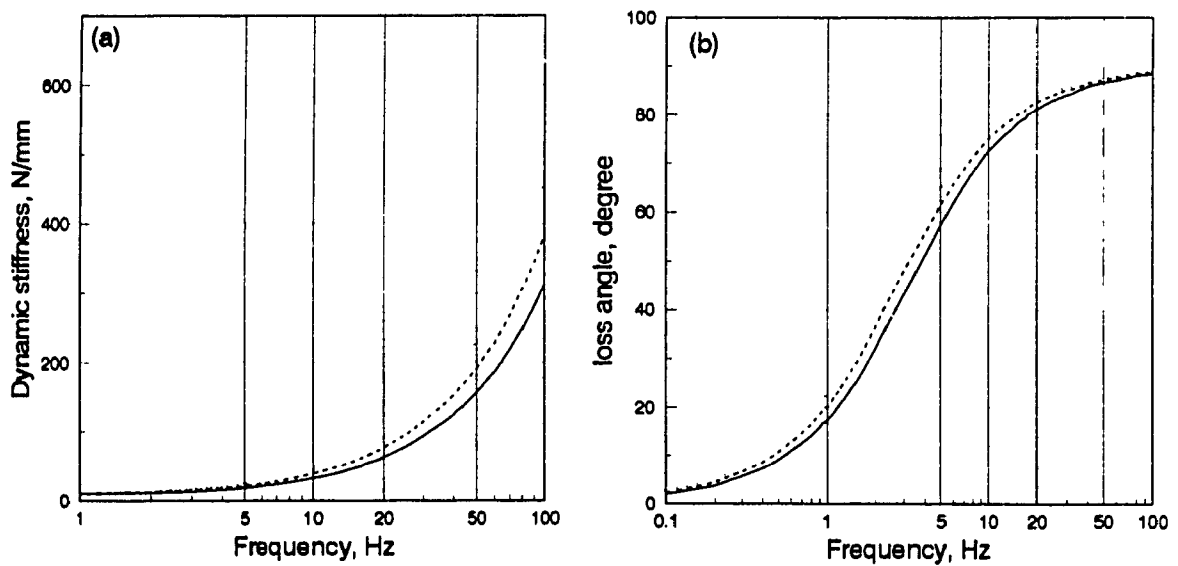


Figure 4.7 Effect of damping parameter on dynamic characteristics of a high-low damper. Transition point of damping ratio,  $\beta$ , —, 1.4; ----, 2.0; ·····, 2.6. ( $A = 10\text{mm}$ ,  $\alpha = 3$ ,  $\zeta = 0.25$ ;  $X_1 = 40\text{mm}$ ).

increase in damping ratio, the increase in dynamic stiffness and loss angle does not occur like low-high damper. The trend in both cases are, however, very similar.

(b) Effect of Transition Factor  $\alpha$  for Displacement: The transition factor  $\alpha$  for displacement dictates the motion required for transition from one damping value to the other. For the case of a low-high damper, increase in transition factor  $\alpha$  for displacement increases the relative displacement or time required to reach the higher damping ratio, thus reducing the effective damping. This can also be viewed as the relative velocity being exposed to higher damping ratio for lesser time, therefore, the dynamic stiffness and loss angle will decrease. Figure 4.8 shows the effect of variation of  $\alpha$  on the characteristics of the damper. The transition in damping ratio from  $\zeta_1$  starts at  $A = 10$  mm and the linear increment in damping ratio is stopped at  $\alpha A = 20$  mm, 40 mm and 60mm. Therefore, the increase in transition factor for displacement is varied as 2, 4 and 6. Other parameters are taken as  $\zeta_1 = 0.25$  and  $\zeta_2 = 0.50$ . As expected, it is found that an increase in  $\alpha$  decreases the dynamic stiffness of the damper throughout the whole range of frequency (Figure 4.8a) except at low frequency where dynamic stiffness is equal to spring stiffness. For the same reason, the loss angle decreases with the increase in transition factor  $\alpha$  (Figure 4.8b).

For the case of a high-low damper, increase in transition factor for displacement increases the transition region [region (b) in Figure 2.2] of the damper which turns it into a damper of higher damping ratio. So, the increase in  $\alpha$  for high-low damper increases the dynamic stiffness and loss angle as shown in the Figures 4.9a and 4.9b. This effect is quite contrary to that of low-high damper where increase in  $\alpha$  decreases the dynamic stiffness. Although the effect is opposite, the trend in variation in both cases are very similar.

(c) Effect of Amplitude of Excitation: Amplitude of excitation may have important effect on the characteristics of a dual-phase damper as it dictates the

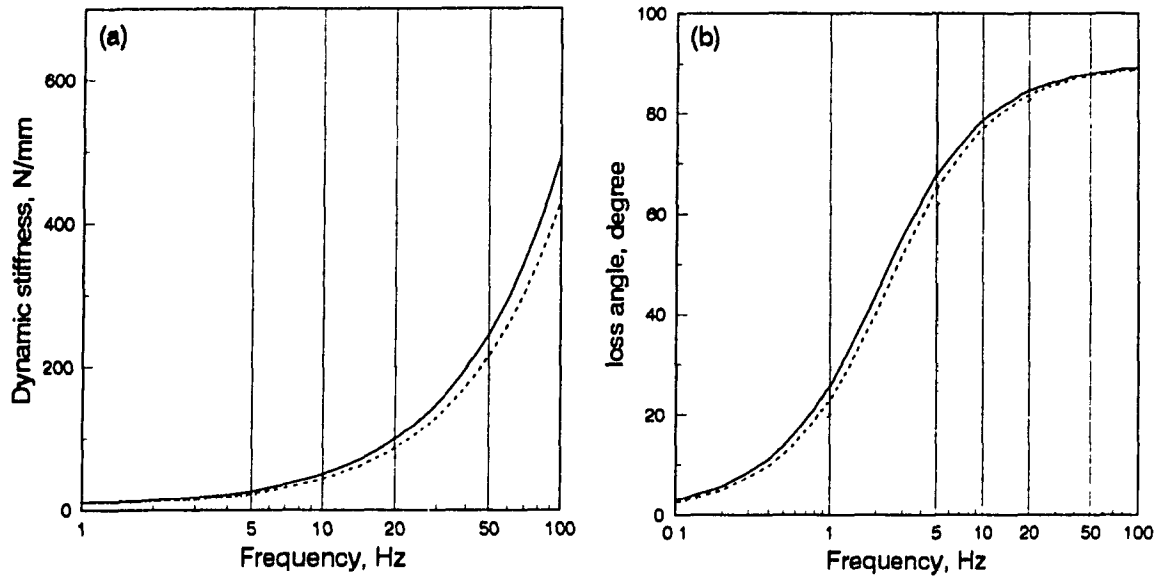


Figure 4.8 Effect of transition point of relative displacement on dynamic characteristics of a low-high damper;  $\alpha$ , —, 2.0; ----, 4.0; ·····, 6.0. ( $A = 10\text{mm}$ ,  $\alpha = 3.0$ ,  $\zeta = 0.25$ ;  $X_1 = 40\text{mm}$ ).

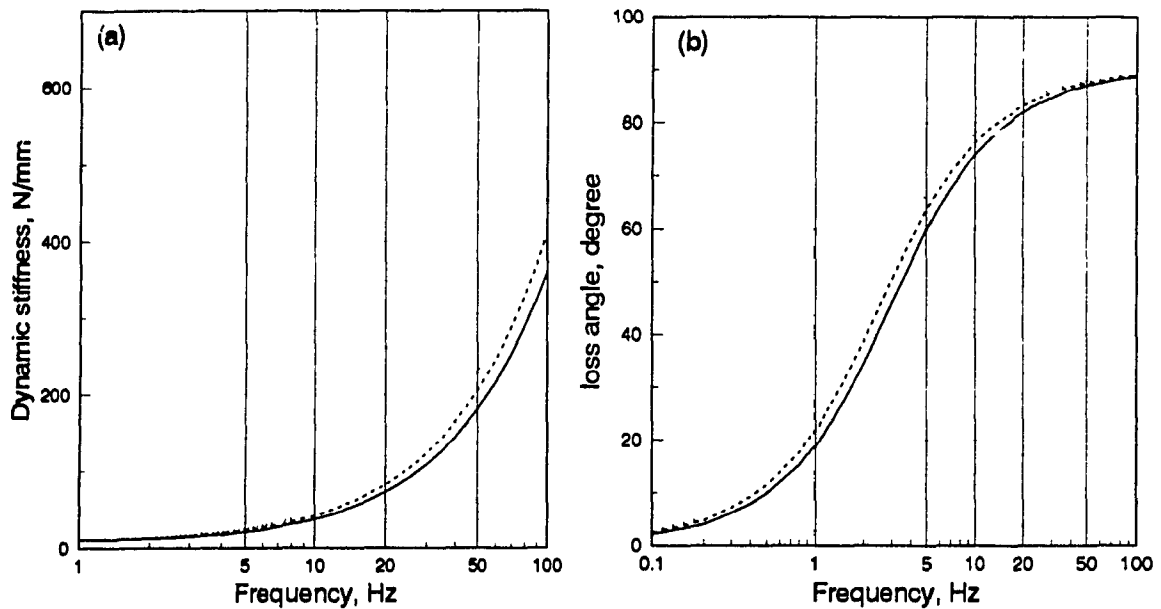


Figure 4.9 Effect of transition point of relative displacement on dynamic characteristics of a high-low damper;  $\alpha$ , —, 2; ----, 4; ·····, 6. ( $A = 10\text{mm}$ ,  $\alpha = 3$ ,  $\zeta = 0.25$ ;  $X_1 = 40\text{mm}$ ).

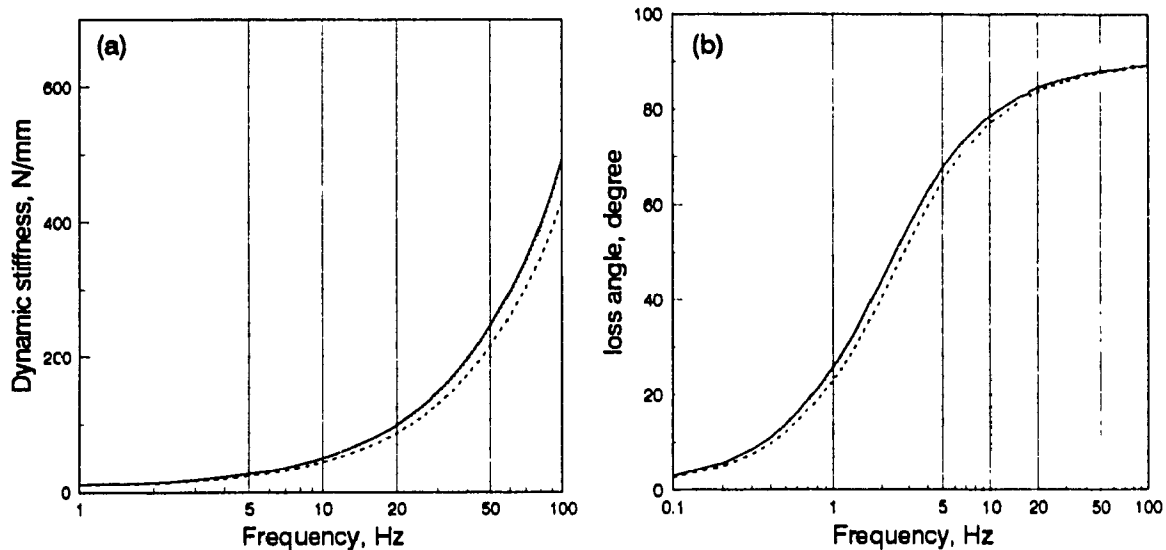


Figure 4.10 Effect of amplitude of excitation on dynamic characteristics of a low-high damper;  $\alpha$ , —, 2.0; ----, 4.0; ·····, 6.0. ( $A = 10\text{mm}$ ,  $\alpha = 3$ ,  $\zeta = 0.25$ ;  $X_1 = 40\text{mm}$ ).

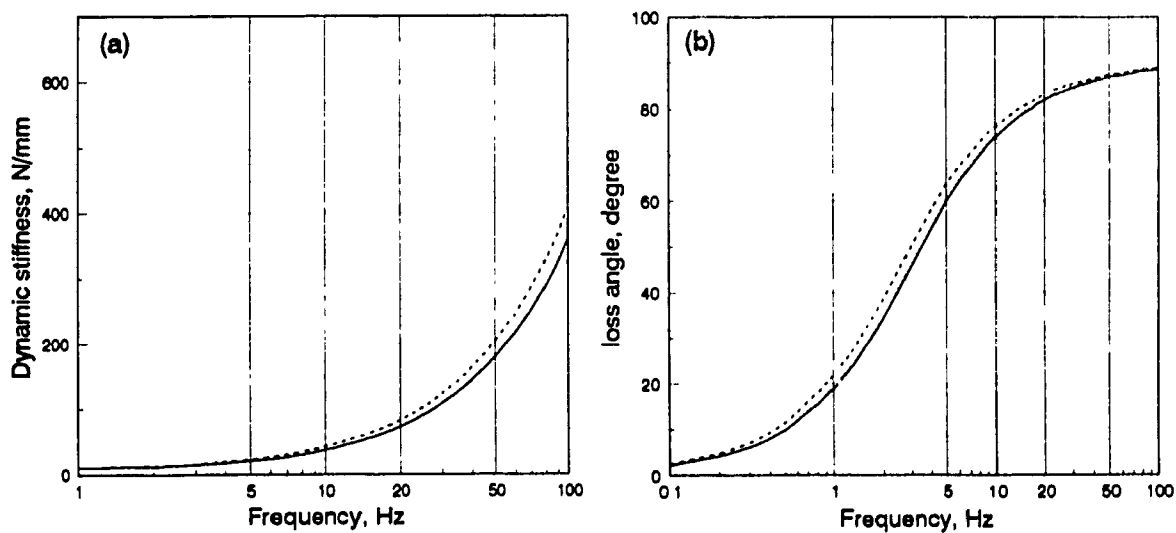


Figure 4.11 Effect of amplitude of excitation on dynamic characteristics of a high-low damper;  $\alpha$ , —, 2; ----, 4; ·····, 6. ( $A = 10\text{mm}$ ,  $\alpha = 3$ ,  $\zeta = 0.25$ ;  $X_1 = 40\text{mm}$ ).

phases of the damper that is included in a motion. A decrease in excitation amplitude will result in same effect as that of increasing the transition value  $\alpha$ . Figure 4.10 shows the effect of excitation amplitude for nominal low-high damper. The amplitude is varied as 10 mm, 20 mm and 40 mm. It is seen that decrease in dynamic stiffness for a change in amplitude from 10 mm to 20 mm is not noticeable, but the change in amplitude to 40 mm decreases both the dynamic stiffness and loss angle of the damper.

Similar to the effect of transition factor  $\alpha$  on the high low damper, the effect of excitation amplitude is opposite in the case of high-low damper. Increase in excitation amplitude increases the dynamic stiffness and loss angle as show in Figure 4.11. Like before, change in amplitude from 10 mm to 20 mm is not noticeable but an increase to 40 mm increases the dynamic stiffness and loss angle of the high-low damper.

### **4.3 Performance of the Damper**

The model developed for dual-phase damper in this study based on integral formulation of damping force characteristics provides significantly different property and performance as demonstrated in chapter 2. The objective of this section is to carry out a detailed performance evaluation of both low-high and high-low dual-phase dampers.

The performance evaluation is carried out by utilizing a one ODF mass-spring-damper system as shown in Figure 2.5. The suspended mass weighs 75 kg and the isolator consists of a dual-phase damper and a linear spring of stiffness 10 N/mm. The value of spring constant is chosen such that the undamped natural frequency is close to 2 Hz. The suspension system of a vehicle has natural frequency within the range 1.5 to 2 Hz. A linear spring is chosen so that the nonlinearity within the damper can be analyzed in depth. The base of the system is excited either

sinusoidally or by the application of shock of different severity. The response due to the application of external input is measured at the sprung mass. For sinusoidal input, response characteristics are determined by the acceleration transmissibility and relative displacement transmissibility in the frequency domain. The range for the frequency of excitation is chosen from 1 to 10 as frequency ratio. The frequency ratio is defined as the ratio of excitation frequency to the system's natural frequency ( $\omega/\omega_0$ ). The frequency response is obtained utilizing the local equivalent linearization technique formulated and shown to be highly effective in chapter 2.

The rounded pulse type of shock input is chosen to evaluate its performance under shock input. The rounded pulse input of different severity is commonly used for performance evaluation of isolators [43]. The response of the mass in terms of acceleration ratio, velocity ratio, displacement ratio and relative displacement ratio are obtained in time domain for a given shock severity. The response is also obtained in terms of shock acceleration ratio (SAR), shock velocity ratio (SVR), shock displacement ratio (SDR) and shock relative displacement ratio (RDR) as a function of shock severity ranging from 0.05 to 5. Such performance indices are also common for comparison of isolators [21, 38].

#### **4.3.1 Application of Sinusoidal Input**

The mass-spring-damper system is base excited using a sinusoidal signal of amplitude of 40 mm for a range of frequency ratio of 1 to 10. The transmissibility curves for the low-high dual-phase damper is shown in Figure 4.12. As the system is nonlinear, the response due to the sinusoidal input is not purely sinusoidal but periodic. Therefore, the response of the system is defined as the root mean square (rms) acceleration transmissibility and rms relative displacement transmissibility.

The rms acceleration transmissibility is defined as the ratio of the rms acceleration of the sprung mass to the rms acceleration of the input.

Figure 4.12a shows the rms acceleration transmissibility characteristics of a low high damper (solid line) with parameters  $A = 10$  mm,  $\alpha = 3$ ,  $\zeta_1 = 0.25$  and  $\zeta_2 = 0.35$  (or  $\beta = 1.4$ ). Transmissibility performance is found excellent around resonance frequency as well as around high frequency zone. Relative displacement transmissibility just passes unity at around resonance frequency and remains at unity throughout the high frequency zone, which is illustrated in Figure 4.12b.

Figure 4.13 shows the performance characteristics of a high-low damper (solid line) with identical parameters as those used for the low-high damper. It is observed earlier that for similar parameters, the high-low damper produces lower dynamic stiffness, therefore it will produce higher transmissibility around resonance zone and lower transmissibility around high frequency zone. Compared to Figure 4.12, the high-low damper has an acceleration transmissibility greater than 2 but high frequency transmissibility is better than that of low-high damper. So for a better high frequency transmissibility requirement, a high-low damper is desirable. For a high-low damper, relative displacement transmissibility at resonance is also higher as shown in Figure 4.13b.

#### **4.3.1.1 Parametric study**

Parametric study is also carried out to investigate the influences of damper parameters pertaining to better response characteristics of the dual-phase damper. The parameters chosen as variables for the parametric study are (a) transition point in damping ratio  $\beta$ , and (b) transition point in displacement  $\alpha$ . The effect of amplitude of excitation on the dynamic performance of the damper is also studied. One parameter is varied at a time while all others are kept equal to their nominal values.



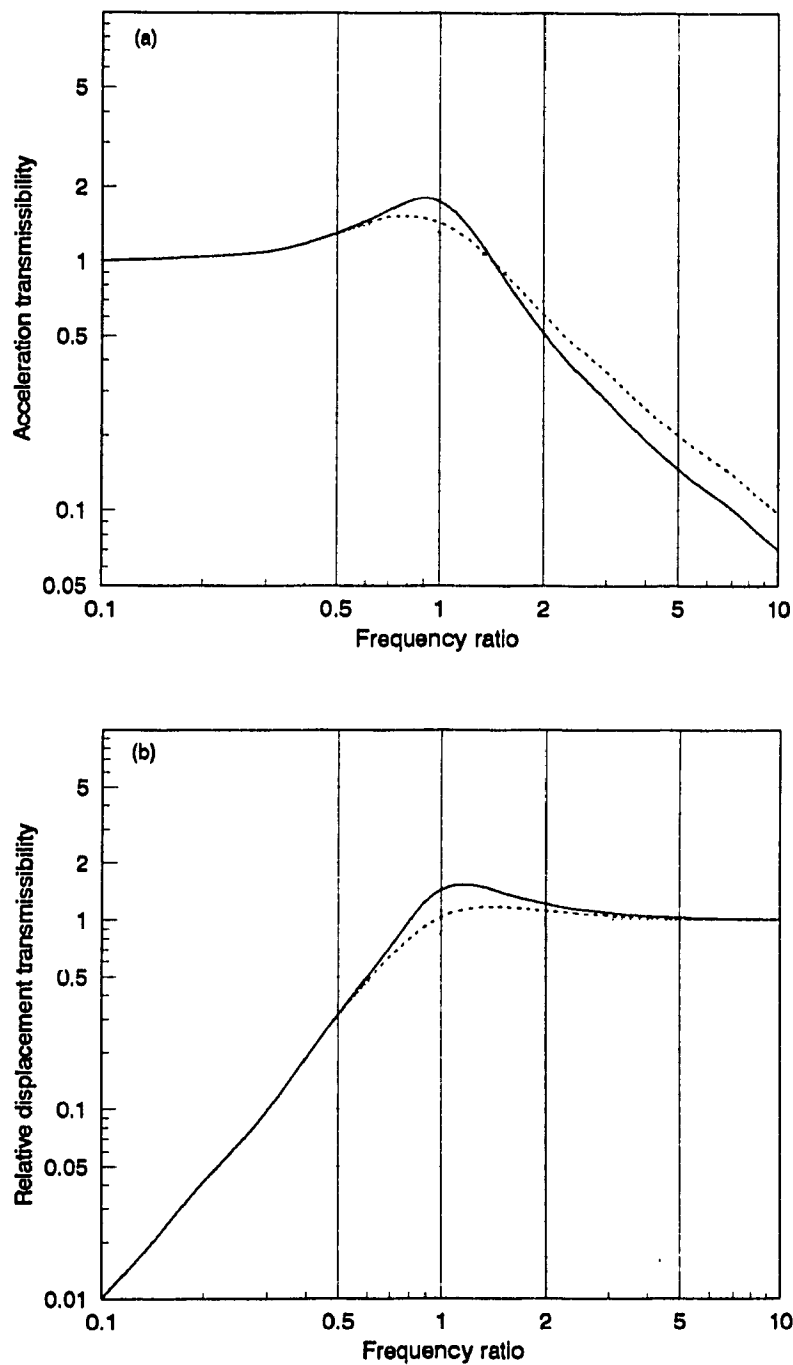


Figure 4.12 Performance of a low-high damper with the variation in transition point of damping ratio  $\beta$ , —, 1.4; ----, 2.0; ·····, 2.6; ( $A = 10\text{mm}$ ,  $\alpha = 3$ ;  $\zeta = 0.25$  and  $X_1 = 40\text{mm}$ ).

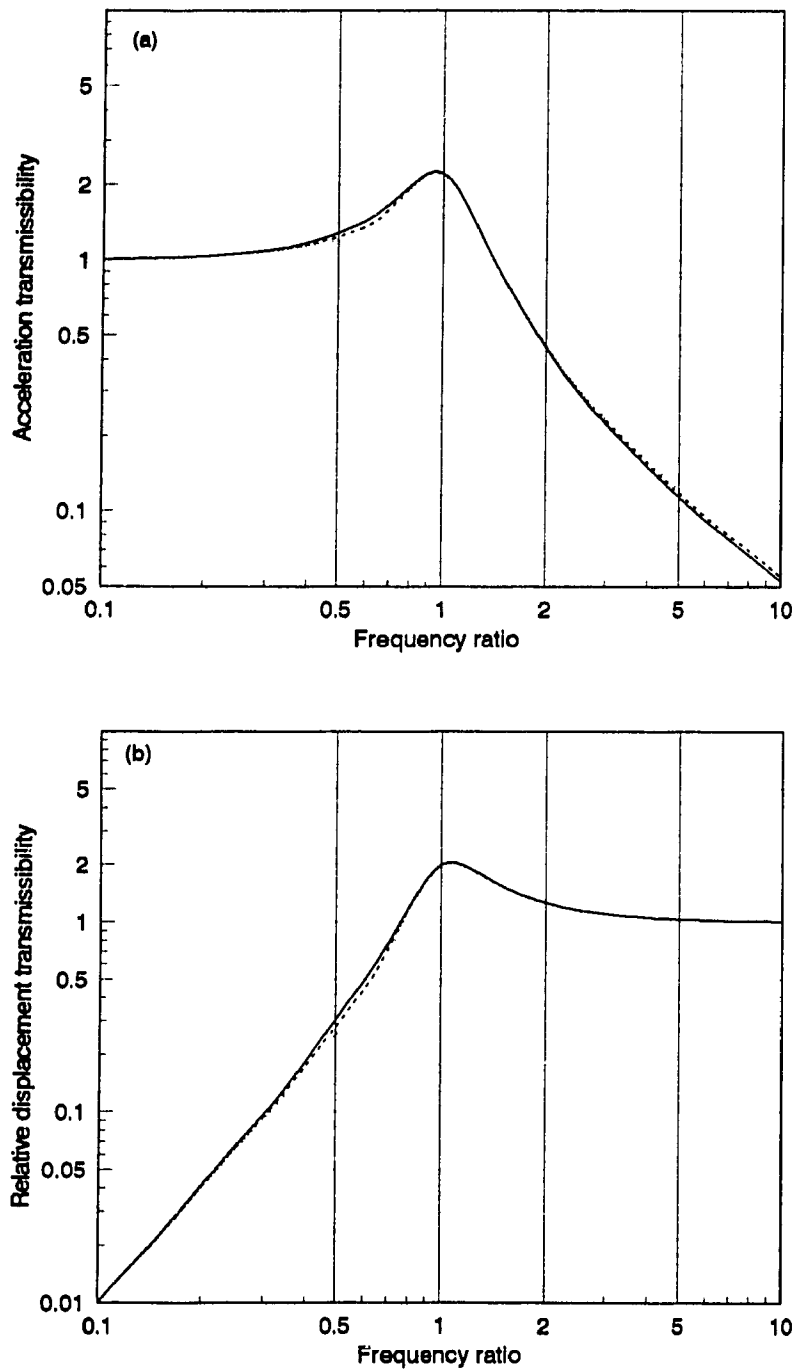


Figure 4.13 Performance of a high-low damper with the variation in transition point of damping ratio  $\beta$ , —, 1.4; ----, 2.0; ·····, 2.6; ( $A = 10\text{mm}$ ,  $\alpha = 3$ ;  $\zeta = 0.25$  and  $X_1 = 40\text{mm}$ ).

(a) Effect of Transition Point in Damping Ratio,  $\beta$  : Figure 4.12 presented earlier further shows the effect of transition point in damping ratio on the acceleration transmissibility and relative displacement transmissibility of a low-high damper. The higher damping ratio is varied as 0.35, 0.50 and 0.65, therefore, the values of transition point in damping ratio,  $\beta$  are 1.4, 2.0 and 2.6 respectively. The other parameters are  $\zeta_1 = 0.25$ ,  $A = 10$  mm and  $\alpha = 3$ . The amplitude of excitation is taken as 40 mm. It is observed that the increase in  $\beta$  decreases the transmissibility at resonance even lower (around 1.5) with a sacrifice in transmissibility at high frequency. It may be noticed that the increase in  $\beta$  value from 2.0 to 2.6 does not affect the transmissibility at resonance to that extent as it does at high frequency transmissibility. Therefore, there exists an optimal  $\beta$  value that can improve resonance performance without significant loss at high frequency.

Increase in  $\beta$  value is, however, very contributory for the performance as relative displacement transmissibility. As shown in Figure 4.12b, the relative transmissibility at resonance reduces for larger  $\beta$  which is desirable for the efficient and compact design of the system. At higher  $\beta$  value (2.6) the transmissibility goes much below than unity at resonance frequency which is highly satisfactory.

The effect of  $\beta$  value for the case of high-low damper is shown in Figure 4.13. It may be recalled that Figure 2.12 shows increase in equivalent damping ratio only at low frequency, with very little changes around resonance and high frequencies for an increase in  $\beta$  value. That observation is reflected into Figure 4.13a and 4.13b. It is found that the increase in  $\beta$  value does not change the resonance transmissibility for both acceleration and relative displacement. The changes observed can be considered negligible. Such behavior for the high-low dual-phase damper can not be predicted using the traditional approach for damping

force [36]. Since the effect of  $\beta$  in that case is more significant for both resonance and high frequency damping ratio as shown in Figure 2.12.

(b) *Effect of Transition Point in Displacement,  $\alpha$*  : The response of the dual-phase damper is observed for both low-high and high-low types with the variation of transition point in displacement,  $\alpha$ . Variation of  $\alpha$  influences the effective damping ratio of both the systems which, in turn, affects the systems' transmissibility. In the parametric study of damper characteristic presented in section 4.2.1 it is found that for low-high damper, an increase in  $\alpha$  value decreases the effective damping ratio throughout the frequency range. This, in turn, will lead to higher transmissibility at resonance frequency and lower high frequency transmissibility. Figure 4.14 shows the effect of  $\alpha$  on acceleration transmissibility and relative displacement transmissibility for a low-high damper. The  $\alpha$  is varied as 2, 4 and 6 which makes the damper reach the higher damping ratio  $\zeta_2$  at displacements of 20 mm, 40 mm and 60 mm, respectively. It is seen that the increase in  $\alpha$  value increases the resonance transmissibility and decreases the high frequency transmissibility. It is found that increase in  $\alpha$  value from 4 to 6 makes a significant decrease in high frequency transmissibility with a minor increase in resonance transmissibility both in acceleration and relative displacement. Therefore, once again, there exists an optimal value for  $\alpha$  in the case of low-high damper which will provide a better compromise between resonance and high frequency response.

Effect of transition factor  $\alpha$  on to the high-low damper is shown in section 4.2.1 to be contrary to that of a low-high damper. Figure 4.15 further shows that increase in  $\alpha$  slightly improves the resonance transmissibility, for a worst performance at high frequency. The results presented in Figure 4.15 further indicate that although relative displacement transmissibility is not significantly

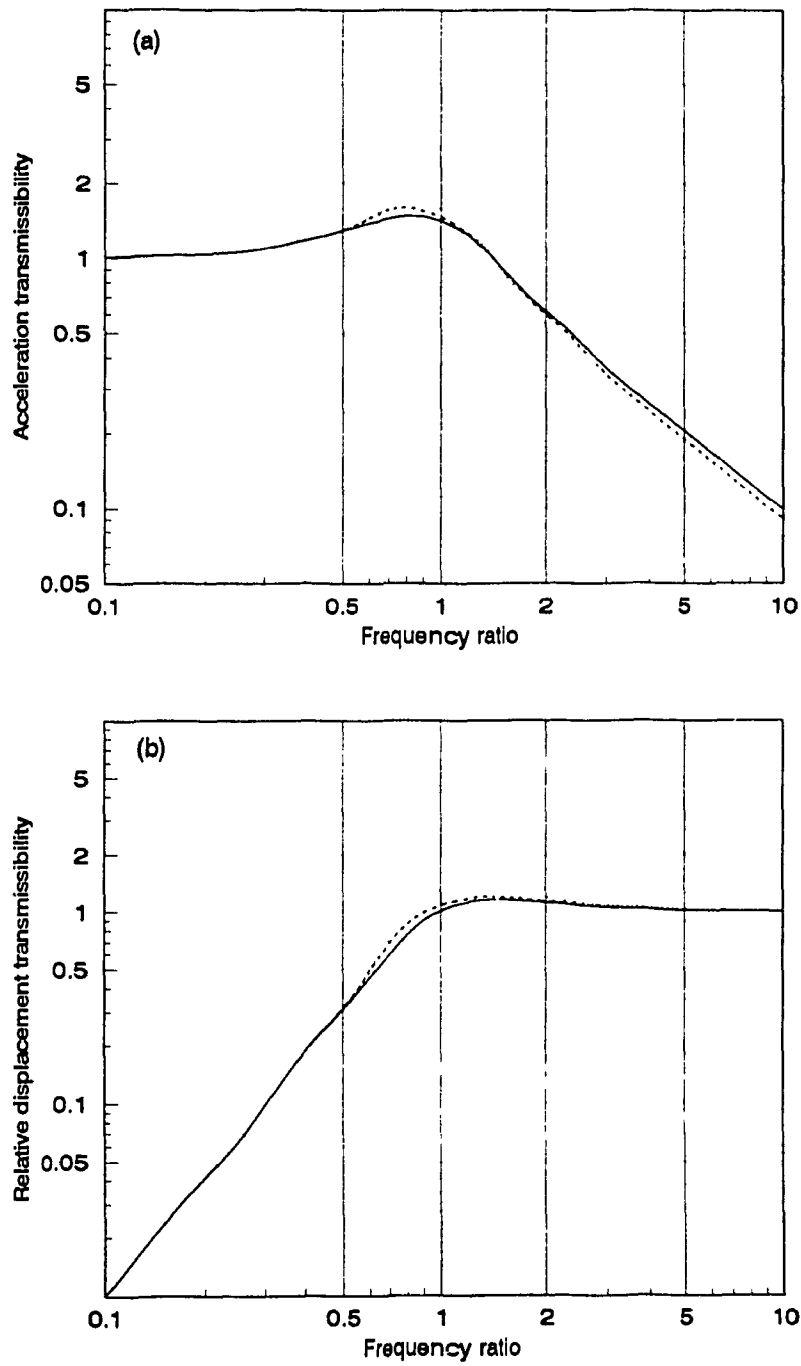


Figure 4.14 Performance of a low-high damper with the variation in transition point in relative displacement  $\alpha$ ; —, 2; ----, 4; ·····, 6; ( $A = 10\text{mm}$ ,  $\beta = 2$ ;  $\zeta = 0.25$  and  $X_1 = 40\text{mm}$ ).

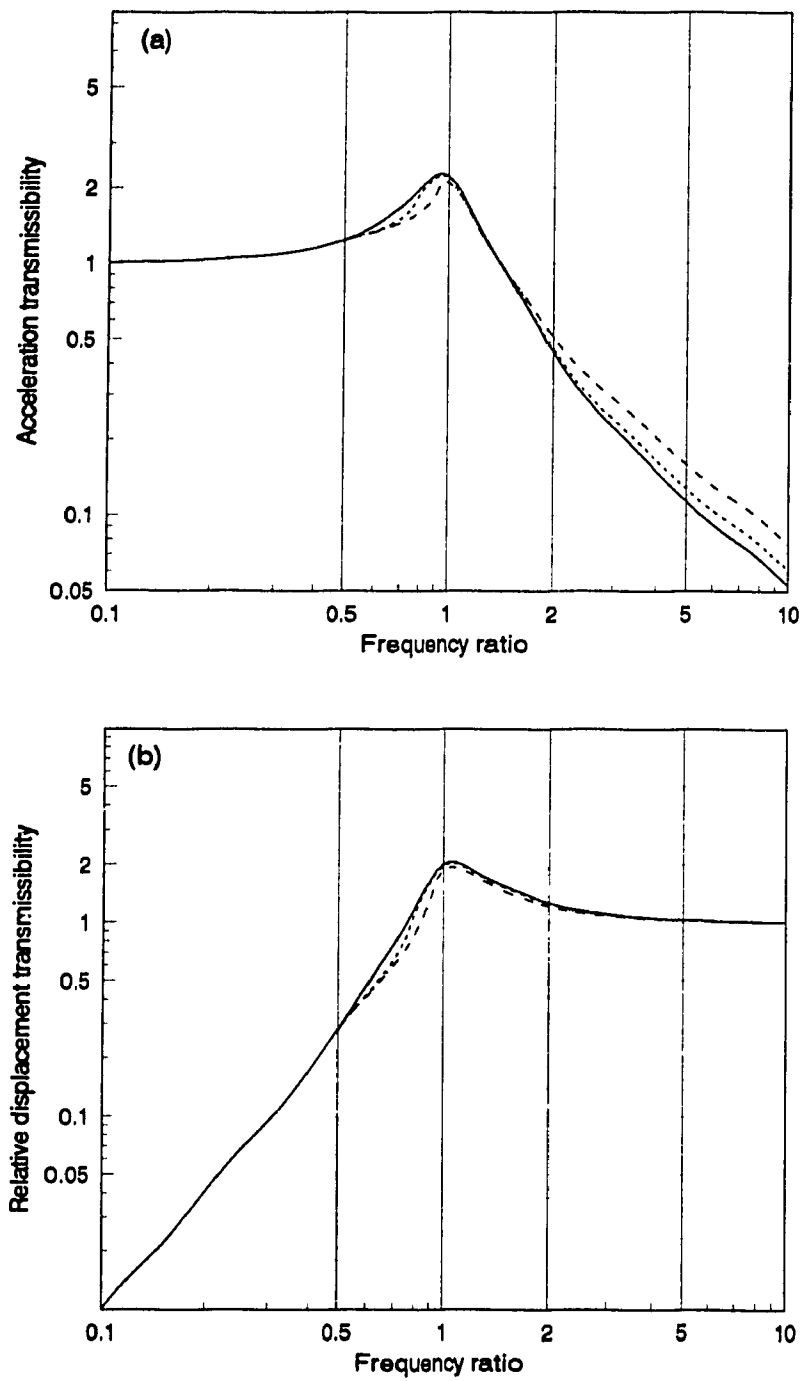


Figure 4.15 Performance of a high-low damper with the variation in transition point in relative displacement  $\alpha$ ; —, 2; ----, 4; ·····, 6; ( $A = 10\text{mm}$ ,  $\beta = 2$ ;  $\zeta = 0.25$  and  $X_1 = 40\text{mm}$ ).

affected by  $\alpha$ , an increase in  $\alpha$  will primarily lead to poor high frequency performance.

(a) Effect of Amplitude of Excitation: The influence of excitation amplitude on the performance of dual-phase dampers is finally examined. The models with baseline parameters are considered under three different amplitude of excitations. The amplitudes used are 10 mm, 20 mm and 40 mm. Results in terms of acceleration transmissibility and relative displacement transmissibility are plotted in Figure 4.16 for a low-high damper and in Figure 4.17 for a high-low damper.

For the case of a low-high damper, lower amplitude of excitation means the damper is active only for lower range of damping ratio. Therefore, transmissibility will be higher at resonance and lower at high frequency. It is seen from the Figure 4.16 that the increase in amplitude of excitation improves the transmissibility at resonance with the expense of higher transmissibility at high frequency. Relative transmissibility (Figure 4.16b) also decreases with the increase in amplitude of excitation. The effect is typical to that of damping ratio variation in a linear system.

In general, the opposite effect occurs for the case of high-low dual-phase damper with identical parameters. With the increase in amplitude, transmissibility at resonance deteriorates severely but the transmissibility at high frequency improves. In this case, however, the effect is not linear. It is interesting to note that a high-low damper for the given parameter and excitation of 40 mm amplitude (Figure 4.17, chained line) produces similar performances to that of a low-high damper with the excitation of 10 mm amplitude (Figure 4.16, solid line). The reverse also holds true. This parametric study clearly indicates that a dual-phase damper, specifically displacement sensitive, must be designed for isolation of a given vibration environment in order to achieve its potential performance.

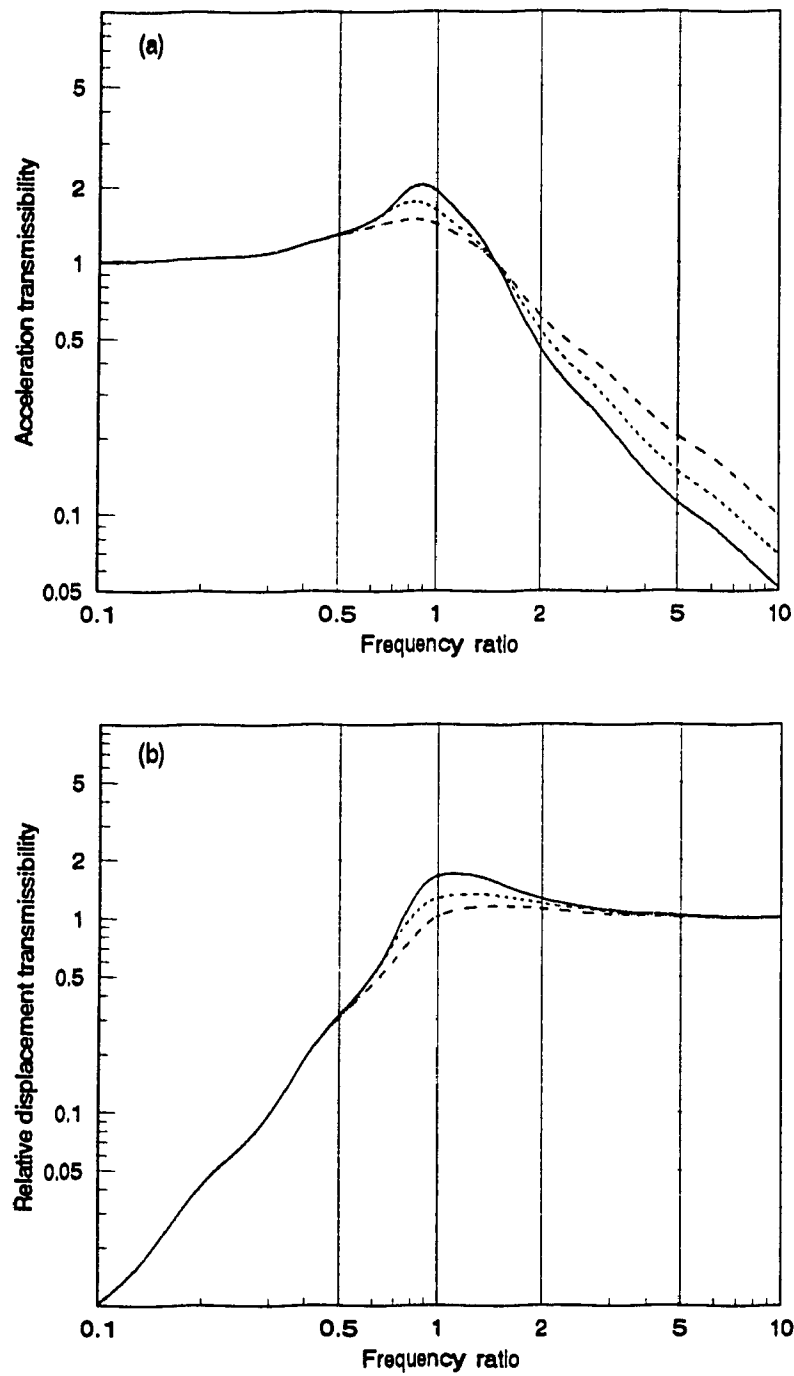


**Figure 4.16** Transmissibility characteristics of a low-high damper.  $X_1$  —, 10mm; ---, 20mm; ···, 60mm. ( $A = 10\text{mm}$ ,  $\alpha = 3$ ;  $\zeta = 0.25$  and  $\beta = 2$ ).



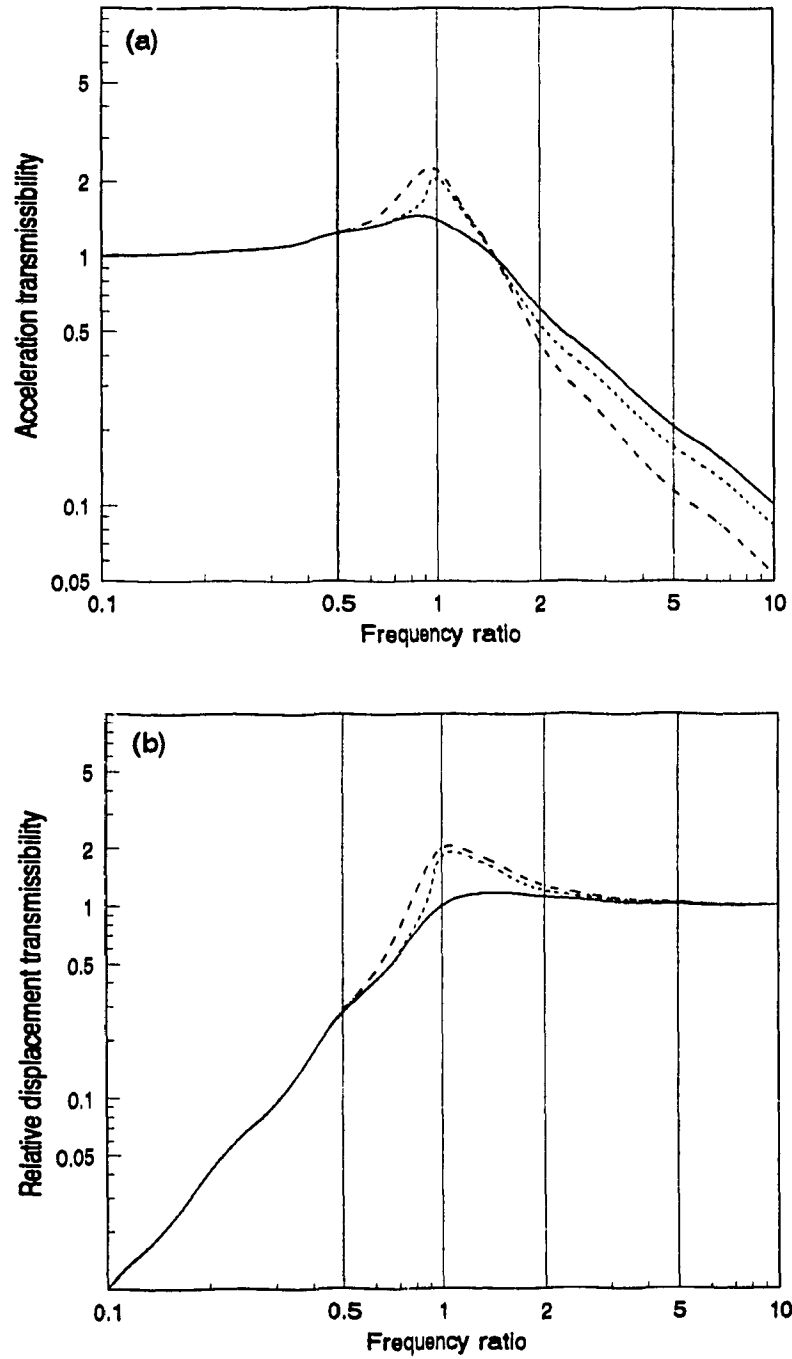


Figure 4.17 Transmissibility characteristics of a high-low damper.  $X_1$  —, 10mm; ---, 20mm; ···, 60mm. ( $A = 10\text{mm}$ ,  $\alpha = 3$ ;  $\zeta = 0.25$  and  $\beta = 2$ ).

A comparative result is finally presented to demonstrate the potential of dual-phase dampers. Figure 4.18 shows a good set of performance for low-high damper. These results are superimposed by the response of linear viscous dampers ( $\zeta = 0.25$  and  $0.50$ ) corresponding to the low or high value of damping. It is observed from the figure that, for high linear damping provides good isolation in the low frequency range but performs poorly in the high frequency range. However, lower damping provides good isolation at high frequencies, but performance is very poor in the low frequency region. But for any value of  $\alpha$ , the dual-phase damper with these two damping value ( $0.25$  and  $0.50$ ) show better transmissibility response both in resonance and high frequency. Its performance at resonance is much better than that of linear damper with low damping but slightly higher than that of linear damper with high damping. Opposite effect is true for high frequency response. It is, thus, appropriate to say that the dual-phase damper has a compromising performance in the low frequency as well as high frequency range.

#### 4.4 Description of Shock Input

Isolators designed for attenuation of vibration may often be subjected to shock inputs in practice. Unless an isolator is designed only for vibration, its performance should be evaluated based on its potential in isolating both vibration and shock. This section of the chapter is devoted towards the performance of displacement sensitive dual-phase dampers in isolation of shock excitation. In all cases, rounded pulse displacement of various severity is used as input. The following subsections describes these inputs and the performances for both low-high and high-low dampers. The performances are evaluated in terms of sprung mass displacement, velocity and acceleration responses as well as relative displacement both as a function of time and shock severity.

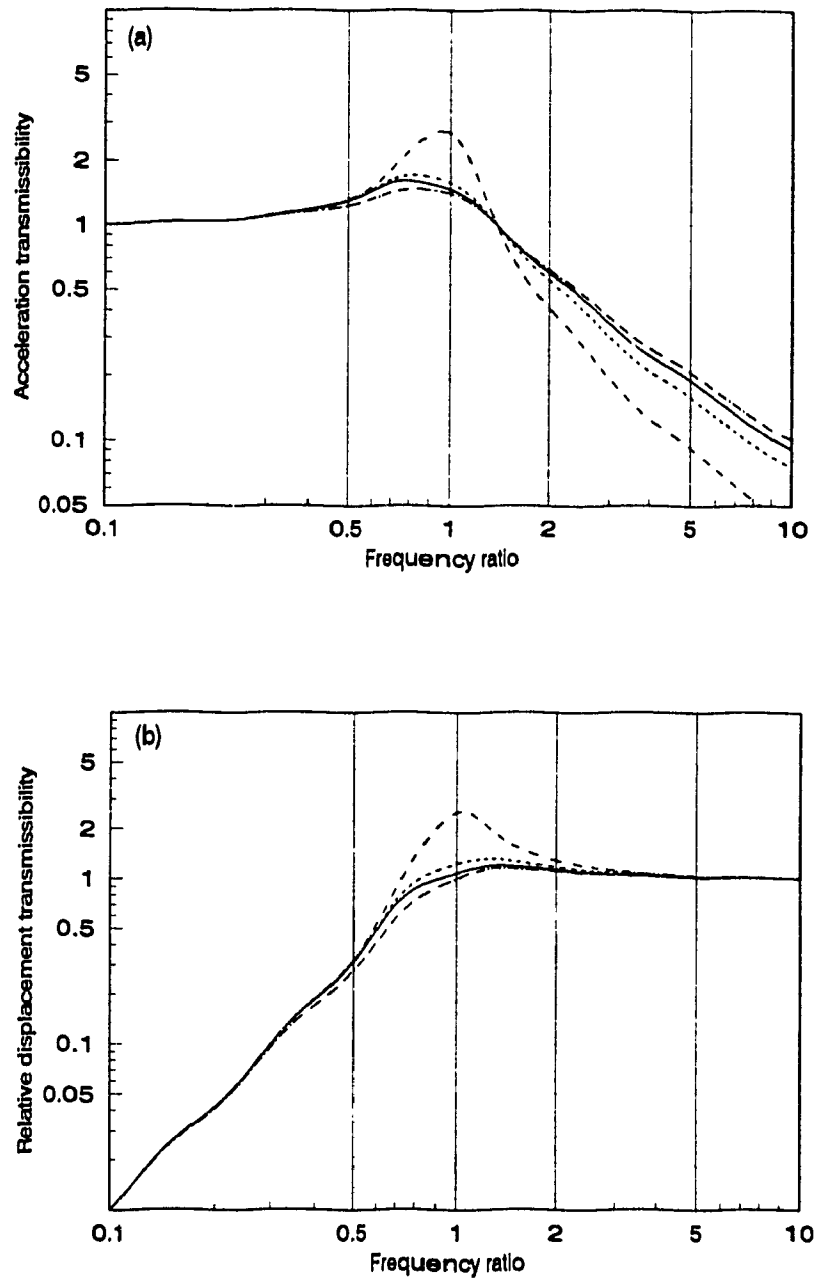


Figure 4.18 Comparison of a low-high damper with linear dampers of high and low damping value.  $\alpha$  —, 4; ----, 6; ···  $\zeta = 0.50$  (linear); - · -  $\xi = 0.25$  (linear); ( $X_1 = 40\text{mm}$ ,  $A = 10\text{mm}$ ,  $\zeta = 0.25$  and  $\beta = 2$ ).

#### 4.4.1 Characteristics of Shock Input

Two types of shock displacements may be considered to evaluate the dual-phase damper performances. These inputs commonly used [21,38,43,59] for evaluation of shock isolation performance of isolators, include:

(a) rounded pulse displacement input

(b) rounded step displacement input

(a) Rounded pulse displacement: A rounded pulse displacement may be defined by the following mathematical form.

$$y_s(t) = \frac{1}{4} Y_s (v\omega_o t)^2 e^{2-v\omega_o t} \quad (4.1)$$

where  $Y$  is the maximum magnitude of displacement,  $e = 2.71828..$  and  $v_p$  is the shock severity parameter. The shock severity parameter is defined as the ratio of half-period of the natural vibration of the system to the duration of the pulse; thus

$$v = \frac{T}{2\tau_p} = \frac{\pi}{\omega_o \tau_p} \quad (4.2)$$

where the duration  $\tau_p$  is defined as the length of an equivalent rectangular pulse that has the same area as that of the rounded pulse, but which is higher by 17.6% than  $Y_s$  and  $\omega_o$  is the natural frequency of the system.

Figure 4.19a shows the rounded pulse displacement for various shock severity parameter for a frequency of 7.5 Hz. This frequency corresponds to the natural frequency of the system considered as discussed in section 4.5.2. The shock severity parameter  $v$  for a rounded pulse input may be defined as the length of an equivalent rectangular pulse that has the same area as that of the rounded pulse, but which has a peak 17.6% higher than  $Y_s$ . The higher the value of  $v$  the higher the shock severity. As shown in Equation (4.2), the shock severity parameter  $v$  is a relative parameter, relative to the resonance frequency of the system. The same

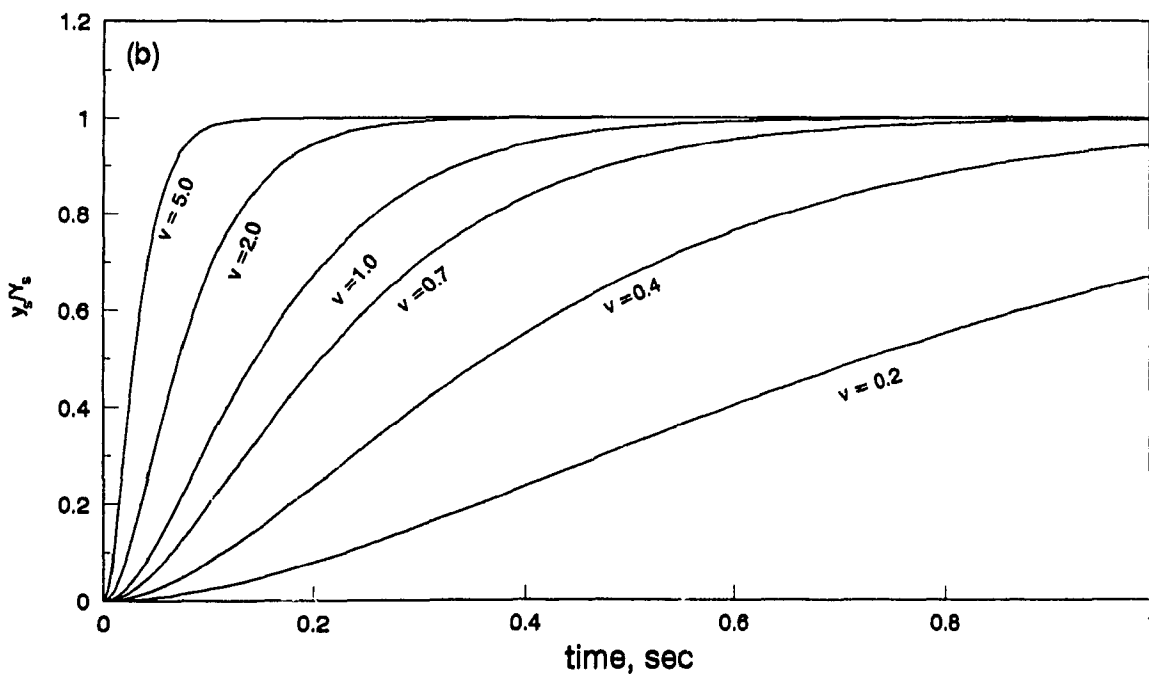
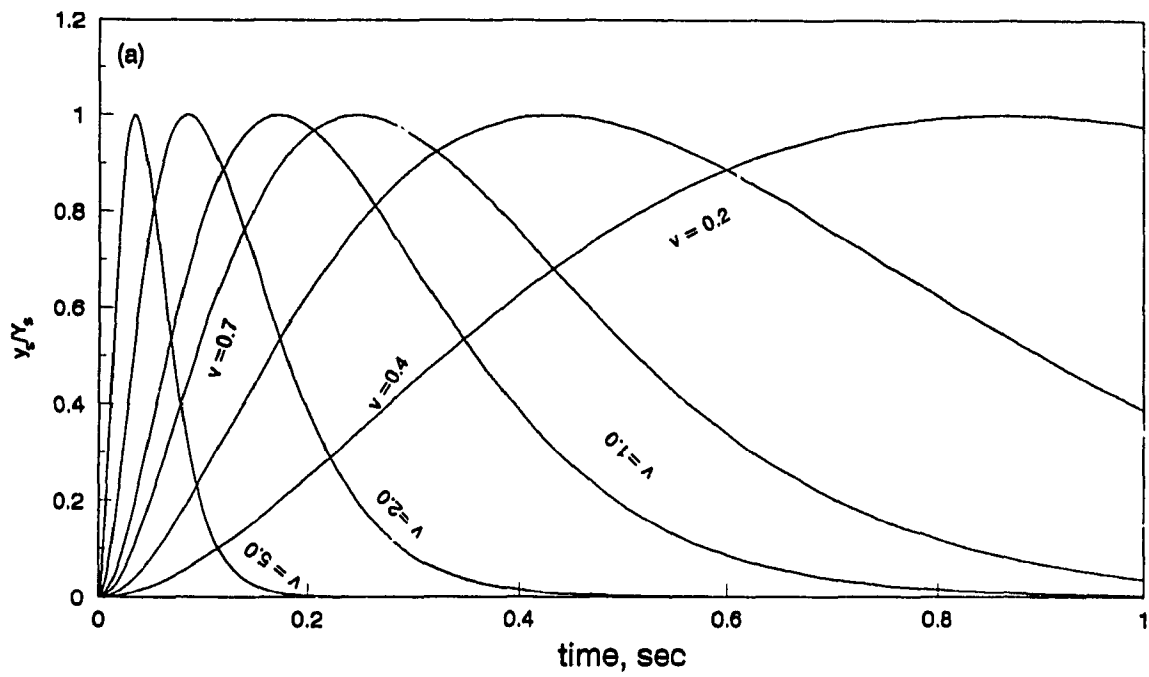


Figure 4.19 Displacement shock characteristics under different shock severity. (a) rounded pulse displacement (b) rounded step displacement.

value of the parameter will lead to more severe shock input for a system with a higher natural frequency.

(b) Rounded step displacement: A rounded step displacement input may be defined by the following pairs of equations.

$$y_s(t) = 0, \quad t < 0 \quad (4.3)$$

$$y_s(t) = Y_s [1 - e^{-\nu \omega_0 t} (1 + \nu \omega_0 t)] , \quad t \geq 0 \quad (4.4)$$

Here, the shock severity parameter is defined in the same manner but the duration of the pulse  $\tau_s$  of the rounded step displacement is defined as the time required for the displacement to reach 82% of its final value. The severity factor  $\nu$  in terms of  $\tau_s$  and  $\omega_0$  is:

$$\nu = \frac{T}{2\tau_s} = \frac{\pi}{\omega_0 \tau_s} \quad (4.5)$$

The rounded step displacement is shown in Figure 4.19b for different shock severity parameter for the natural frequency of 7.5 Hz.

In addition to the above mentioned shock displacement, a third type of shock input is also available in the literature known as oscillatory displacement step [43]. The use of such input is not common for evaluation of isolators. The rounded pulse displacement is the mostly appropriate shock input for common isolators, as for example, it represents a bump or a pot hole on a damaged road. Performance of the dual-phase dampers, in this investigation is only considered under the application of the rounded pulse displacement.

#### 4.4.2 Shock Performance Index

The performance of the dual-phase damper under the shock load is evaluated both in time domain and shock severity parameter domain. Again, there are commonly

used performance indices [21, 38] that can be used effectively for evaluation of performance and comparative study.

(i) Shock Acceleration Ratio (SAR) defined as the ratio of the maximum acceleration of the response to the maximum acceleration of the input:

$$SAR = \frac{|\ddot{x}_s(t)|_{\max}}{|\ddot{y}_s(t)|_{\max}} \quad (4.6)$$

where maximum acceleration for the rounded pulse displacement input is defined as:

$$|\ddot{y}_s(t)|_{\max} = 3.69453 \, v^2 \omega_0^2 Y_s \quad (4.7)$$

where  $v_p$  is the shock severity factor,  $\omega_0$  is the system natural frequency and  $Y$  is the maximum displacement of pulse defined in Equation (4.1).

(ii) Shock Velocity Ratio (SVR) defined as the ratio of the maximum velocity of the response to the maximum velocity of the input.

$$SVR = \frac{|\dot{x}_s(t)|_{\max}}{|\dot{y}_s(t)|_{\max}} \quad (4.8)$$

where maximum velocity for the rounded pulse displacement input is defined as

$$|\dot{y}_s(t)|_{\max} = 0.85188 \, v \, \omega_0 Y_s \quad (4.9)$$

where the various variables are same as those in Equation (4.7)

(iii) Shock Displacement Ratio (SDR) defined as the ratio of the maximum displacement of the response to the maximum displacement of the input.

$$\text{SDR} = \frac{|x_s(t)|_{\max}}{|y_s(t)|_{\max}} \quad (4.10)$$

(iv) Shock Relative Displacement Ratio (RDR) defined as the ratio of the maximum relative displacement of the response to the maximum displacement of the input.

$$\text{RDR} = \frac{|x_s(t) - y_s(t)|_{\max}}{|y_s(t)|_{\max}} \quad (4.11)$$

#### 4.5 Shock Response of Dual-phase Damper

The dual-phase damper is excited at the base by the rounded pulse displacement type of shock input and the response is measured at the sprung mass of the system. The system chosen has the undamped natural frequency of 7.5 Hz and maximum input displacement of the shock is taken as 40 mm. The reason for choosing higher natural frequency is that the response of the dual-phase damper will be compared with the response of the dampers with flexible chambers. The natural frequency of the flexible chambered damper is 7.5 Hz. The natural frequencies are maintained equal in order to keep the shock severity parameter same. The shock isolation characteristics of the damper is evaluated in two ways (a) in time domain for some selected shock severity parameter and (b) in shock severity domain.

(a) Response in time domain: Figure 4.20 shows the shock response of a low-high damper in terms of acceleration ratio and velocity ratio. The damper chosen has the following parameters  $A = 10$  mm,  $\alpha = 4$ ,  $\zeta = 0.25$  and  $\beta = 2$ . The shock severity parameter considered are 0.1, 0.2, 0.5 and 1.0 which covers a wide range of shock severity for effective demonstration of performance in time domain. As the results show, the peak acceleration ratio diminishes within two cycles for all



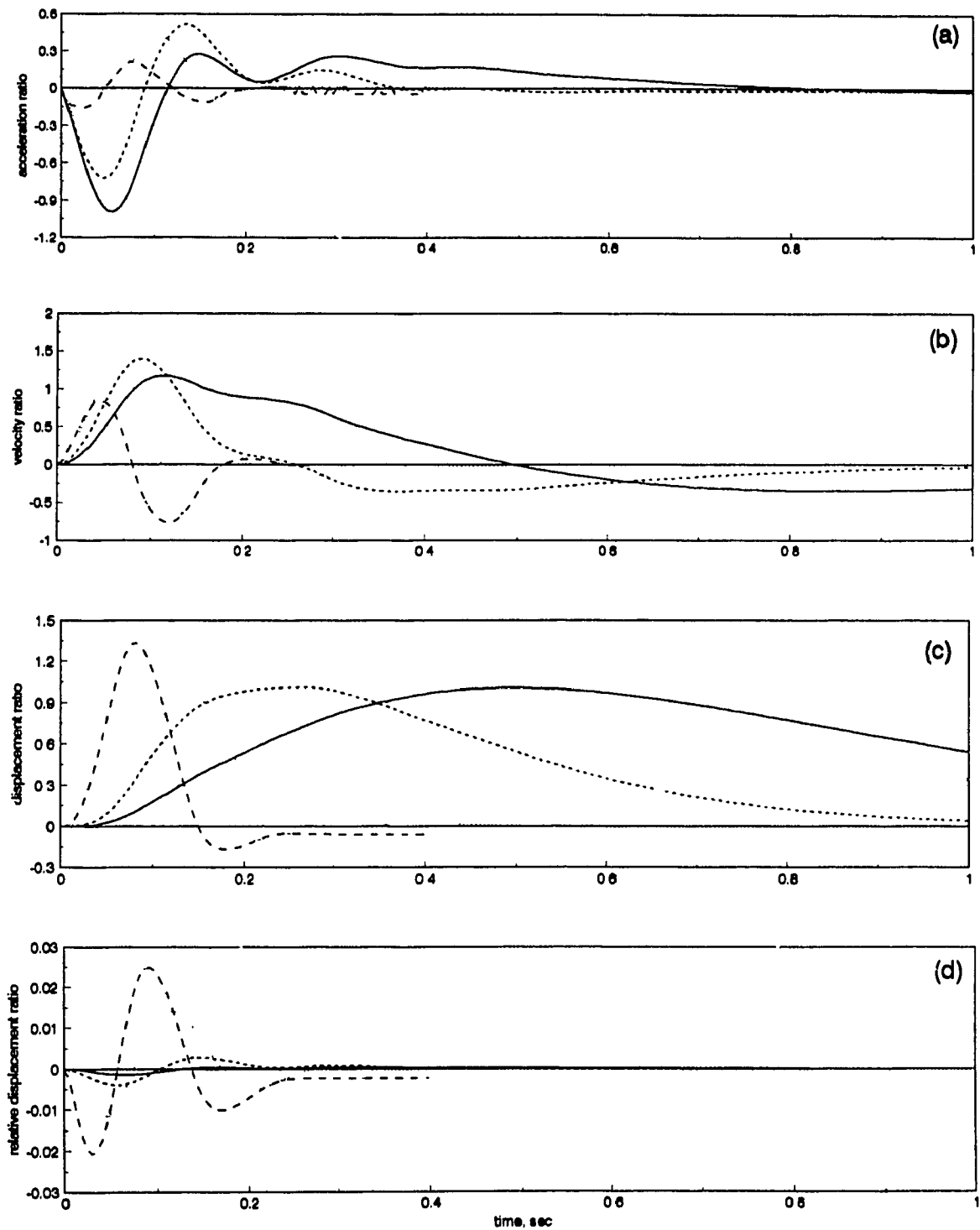


Figure 4.20 Shock response characteristics of a low-high damper. (a) acceleration ratio (b) velocity ratio (c) displacement ratio (d) relative displacement ratio. Shock severity, —, 0.10; ---, 0.20; ···, 0.50; -·-·-, 1.0 ( $A = 10\text{mm}$ ,  $\alpha = 4$ ,  $\zeta = 0.25$ ,  $\beta = 2$ ,  $Y_s = 40\text{ mm}$ ).

severity except for the lowest severity when  $\nu = 0.1$ . The maximum acceleration decreases with the increase in shock severity parameter.

The velocity response takes time equivalent twice as long (Figure 4.20b) to diminish to 20% of its maximum value and the velocity increase with the increase in shock severity and then gradually decreases. However, at higher shock severity, velocity dies out within one cycle. Peak displacement ratio tends to increase with increase in severity parameter as shown in Figure 4.20c. The diminishing period, however, reduces as the shock severity is increased. Relative displacement ratio (Figure 4.20d) increases with the increase in shock severity, but irrespective of the severity parameter, relative displacement reduces to zero within the period of two cycles.

Figure 4.21 shows the shock response for a high-low dual-phase damper under the application of same shock input. The parameters for the damper is also kept as that of low-high damper in order to compare their performances. It is seen from the Figure 4.21a that although the peak acceleration and the trend remain the same for both low-high and high-low dampers, the acceleration disappears relatively faster in the case of high-low damper. In comparison to low-high damper, there is no significant difference in the trend of velocity, displacement and relative displacement responses when high-low damper ( Figure 4.21b,c,d) is used. These responses are, however, marginally better in comparison to a low-high damper. It might be possible that the high-low damper has better potential for isolation of shock for a optimal set of parameters. This will be explored further in the following subsection.

(b) Response versus shock severity: Here the peak response ratios are obtained for variation of shock severity parameters in the range of 0.05 to 5. Figure 4.22 shows the response characteristics of the low-high damper in terms of shock acceleration ratio shock velocity ratio, shock displacement ratio and shock relative

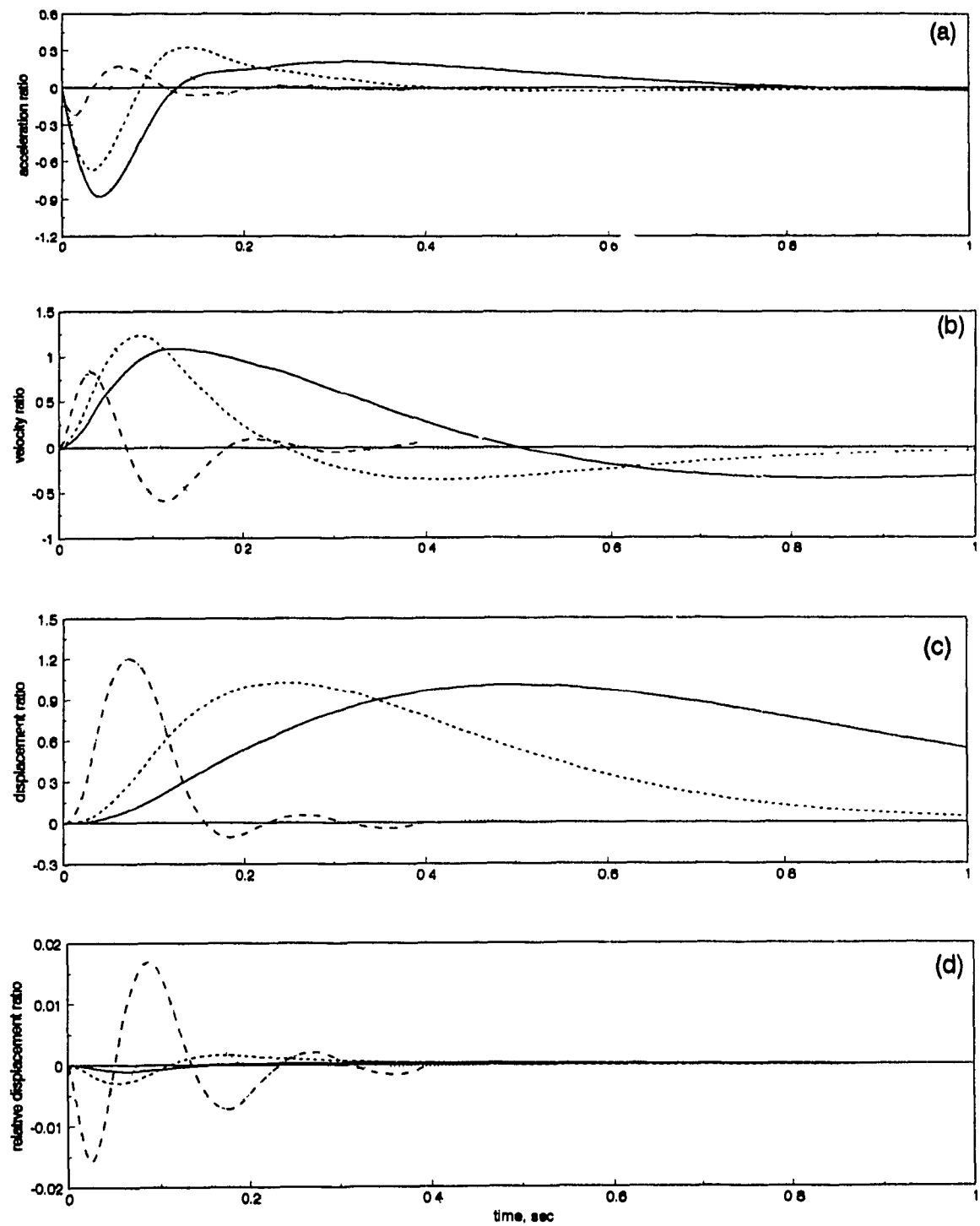


Figure 4.21 Shock response characteristics of a high-low damper. (a) acceleration ratio (b) velocity ratio (c) displacement ratio (d) relative displacement ratio. Shock severity, —, 0.10; ---, 0.20; ···, 0.50; - · - ·, 1.0 ( $A = 10\text{mm}$ ,  $\alpha = 4$ ,  $\zeta = 0.25$ ,  $\beta = 2.0$ ,  $Y_s = 40\text{mm}$ ).

displacement ratio. The parameters are  $A = 10$  mm,  $\alpha = 2$ ,  $\zeta = 0.25$  and  $\beta$  is varied as 1.4, 2 and 2.6 to examine the effect of higher damping ratio on its performance. It is found that the acceleration ratio diminishes quickly with the increase in shock severity and reaches very low at high shock severity. The increase in damping ratio is found to have influence only at higher shock severity ( $> 0.40$ ) where an increase in  $\beta$  deteriorates the acceleration ratio. At lower shock severity, the relative displacement is low, therefore, the damper remains within the low damping region. That is why the SAR is identical until  $v = 0.4$  after which relative displacement goes to higher damping ratio and it affects the damper performance. Higher damping ratio deteriorates the acceleration at higher shock severity as observed in Figure 4.22a.

The shock velocity ratio (SVR), for the same set of parameters, is shown in Figure 4.22b. SVR increases with the increase in shock severity up to certain shock severity ( $v = 0.3$ ) after which SVR tends to reduce rapidly with the increase in shock severity. The effect of variation of damping ratio does not change the SVR significantly as seen in Figure 4.22b. The shock displacement ratio for the low-high damper shown in Figure 4.22c indicates that the response remains unity until  $v = 0.3$ , it then starts to increase with increase in  $v$  and after crossing  $v = 0.8$ , it falls rapidly with increase in severity parameter. Increase in damping parameter  $\beta$  decreases the SDR at higher  $v$  value. At lower  $v$ , the shock displacement response is insensitive to the higher damping parameter of a low-high damper.

The relative displacement ratio (RDR) response of the low-high damper shown in Figure 4.22d indicates a rapid increase in the response with increase in shock severity. The RDR response goes up to 0.8 which is higher compared to the sequential damper proposed by the Rakheja and Sankar [21]. However, when other response characteristics are compared, the dual-phase damper performs better throughout the whole range of shock severity.

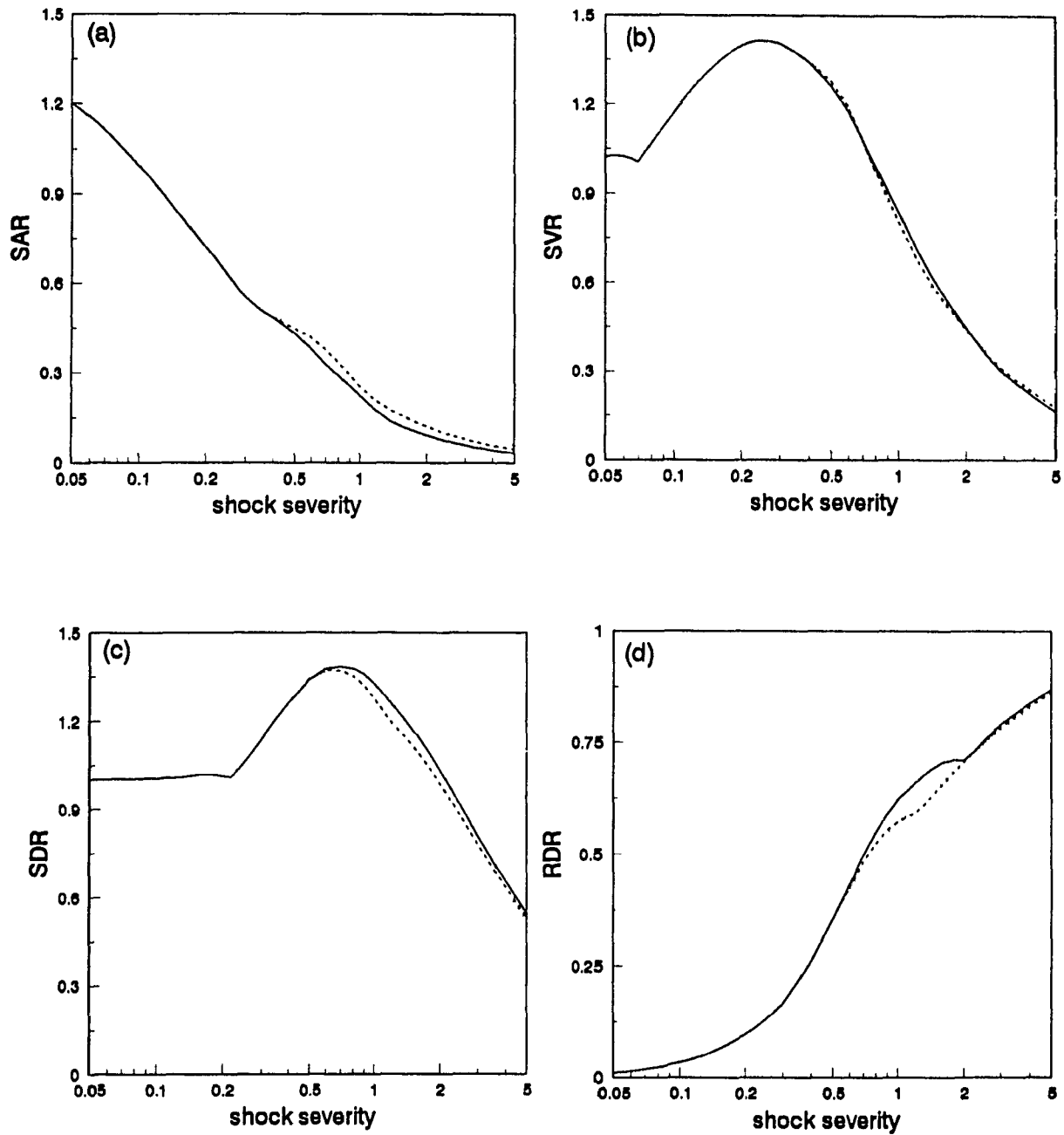


Figure 4.22 Shock response characteristics of a low-high damper. (a) SAR (b) SVR (c) SDR and (d) RDR.  $\beta$ , —, 1.4; ----, 2.0; ····, 2.6. ( $A = 10\text{mm}$ ,  $\alpha = 4$ ,  $\zeta = 0.25$ ,  $Y_s = 40\text{mm}$ ).

Shock isolation characteristics of the high-low damper are shown in Figure 4.23. The trend in this case is very similar to that of low-high damper response. It, however, performs better than a low-high dual-phase damper and is sensitive to the change in damping parameter  $\beta$  throughout the range of severity. Figure 4.23a shows that SAR of the damper is much lower throughout the whole range of shock severity. The SAR decreases with the increase in  $\beta$  at lower shock severity because high damping produces better performance at lower shock severity. But it increases the SAR at higher shock severity. Figure 4.23b shows the shock velocity ratio (SVR) with the variation of shock severity. Compared to low-high damper, it exhibits much lower shock velocity ratio and SVR reduces even further with the increase in higher damping parameter  $\beta$ . The effect of  $\beta$  is similar on SVR as that of SAR.

The shock displacement ratio (SDR) is also much lower for the case of high-low damper compared to a low-high damper for all ranges of shock severity (Figure 4.23c). Higher damping parameter  $\beta$  decreases the SDR with a minor increase at very high shock severity. Relative displacement ratio (RDR) remains similar to that of a low-high damper (Figure 4.23d). But unlike the low-high damper, RDR decreases significantly with the increase  $\beta$ .

#### **4.6 Summary**

A detail investigation regarding the characteristics and performance of the dual-phase damper is carried out here. Two types of displacement sensitive dampers, i.e., low-high and high-low are considered. Characteristics of the damper is determined in terms of dynamic stiffness and loss angle. It is observed that, generally, the low-high damper exhibits higher dynamic stiffness and loss angle compared to a high-low damper. Response characteristics of the damper is evaluated under the application of both sinusoidal and shock excitation. Detailed

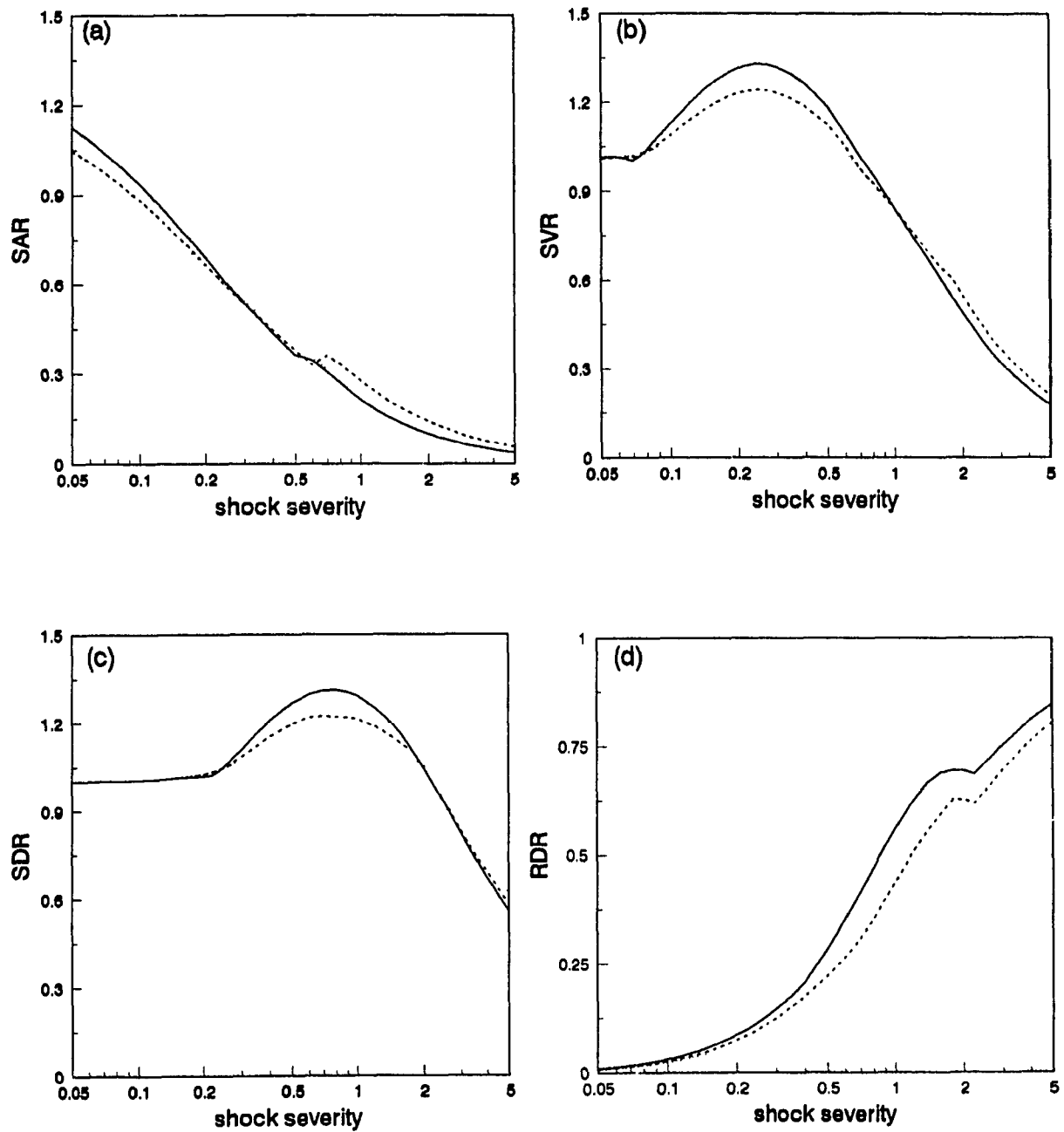


Figure 4.23 Shock response characteristics of a high-low damper. (a) SAR (b) SVR (c) SDR and (d) RDR.  $\beta$ , —, 1.4; ----, 2.0; ·····, 2.6. ( $A = 10\text{mm}$ ,  $\alpha = 4$ ,  $\zeta = 0.25$ .  $Y_s = 40\text{mm}$ ).

parametric study for both low-high and high-low dampers indicate that a low-high damper has better potential for improved performance over a wide range of frequency. The study further indicates that a dual-phase damper, specifically displacement sensitive must be designed for isolation of a given vibration amplitude in order to achieve its best performance.

The shock response analysis under rounded pulse input indicates suitability of such damper in isolation of shock. For both low-high and high-low dampers, the shock acceleration response increases and relative displacement ratio decreases as shock severity is increased. For shock velocity and displacement ratios, the response first increases and then decreases as shock severity is increased. The effect of dual-phase damper parameter  $\beta$  (ratio of high to low damping ratio) has more significant effect on the performance of high-low damper leading to a superior performance under shock excitation.



## **CHAPTER 5**

# **CHARACTERISTICS AND PERFORMANCE OF SHORT ORIFICE HYDRAULIC DAMPER**

### **5.1 Introduction**

A detailed nonlinear model for hydraulic damper with flexible chamber and short orifice of different openings is developed as presented in chapter 3. This part of the study considers the damper characteristics and its performance in isolation of vibration and shock. The method of simulation outlined in section 3.2.5 is adopted to establish the characteristics and performance. The results are obtained in both time and frequency domain to demonstrate the damper characteristics in terms of internal variables like orifice flow, top chamber pressure, damping force and transmitted force. Dynamic stiffness and loss angle of the damper are also presented in frequency domain. Acceleration transmissibility and relative displacement transmissibility of the single DOF system utilizing the damper are observed to evaluate its performance. A detailed parametric study is carried out to examine the influence of various damper parameters on the dynamic stiffness and transmissibility response. The effect of different orifice openings has also been investigated. The nominal parameters selected for the simulation are: orifice diameter 6 mm; orifice length 5 mm; suspended mass 125 kg. These are based on a realistic system where the mass represents an engine supported on mounts with system natural frequency 7.5 Hz. The natural frequency in this case is, however,

highly sensitive to damper parameters due to the creation of additional stiffness from the compliance of the top chamber. The following subsection presents the characteristics of the damper along with a detailed parametric study. Results are further presented for transmissibility performance response under both sinusoidal excitation and shock.

## **5.2 Characteristics of the Damper**

A hydraulic damper with short orifice of diameter 4.5 mm is chosen to carry out the investigation of its characteristics. Projected piston diameter is taken as 70 mm. A mass of 125 Kg is supported by the damper with a base excitation of 1 mm sinusoidal of frequency 10 Hz. The mass is considered equivalent to the mass of the engine where the damper will act as a mounting device on the chassis. From table 3.3, the static pressure for the above configuration is obtained as 111.45 KPa when Comp\_A type top chamber material is implemented. The characteristics of the damper is compared with the experimentally obtained characteristics [17] for long orifice hydraulic damper. The reasons for selecting long orifice damper for validation are (1) to the knowledge of the author, no literature is yet available for characteristics of the short orifice damper, and (2) the long orifice damper has similar trends in characteristics of short orifice damper. The peak values of internal parameters, the trend in time domain as well as in frequency domain do not exhibit wide variation due to the functional and construction similarities of the dampers.

### **5.2.1 Time Domain Analysis**

The system associated with the flexible chambered hydraulic damper is highly nonlinear due to compliance, chamber material properties, etc. Therefore, the behavior of the systems' internal variable are also nonlinear. Hence, it is desirable to analyze its characteristics in time domain. In each simulation, sufficient time is

allowed to ensure that steady state has been reached. The response variable data are stored for three cycles after passing 30th cycle of input excitation.

Using a frequency sweep in the range of 1 to 100 Hz, it is first established that the given system has a natural frequency close to 10 Hz. The steady state time history is, therefore, obtained at 6, 10 and 20 Hz to examine the orifice flow rate from one chamber to the other. The results presented in Figure 5.1 include a dotted curve which represents the excitation frequency. The positive part of the flow shows flow from bottom chamber to top chamber (reverse flow) and the negative part shows the opposite or forward flow. Figure 5.1a shows that the forward flow occurs after 33.33 ms of the onset of the forward stroke which is equivalent to 71.93 degree phase lag. However, this time delay decreases with increase in excitation frequency (14.0 ms or 50.4 degree at 10 Hz and 3 ms or 21.6 degree at 20 Hz). The asymmetric orifice flow rate characteristics, shows nonsinusoidal behavior, although the application of excitation is purely sinusoidal. For each cycle, duration of maximum flow is higher in reverse flow than in forward flow and this fact increases with increase in frequency.

The reason for this behavior may be explained from Figure 5.2 which represents the time history of top chamber pressure distribution for the three given frequencies. The distribution is purely asymmetric in nature where minimum pressure goes as low as 37.81 KPa which is below atmospheric. This sub-atmospheric pressure distribution for the damper agrees quite well with the experimentally obtained one for a long orifice hydraulic damper [17]. The period for higher pressure difference between chambers which governs orifice flow is longer during reverse flow but magnitude of peak flow is higher during forward flow. This way the total volume in one cycle is balanced. The peak value of the pressure is around 216 KPa which varies with the variation of orifice diameter, chamber compliance and amplitude of excitation as discussed later.

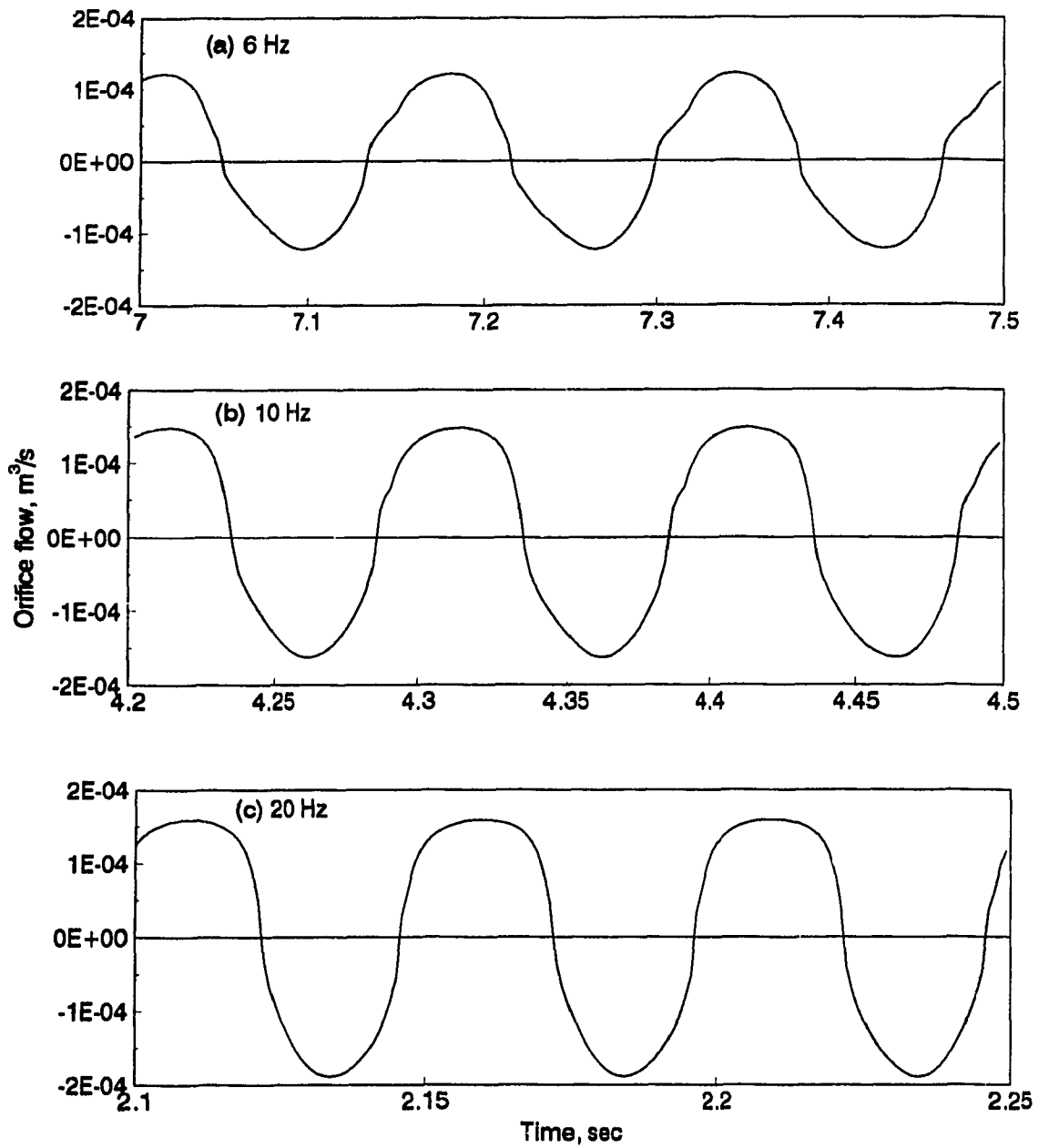


Figure 5.1 Orifice flow time history of the hydraulic damper at different frequencies. ( $X_1 = 1\text{mm}$ ; piston diameter 70mm).

Figure 5.2 further shows that increase in frequency increases the magnitude of the pressure and the creation of sub-atmospheric pressure. Although the bottom chamber has a very high compliant element, pressure build up in top chamber increases with frequency. Smaller diametered orifice cannot pass the bulk of fluid as quickly as the forward stroke, which leads to rapid rise in pressure. Due to the same reason, more vacuum is created in high frequency excitation during reverse stroke. It is interesting to indicate that time response above atmospheric pressure is completely different from time response below atmospheric pressure. Compliance of the chambers works only when there is a pressure buildup above atmospheric pressure. When the pressure is below atmospheric, 'negative compliance' phenomenon occurs as discussed earlier in section 3.2.2.2 for nonlinear compliances. It is simulated by considering that entrapped air bubbles get released at low pressure and pressure-volume relationship for air holds good during that time [17].

Figure 5.3 shows the time history for variation of bottom chamber pressure. Clearly, due to high compliance nature of the bottom chamber, variation of pressure is very low compared to that of the top chamber. Here the variation is about the static pressure of 111 KPa, where peak to peak difference is only 6.16 KPa at 10 Hz. The results further show a decreasing tendency for the peak to peak difference as frequency is increased. This results from increase in orifice flow leading to lower volume increment from the condition  $P_B = P_{AT}$ . Consequently, it leads to lower buildup of pressure in the bottom chamber. Such behavior in short orifice is contrary to the known behavior of the long orifice system.

For the same simulation, Figure 5.4 shows the time history for damping force at three different frequencies. These results reflect the top chamber pressure distribution obtained earlier in Figure 5.2. The pattern of distribution can be considered identical with a phase shift of 180 degree. This is due to the fact that

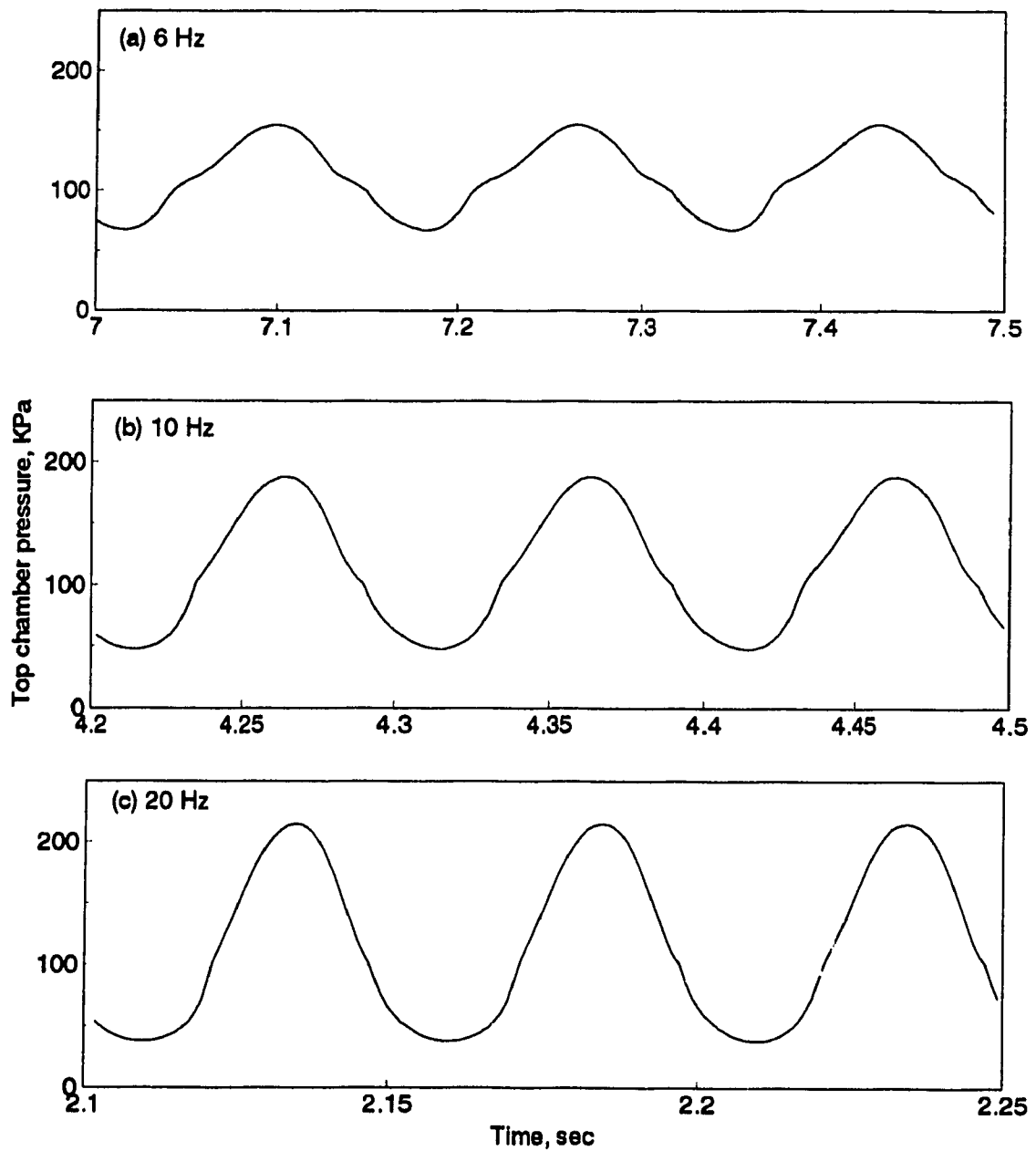


Figure 5.2 Top chamber pressure of the hydraulic damper in time domain at different frequencies. ( $X_1=1\text{mm}$ ; piston diameter 70mm).

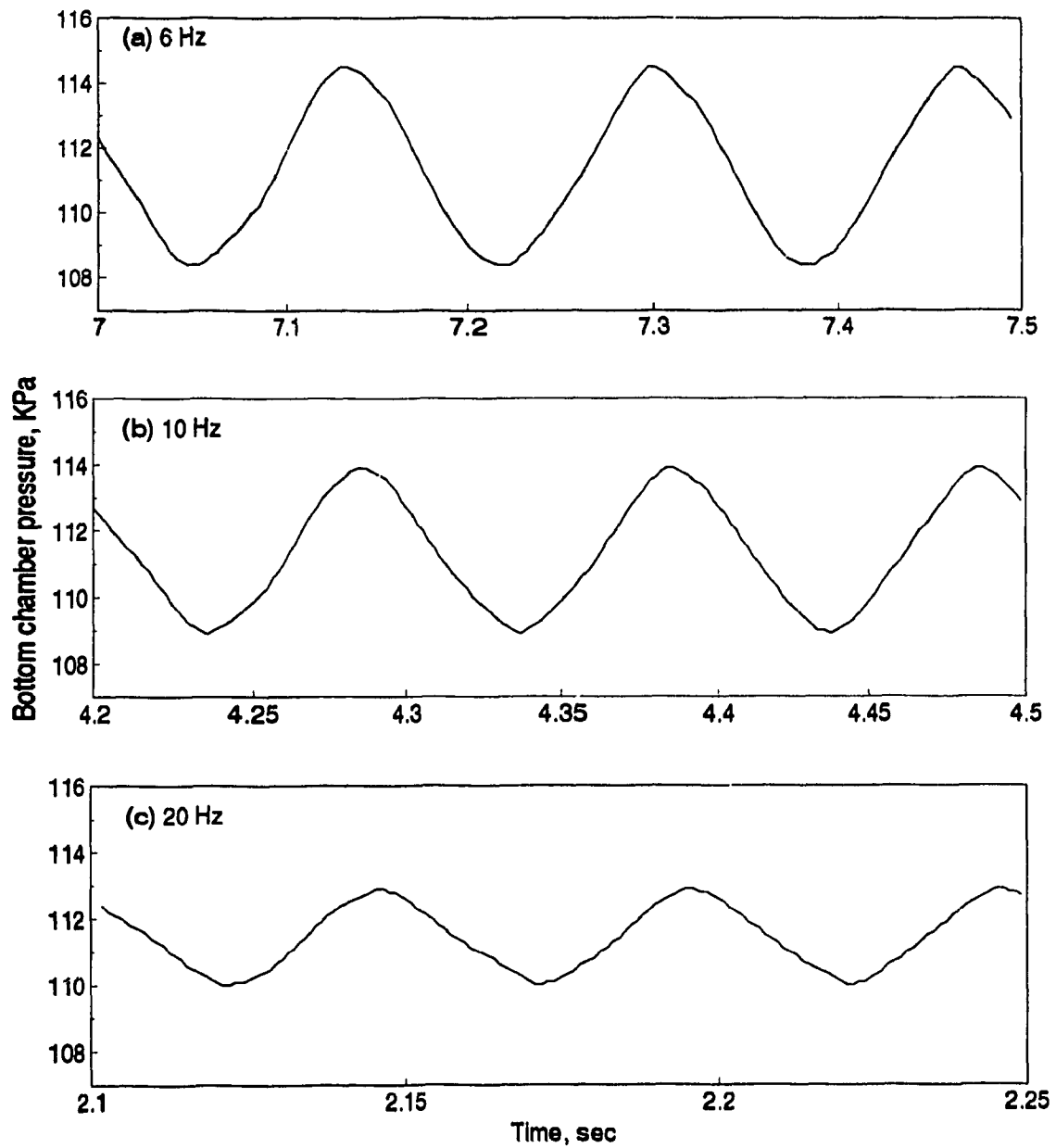


Figure 5.3 Bottom chamber pressure of the hydraulic damper in time domain at different frequencies. ( $X_1 = 1\text{mm}$ ; piston diameter 70mm).

top chamber pressure distribution is the only contributory factor for damping force. At low frequency, (Figure 5.4a) damping force development during forward stroke and reverse stroke are almost same and exhibits a phase shift of 64.8 degree with excitation frequency. With increase in frequency, damping force also increases with higher magnitude during forward stroke than reverse stroke. At 20 Hz, peak damping force at the end of forward stroke is 404.69 N whereas at the end of reverse stroke damping force is 281.5 N. In reverse stroke, development of pressure difference is limited due to formation of sub-atmospheric pressure. Therefore, increase in damping force with frequency during reverse stroke is much lower than the increase in forward stroke. Like orifice flow, phase difference also decreases with increase in frequency, 46.8 degree at 10 Hz and 25.2 degree at 20 Hz.

Simulated results for force transmitted to the ground by the damper is shown in Figure 5.5. It shows the nonlinear distribution of transmitted force as a function of time for the three different frequencies. Like damping force, transmitted force also increases with frequency. Peak transmitted force at 6 Hz is 400 N whereas, at 10 Hz, it is 551 N and at 20 Hz, it is 684 N. Figure 5.6 shows the excitation displacement verses transmitted force plot. The encircled area, thus formed, shows the amount of damping (energy dissipation) developed by the system. It also exhibits the extent of nonlinearity present in the system. The results show that the hydraulic damper develops higher damping at 10 Hz compared to 6 Hz. With the increase in frequency, damping effect tends to diminish (width of the Lissajous plot tends to be narrower). The Figure also displays that, with increase in frequency, the hydraulic damper shows more nonlinearity.



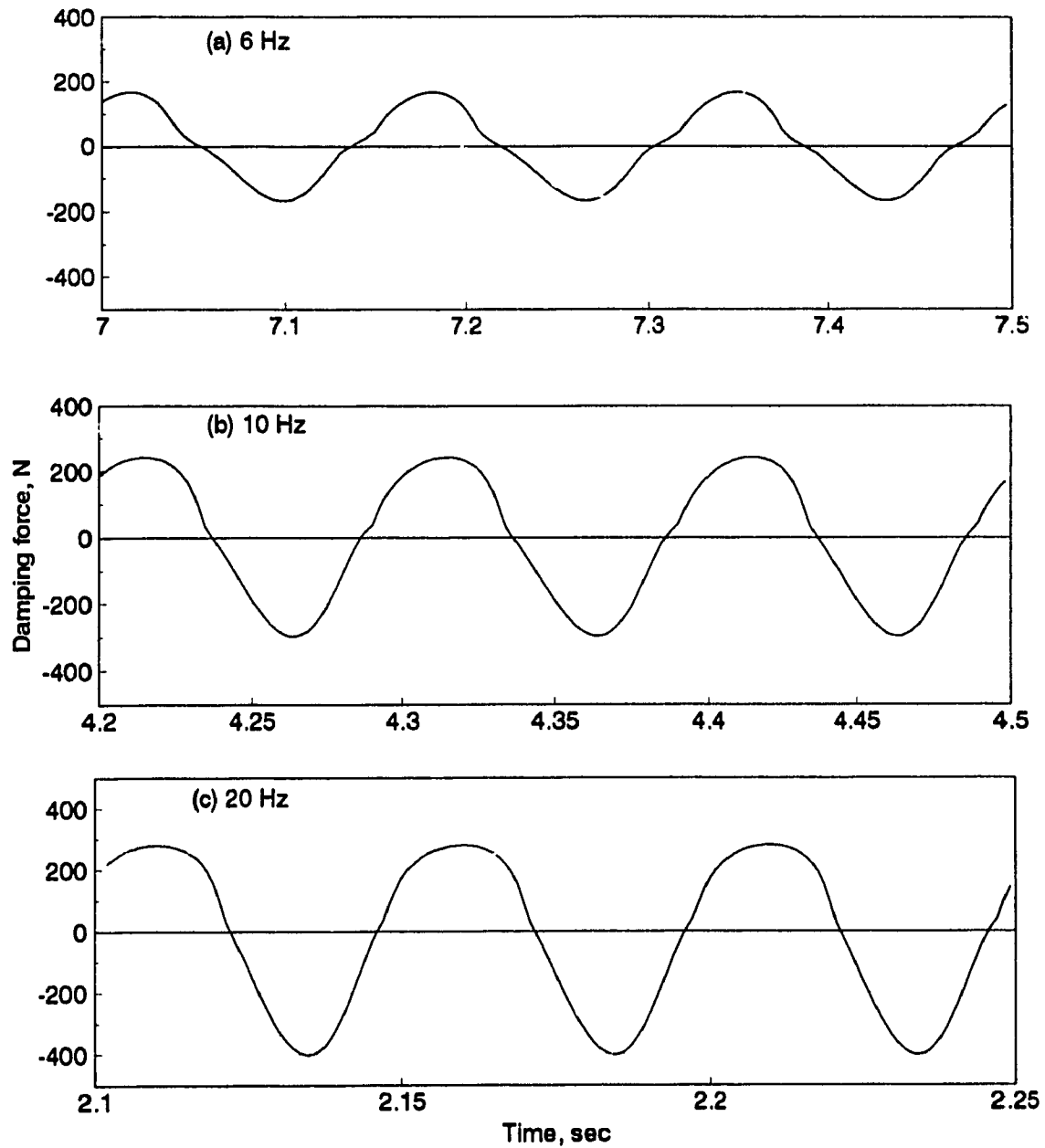


Figure 5.4 Damping force of the hydraulic damper in time domain at different frequencies. ( $X_1 = 1\text{mm}$ ; piston diameter 70mm).

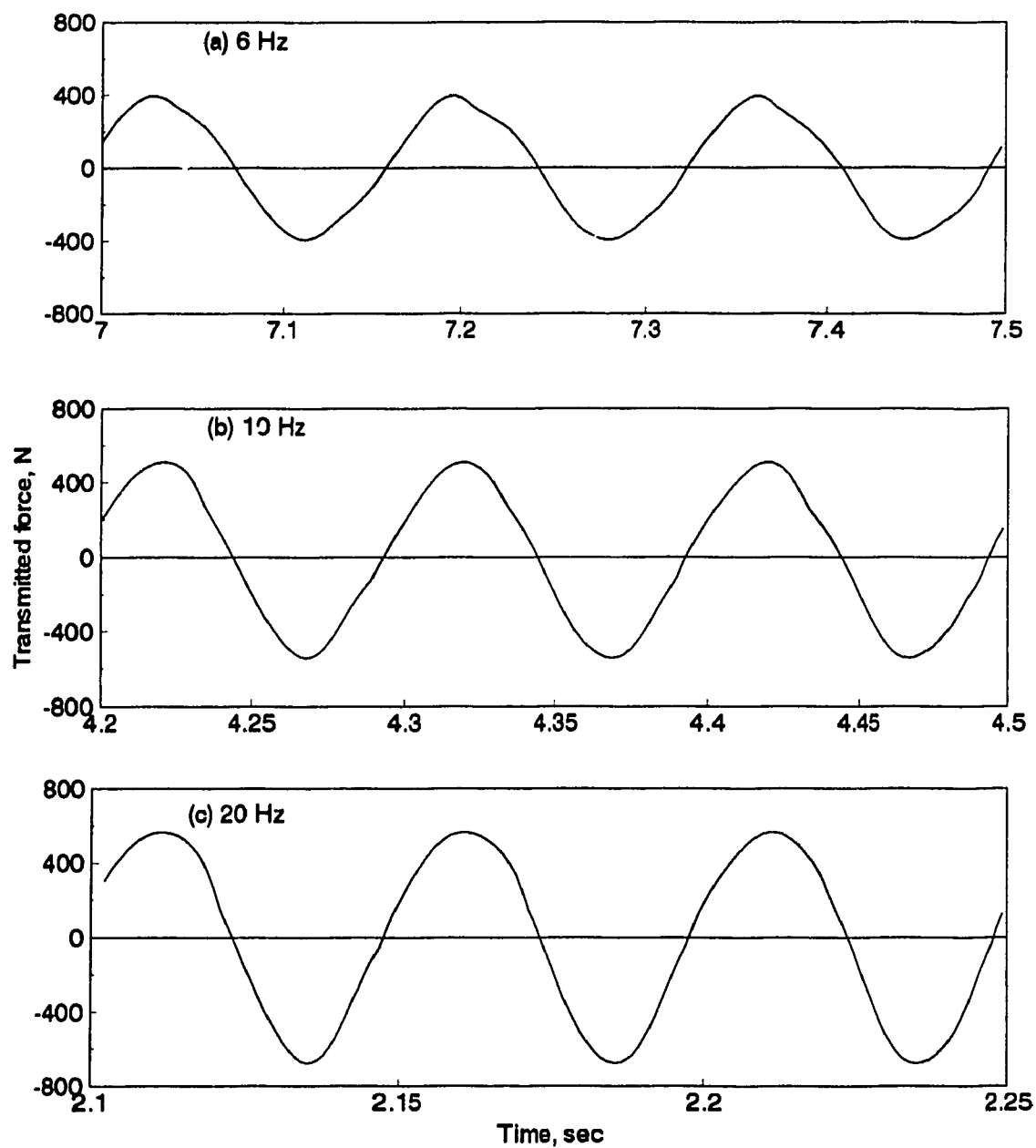
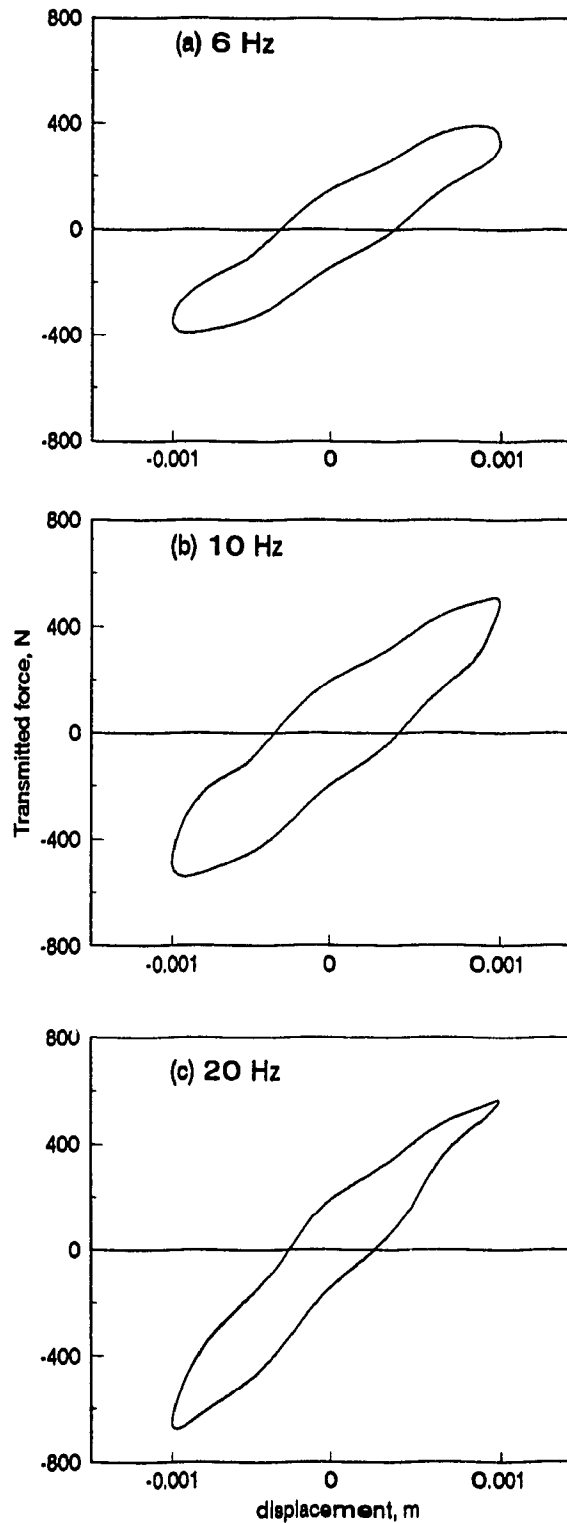


Figure 5.5 Transmitted force characteristics of the hydraulic damper at different frequencies. ( $X_1=1\text{mm}$ ; piston diameter 70mm).



**Figure 5.6** Lissajous plots of the hydraulic damper at different frequencies. ( $X_1 = 1\text{mm}$ ; piston diameter 70mm).

### 5.2.1.1 Parametric Study

For the parametric study in time domain, the two most important parameters that significantly change the characteristics of the damper will be varied to analyze their effect. These parameters include: (i) orifice diameter and (ii) piston diameter (top chamber diameter). One parameter is varied at a time while the other is held constant and equal to its nominal value presented in section 5.1.

(a) Orifice diameter: Figure 5.7 shows the effect of orifice diameter on the orifice flow rate, top chamber pressure and transmitted force. These results are obtained for orifice diameter 4.5 mm, 6 mm and 7.5 mm. Excitation amplitude is 1 mm at a frequency of 10 Hz. With the increase in orifice diameter, the flow rate increases and consequently, the chamber pressure decreases. This decrease in pressure, in turn, results in the decrease in transmitted force. Flow rate increases because of the reduction in the flow restriction due to greater orifice area. Except around the zero flow rate zone, phase angle at each point varies significantly for different diameters. One possible explanation might be that the smaller diameter creates additional stiffness due to top chamber compliance developing significant phase difference. The greater the orifice diameter, the lesser the effect of compliance will be, one can see the phase difference is also decreasing. Asymmetry also tends to decrease with the increase in diameter (Figure 5.7a) because the difference in pressure during both forward and reverse flow tends to become equal.

Increase in diameter means decrease in flow restriction which, in turn, reduces the building up of pressure. Therefore, larger diameter reduces the pressure in the top chamber. With the increase in diameter, phase shift and waviness in the curve are also observed in Figure 5.7b. Similar trend is also visible in the transmitted force curve (Figure 5.7c) with minimum phase shift.

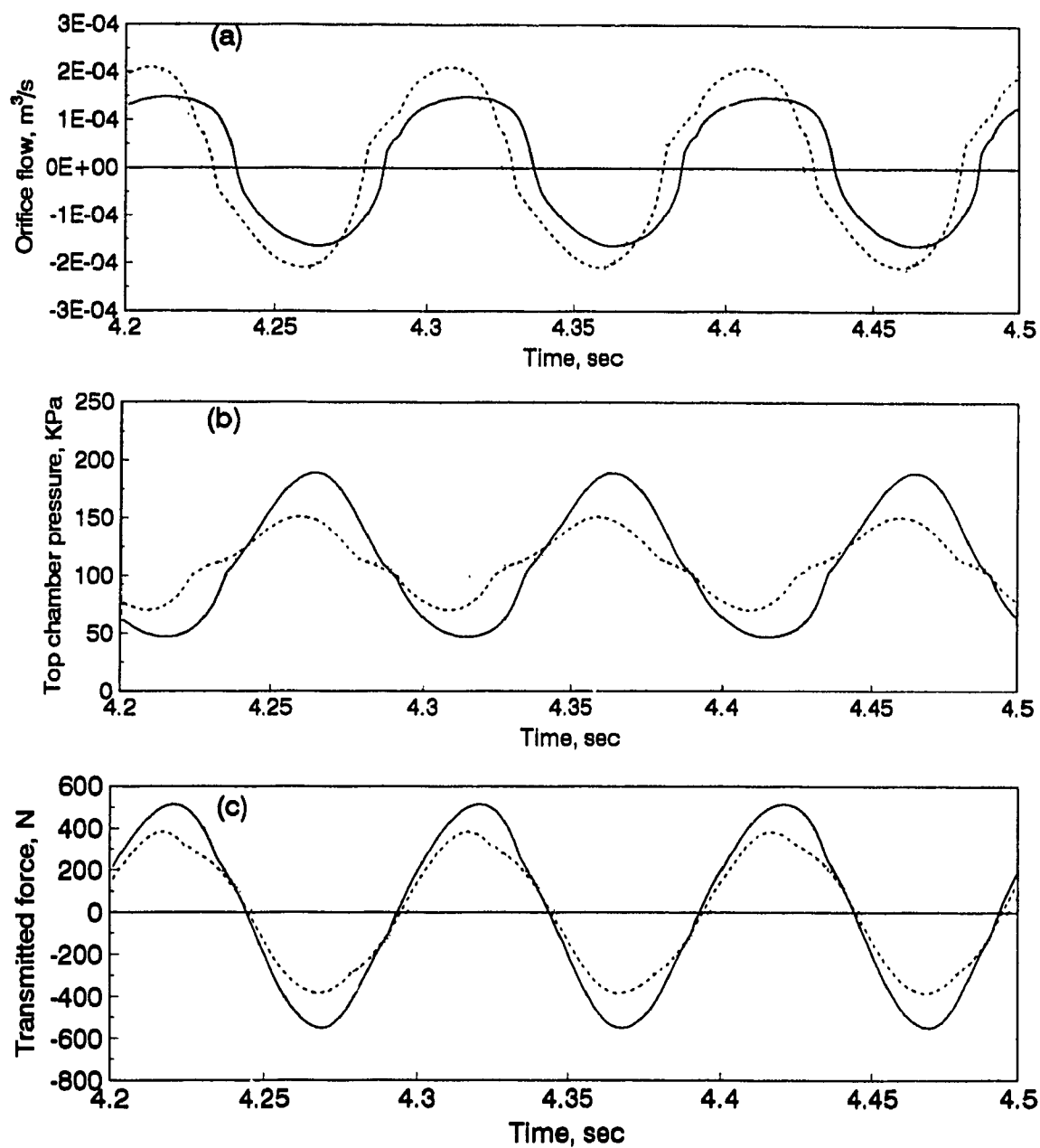


Figure 5.7 Effect of orifice diameter on the internal variables of the damper.  $X_1=1.0$  mm at 10 Hz ; piston diameter 70mm; orifice diameter, —, 4.5mm; ---, 6mm; ···, 7.5mm.

(b) Piston diameter: The piston dia of the top chamber is varied as 70 mm (area 3850 mm<sup>2</sup> ), 80 mm (area 5025 mm<sup>2</sup> ), and 90 mm (area 6362 mm<sup>2</sup> ) and effects of these variation on damper characteristics are investigated for orifice flow, top chamber pressure and transmitted force. Figure 5.8a shows the effect of increase in top chamber diameter on orifice flow. Larger diameter means larger thrust area for working fluid displacement, therefore, more flow to and from the chambers. For a 23.4% increase in piston area there is a 20.1% increase in peak flow rate. A 65.3% increase in piston area results in 39.7% increase in the peak flow rate. Therefore, increase in piston area is not proportional to the increase in orifice flow. It is also observed that when piston area is increased, it takes longer time to complete reverse flow and shorter time to complete forward flow.

For the fixed orifice size, increase in orifice flow creates more pressure build up, i.e., increase in piston area increases the top chamber pressure as shown in Figure 5.8b. For an increase in piston area to 23.4% creates a 21.4% rise in peak chamber pressure which results in 88.7% increase in damping force. Again 65.3% increase in piston area produces increase in peak pressure by 48% where the damping force increases by 226%. On the other hand, piston area has little effect on sub-atmospheric pressure developed during reverse stroke, i.e., there is very minor increase in vacuum.

Increase in piston area affects the nonlinear nature of the force transmitted to the ground as shown in Figure 5.8c. For the damper with piston diameter of 70 mm, transmitted force curve shows a trend almost similar to the sinusoidal excitation. But as the piston diameter is increased the force become nonlinear and asymmetric. Figure 5.8d presents the transmitted force-displacement characteristics for the three piston areas where the nonlinearity of the damper is quite apparent. The peak magnitude of the transmitted force also increases prominently with the increase in piston area. The following table furnishes the

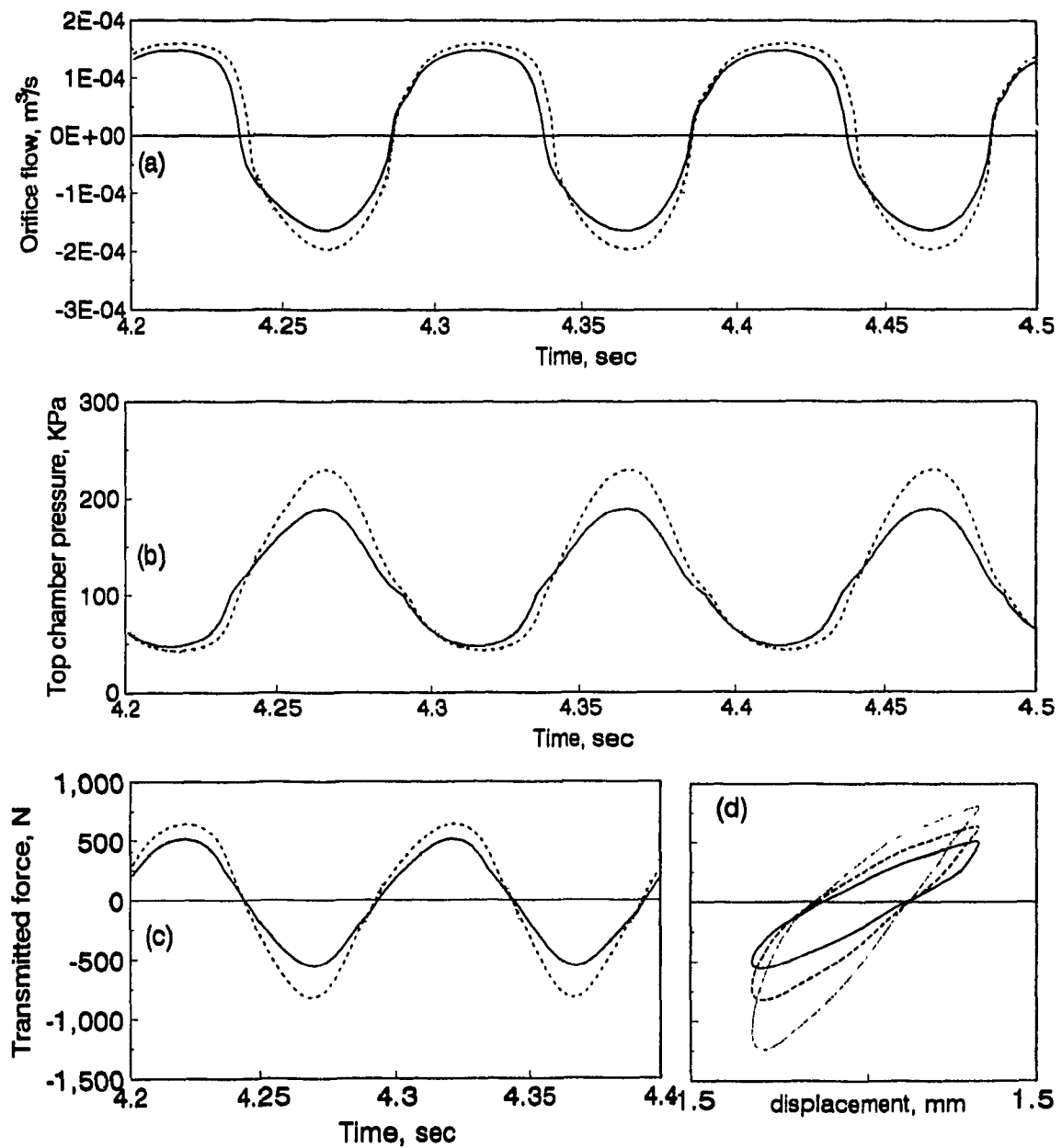


Figure 5.8 Effect of piston diameter on the internal variables of the damper.  $X_1=1.0$  mm at 10 Hz; orifice diameter 4.5mm; piston diameter, —, 70mm; ---, 80mm; ···, 90mm.

summary of the increase in different parameter with the increase in piston diameter

Table 5.1 Percentage increase in some parameters with the increase in piston area based on piston diameter of 70 mm.

piston area	peak orifice flow	peak pressure	peak damping force	peak transmitted force
23.4	20.1	21.4	88.7	48.2
65.3	39.7	48.1	221.0	124.0

Influence of these and other parameters will be further examined in the following section as peak response in frequency domain.

## 5.2 Frequency Domain Analysis

The short orifice hydraulic damper characteristics is next evaluated in frequency domain. The parameters evaluated include: dynamic stiffness; loss angle; chamber pressure; orifice flow and peak damping force. The damper characteristics in terms of rms (root mean square) dynamic stiffness and loss angle as a function of frequency is presented in Figure 5.9. The curve is obtained for amplitude of excitation 1 mm in the frequency range of 1 to 100 Hz. Damper parameters are: orifice diameter 4.5 mm, length 5 mm. Static pressure is obtained at 111.05 KPa. As shown in the Figure, the dynamic stiffness of the damper is constant and is equal to the rubber stiffness for low frequencies less than 5 Hz. In the range of 5 to 50 Hz, the dynamic stiffness increases rapidly with increase in frequency, and is relatively insensitive to frequencies greater than 50 Hz. For the selected parameters, the dynamic stiffness at high frequency goes almost 2.5 times greater than that of low frequencies.



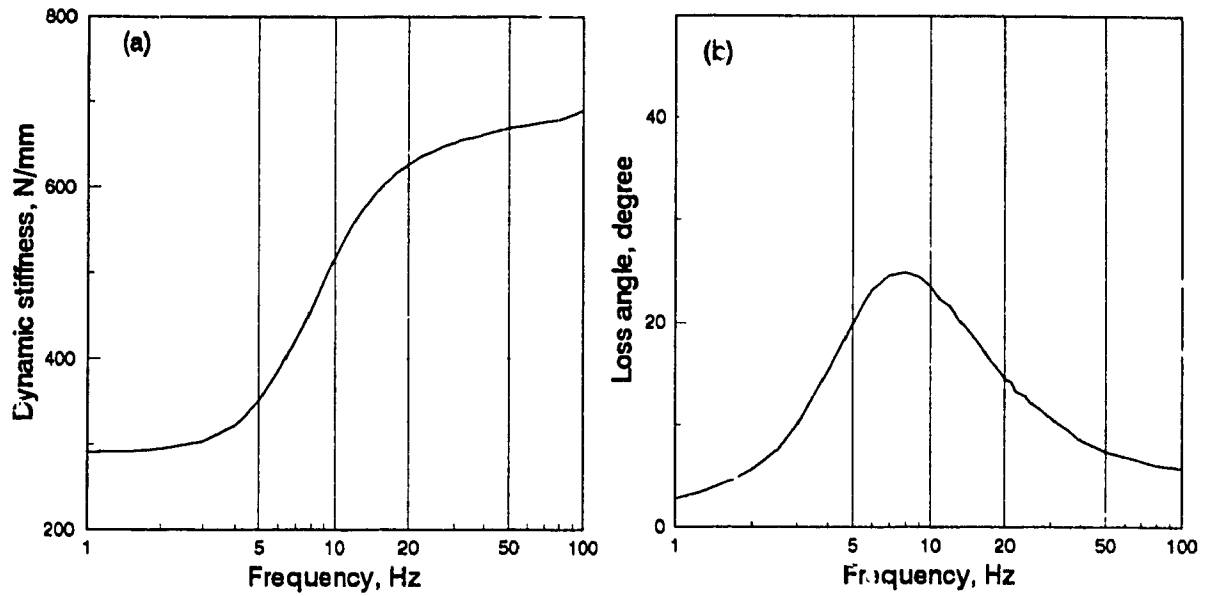


Figure 5.9 Effect of frequency of excitation on (a) dynamic stiffness and (b) loss angle. ( $X_1 = 1\text{mm}$ ; piston diameter 70mm; orifice dia 4.5mm).

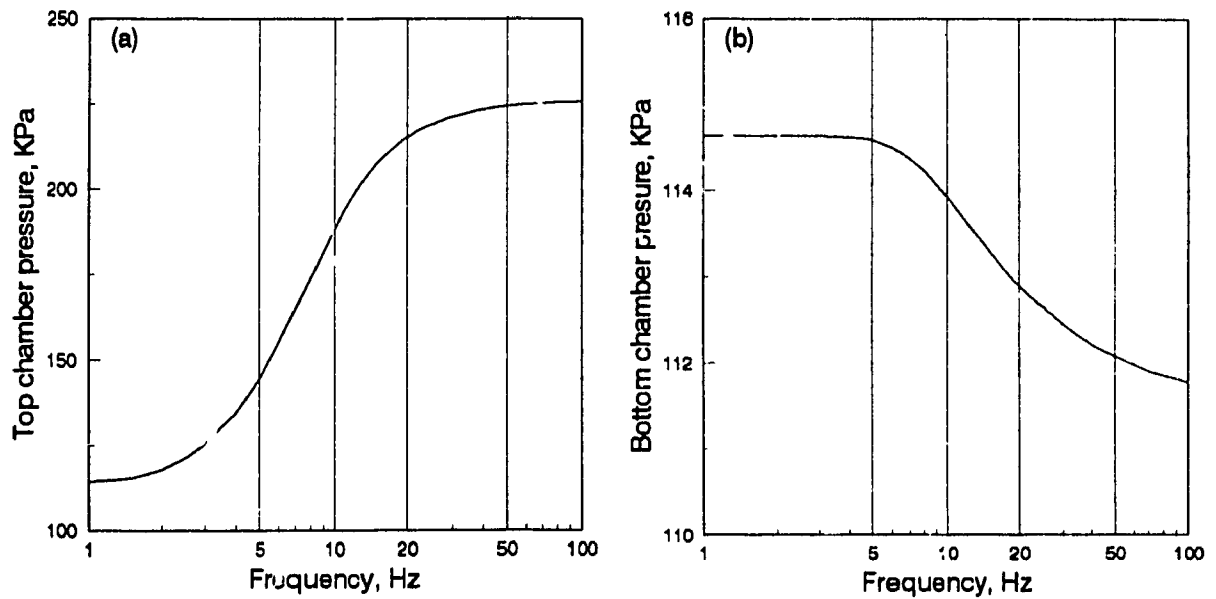


Figure 5.10 Effect of frequency of excitation on (a) top chamber pressure and (b) bottom chamber pressure. ( $X_1 = 1\text{mm}$ ; piston diameter 70mm; orifice dia 4.5mm).

The chief objective in using such damper is to attain enough damping for isolation of resonance. Figure 5.9b shows the damping developed by the damper in terms of loss angle in a wide frequency range. In fact, high damping is desirable within the natural frequency of excitation and low damping is required for high frequency. At 8 Hz loss angle is maximum, 24.83 degree and it decreases rapidly with increase in frequency. Thus a short orifice hydraulic damper is very suitable for high frequency, low amplitude vibration isolation.

Distribution of peak top chamber pressure as a function of frequency shown in Figure 5.10a, exhibits that there is negligible pressure buildup (116 KPa) for frequencies of up to 3 Hz. The pressure then increases rapidly through the resonance frequency (7.1 Hz) and approaches a maximum value of about 226 KPa after 20 Hz. It is interesting to note that the trend of dynamic stiffness curve is very similar to the top chamber pressure curve. The reason is that the top chamber pressure is the major contributing factor for dynamic stiffness development.

It was shown earlier (Figure 5.3) that the bottom chamber pressure decreases nonlinearly with frequency; Figure 5.10b confirms this effect for frequency 1 to 100 Hz. Up to 5 Hz, chamber pressure remains constant from which it begins to decrease, gradually, with increasing frequency.

Figure 5.11 shows the variation of peak orifice flow and damping force as a function of frequency. Unlike to top chamber pressure development, orifice flow starts rising gradually with increase in frequency up to 20 Hz (Figure 5.11a), showing no further increment in orifice flow. Development of peak damping force shows mostly similar trend like peak top chamber pressure, as they are directly related. Although Figure 5.9b shows that the damping (loss angle) development by such damper diminishes with increase in frequency, here, damping force is high due to the fact that damping force is function of velocity and which, in turn, is a function of frequency.

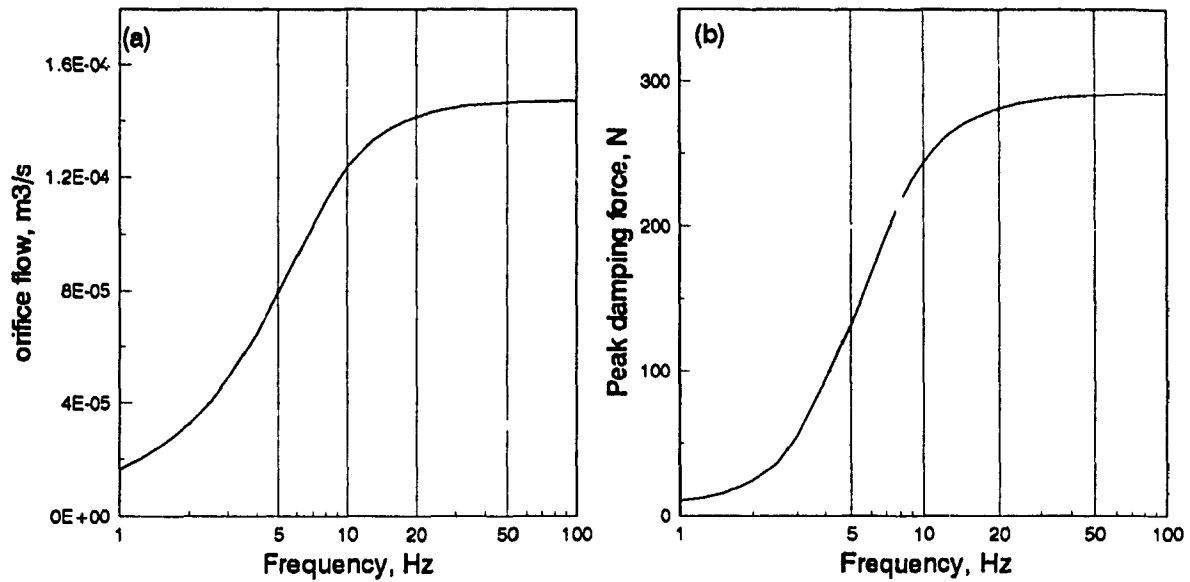


Figure 5.11 Effect of frequency of excitation on (a) orifice flow and (b) damping force. ( $X_1 = 1\text{mm}$ ; piston diameter 70mm; orifice diameter 4.5mm).

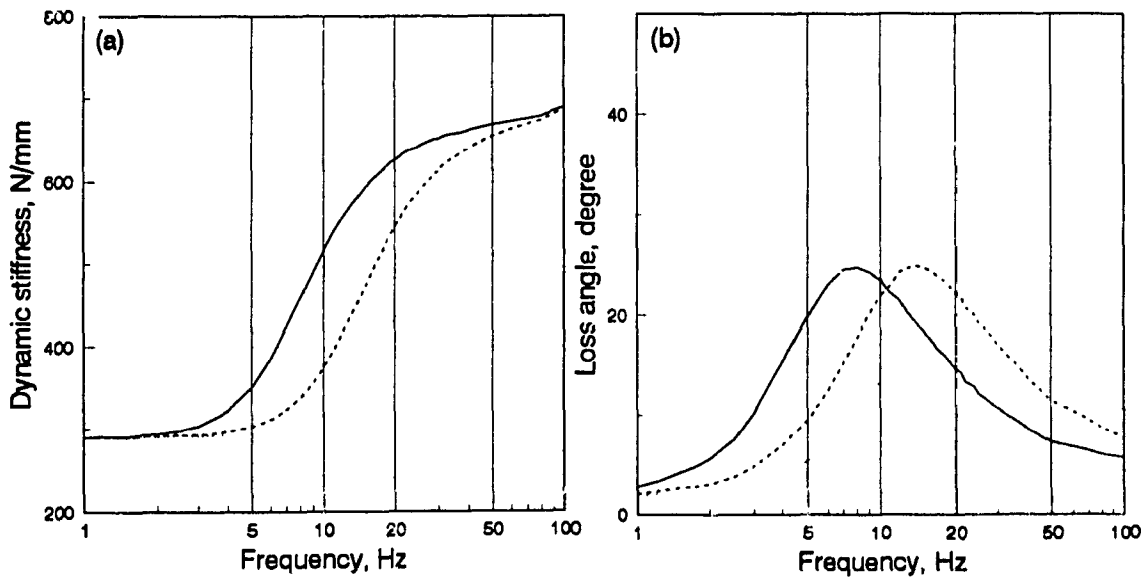


Figure 5.12 Effect of orifice diameter on (a) dynamic stiffness and (b) loss angle. Amplitude 1mm; piston diameter 70mm; orifice diameter, —, 4.5mm; ----, 6mm; ····, 7.5mm.

### 5.2.2.1 Parametric Study

A parametric study is next carried out in the frequency domain. Several damper parameters considered include: orifice diameter; piston diameter; top and bottom chamber compliance as well as shape of orifice opening and amplitude of excitation. Again one parameter is varied at a time while the others are kept equal to their nominal values.

(a) Orifice diameter: Fig. 5.12 shows the variation of rms dynamic stiffness and loss angle with the variation of orifice diameter. The amplitude of excitation is 1 mm and the static pressure in the chambers is 111.05 KPa. As the orifice diameter is increased, the frequency where the stiffness starts to increase from the static stiffness shifts to the right, as the pressure build up takes place at a higher frequency. At high frequency (100 Hz), however, the dynamic stiffness for all orifice size approaches the same value regardless of the size of the orifice, since the pressure in top chamber also approaches the same value. For larger orifice diameter, as the pressure develops at higher frequency, occurrence of maximum loss angle also shifts towards higher frequency. Figure 5.12b shows that for diameter of 6 mm, maximum loss angle occurs at 14 Hz and for 7.5 mm at 24 Hz. The maximum damping as loss angle in each case is identical. For a frequency of 100 Hz, however, the value of loss angle is higher for larger orifice size as the curves shift to the right.

The effect of orifice diameter on the top and bottom chamber pressure is shown in Figure 5.13. These results reconfirm the observations made in Figure 5.12. The trend for top chamber pressure is identical to that of dynamic stiffness. The orifice diameter has similar effect on the bottom chamber pressure as shown in Figure 13b. The drop in bottom chamber pressure is observed at higher frequency as the orifice size is increased.

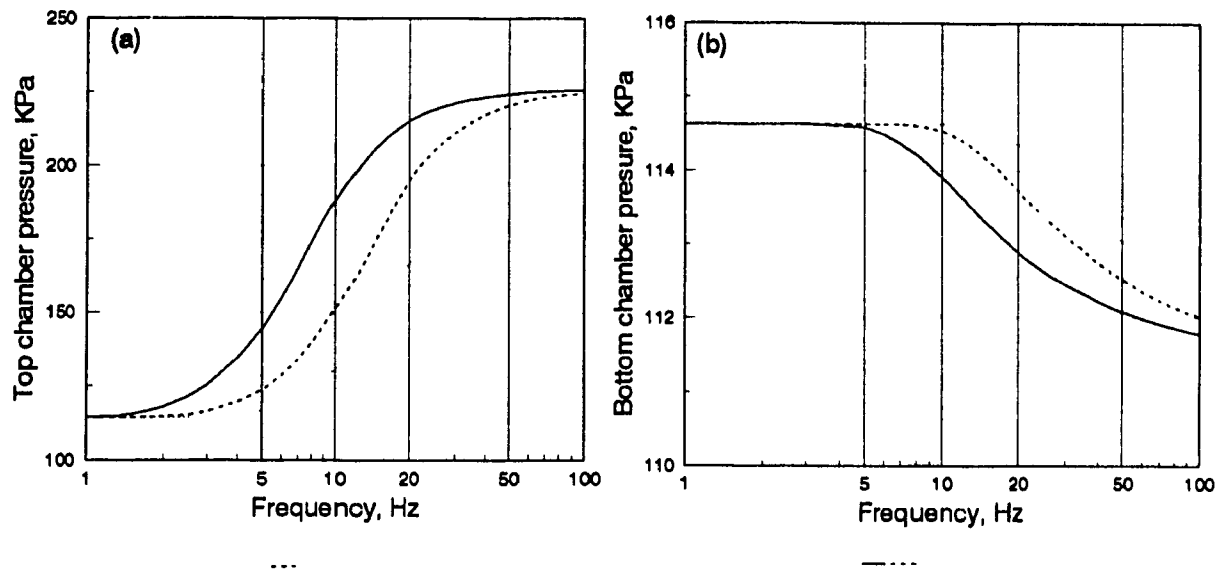


Figure 5.13 Effect of orifice diameter on (a) top chamber pressure and (b) bottom chamber pressure. Amplitude 1mm; piston diameter 70mm. Orifice diameter ; —, 4.5mm; ----, 6mm; ····, 7.5mm.

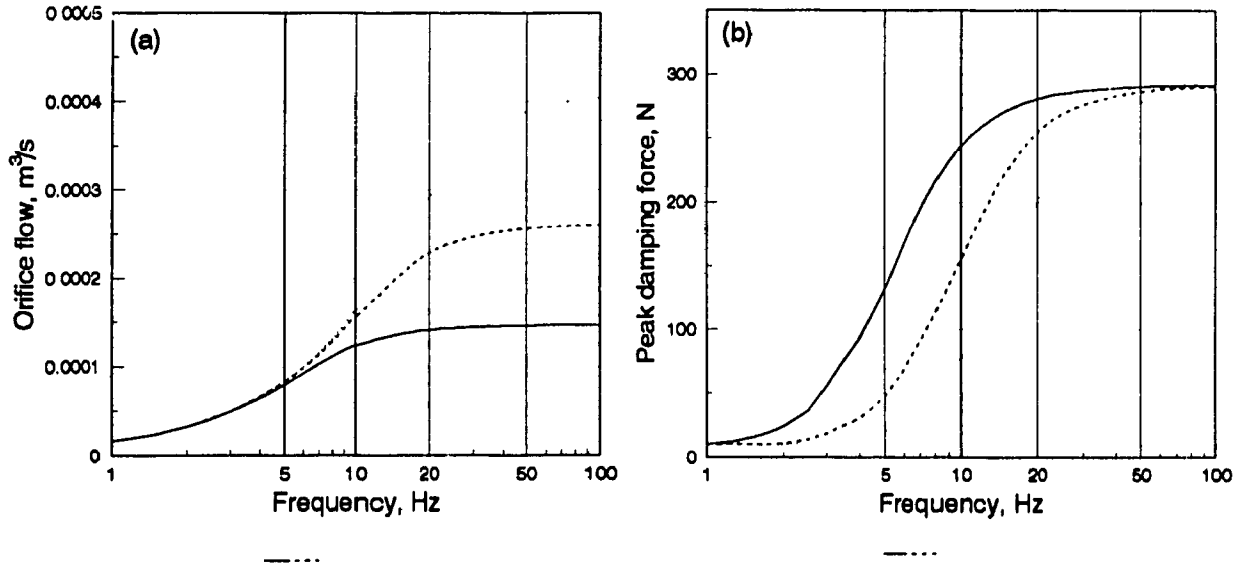


Figure 5.14 Effect of orifice diameter on (a) orifice flow rate and (b) peak damping force. Amplitude 1mm; piston diameter 70mm. Orifice diameter; —, 4.5mm; ----, 6mm; ····, 7.5mm.

The increase in orifice flow rate with frequency for the three orifice sizes is demonstrated in Figure 5.16a. At low frequency, up to 6 Hz, change in diameter causes very little increase in flow rate. Around 20 Hz, flow rate due to 7.5 mm orifice is double of that produced by 4.5 mm. At 50 Hz this increase almost triples and becomes steady. The final result presented in terms of peak damping force in Figure 5.14b again shows identical trend as that of top chamber pressure due to change in orifice size.

(b) Piston diameter: Since the effect of damper parameter is similar on dynamic stiffness, top chamber pressure and peak damping force, the effect of piston diameter only obtained for dynamic stiffness and loss angle. It was observed in Figure 5.8 that, at 10 Hz, increase in piston diameter increases the top chamber pressure. This trend holds for the whole frequency range of interest, 1 Hz to 100 Hz. Figure 5.15a shows the effect of piston diameter on dynamic stiffness and 5.15b shows its effect on loss angle for piston diameter 70 mm, 80 mm and 90 mm. It shows that at 90 mm piston diameter, dynamic stiffness almost doubles in comparison to the dynamic stiffness at 70 mm dia. By increasing piston diameter only by 30%, dynamic stiffness can be increased by more than 100%. But, as shown in Figure 5.15b, variation of piston diameter virtually has no effect on loss angle beyond 15 Hz, where all three curves coincide each other. Piston diameter has very important effect on magnitude and frequency of occurrence of peak loss angle. Peak loss angle is an important parameter as it can be utilized to isolate resonance response. Figure 5.15b shows that for 70 mm piston diameter, peak damping occurs at 8 Hz which shifts to 6 Hz with higher magnitude for larger piston diameter (90 mm). Therefore, if the maximum damping is required at lower frequency, piston diameter can be increased.

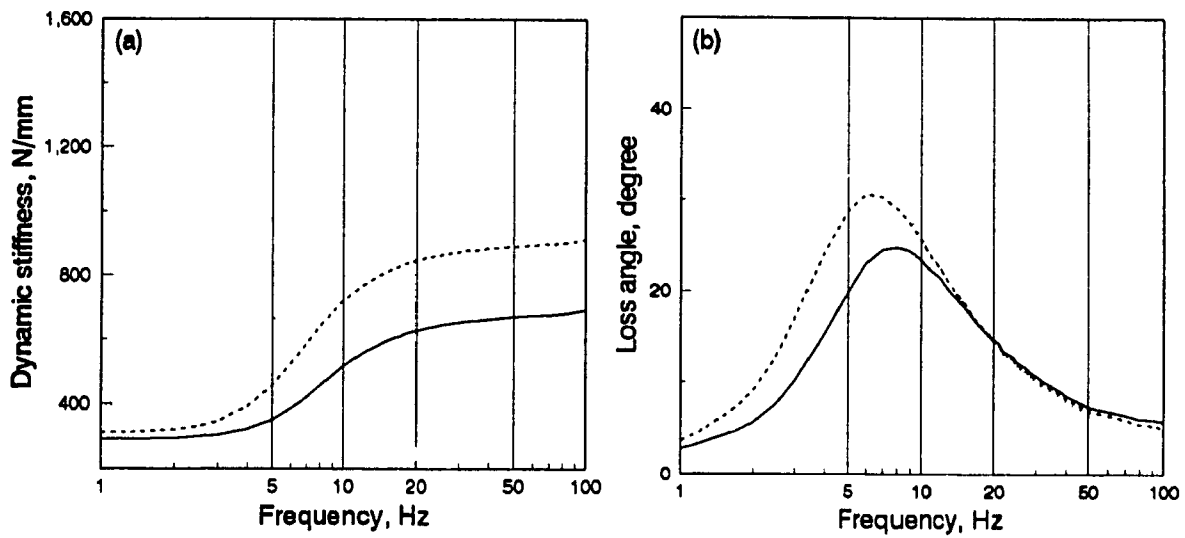


Figure 5.15 Effect of piston diameter on (a) dynamic stiffness and (b) loss angle.  $X_1=1\text{mm}$  at 10 Hz; piston diameter; —, 70mm; ---, 80mm; . . . , 90mm.

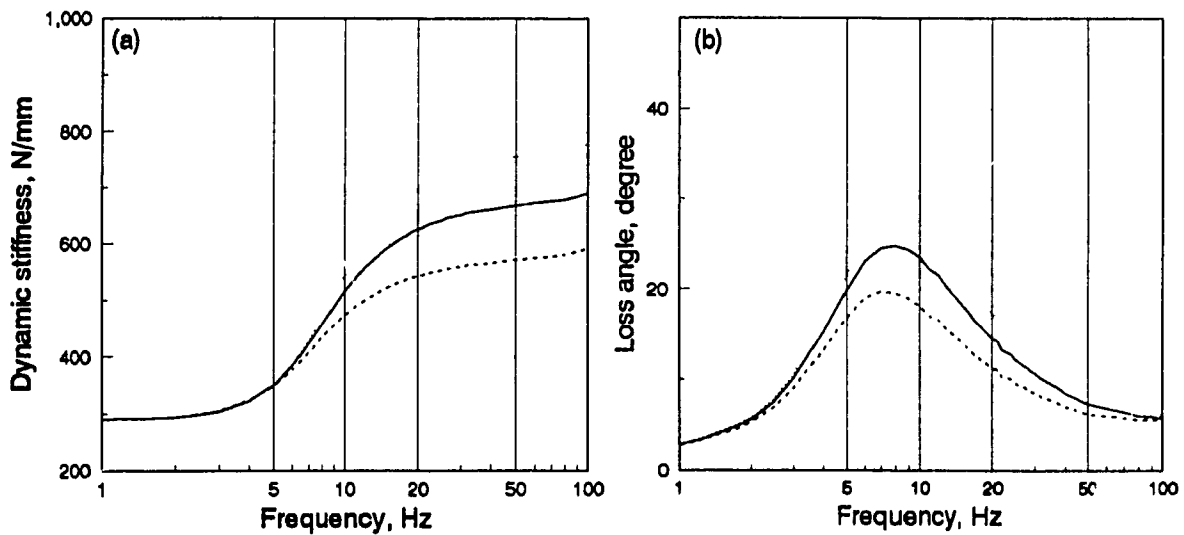


Figure 5.16 Effect of top chamber compliance on (a) dynamic stiffness and (b) loss angle.  $X_1=1\text{mm}$  at 10 Hz; orifice dia 4.5mm; piston diameter 70mm. —, Comp\_A; ---, Comp\_B; . . . , Comp\_C.

Similar to previous parameter, the effect of top chamber compliance is next examined for three different compliance, where results are only obtained for dynamic stiffness and loss angle.

(c) Top chamber compliance: Figure 5.16a shows the influence of top chamber compliance on the dynamic stiffness. Three different nonlinear compliances, Comp\_A, Comp\_B and Comp\_C as defined in section 3.2.2.2 and shown in Figure 3.2 are used. Comp\_B is more compliant than Comp\_A and Comp\_C is less compliant than Comp\_A. As the results show, the compliance of top chamber has small effect on the dynamic stiffness up to 10 Hz. However, the dynamic stiffness at high frequency is strongly influenced by compliance, where, an increase in the value of compliance (more compliant) results in lower dynamic stiffness. The effect of top chamber compliance on the loss angle as shown in Figure 5.16b is prominent only around the peak. An increase in compliance leads to a lower peak for loss angle characteristics.

(d) Bottom chamber compliance: Figure 5.17 presents the results for variation in bottom chamber compliance. Two nonlinear compliances referred to as Comp\_D and Comp\_E presented in section 3.2.2.2 and Figure 3.3 are used, while Comp\_A is retained for the top chamber. In this case Comp\_E is lower than Comp\_D. Due to the very high compliance of the bottom chamber wall, its effect on top chamber pressure is very small. The results (Figure 5.16b) also, show that a decrease in bottom chamber compliance produces a negligible increase in dynamic stiffness, and a small increase in the peak loss angle value. Here the shifts in curves are primarily for the change in static characteristics as the compliance is changed.

The model developed in this investigation includes the effect of orifice geometry as discussed in section 3.2.2.



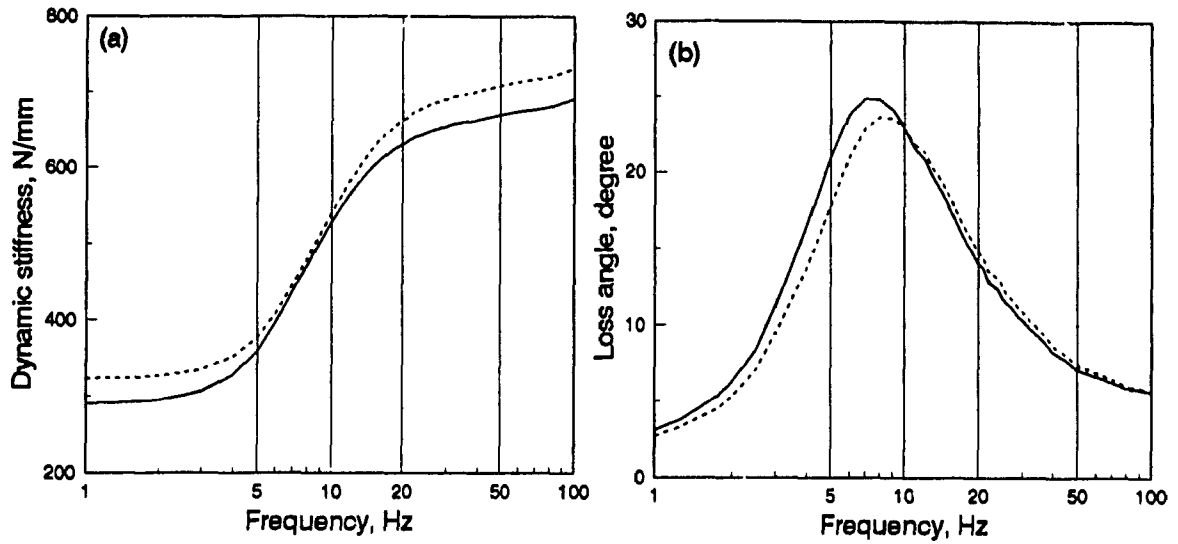


Figure 5.17 Effect of bottom chamber compliance on (a) dynamic stiffness and (b) loss angle.  $X_1=1\text{mm}$  at 10 Hz; orifice dia 4.5mm; piston diameter 70mm. Comp\_D; -----, Comp\_E.

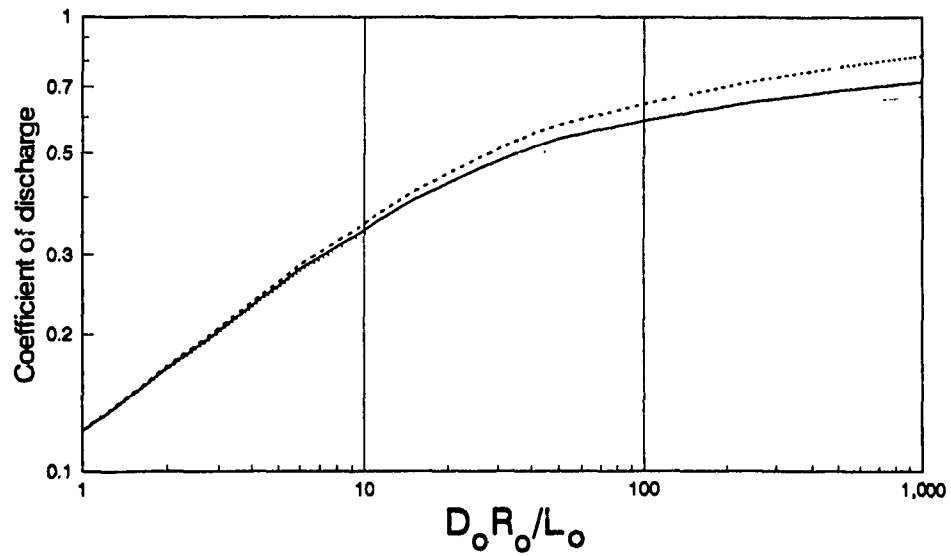


Figure 5.18 Coefficient of discharge for various orifice opening. —, sharp edge; -----, rounded edge; . . . , projected edge.

(e) Opening of orifice: Three different geometry of orifice entrances and exits are considered in this investigation, namely, i) sharp-edged, ii) well-rounded edge and iii) projected edge. These geometry and their parameters were presented in Table 3.1. Figure 5.18 shows the changes of coefficient of discharge due to the change of orifice opening. It shows that orifice with projected edge has the minimum coefficient of discharge for any Reynolds number. The orifice with rounded edge has the maximum coefficient of discharge (minimum resistant). Figure 5.19 presents the dynamic stiffness characteristics and loss angle of the hydraulic damper for the different orifice opening. As the results show, the dynamic stiffness is not highly influenced by the shape of the orifice. However, well rounded orifice opening has the minimum resistance coefficient ( $k=0.05$ ), leading to minimum dynamic stiffness, whereas projected edge ( $k=0.80$ ) develops maximum dynamic stiffness. In the case of loss angle, changes in orifice opening only change the frequency for occurrence of the peak value.

(f) Amplitude of excitation: To examine the influence of excitation amplitude, the dynamic stiffness characteristic is obtained for excitation amplitudes of 1, 0.75 and 0.5 mm as shown in Figure 5.20a. As the results show, lower excitation leads to higher dynamic stiffness for higher frequencies ( $>20$  Hz), whereas within the range of 4-20 Hz, dynamic stiffness decreases with decrease in amplitude. Previous investigation such as Reference [1] shows the opposite effect i.e., higher dynamic stiffness at lower amplitude of excitation for all range of frequency which is not feasible from practical point of view. Smaller amplitude of excitation leads to low pressure development with increase in frequency, and consequently lower damping force is developed. Lower amplitude means low orifice flow rate and less pressure buildup. Although pressure decreases throughout the whole range of frequency with decrease in amplitude, the reason for dynamic stiffness increase at higher frequency results from its definition. For a particular frequency, peak

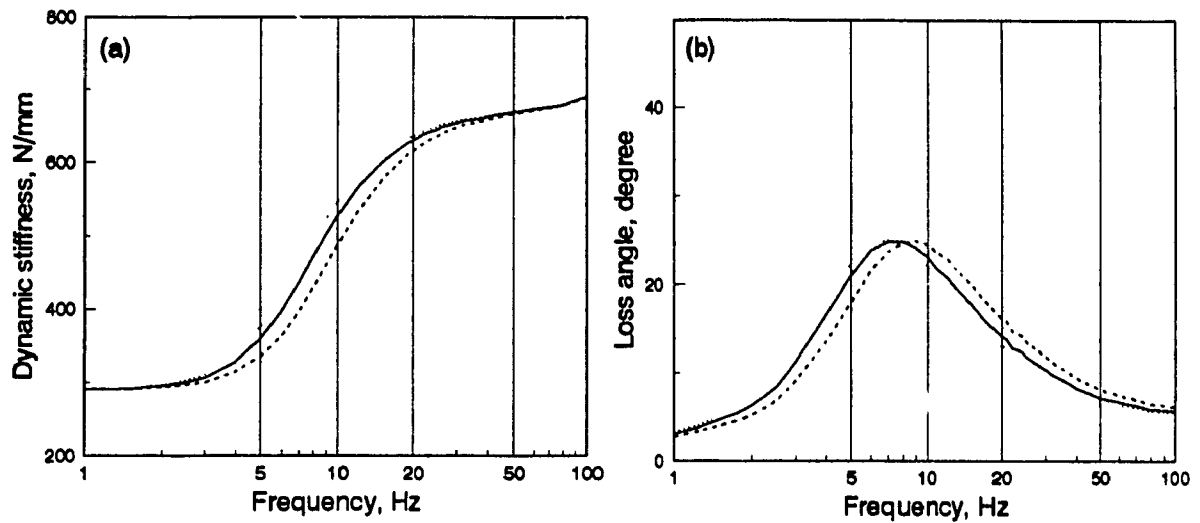


Figure 5.19 Effect of orifice opening on (a) dynamic stiffness and (b) loss angle.  $X_1=1\text{mm}$  at 10 Hz; orifice dia 4.5mm; piston diameter 70mm. —, squared edge; ----, sharpened edge; ····, extended edge.

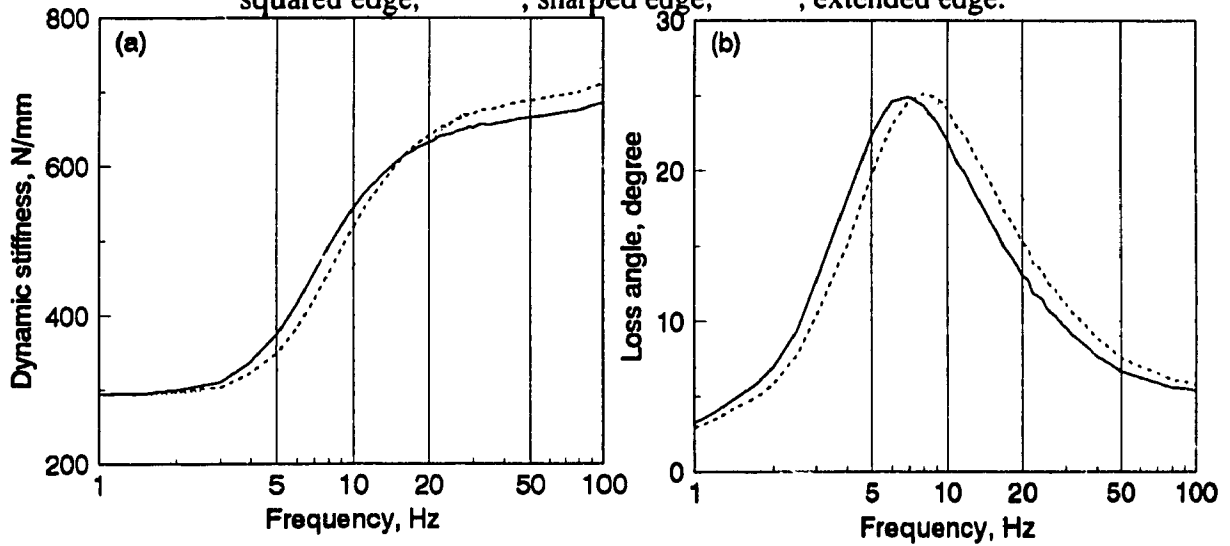


Figure 5.20 Effect of amplitude of excitation on (a) dynamic stiffness and (b) loss angle. Orifice dia 4.5mm; piston diameter 70mm. Amplitude —, 1mm; ----, 0.75mm; ····, 0.50mm.

transmitted force divided by peak amplitude gives the dynamic stiffness. The simulation results obtained here show that at high frequencies the decrease in pressure for a decrease in amplitude is not proportional which leads to higher dynamic stiffness. Lower amplitude of excitation simply shifts the loss angle curve to the right as shown in Figure 5.20b. The peak value of loss angle is not affected by the amplitude of excitation considered.

### **5.3 Performance Analysis of Hydraulic Damper**

To the best knowledge of the author, performance analysis of short orifice flexible chamber damper is not available in the literature. The objective in this section is to carry out a detailed performance evaluation of the damper both under vibration and shock excitations. For this, the nonlinear damper mounted on a simple system as shown in Figure 3.7 is used, where the hydraulic isolator with the flexible chamber provides both stiffness and damping. Results are obtained as acceleration and relative displacement transmissibility in the frequency domain. A parametric study is carried out for variation of important damper parameters which include: orifice diameter; piston diameter and top chamber compliance. The performance under shock input is obtained both in time domain and as a function of shock severity. The nominal parameters for the system include: sprung mass 125 kg; orifice diameter 6 mm; length 10 mm; diameter of the piston 70 mm and Comp\_A and Comp\_D compliances.

#### **5.3.1 Performances Under Sinusoidal Excitation**

Rms acceleration transmissibility for the single DOF system with nominal damper parameters for three different amplitude of excitation is shown in Figure 5.21(a). Corresponding rms relative displacement transmissibility is shown in Figure

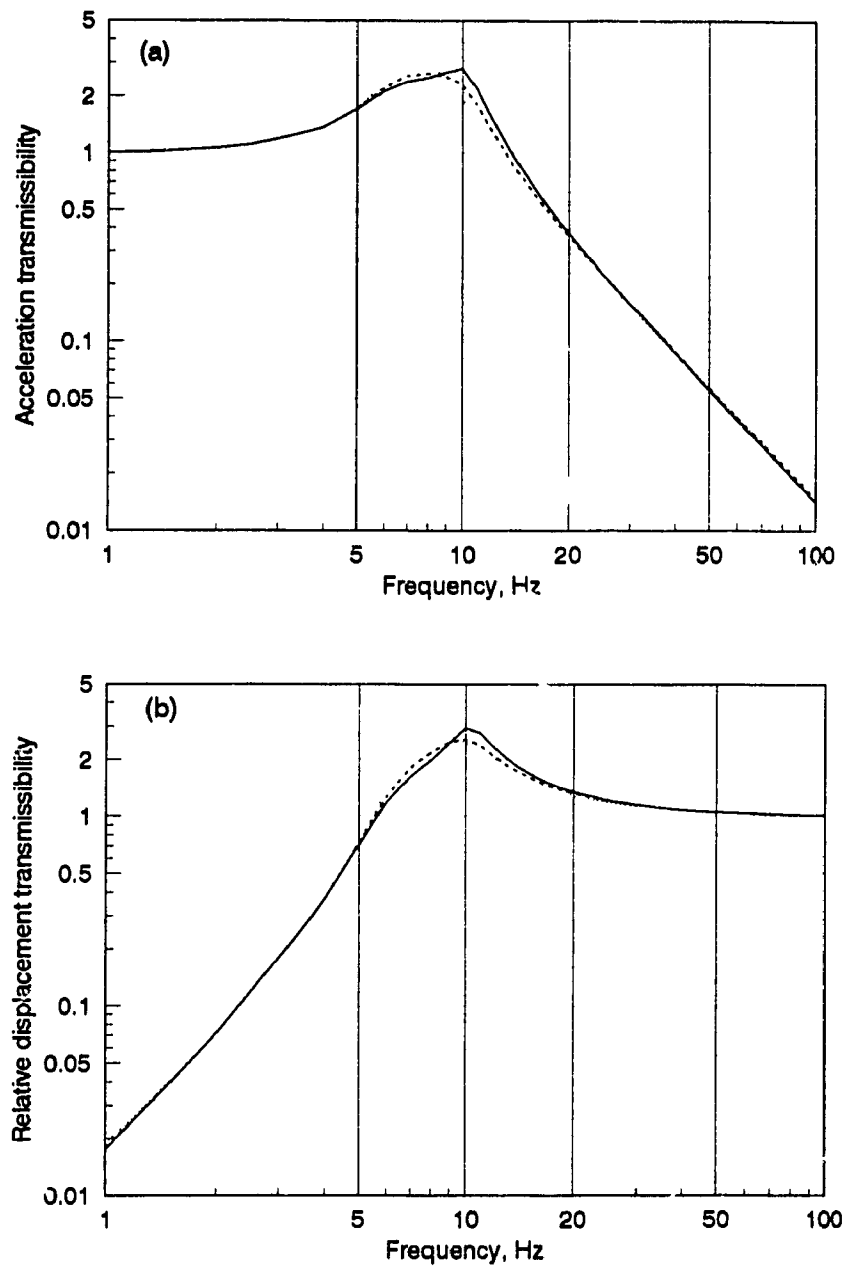


Figure 5.21 Effect of amplitude of excitation on (a) acceleration transmissibility and (b) relative displacement transmissibility. Orifice dia 6mm; piston diameter 70mm. Amplitude; —, 1mm; ---, 0.75mm; ···, 0.50mm.

5.21(b). It is seen that around resonance frequency the acceleration transmissibility is rather high in all cases, where higher amplitude of excitation leads to poor performance for a range of frequency beyond resonance. For all amplitudes considered, high frequency transmissibility shows inert to the amplitude, where such dampers provide superior performance. At low frequency, relative transmissibility is independent of excitation amplitude and at resonance frequency zone lower amplitudes shows lower transmissibility. Relative transmissibility finally reaches to unity at high frequency. Such damper can be tuned to give superior performance for high frequency low amplitude vibration isolation such as isolation of noise. The tunability of such damper can be better understood from a parametric study that examines the influences of important parameters on the transmissibility performance

#### 5.3.1.1 Parametric Study

For the parametric study in this section, the damper parameters that are considered include: (a) diameter of the orifice, (b) diameter of the piston; and (c) the top chamber compliance. One parameter is varied at a time while all other held equal to their nominal values. Responses are obtained for 1 mm amplitude of excitation.

(a) Orifice diameter: Effect of orifice diameter on the rms acceleration transmissibility as well as on rms relative displacement transmissibility as a function of frequency is shown in Figure 5.22. Four different diameters in the range of 5 to 10 mm are chosen to examine their influence when the compliance of the chamber is fixed. As the results show, the orifice diameter, in addition to the compliance property, has significant influence on resonance as well as high frequencies. In general larger orifice diameter produces superior high frequency performance. The resonance performance in this case is interesting as the peak response first decreases and then increases as the diameter is reduced from 10 to 5

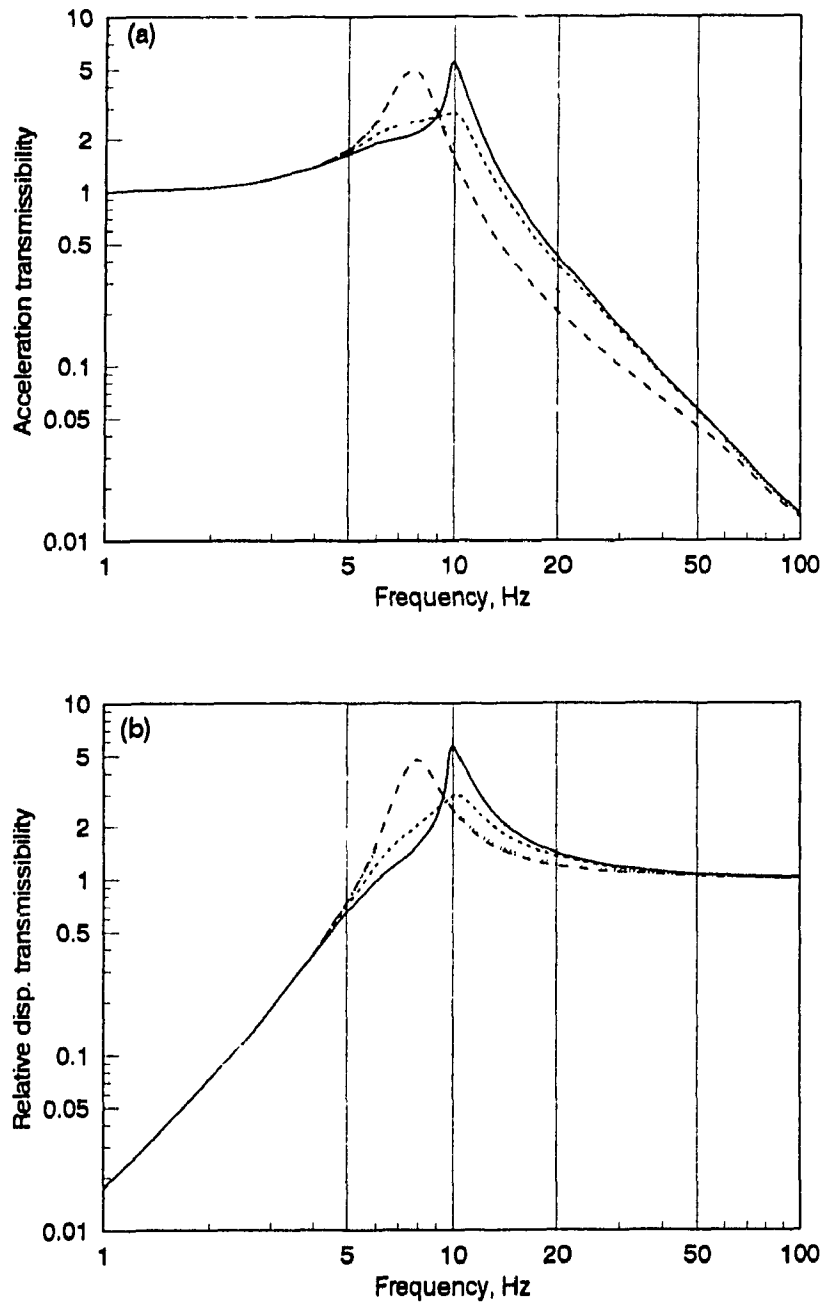


Figure 5.22 Effect of orifice diameter on (a) acceleration transmissibility and (b) relative displacement transmissibility. Amplitude 1mm; piston diameter 70mm. Orifice diameter, —, 5mm; ----, 6mm; — · —, 8mm; ····, 10mm.

mm. The reason behind this outcome may be explained in the following manner. As the diameter is decreased, the damping effect increases up to certain limit. For a given compliance, when the diameter is less than a certain value (between 5 and 6 mm), enough fluid can not flow through the orifice, and a greater portion of the fluid remains in the top chamber. The compliance of the chamber in turn receives the fluid leading to higher dynamic stiffness. The resonance therefore, occurs at a frequency much higher than system's natural frequency (7.9 Hz). As the diameter is made very large, (10 mm) the damping is again low, but in this case the compliance of the chamber does not receive additional fluid to increase the dynamic stiffness. Here the dynamic natural frequency is equal to the system's natural frequency. That means top chamber is not making the system stiffer, and is acting as a piston only. Similar observation can be made for relative displacement transmissibility too as shown in Figure 5.22b.

(b) Piston Diameter: The diameter of the upper element of the top chamber which acts as a piston is varied to analyze its effect on dynamic performance. To minimize the effect of compliance, orifice diameter is chosen as 7.5 mm. The rms acceleration transmissibility response is shown in Figure 5.23. It shows that the larger the piston area, the higher the damping and the better is the resonance transmissibility. The improvement in resonance response is, however, obtained at a significant expense of high frequency response.

(c) Top Chamber Compliance: The influence of top chamber compliance on the acceleration transmissibility is shown in Figure 5.24. The compliances used are same as those presented in section 3.2.2.2 and referred to as Comp\_A, Comp\_B and Comp\_C. As shown in Figure 3.2, Comp\_B is more compliant than Comp\_A and Comp\_C is less compliant than Comp\_A. This parameter has some influence on both resonance and high frequency response. Larger top chamber compliance



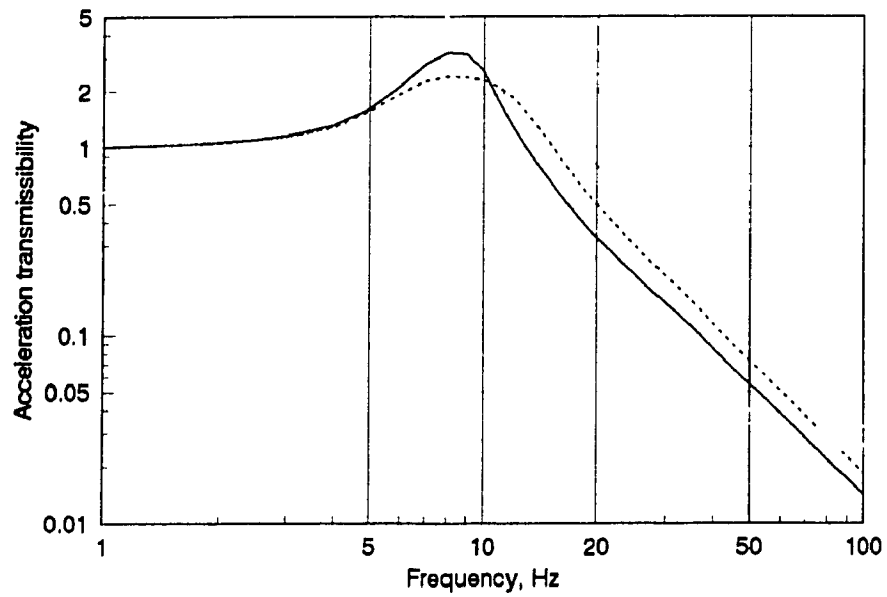


Figure 5.23 Effect of piston diameter on (a) acceleration transmissibility. Amplitude 1mm; orifice diameter 7.5mm. Piston diameter, —, 70mm; ----, 80mm; ····, 90mm.

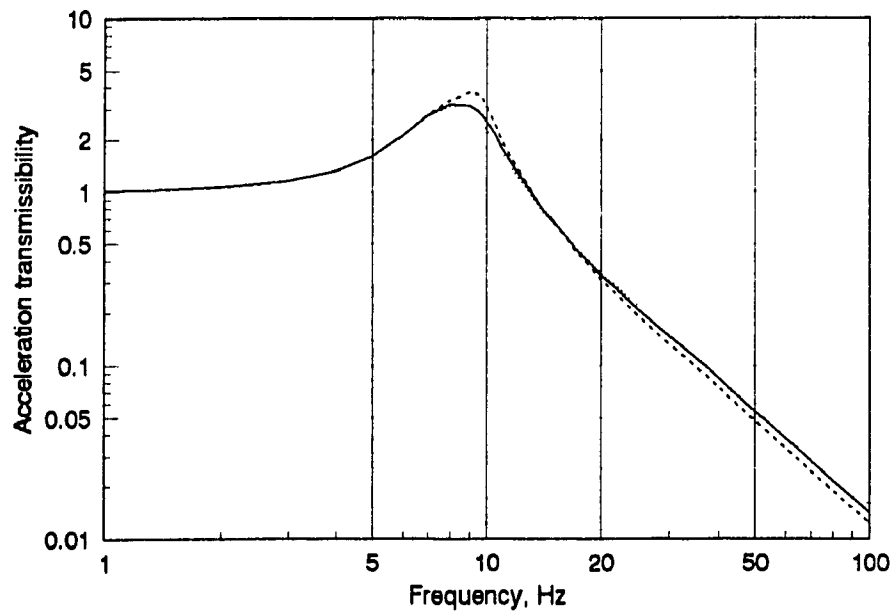


Figure 5.24 Effect of chamber compliance on (a) acceleration transmissibility. Amplitude 1mm; orifice diameter 7.5mm. —, Comp\_A ; ----, Comp\_B; ····, Comp\_C.

effectively reduces the damping effect throughout the frequency range leading to higher response at resonance and lower response at high frequencies.

### **5.3.2 Performances Under Shock Displacement**

The performance of the short orifice hydraulic damper (SDHF) under the application of shock displacement is investigated in time domain and in shock severity domain for different shock severity. The characteristics of the shock input is discussed and presented in detail in section 4.5.1. The shock excitation characteristics for different shock severity is presented in Figure 4.18. The range for the shock severity is varied from 0.05 to 5, which is a satisfactory range to cover all levels of shock the hydraulic damper may encounter for different applications. As discussed in section 4.5.1, the shock severity number is a relative term, depending both in duration of shock and natural frequency of the system. The lower the natural frequency, the lower the shock severity number, although the intensity of the shock remains the same. Similar to dual-phase damper, SDHF is also subjected to a rounded pulse shock displacement, shown in Figure 4.18a. The shock input is applied to the base of the one DOF system with an amplitude of 20 mm. The performance of the damper is shown in time domain in terms of acceleration ratio, velocity ratio, displacement ratio and relative displacement ratio. In shock severity domain the responses are taken as shock acceleration ratio, shock velocity ratio, shock displacement ratio and shock relative displacement ratio. These performance indices are also defined in section 4.5.1.

#### **5.3.2.1 Time Domain Analysis**

Figure 5.25 shows the acceleration ratio and velocity ratio of the one ODF system encountered by the shock displacement with severity of magnitude 0.1, 0.5 and 1.0. The shock severity below 0.5 is considered static region because the period of

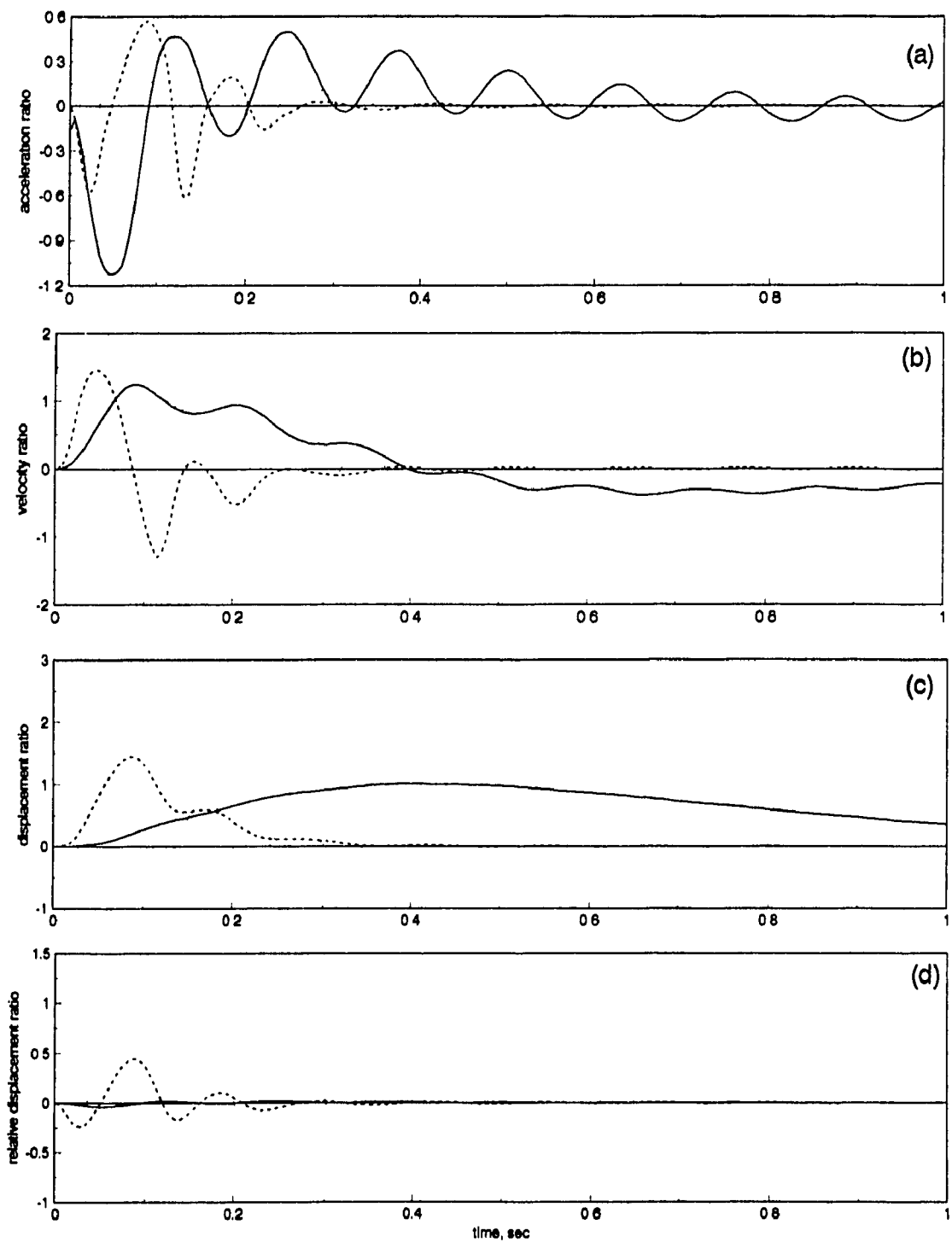


Figure 5.25 Shock responses in time domain. Shock severity, —, 0.1; ----, 0.5; ···, 1.0; (a) acceleration ratio, (b) velocity ratio, (c) displacement ratio, (d) relative displacement ratio.

the natural frequency is higher than the duration of the pulse. The damper parameters are: orifice diameter 6 mm, piston diameter 75 mm.

The acceleration ratio for shock severity  $\nu = 0.1$  seems to be unsatisfactory as the ratio decreases within a cycle but it continues to oscillate for a long time (more than one second). The acceleration for other shock severity tends to decrease rapidly but still it makes more than three oscillations before it diminishes. The peak acceleration ratio decreases with the increase in shock severity and duration of acceleration tends to decrease with shock severity. This observation is similar to those observed for dual-phase damper. The velocity ratio of the sprung mass shown in Figure 5.25b exhibits highest peak for the highest shock severity ( $\nu = 1$ ). Again the trend is same as that of a dual-phase damper. The displacement ratio and relative displacement ratio in time domain are shown in Figure 5.25c and 5.25d. It is obvious from Figure 5.25c that the displacement ratio at  $\nu = 0.1$  and 0.5 are static one, where the effect is not significant. At  $\nu = 1.0$ , it takes three oscillations before the response diminishes, which is not a good response compared to other types of dampers. The peak relative displacement ratio increases with the increase in shock severity as seen in Figure 5.25d. The duration of relative displacement in terms of number of oscillation also increases for increased severity. The shock response of this damper in general shows similar trend as that of a dual-phase damper, but is inferior in all categories.

#### **5.3.2.2. Performance Analysis in Shock Severity Domain**

Figure 5.26 exhibits the shock acceleration ratio (SAR), shock velocity ratio (SVR), shock displacement ratio (SDR) and relative displacement ratio (RDR) of the short orifice hydraulic damper as a function of shock severity. The results presented here are obtained for three different sizes of short orifice diameter. At very low shock severity, acceleration increases with the increase in orifice

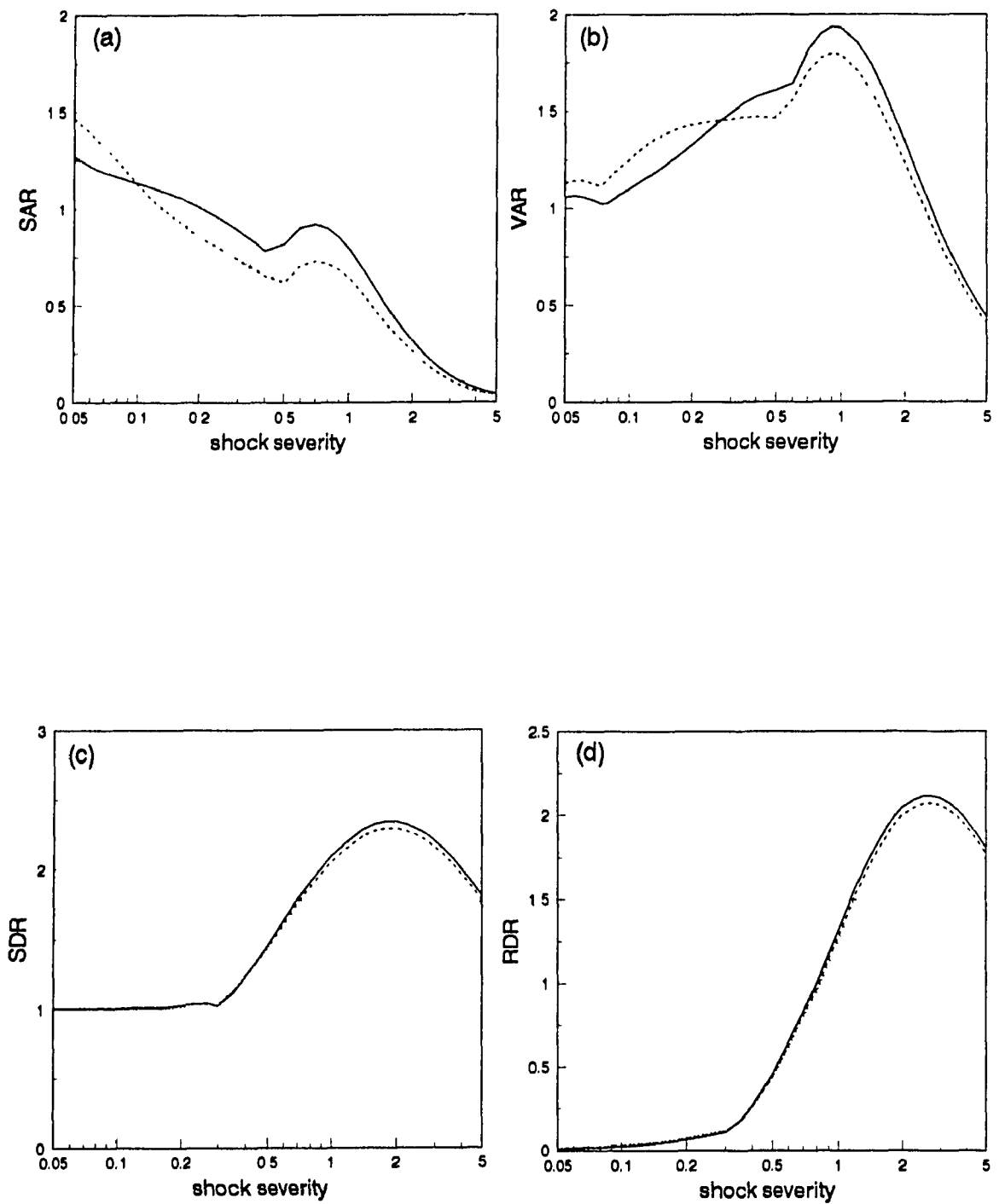


Figure 5.26 Shock responses as a function of shock severity with the variation of orifice diameter; —, 4mm; ---, 6mm; ···, 8mm; (a) SAR, (b) VAR, (c) SDR, (d) RDR.

diameter but for mid range of shock severity considered, large orifice diameter leads to significantly better SAR performance. The SAR performance of the short orifice damper is comparable to that of a dual-phase damper where high-low type dual-phase provides the best performance.

The shock velocity ratio (SVR) of the damper as shown in Figure 5.26b, increases with the increase in orifice diameter for up to a value of severity where duration of pulse equal to the natural period of the system (static region). For higher severity, SVR decreases considerably as the orifice diameter is increased.

The static region is clearly visible in shock displacement response (SDR) and shock relative displacement response (RDR) as presented in Figure 5.26c. The SDR is unity for severity of up to 0.4 and increases to a maximum at  $\nu = 2$ . Here also larger orifice diameter makes the damper perform better. Similar performance is observed (Figure 5.26d) for RDR response except RDR is close to zero for low shock severity.

The results in shock severity domain clearly demonstrate that, for isolation of shock, hydraulic damper with short orifice requires larger orifice diameter. However, a compromise will be required as larger diameter leads to poor isolation of vibration at resonance. Again comparison of results with dual-phase response in severity domain shows significantly better performance of dual-phase damper under shock excitation.

## 5.4 Summary

The nonlinear model of damper developed in chapter 3 is used with nonlinear chamber compliance and effect of orifice geometry. The damper characteristics is evaluated in time domain at selected frequencies and for various orifice and piston diameter. In general, increase in orifice diameter increases the orifice flow rate leading to reduced transmitted force. Whereas increase in piston diameter

increases orifice flow rate and the peak transmitted force. The characteristics obtained in frequency domain shows identical trend for dynamic stiffness, top chamber pressure and peak damping force. The loss angle characteristics in this case is bell shaped with low value for low and high frequency. Such damper can, therefore, be tuned to provide the maximum damping only near resonance. Among all parameters varied, the effect of bottom chamber compliance and orifice geometry had the least effect, and top chamber compliance and orifice diameter had the most effect on the dynamic characteristics.

In general, the isolation performance of damper is found to be good for low amplitude high frequency vibration. The orifice diameter along with top chamber compliance plays the most important role in performance. Smaller orifice may lead to higher damping and better resonance response until the compliance takes over, where dynamic stiffness will increase leading to low damping and poor resonance response.

The trend for shock isolation performance is found to be similar to that of dual-phase dampers. Increase in shock severity leads to decrease in peak acceleration response while the displacement and relative displacement responses increase. Increase in orifice diameter improves shock responses in all categories except for shock velocity ratio when severity is low. The overall performance of short orifice damper in isolation of shock is considerably poor when compared to that of a high-low dual-phase damper.

## **CHAPTER 6**

# **CHARACTERISTICS AND PERFORMANCE OF LONG ORIFICE HYDRAULIC DAMPER**

### **6.1 Introduction**

A detailed nonlinear dynamic model of long orifice hydraulic damper with flexible chamber was developed and presented in chapter 3. The model includes nonlinear compliance and oscillation effect of the fluid within the long orifice. The model for the long orifice damper was also extended to include a short orifice as bleeder orifice. The objective of this section of the study is to carry out a detailed analysis of the model by investigating the damping characteristics and performance of the damper in isolation of vibration and shock.

The damping characteristics are evaluated by systematic simulation of the model in time and frequency domain. A detailed parametric study is carried out to examine the influences of oscillation effect, compliance and all internal variables of the long orifice damper as well as amplitude of excitation on the time response and dynamic characteristics. The performance of the damper is further evaluated by utilizing it in a single DOF model subjected to sinusoidal as well as shock excitation. Effects of important parameters on these performances are also examined.

This section finally presents the results of the extended model that includes a short bleeder orifice with the long orifice system. Again, the dynamic damper



characteristics and performance of the damper is evaluated for a range of short orifice parameters.

In all cases the damper characteristics are evaluated by applying sinusoidal excitation at the top while keeping the base of the damper fixed. For performance analysis, a mass of magnitude 125 kg is placed on the damper, while the base is excited. The density of the hydraulic fluid is considered  $980 \text{ kg/m}^3$ . The absolute viscosity of the fluid is taken as  $0.004 \text{ kg-sec/m}$ . To avoid vacuum of the chamber during extension stroke of the damper, 0.5 cc air is considered entrapped within the damper which governs pressure volume relationship at negative pressure stage. The procedure used in this was further explained in chapter 3. The nominal parameters for the long orifice damper include: orifice dia 6 mm; orifice length 5 mm; piston dia 75 mm; top chamber compliance Comp\_A and bottom chamber compliance Comp\_D. In all cases amplitude of excitation used is 1 mm unless mentioned otherwise.

## **6.2 Characteristics of the Long Orifice Hydraulic Damper**

The damper characteristics is evaluated by examining the effect of parameter on the internal variables such as orifice flow rate, top chamber pressure as well as damping and transmitted forces. The time responses are again obtained for a few different frequencies. The effect of important parameters such as orifice diameter, length and piston diameter on the time response are also examined. The characteristics are finally obtained in terms of dynamic properties such as dynamic stiffness and loss angle along with the chamber pressure and orifice flow rate as a function of frequency. For each parametric study, one parameter is varied at a time while the others are maintained at their nominal values.

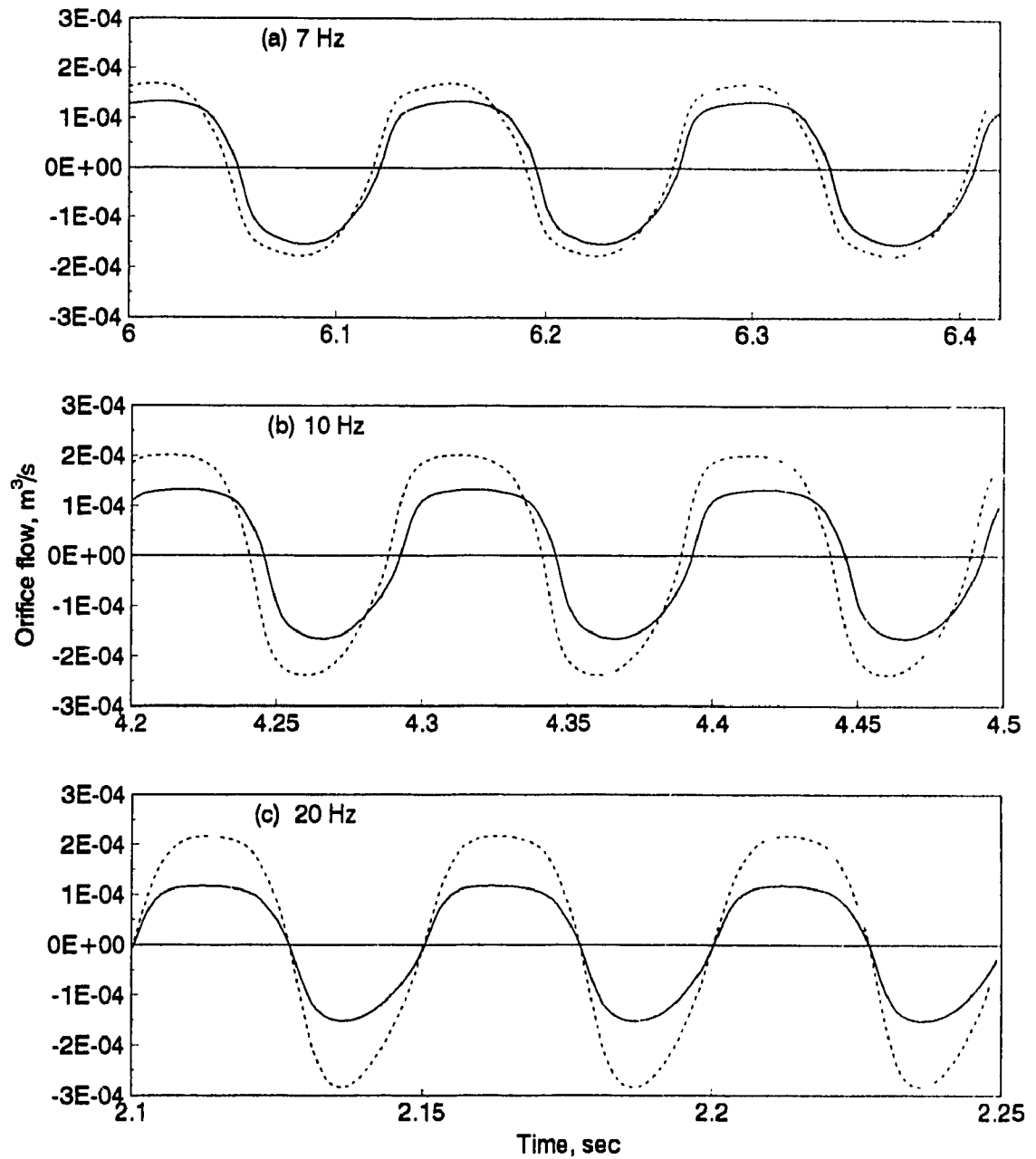


Figure 6.1 Orifice flow characteristics in time domain at different frequencies; oscillation effect, —, considered; ---, not considered; ( $X_1=1\text{mm}$ ;  $L_o=50\text{mm}$ ,  $D_o=6\text{mm}$ ).

### 6.2.1 Time Domain Analysis

Since the model developed in this study includes the effect of fluid oscillation within the orifice, one of the first results obtained is to examine its influence. Figure 6.1 presents the steady state time variation of orifice flow rate at three different frequencies (7, 10 and 20 Hz). The solid line is obtained from the analysis with the consideration of oscillation effect. The dotted lines are for without oscillation effect. It is clearly visible that ignorance of oscillation effect during analytical estimation greatly overestimates the orifice flow. This overestimation is more than 100% at higher frequency (20 Hz). Peak orifice flow rate, with the consideration of oscillation effect, decreases with increase in frequency whereas the flow rate increases with frequency when oscillation effect is not considered. The orifice flow rate calculation without the effect of oscillation is based on the established flow equation for a steady flow through pipe. But in practice, the flow is highly oscillatory specially at higher frequencies. For a given frequency, the amount of fluid flowing during forward cycle get hindered during reverse flow due to inertia effect of the fluid along the boundary layer. Therefore, at steady state, effective flow rate reduces and the effect is more prominent and highly significant at higher frequencies. A comparison of long orifice flow rate with that of short orifice (SDHF) presented in Figure 5.1 indicates a similarity except that during reverse flow (bottom chamber to top chamber half cycle), flow rate sharply reaches to maximum flow and retains as maximum flow. This phenomenon is prominently visible at higher frequency and with consideration of oscillation effect. The pressure difference during reverse flow, which is responsible for orifice flow, remains constant for longer time.

Figure 6.2 shows the variation of top chamber pressure of the damper with time at different frequencies. Result is obtained with the consideration of oscillatory flow. Like SDHF, variation of top chamber pressure is highly nonlinear

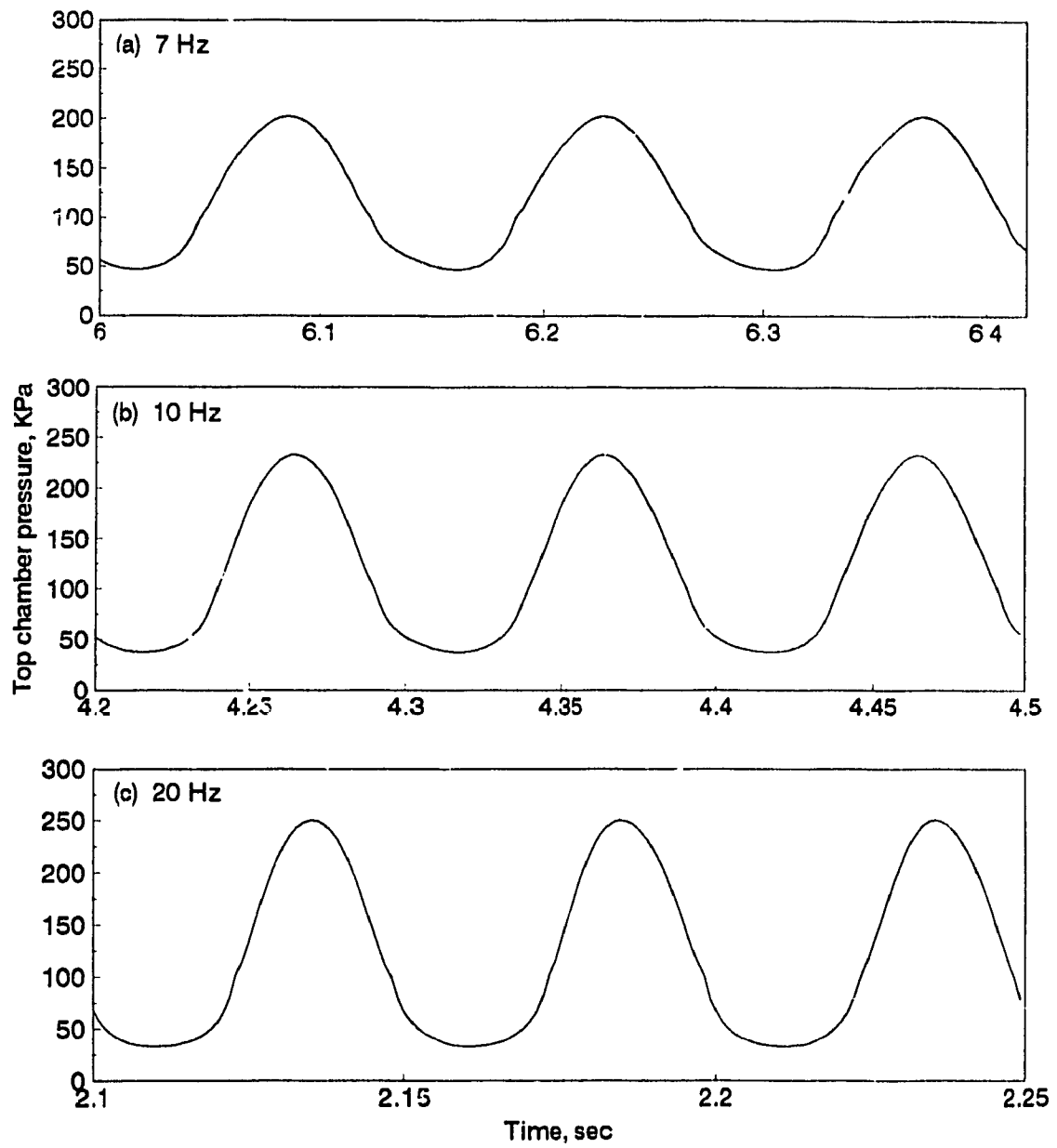


Figure 6.2 Top chamber pressure characteristic in time domain at different frequencies. ( $X_1=1\text{mm}$ ;  $L_o=50\text{mm}$ ,  $D_o=6\text{mm}$ ).

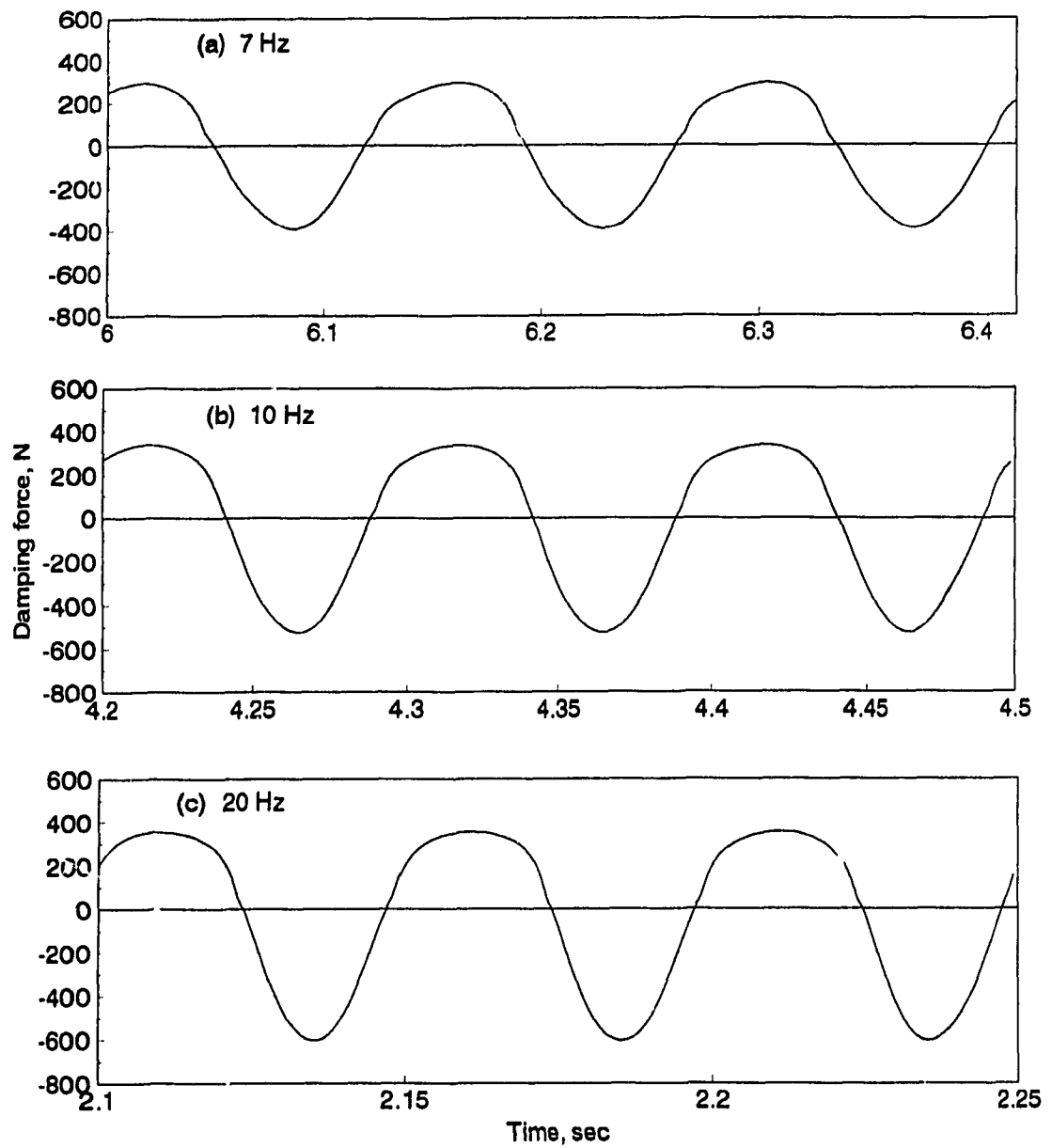


Figure 6.3 Damping force characteristic in time domain at different frequencies. ( $X_1=1\text{mm}$ ;  $L_o=50\text{mm}$ ,  $D_o=6\text{mm}$ ).

and increases with frequency. Sub-atmospheric pressure occurs during reverse stroke at all frequencies. At 10 Hz, minimum pressure goes as low as 37.4 KPa at the top chamber and minimum pressure at the bottom chamber is 112 KPa. Therefore minimum pressure ratio between top and bottom chamber might be in the range of 0.30 to 0.35. By observing the discharge coefficient curves for cavitation considered [31], this ratio indicate that slight cavitation might occur at high Reynolds number. This means that for a very shorter period of cycle the fluid may contain liquid vapor mixture which disappears as soon as pressure ratio rises above 0.35. At very low frequency and at low amplitude of excitation negative pressure does not exist. The trend of pressure variation and magnitude of minimum and maximum pressure correlate quite well with the results obtained experimentally for nearly similar type of LDHF by Kim and Singh [17].

The damping force characteristic of the nominal LDHF damper in time domain is shown in Figure 6.3. The propensity of the curve is the opposite phase of top chamber pressure distribution with time, because top chamber pressure is the only contributing factor for damping force. The asymmetry of the damping force i.e., difference in variation during forward stroke and variation during reverse stroke exists and damping force during forward stroke increases with frequency as shown by figure 6.3(a), (b) and (c) but the increment with frequency during reverse stroke does not exist.

The transmitted force-time history of the nominal LDHF damper is shown in Figure 6.4 for three different frequencies. These curves show the variation in the trend of the transmitted force. At 7 Hz, variation of transmitted force is nonsinusoidal and symmetric. But with the increase in frequency (10 Hz and 20 Hz), asymmetry as well and nonsinusoidal nature increases. The transmitted force versus excitation displacement (Lissajous plots), at those frequencies are plotted in Figure 6.5. Second column in the figure shows the same but without

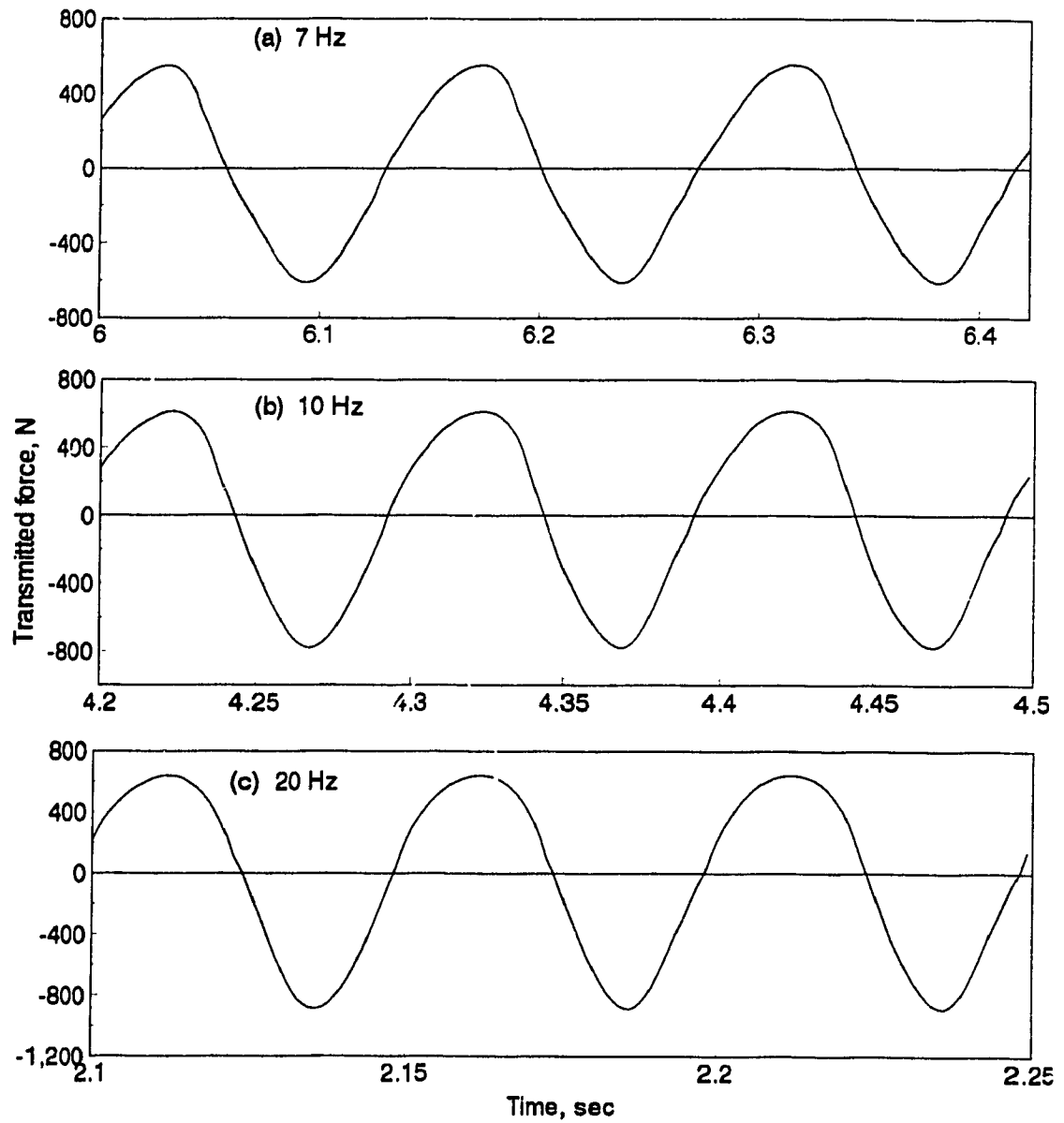


Figure 6.4 Transmitted force characteristic in time domain at different frequencies. ( $X_1=1\text{mm}$ ;  $L_0=50\text{mm}$ ,  $D_0=6\text{mm}$ ).

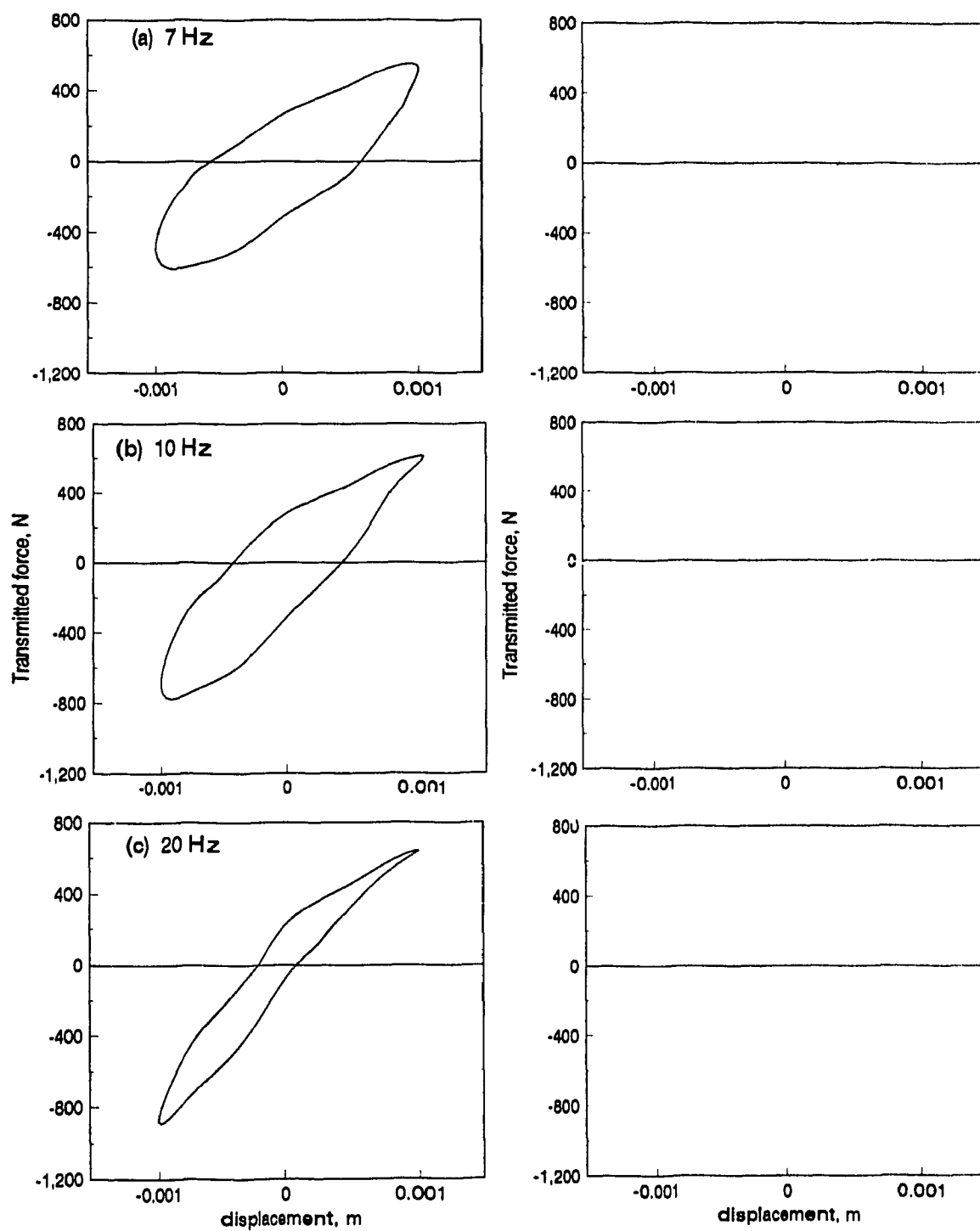


Figure 6.5 Lissajous plots for the damper at different frequencies. Oscillation effect, —, considered;   , not considered; ( $X_1=1\text{mm}$ ;  $L_0=50\text{mm}$ ,  $D_0=6\text{mm}$ ).



considering oscillation effect. The area contained within the plots shows the amount of energy dissipated (measure of damping) per cycle. It shows that the energy dissipated per cycle decreases with increase in frequency and at high frequency it tends to diminish rapidly (Figure 6.5c). Again it is interesting to note that overlooking the oscillation effect causes underestimation of energy dissipation. At each frequency, the area is larger for the plot with consideration of oscillation effect than that of the area without oscillation effect. That is why the experimental energy dissipation was found higher than the analytical one obtained by Kim and Singh [17] neglecting oscillation effect. At high frequency (20 Hz), energy dissipation is almost 50% more in the model considering oscillation effect.

#### **6.2.1.1 Parametric Study**

The major parameters which may affect the characteristics of the LDHF dampers substantially, include: (a) orifice diameter; (b) orifice length; and (c) piston diameter. There are other factors such as compliance of the chambers, geometry of the cross-section of the orifice, orifice openings, etc., which were considered for SDHF dampers and the effect was found to be minor. This section presents steady state time history of orifice flow rate, top chamber pressure and transmitted force for a frequency of 10 Hz.

(a) Orifice diameter: Figure 6.6 shows the results for the dampers with the variation of orifice diameter. Diameters considered are 4.5 mm, 6 mm and 7.5 mm while length is held constant and equal to 50 mm. As expected, the orifice flow increases with the increase in diameter (Figure 6.6a), where 33% increase in diameter produces 100% more orifice flow. It is interesting to note that changes in orifice diameter also changes the phase difference with excitation frequency. Larger diameter leads to greater shift in phase.

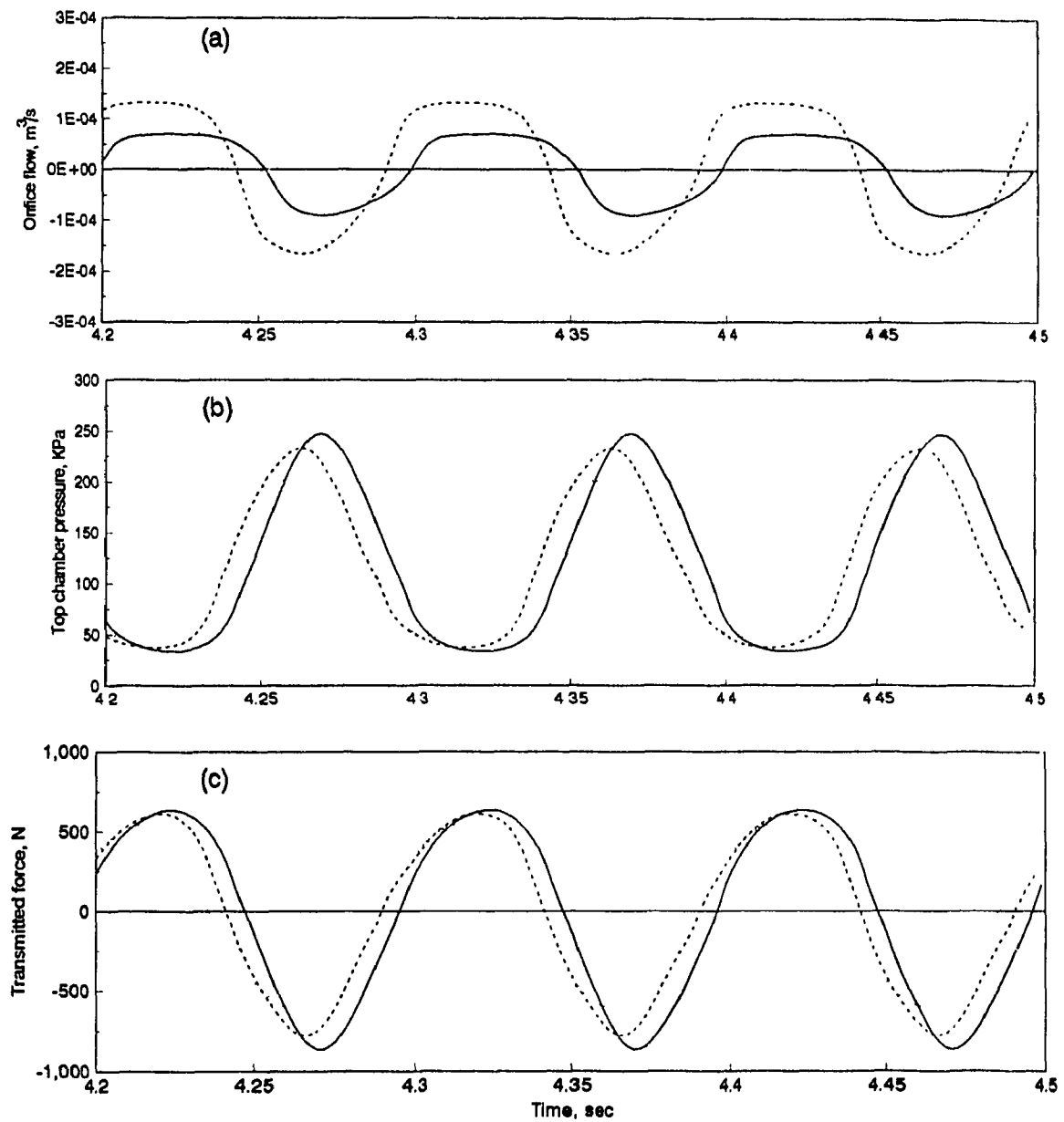


Figure 6.6 Effect of orifice diameter on the internal variables of the damper; orifice diam —, 4.5mm; ----, 6mm; . . . , 7.5mm; ( $X_1=1$ mm at 10 Hz;  $L_o=100$ mm,  $D_p=75$ mm).

Increase in orifice diameter leads to reduction in top chamber pressure build up as shown in Figure 6.6b. At 4.5 mm orifice diameter, peak pressure is noted as 247.2 KPa whereas at 6 mm diameter, peak pressure is 201.5 KPa. Unlike in the case of SDHF damper, orifice diameter does not contribute in changing sub-atmospheric pressure to that considerable extent as shown in Figure 6.6b.

As the top chamber pressure is decreased with the increase in diameter, transmitted force is also decreased. But the trend in decrement is different from what is obtained for SDHF damper. Difference is prominent during forward stroke only. The reason for this asymmetric observation might be that the creation in vacuum in reverse stroke is more in the case of LDHF damper.

(b) Orifice length: The orifice length is varied as 50 mm, 100 mm and 150 mm, keeping diameter constant, at 6 mm. The results shown in Figure 6.7a indicate that at 10 Hz peak orifice flow rate virtually does not change with changes in orifice length but the phase difference occurs to a small degree. Flatness of the peak orifice flow also decreases with increase in diameter.

Increase in orifice length however leads to increase in the peak top chamber pressure as shown in Figure 6.7b. By increasing orifice length three times, pressure increases only by 13% at this frequency. Transmitted force to the ground (Figure 6.7c) exhibits similar trend to that of top chamber pressure. The increase in the transmitted force during forward stroke is 18% for a three times increase in orifice length.

(c) Piston diameter: Piston diameter affects the characteristics of the chamber significantly. Figure 6.8 depicts the variation of orifice flow, top chamber pressure and transmitted force to the ground for three different values of piston diameter. Piston diameter is considered as 70 mm (area 3850 mm<sup>2</sup>), 80 mm (area 5025 mm<sup>2</sup>) and 90 mm (area 6362 mm<sup>2</sup>). Figure 6.8a shows that increase in piston area increases the orifice flow where the increase in forward stroke is significantly

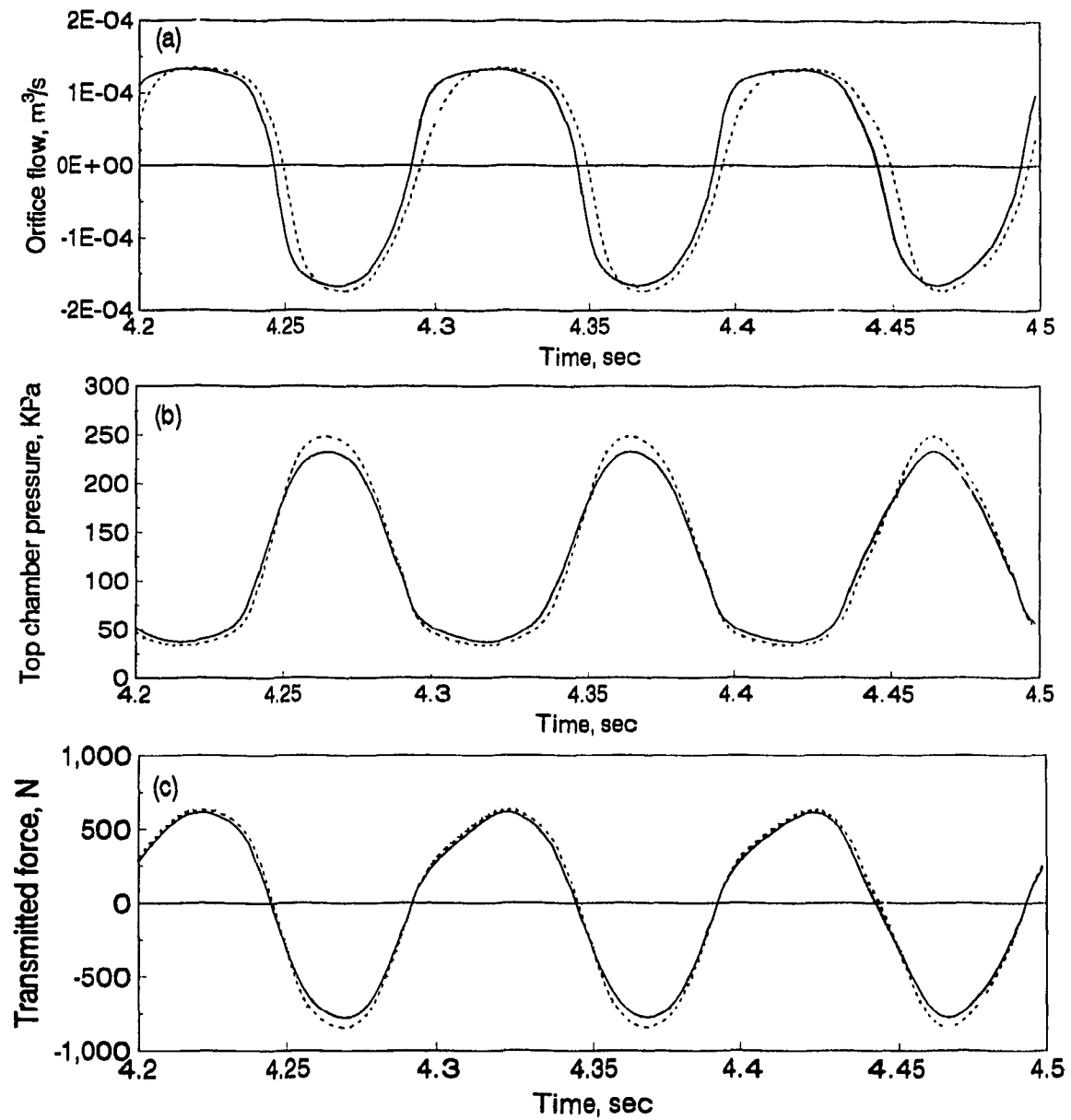


Figure 6.7 Effect of orifice length on the internal variables of the damper; orifice length —, 50mm; ----, 100mm; . . . , 150mm; ( $X_1=1\text{mm}$  at 10 Hz;  $D_o=6\text{mm}$ ,  $D_p=75\text{mm}$ ).

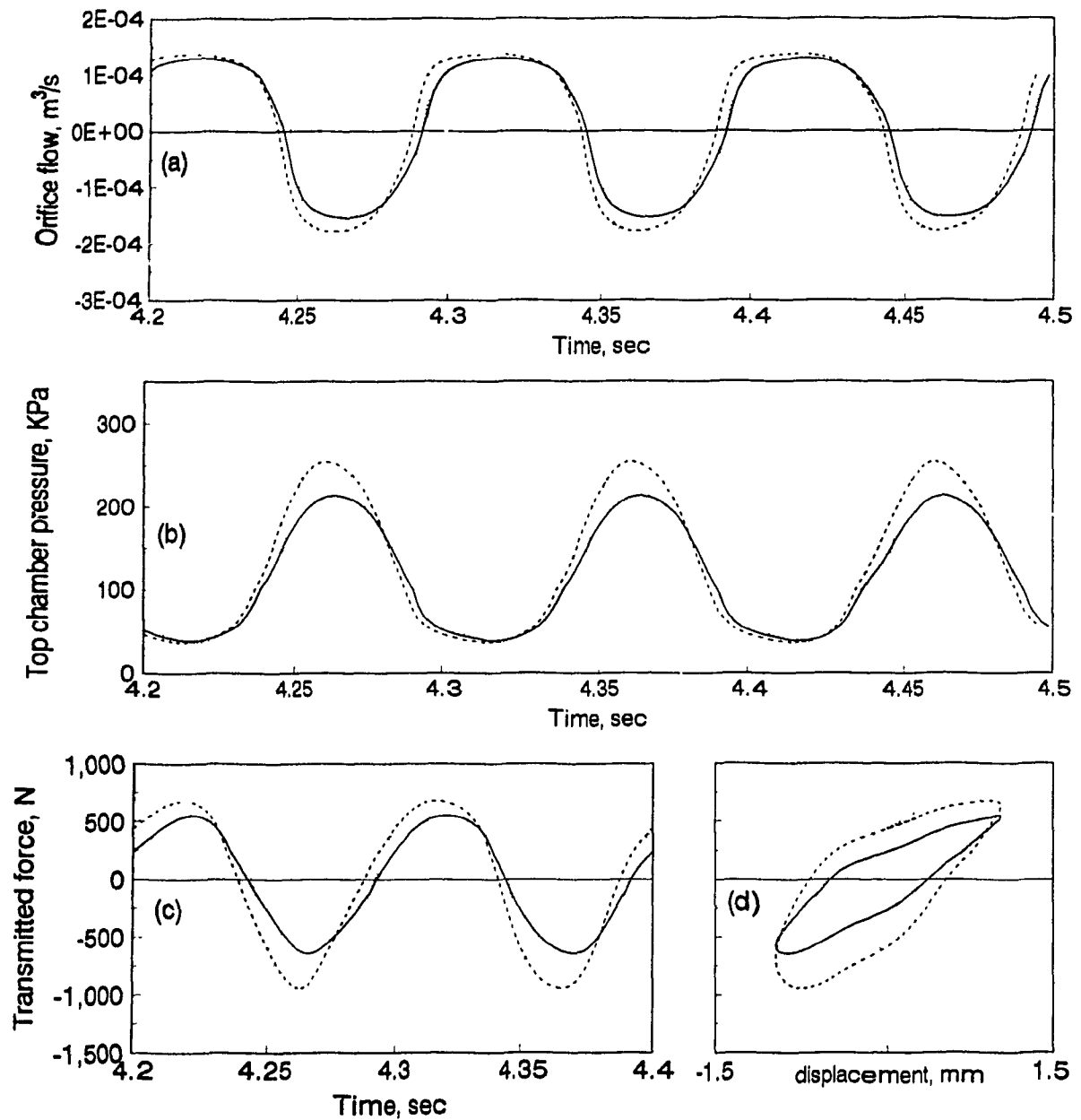


Figure 6.8 Effect of piston diameter on the internal variables of the damper; piston diameter —, 70mm; ----, 80mm; . . . , 90mm; ( $X_1=1\text{mm}$  at 10 Hz;  $D_o=6\text{mm}$ ,  $D_p=75\text{mm}$ ).

greater than the reverse stroke. For a increase in piston area by 65.3%, flow rate during forward direction increases by 32%.

Increase in piston area increases peak value of the top chamber pressure (Figure 6.8b) but the minimum pressure (sub-atmospheric) created during reverse stroke is insensitive to piston diameter. For an increase in piston area by 23.4%, top chamber peak pressure increases by 19.2%. This increase in pressure affects the force transmitted to the ground which increases in a nonlinear fashion as the piston diameter is increased. Figure 6.8c shows the variation of transmitted force with the variation of piston dia in time domain and 6.8d shows the same in the form of Lissajous plot. Figure 6.8d shows the extent of nonlinearity of the damper. It also shows that increase in piston diameter increases energy dissipation per cycle which means more damping is developed with increase in diameter.

### 6.2.2 Frequency Domain Analysis

The nominal damper characteristics in terms dynamic stiffness and loss angle (a measure of damping) in frequency range of 1 to 100 Hz is presented in Figure 6.9. As shown in Figure 6.9a, dynamic stiffness at low frequency is low and equal to rubber stiffness. Starting at 4 Hz, dynamic stiffness starts to rise rapidly with frequency and reaches maximum at around 20 Hz. The dynamic stiffness is found to be insensitive to any further increase in frequency. In comparison to short orifice damper, the dynamic stiffness produced by long orifice is larger and the increase is very rapid within a short range of frequency.

The resulting loss angle characteristics for the long orifice damper is similar to that of short orifice. For long orifice as shown in Figure 6.9b, the loss angle peak is comparatively sharper and larger. It is desirable that the damper produces enough damping around resonance to minimize transmissibility and produce low damping at high frequency. For the parameters used, maximum loss angle occurs at 6 Hz

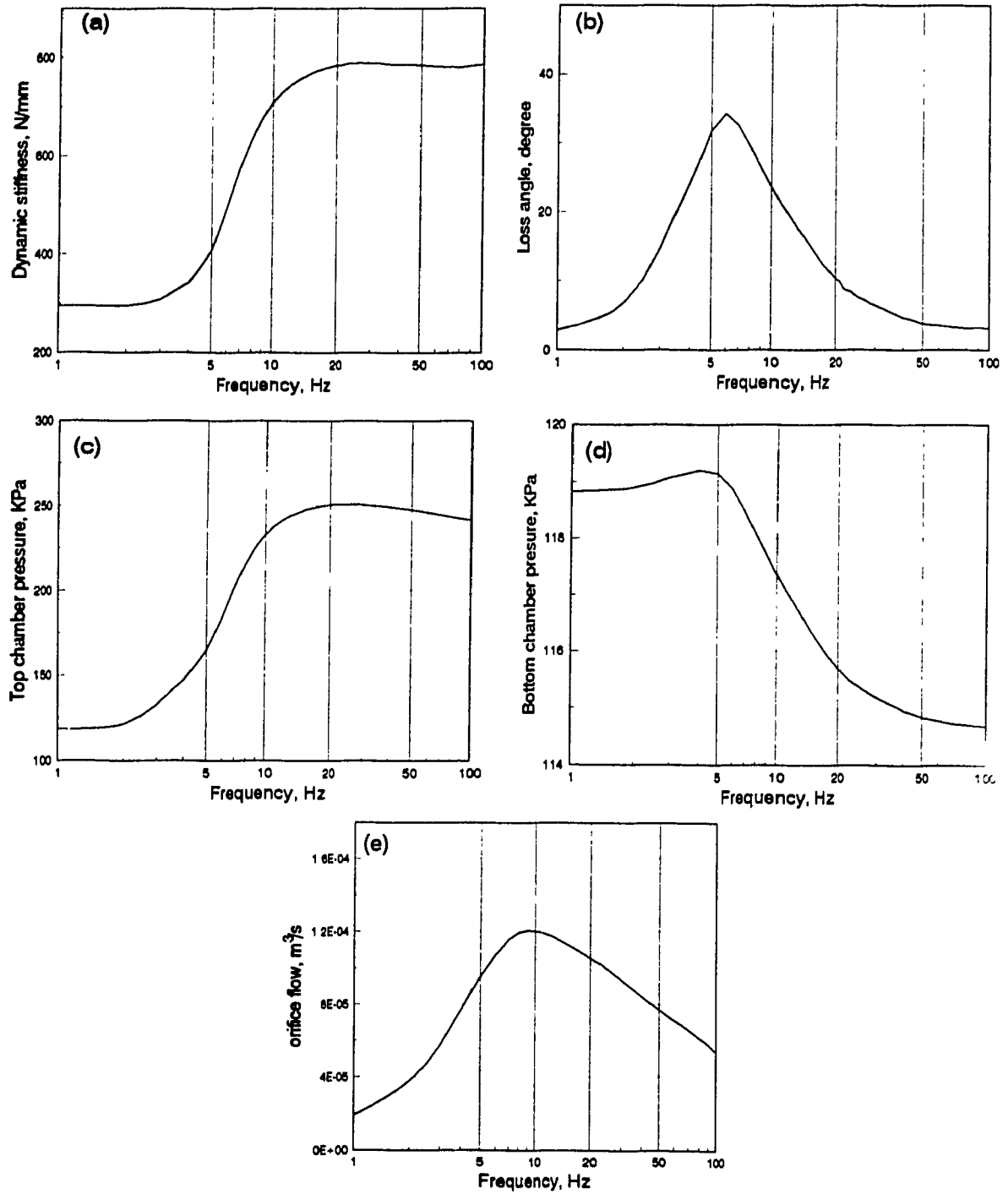


Figure 6.9 Effect of frequency of excitation on (a) dynamic stiffness and (b) loss angle (a) top chamber pressure and (b) bottom chamber pressure (e) orifice flow; ( $X_1=1\text{mm}$ ,  $D_o=6\text{mm}$ ,  $D_p=75\text{mm}$ ).

which is close to system's natural frequency. Such characteristics makes it ideal for application as isolators.

Figure 6.9c and 6.9d show the variation of peak top chamber and bottom chamber pressures as a function of frequency. Similar to dynamic stiffness, top chamber pressure increases rapidly as frequency is increased. There is a slight decline in pressure, however, for frequencies greater than 20 Hz. The maximum peak top chamber pressure produces by the nominal model is 250 KPa, around 20 Hz. Figure 6.10b shows the variation of peak bottom chamber pressure which remains constant at 119 KPa for low frequencies and starts to fall rapidly as the frequency is decreased.

Figure 6.9e presents the orifice flow characteristics of the damper in frequency domain. As the frequency is increased, orifice flow increases rapidly and reaches a maximum around resonance frequency producing high damping. Unlike SDHF, where flow rate continues to grow with frequency (Figure 5.11), the flow rate for LDHF again decreases for frequencies greater than 10 Hz. Oscillation effect greatly contributes for such characteristics of long orifice damper.

#### 6.2.2.1 Parametric Study

Similar to time domain analysis of damper characteristics, a parametric study is next carried out in frequency domain. Results of dynamic characteristics are obtained for variation in internal parameters such as: orifice diameter; orifice length; and piston diameter. The effect of excitation amplitude on the dynamic characteristics is also presented.

(a) Orifice diameter: Figure 6.10 shows the variation in dynamic stiffness and loss angle with the variation of orifice diameter. Orifice diameters used are 4 mm, 6 mm and 8 mm with a constant length of 50 mm. As the results show, an increase in the orifice diameter leads to a shift of the curves towards higher frequency. For



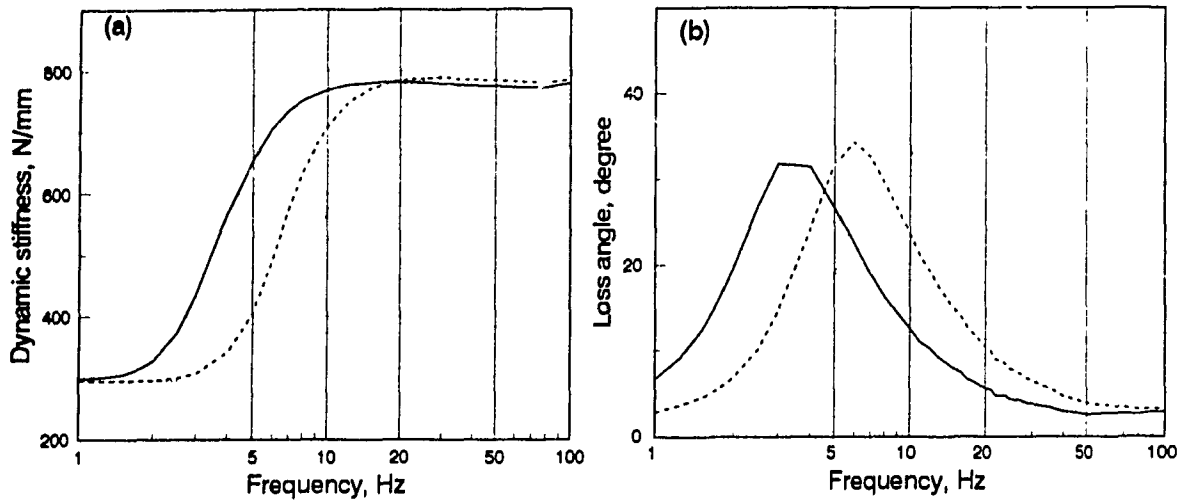


Figure 6.10 Effect of orifice diameter on the (a) dynamic stiffness and (b) loss angle of the damper; oscillation effect is considered; orifice diameter —, 4mm; . . . . ., 6mm; . . . . ., 8mm; ( $X_1=1\text{mm}$ ,  $L_o=50\text{mm}$ ,  $D_p=75\text{mm}$ ).

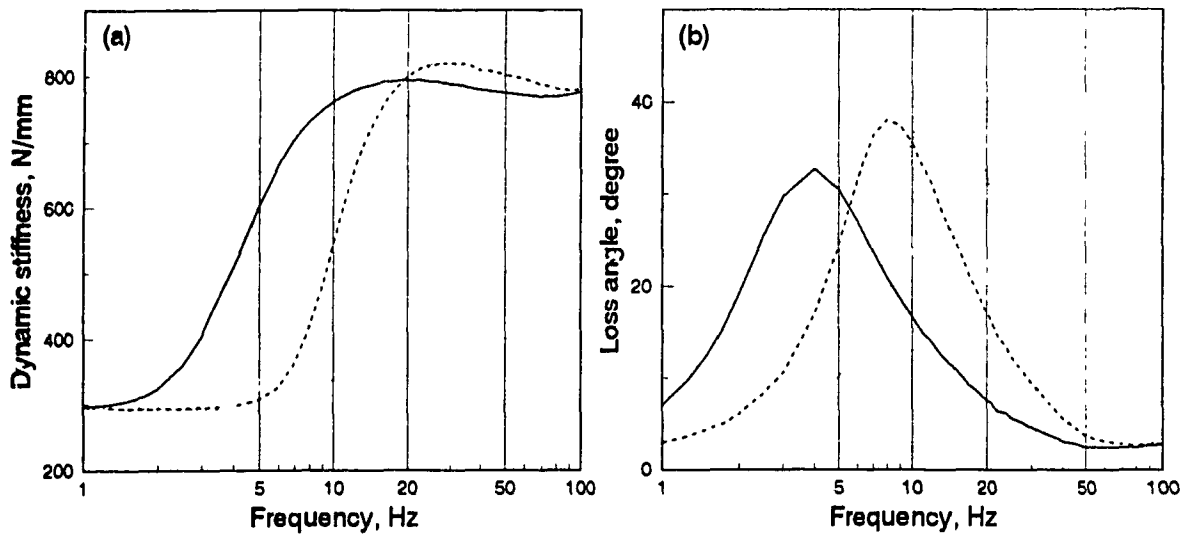


Figure 6.11 Effect of orifice diameter on the (a) dynamic stiffness and (b) loss angle of the damper; oscillation effect is not considered; orifice diameter —, 4mm; . . . . ., 6mm; . . . . ., 8mm; ( $X_1=1\text{mm}$ ,  $L_o=50\text{mm}$ ,  $D_p=75\text{mm}$ ).

example, at 4 mm dia, dynamic stiffness starts rising at 2 Hz and reaches maximum at 10 Hz and peak loss angle (Figure 6.10b) occurs at 3.5 Hz. At diameter of 8 mm, dynamic stiffness starts rising at 5 Hz and reaches maximum at around 20 Hz and peak loss angle occurs at 9 Hz. Orifice diameter, however, has no effect on the peak stiffness or loss angle. The orifice diameter, therefore, appears to be a good parameter for tuning the damper characteristics according to requirement.

The above simulation is next repeated for the model without oscillation effect, results of which is presented in Figure 6.11. Clearly, it may lead to misleading results, which show that increase in orifice diameter not only changes the frequency at which peak damping occurs but also shows increase in the amount of damping (loss angle) with increase in orifice diameter.

(b) Orifice length: Another important parameter of a long orifice hydraulic damper is the length of long orifice. It is a key parameter to obtain higher damping from the same damper. Figure 6.12 shows the variation of the characteristics in terms of dynamic stiffness and loss angle for three different values of orifice length. Here the orifice diameter is maintained at 6 mm while the length is varied as 50 mm, 100 mm, and 150 mm. The results show a completely different trend for the influence of orifice length from that of the influence of orifice diameter. For dynamic stiffness (Figure 6.12a), the major effect of orifice length is in the rate of increase of the stiffness. Larger orifice leads to faster increase in dynamic stiffness and a small increase in the maximum value reached. The peak value for the loss angle is significantly affected by the length of the orifice as shown in Figure 6.12b. Unlike the effect of orifice size where same peak loss angle is provided at different frequency, here the peak value of loss angle increases around the systems' natural frequency as the orifice length is increased. The effect on the frequency where peak loss angle occur is very small. (A reduction of 1 Hz for 3 times increase in

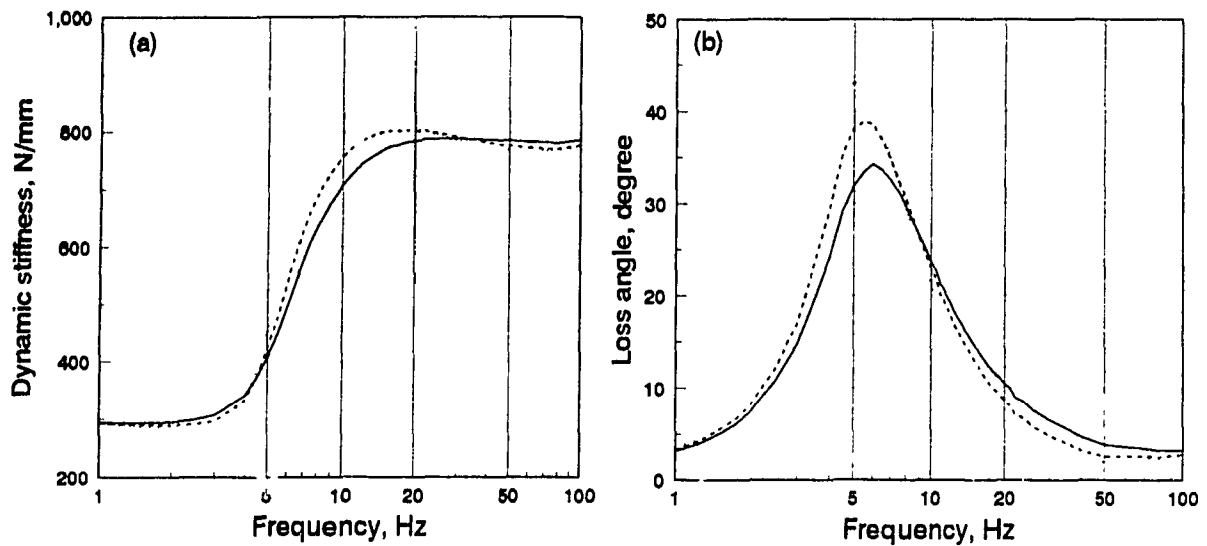


Figure 6.12 Effect of orifice length on the (a) dynamic stiffness and (b) loss angle of the damper; orifice length —, 50mm; ----, 100mm; ····, 150mm; ( $X_1=1\text{mm}$ ,  $D_o=6\text{mm}$ ,  $D_p=75\text{mm}$ ).

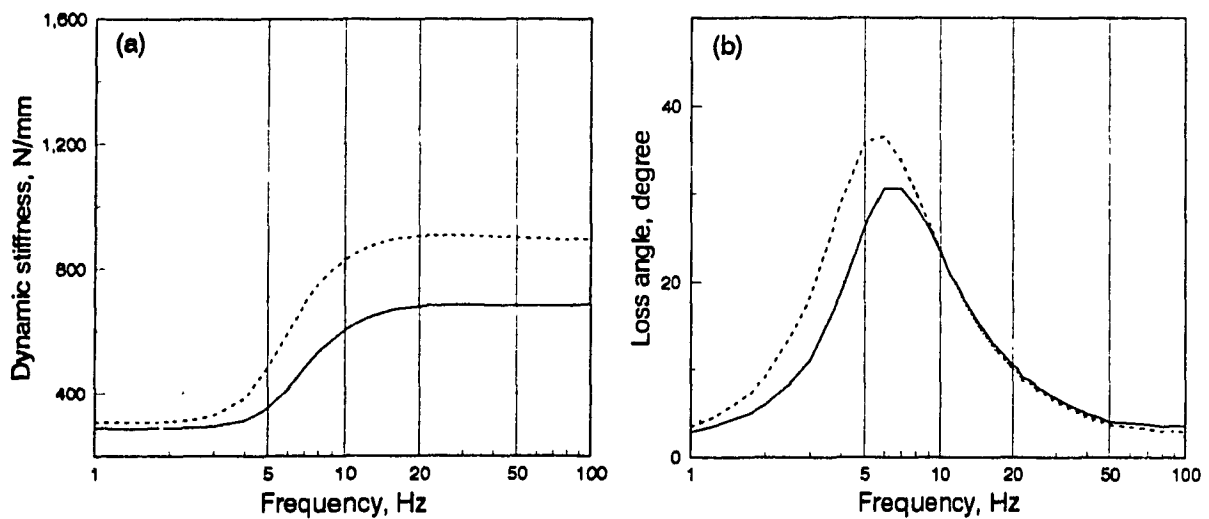


Figure 6.13 Effect of piston diameter on the (a) dynamic stiffness and (b) loss angle of the damper; piston diameter —, 70mm; ----, 80mm; ····, 90mm; ( $X_1=1\text{mm}$ ,  $D_o=6\text{mm}$ ,  $L_o=50\text{mm}$ ).

orifice length). Similar to orifice diameter, orifice length is a highly useful parameter for tuning of the damper for a given application. It may be recommended that a damper designed for a given system be evaluated for variation of orifice diameter to length ratio to arrive at a tuned configuration.

(c) Piston diameter: Piston diameter plays an important role in the development of pressure on dynamic stiffness as well as on the loss angle. Figure 6.13 shows the dynamic stiffness and loss angle characteristics of the damper for the variation of piston diameter. The diameter is varied as 70 mm, 80 mm and 90 mm. It is seen that dynamic stiffness (Figure 6.13a) trend remains the same where both static and maximum dynamic stiffness increase nonlinearly as piston diameter is increased. It is interesting to note that higher piston area affects the dynamic stiffness even at very low frequency. For the given parameters of the damper, increase in piston area increases the loss angle at lower frequency with advancement of frequency at which peak loss angle occurs (Figure 6.13b). At high frequency, beyond 9 Hz, loss angle is practically insensitive to piston diameter. Again, the peak value of loss angle increases nonlinearly as the piston diameter is increased from 70 mm to 90 mm.

Since amplitude of excitation may have strong influence on the characteristics of such nonlinear damper, the dynamic characteristics are next determined for 3 different amplitude of excitation.

(d) Effect of excitation amplitude: Figure 6.14 shows the effect of amplitude of excitation on dynamic stiffness and loss angle of the damper. The amplitude of excitation is varied as 1 mm, 0.75 mm and 0.50 mm. It is seen that (Figure 6.14a) with decrease in amplitude, dynamic stiffness starts to rise at a higher frequency and provides a higher maximum value. At lower amplitude of excitation, loss angle also increases, as shown in Figure 6.14b. The peak value for loss angle and the corresponding frequency also increase almost linearly as the amplitude of

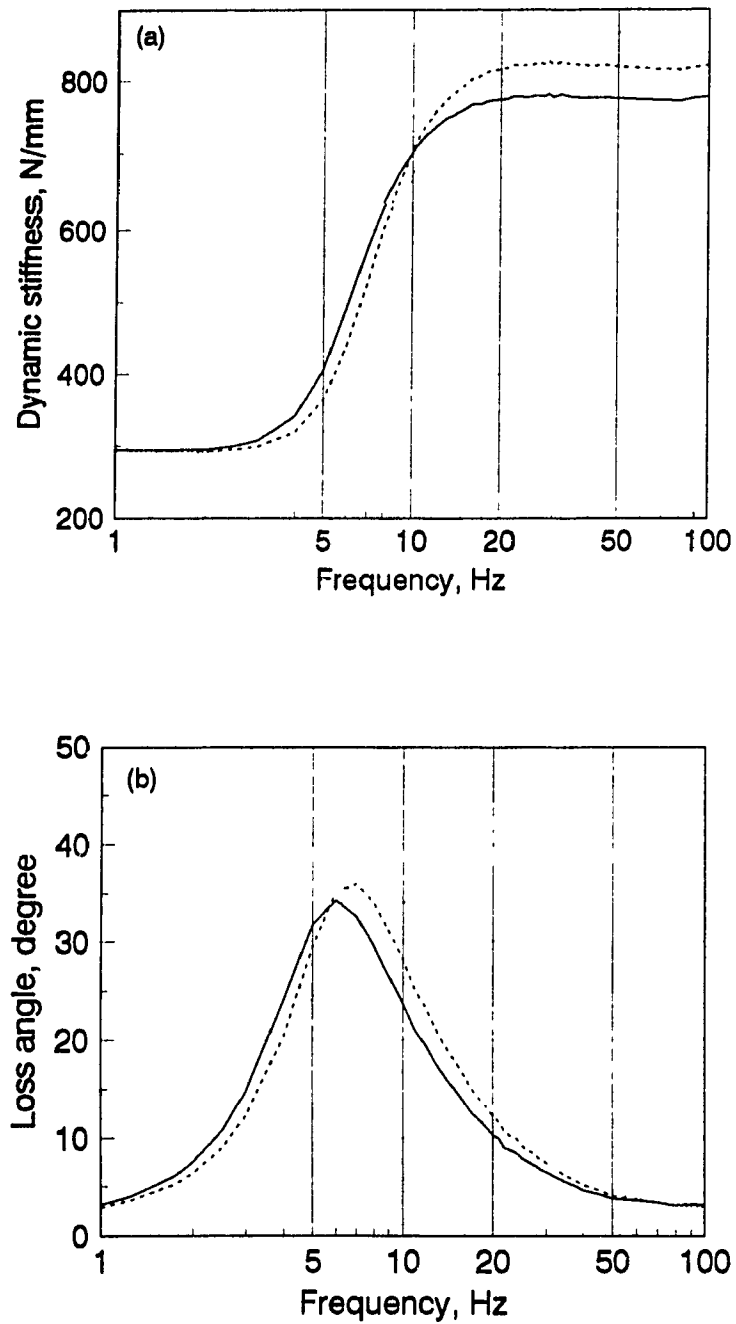


Figure 6.14 Effect of amplitude of excitation on the (a) dynamic stiffness and (b) loss angle of the damper.  $X_1$ ; —, 1mm; ----, 0.75mm; ····, 0.50mm; ( $D_o=6\text{mm}$ ,  $L_o=50\text{mm}$ ,  $D_p=70\text{mm}$ ).

excitation is reduced. It is, therefore, expected that such dampers although may provide excellent vibration isolation performance, it must be at low amplitudes. The performance will be poor under high amplitude and under shock.

### **6.3 Performance Analysis of the Damper with Long Orifice**

The results and analysis so far discussed, constitutes the dynamic characteristics of the damper. This article is devoted to the performance analysis of the LDHF damper. Literature survey shows that very little attention is paid to the performance analysis. Most of the articles are devoted to the dynamic characteristics only [1-10]. To find its dynamic performance, the nonlinear damper is mounted to a single degree of freedom (DOF) system which includes a mass and the damper. As shown in Figure 3.7, the flexible chambered damper also acts as a spring to support the mass. The base of the damper is excited by sinusoidal input and shock input. The response is measured by the absolute motion (absolute transmissibility) and relative motion (relative transmissibility) of the mass for the case of sinusoidal input. For the shock displacement, responses are measured as acceleration ratio, velocity ratio, displacement ratio and relative displacement ratio in time domain. Shock responses are also evaluated in the shock severity domain in terms of common performance indices as used in the previous cases.

The nominal parameters used include: a mass of 125 Kg; orifice diameter 9 mm; orifice length 200 mm; piston diameter 70 mm; Comp\_A for the top chamber and Comp\_B for the bottom chamber. The results in case of parametric variation are obtained for variation in important damper parameters namely: orifice length, orifice diameter and piston diameter.

### 6.3.1 Performance under Sinusoidal Excitation

Figure 6.15 shows the performance curves in terms of acceleration and relative displacement transmissibility for the one DOF system. These results are obtained for three different amplitude of excitations ( 1 mm, 0.75 mm and 0.5 mm). Figure 6.15a shows the rms acceleration transmissibility of the sprung mass for the three amplitudes. As the results show, for all cases of amplitude of excitation, two peaks in the transmissibility curves are observed. The first peak is due to system's natural frequency and second peak is due to inertia of the mass of fluid contained within the long orifice (mass 12.5 gm). Excellent acceleration transmissibility which is around 2 is observed for the first peak although transmissibility corresponding to second peak may be significantly higher for higher amplitude of excitation. The second peak, which is highly sensitive to the amplitude of excitation, is found to be below 2 for an excitation of 0.5 mm. At higher frequency, amplitude of excitation does not affect the transmissibility to any significant extent where response declines very sharply.

Relative displacement transmissibility is equally important as it dictates the space required to accommodate relative motion. The results for the relative displacement transmissibility presented in Figure 6.15b, show identical trend as that of acceleration as the excitation amplitude is varied. Here the first peak corresponding to the system resonance is highly satisfactory but as shown it leads to a significantly higher second peak. The performance can be considered superior for low amplitude of excitation.

The result when compared to that of short orifice damper presented in Figure 5.21 clearly indicates that a much superior resonance performance can be obtained utilizing a long orifice system with a wide deviation of high frequency performance.

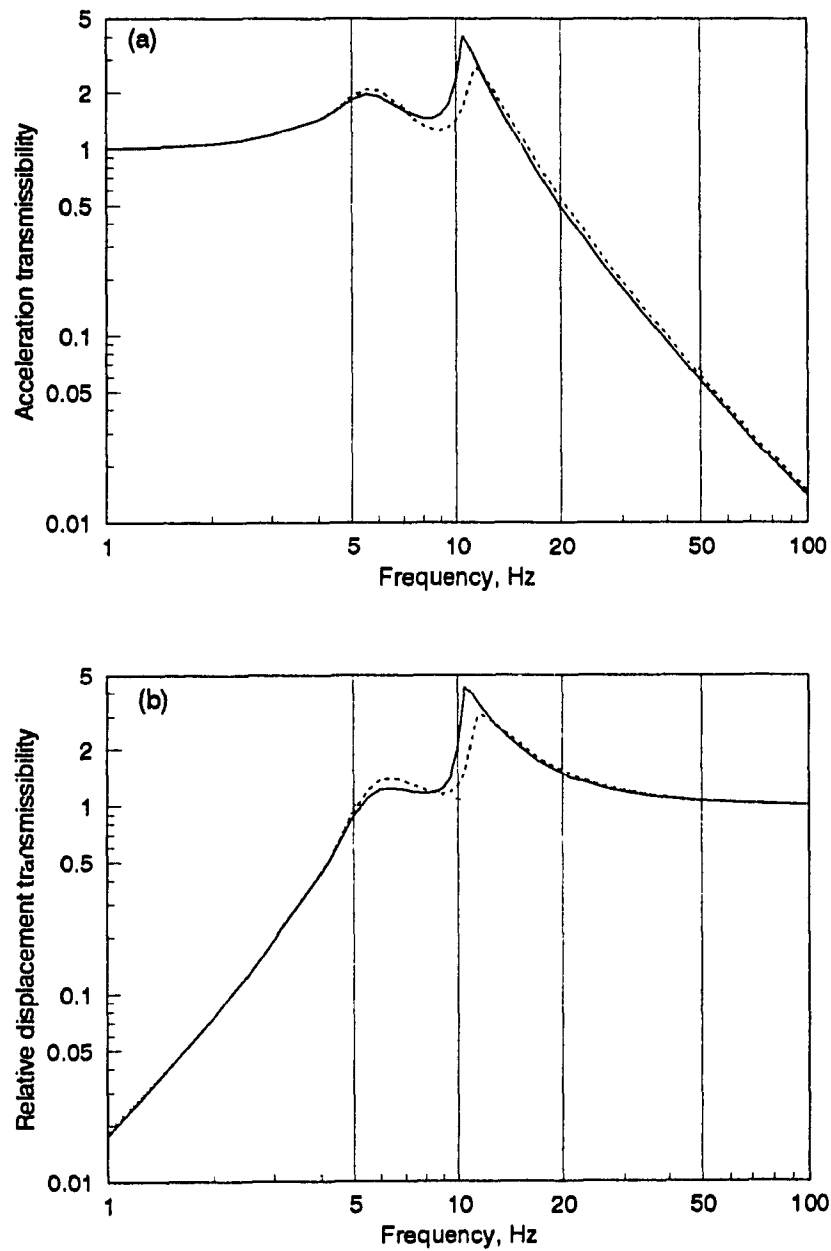


Figure 6.15 Effect of amplitude of excitation on (a) acceleration transmissibility and (b) relative displacement transmissibility;  $X_1$ : —, 1mm; - - -, 0.75mm; ···, 0.50mm; ( $D_o=9\text{mm}$ ,  $L_o=200\text{mm}$ ,  $D_p=70\text{mm}$ ).



#### 6.3.1.1 Parametric Study

Similar to section 6.2.1.1, a parametric study is next carried out to examine the influence of important damper parameters on the dynamic performance. These parameters include: orifice length, orifice diameter and piston diameter. Amplitude of excitation is taken as 0.75 mm which is quite reasonable for the application of flexible chambered damper. As found in the previous section, such dampers are not practical for isolation of high amplitude vibration.

(a) Orifice length: Effect of orifice length on rms acceleration transmissibility and rms relative displacement transmissibility as a function of frequency is shown in Figure 6.16. The orifice lengths used are: 100 mm; 150 mm and 200 mm. Orifice diameter and piston diameter are kept at their nominal value as 9 mm and 70 mm, respectively. The results presented show that for the orifice diameter used, the 100 mm length for orifice produces the most satisfactory result. The results further show that in the region of first peak the response improves with orifice length and the vice versa is true for the region of second peak.

Figure 6.16b shows corresponding relative displacement transmissibility for the variation of orifice length. The trend in the response for changes in orifice length is identical to that of acceleration transmissibility. This trend may be explained from the loss angle characteristics of the damper shown in Figure 6.12. Due to sharp peak in loss angle the resonance is isolated very well in all cases. However, due to the sharp peak the loss angle around 12 Hz (fluid resonance) is significantly lower than the peak. As shown in Figure 6.12, the loss angle at 12 Hz is further reduced for longer length of orifice.

(b) Orifice diameter: Figure 6.17 shows the performance of the nominal damper for different values of orifice diameter. Retaining the orifice length at intermediate value (150 mm), orifice diameter is varied as 7 mm, 8 mm, 9 mm and 10 mm. It is interesting to observe that if the orifice diameter is increased,

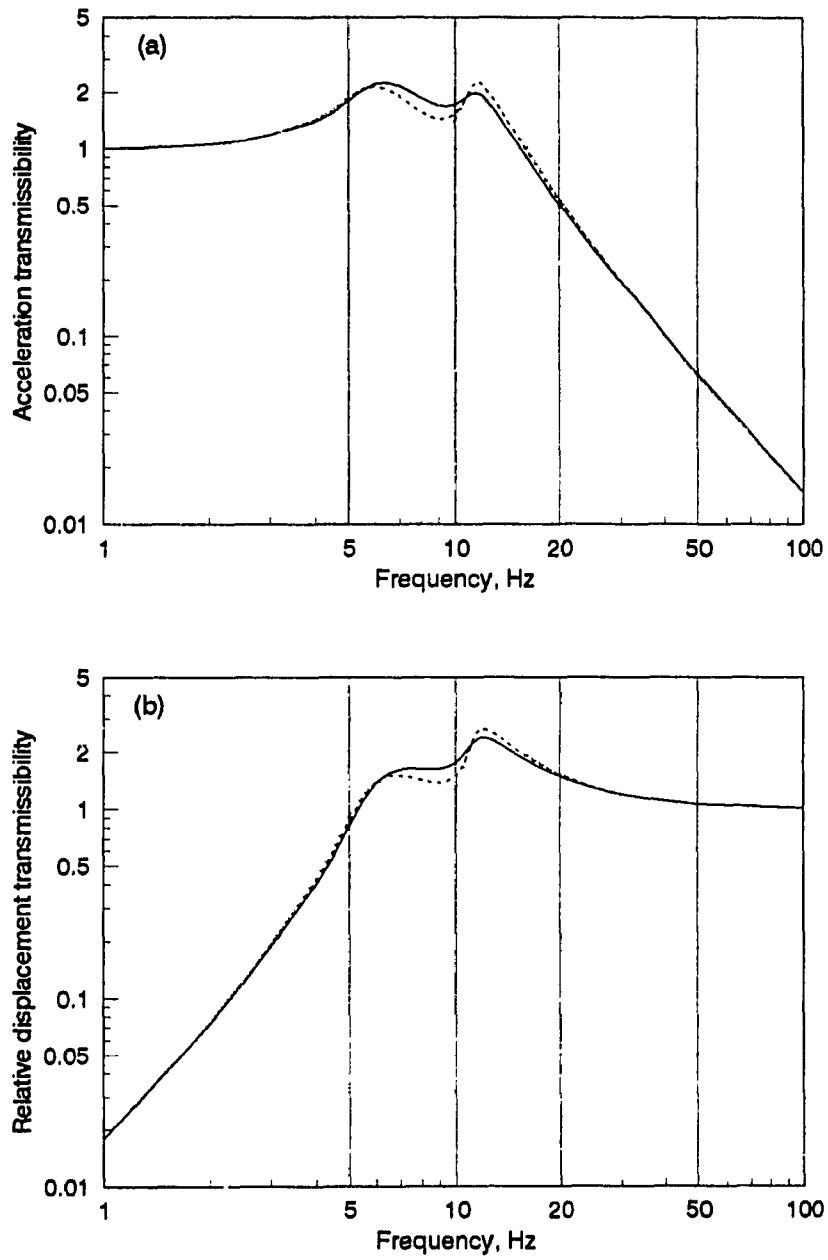


Figure 6.16 Effect of orifice length on (a) acceleration transmissibility and (b) relative displacement transmissibility; orifice length; —, 100mm; - - -, 150mm; ···, 200mm; ( $X_1 = 0.75\text{mm}$ ,  $D_o = 9\text{mm}$ ,  $D_p = 70\text{mm}$ ).

transmissibility around first resonance area is increased with a great reduction in the transmissibility around second resonance frequency. As for example, at 7 mm orifice dia, transmissibility at second resonance is 6 whereas at 10 mm dia it goes down to 1.47. At orifice diameter of 9 mm, both the transmissibility peaks are at the same level (dotted line), which is an optimal performance. Similar trend is again observed for relative displacement transmissibility shown in Figure 6.17b. In this case, 10 mm orifice produces the optimal performance.

Similar to previous section, this opposite trend can be explained from the loss angle characteristics presented in Figure 6.12. As shown, the peak loss angle shifts to higher frequency as orifice diameter is increased. For a diameter of 10 mm, the peak loss angle will be around 12 Hz which in turn will provide significantly lower damping at the first resonance frequency. This parameter should be used to tune the damper such that the peak loss angle occur at a frequency between the two resonance.

(c) Piston diameter: The final parameter examined is the influence of piston diameter on the frequency response of the system. For this, the nominal system parameters with an orifice diameter of 9 mm and length of 100 mm is used as it was proven to perform best under the given excitation. As it was shown in Figure 6.13, an increase in piston diameter leads to higher dynamic stiffness and loss angle. The increase in loss angle is, however, only for frequencies less than 10 Hz. This trend for change in piston diameter is now reflected on the acceleration and relative displacement transmissibility shown in Figure 6.18. These results show that piston diameter has influence on the response throughout the frequency range. As the piston diameter is increased, the increase in dynamic stiffness effectively moves the response curves to the right. And in doing so, the effective loss angle at the resonance is reduced leading to higher peak resonance. Near the first

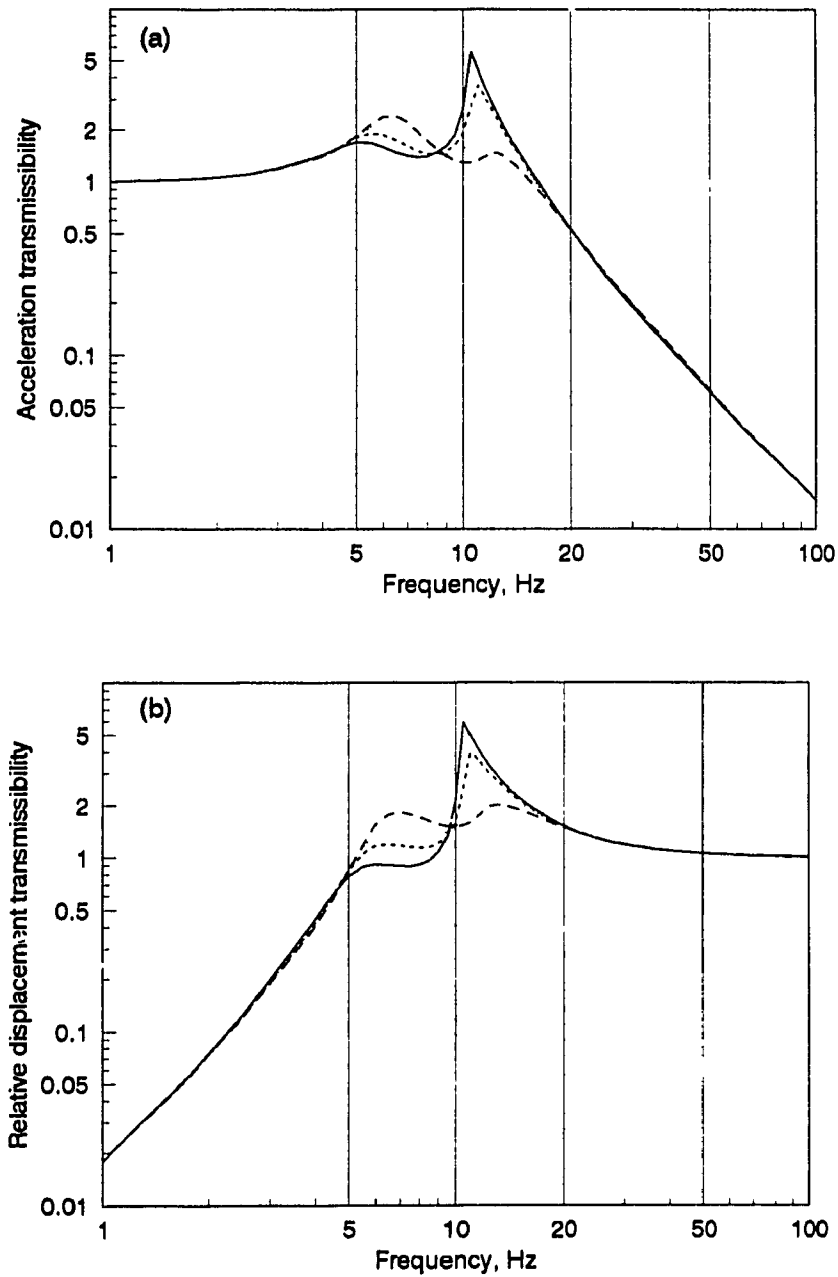


Figure 6.17 Effect of orifice diameter on (a) acceleration transmissibility and (b) relative displacement transmissibility; orifice diameter; —, 7mm; ----, 8mm; ····, 9mm, — —, 10mm; ( $X_1=0.75\text{mm}$ ,  $L_o=150\text{mm}$ ,  $D_p=70\text{mm}$ ).

resonance, however, (frequency  $< 10$  Hz, Figure 6.13) the damping increases with increase in piston diameter leading to better response.

### **6.3.2 Performances Under Shock Displacement**

The performance of the LDHF damper under the application of shock displacement is analyzed in time domain for different shock severity as well as peak response in shock severity domain. The shock displacement input and the performance indices are same as those used for dual-phase and short orifice dampers. The details for the inputs and performance indices are presented in section 4.4.1 and 4.4.2, respectively. The nominal parameters for the damper include: orifice diameter, 8 mm; orifice length, 100 mm; piston diameter, 75 mm. The performance is evaluated for shock severity in the range of 0.05 to 1.0. The shock displacement applied in all cases is a rounded pulse input of amplitude 20 mm.

#### **6.3.2.1 Time Domain Analysis**

The acceleration ratio, velocity ratio, displacement ratio and relative displacement ratio for the sprung mass of the single DOF system under rounded pulse displacement are shown in Figure 6.19. The results are obtained for four different shock severity  $v = 0.1, 0.2, 0.5$  and  $1.0$ . As the results indicate, shock severity below 0.5 is basically the static region which leads to non-oscillating motion. A comparison of response for shock severity of 0.5 and 1.0 indicate that the peak response in all cases increases with severity except for acceleration which show a decrease. A comparison of these results with those of short orifice in Figure 5.25 indicates that the peak response for long orifice is as bad as that of short orifice. Furthermore, it takes longer and more cycle to subside.

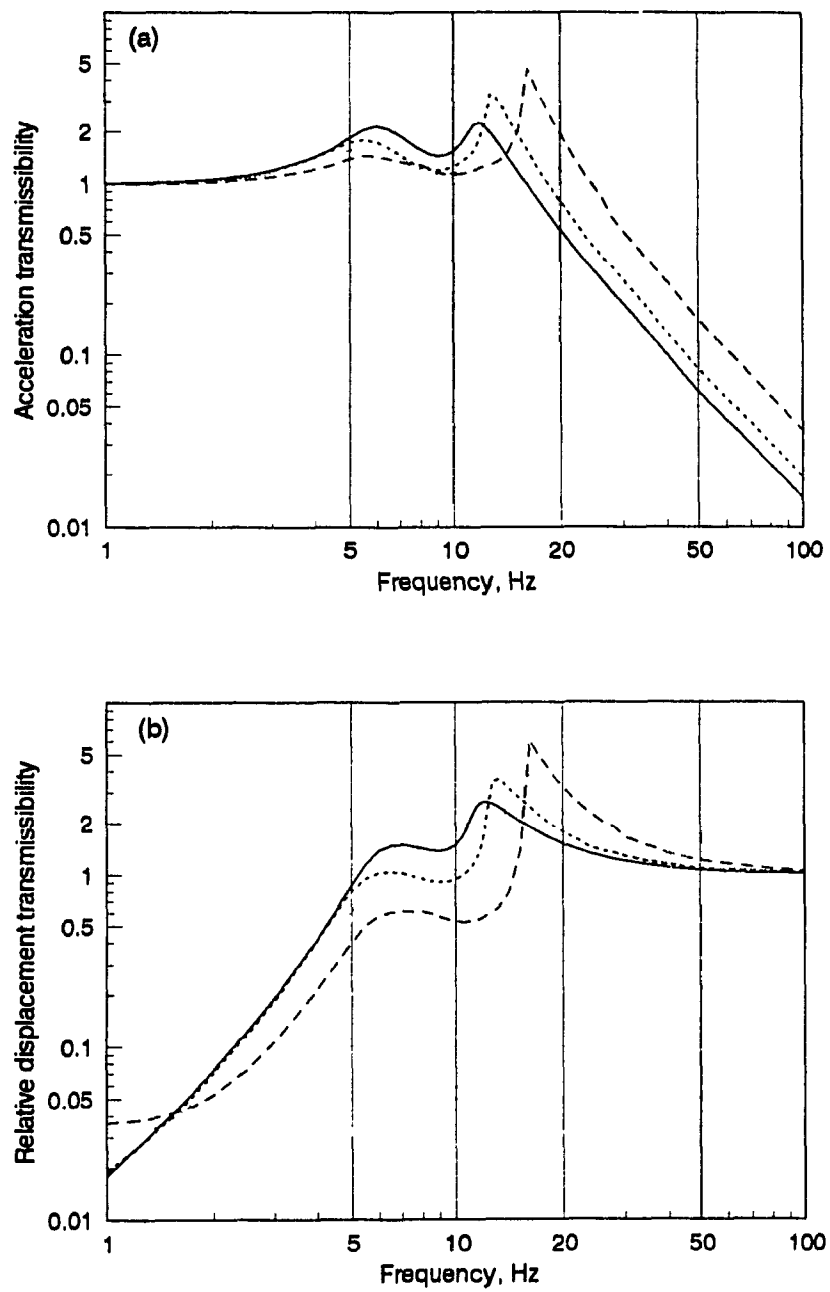


Figure 6.18 Effect of piston diameter on (a) acceleration transmissibility and (b) relative displacement transmissibility; piston diameter, —, 70mm; ----, 80mm; ····, 90mm; — · —, 100mm; ( $X_1=0.75\text{mm}$ ,  $L_o=150\text{mm}$ ,  $D_o=9\text{mm}$ ).

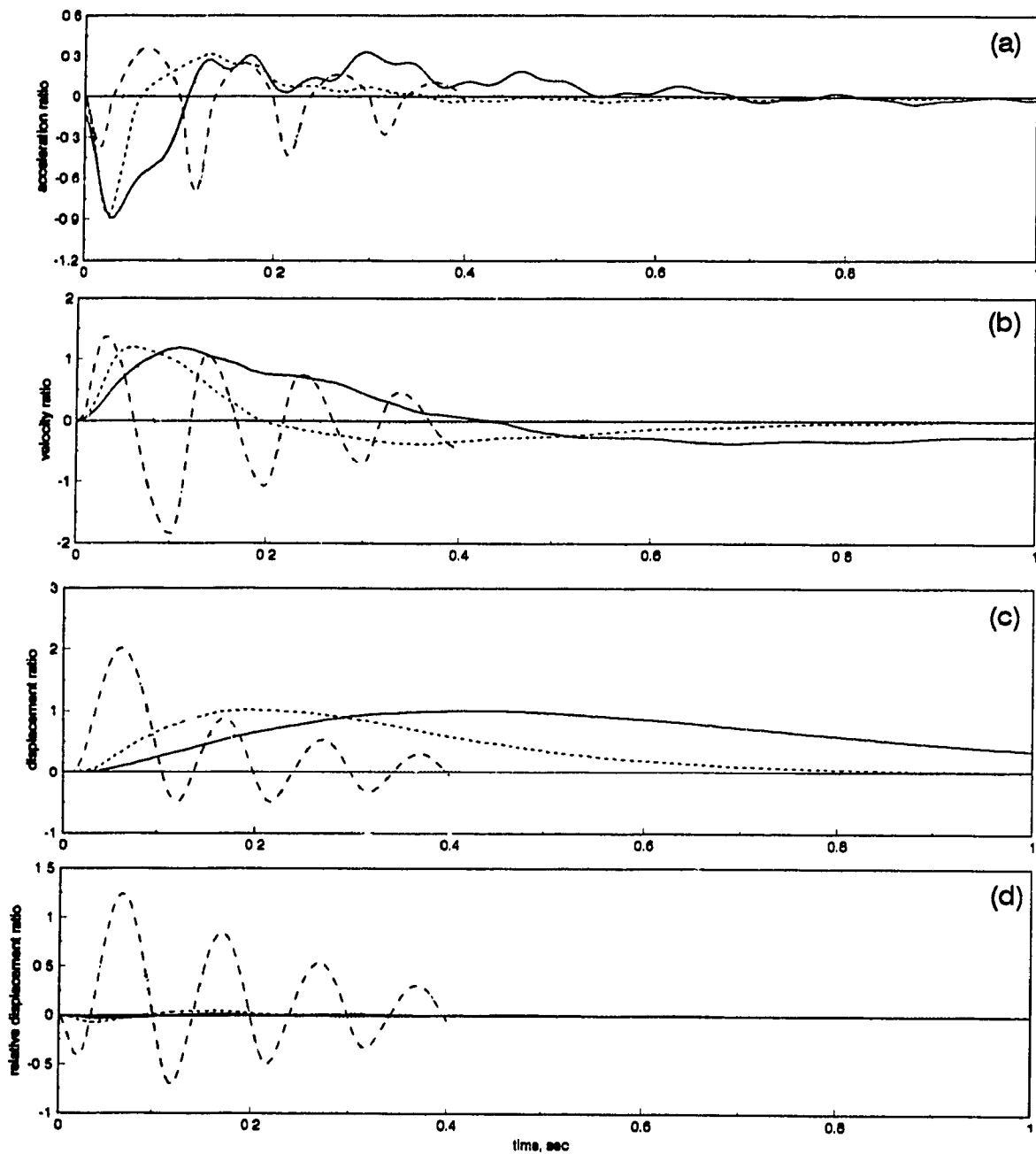


Figure 6.19 Shock responses in time domain. Shock severity, —, 0.1; ----, 0.2, 0.5; - · - · - , 1mm; (a) acceleration ratio, (b) velocity ratio, (c) displacement ratio, (d) relative displacement ratio.

### **6.3.2.2 Shock Severity Domain Analysis**

Figure 6.20 shows the shock acceleration ratio (SAR) and shock velocity ratio (SVR) for the long orifice hydraulic damper subjected to shock severity in the range of 0.05 to 5. These results are obtained for orifice diameter 6 mm, 7 mm and 8 mm. The response in shock severity domain is found very similar to those of short orifices presented in Figure 5.26 with higher magnitudes for long orifice. These results (Figure 6.20) further show similar influence of orifice diameter where the response increases at low severity and decreases at high severity as the orifice diameter is increased. In the case of long orifice the influence is, however, significantly less than that of short orifice.

The response in terms of shock displacement and shock relative displacement also presented in Figure 6.20 again indicates very similar response as that of short orifice damper both in magnitude and trend. Again short orifice damper (Figure 5.26) showed potential for improvement via large orifice diameter which is not present in the case of long orifice.

The shock severity domain analysis was also carried out for variation in orifice length and piston diameter. These results not presented here reconfirm above findings which indicate a lack of potential for long orifice dampers in isolation of shock.

## **6.4 Characteristics of the LSDHF Damper**

Due to conflicting performance of long orifice damper in isolation of low amplitude vibration and shock, the model is extended to include a combination of long and short orifice referred to as LSDHF damper. The models and its equations are presented in chapter 3. To the best knowledge of the author, characteristics or performance of such LSDHF is not available in the literature. Some characteristics of similar concept known as hydraulic damper with decoupler is available in the



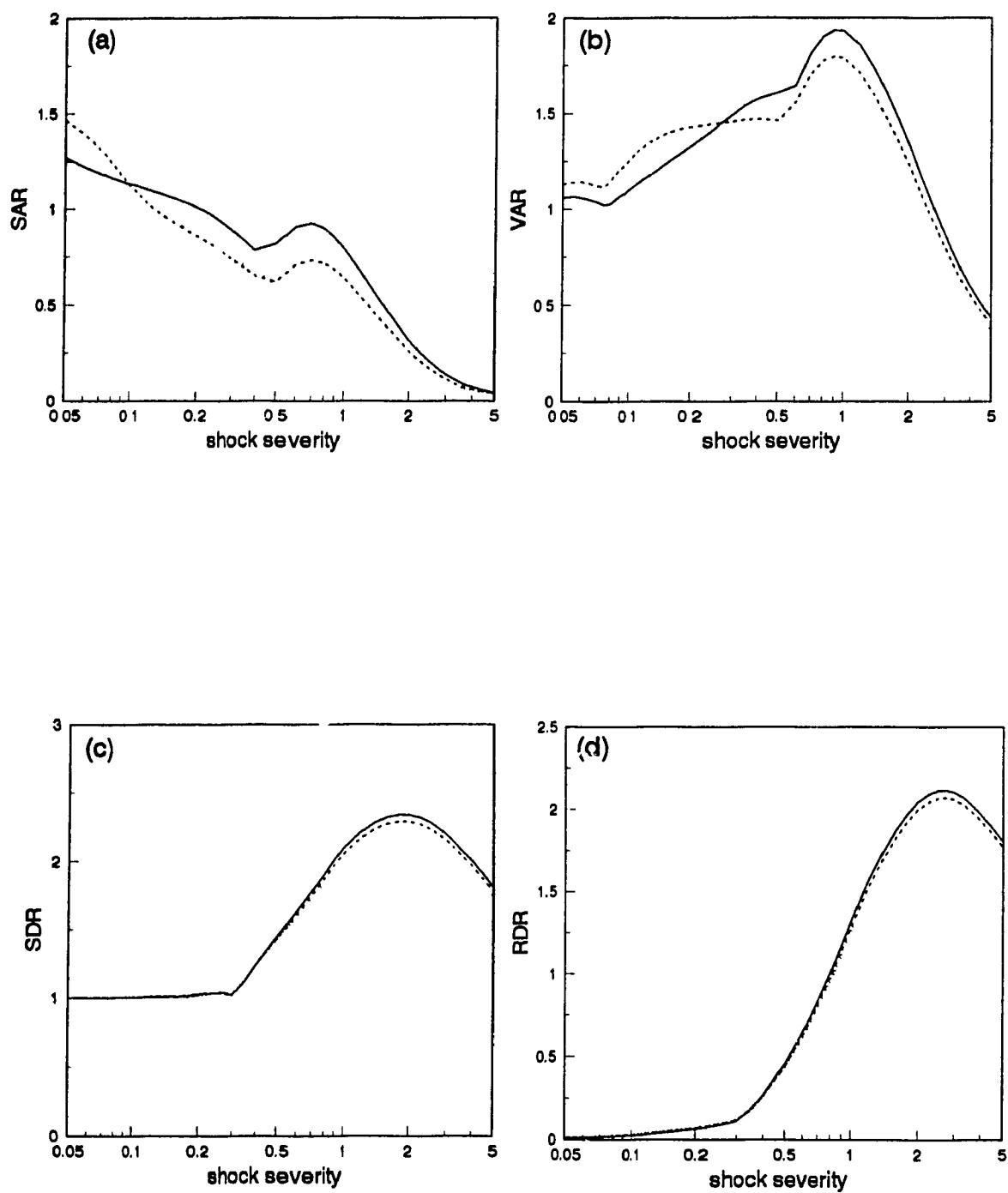


Figure 6.20 Shock responses as a function of shock severity with the variation of orifice diameter; —, 6mm; ----, 7mm; ···, 8mm; (a) SAR, (b) VAR, (c) SDR, (d) RDR.

literature [4,16]. A decoupler is a short orifice with a valve floating into the openings of the orifice with some predetermined displacement. The key difference between long and short orifice damper, and decoupler damper is that the decoupler orifice only works at lower amplitude of excitation. The objective of this section is to establish the dynamic characteristics of the LSDHF damper which can be readily compared with the other systems studied in this investigation. The damper characteristics for LSDHF are evaluated in terms of orifice flow through both long and short orifices, dynamic stiffness and loss angle. The parameters for long orifice are: length of long orifice 150 mm, diameter 7 mm, piston diameter 75 mm. The orifice diameter of the short orifice is varied as 0.0 mm (without short orifice), 3 mm, 4 mm and 5 mm to see its effect on the characteristics. The amplitude of excitation is taken as 1 mm, 2.5 mm and 5 mm. The rationale in selecting larger amplitude is that the short orifice is added in attempts to use such damper for larger amplitude of excitation.

Figure 6.21 shows the orifice flow through long orifice (Figure 6.21a) and short orifice (Figure 6.21b) under the excitation of 1 mm amplitude. The solid line in Figure 6.21a represents flow through long orifice in absence of short orifice. When the short orifice of diameter 3 mm is introduced, orifice flow reduces which at high frequency merges with the solid line. The decrease in long orifice flow continues as short orifice diameter increases. On the other hand, short orifice flow increases with the increase in orifice diameter throughout the whole range of frequency. But for each orifice diameter, the short orifice flow reaches a maximum value and maintains it throughout the high frequency range. At high frequency, the orifice flow for 4 mm orifice is almost twice the orifice flow for 3 mm orifice. At 5 mm short orifice diameter, the short orifice flow exceeds long orifice flow although the long orifice diameter (7 mm) is greater than the short orifice dia. This results from the oscillation effect of the fluid in the long orifice.

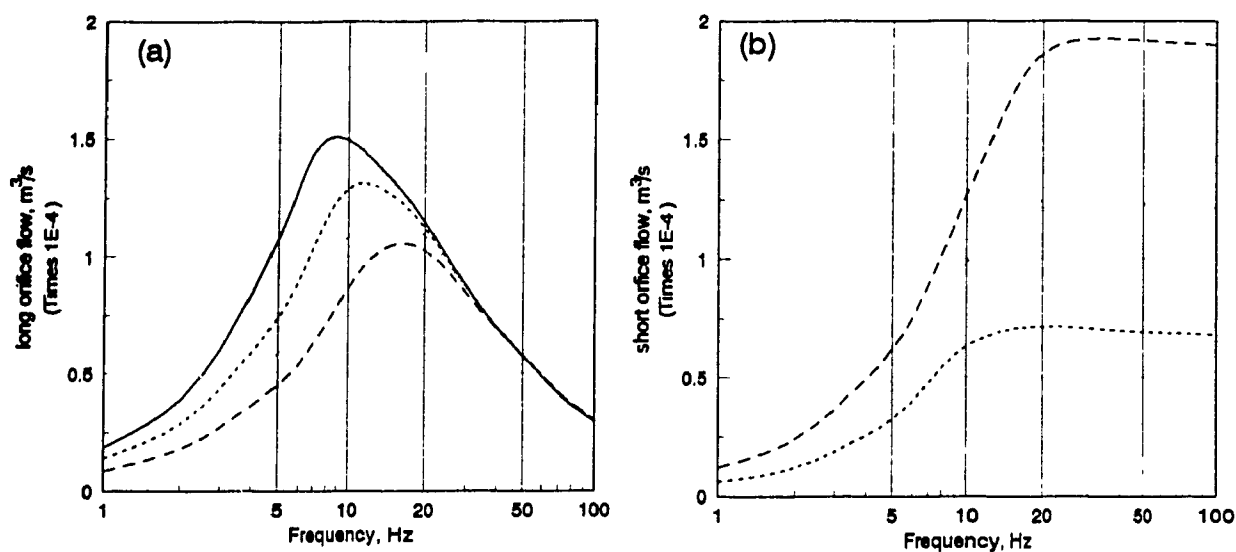


Figure 6.21 Effect of bleeder orifice diameter on the (a) long orifice flow and (b) short orifice flow of the damper; short orifice diameter, —, 0.0mm (without); ·····, 3mm; — · — ·, 4mm — — —, 5mm. ( $X_1=1\text{mm}$ ,  $L_o=150\text{mm}$ ,  $D_o=7\text{mm}$ ).

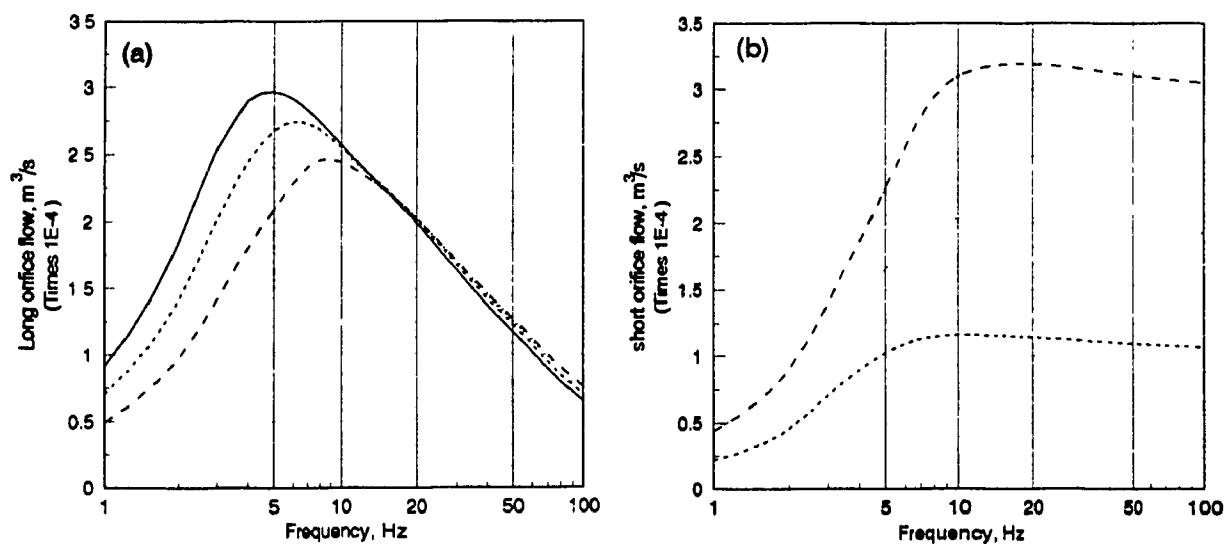


Figure 6.22 Effect of bleeder orifice diameter on the (a) long orifice flow and (b) short orifice flow of the damper; bleeder orifice diameter, —, 0.0mm (without); ·····, 3mm; — · — ·, 4mm — — —, 5mm. ( $X_1=5\text{mm}$ ,  $L_o=150\text{mm}$ ,  $D_o=7\text{mm}$ ).

The results of the same simulation repeated for 5 mm excitation is shown in Figure 6.22. The same trend of orifice flow like Figure 6.21 is observed. But the maximum long orifice flow occurs at lower frequency for high amplitude of excitation. Flow rate through both the orifices is much higher than the flow for low amplitude excitation. Like long orifice flow, short orifice flow also reaches its maximum limit at a lower frequency and retains that maximum value for higher frequencies.

Figure 6.23a shows the characteristics of the LSDHF damper in terms of dynamic stiffness and loss angle for an excitation of 1 mm. Out of four curves in each figure, the solid line represents the characteristics for long orifice without the short orifice. Other curves represent the characteristics when bleeder orifice of diameter of 3 mm, 4 mm and 5 mm are included. Figure 6.23b and Figure 6.23c represent the same characteristics but at higher amplitude of excitation, 2.5 mm and 5 mm respectively. It is observed from the figures that addition of bleeder orifice actually shifts the sharp rise in dynamic stiffness to a higher frequency. Inclusion of short orifice also shifts the frequency at which peak damping occurs as shown in Figure 6.23d. For example, peak damping occurs at 6 Hz without the orifice which shifts to 8 Hz when a short orifice of 3 mm is added. For orifice dia of 4 mm, peak damping occurs at 9.5 Hz and for 5 mm orifice dia the frequency is at 12 Hz. The magnitude of peak damping reduces with increasing orifice diameter. This also leads to higher damping value at high frequency, which may effect the high frequency performance.

As shown in Figure 6.23b and 6.23c, increase in amplitude of excitation causes the rise in dynamic stiffness to occur at a lower frequency and the peak value of dynamic stiffness decreases as the excitation is increased. The amplitude of excitation also has effect on loss angle developed by the damper. The higher the amplitude, the lower the frequency at which peak loss angle occurs. And the

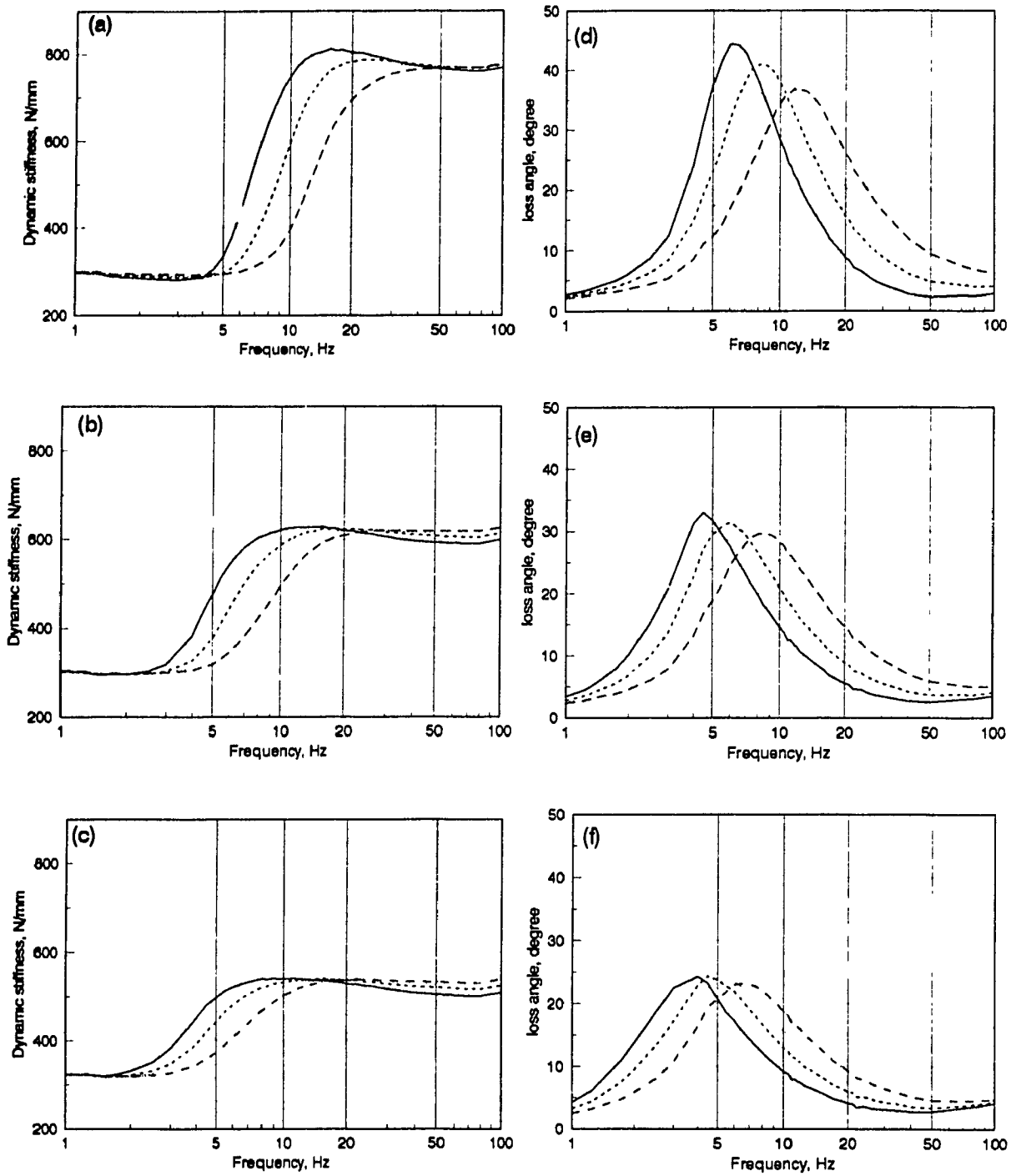


Figure 6.23 Effect of bleeder orifice diameter on the dynamic stiffness and loss angle of the damper. bleeder orifice diameter, —, 0 mm (without); ----, 3mm; — · —, 4mm; · · · · ·, 5mm; (a)  $X_1=1\text{mm}$ , (b)  $X_1=2.5\text{mm}$ , (c)  $X_1=5\text{mm}$ ; ( $L_o=150\text{mm}$ ,  $D_o=7\text{mm}$ ).

addition of short orifice and an increase in its diameter leads to a shift towards higher frequency. Amplitude of excitation also has significant influence on the peak value of loss angle which reduces significantly as the amplitude is increased.

Figure 6.24 shows the comparison of LDHF damper and LSDHF dampers in terms of transmitted force versus excitation displacement for the three amplitude of excitation. The two columns show the Lissajous' plot at two different frequencies; one at 7 Hz, close to first resonance, the other at 12 Hz, near second resonance. The solid line represents plot for LDHF damper. The broken lines are for LSDHF with gradual increase in orifice diameter; 3 mm, 4 mm and 5 mm. As the area within the boundary of Lissajous plot represents the amount of energy dissipated by the damper, it is observed that at 7 Hz and 1 mm amplitude, inclusion of short orifice reduces the damping. At 12 Hz, amount of damping remains the same where the asymmetry is reduced. It is, however, obvious from other figures that the inclusion of bleeder orifices increase the damping and the amount of damping increase with the increase of bleeder orifice diameter. Thus it appears that by adding a bleeder orifice, the long orifice damper energy dissipation can be increased in order to use such damper for isolation of high amplitude vibration.

The potential of such damper in isolation of high amplitude vibration as well as shock is next examined.

## 6.5 Performance Analysis of the Damper

The LSDHF damper applied to a one DOF system is simulated to observe its performances in terms of acceleration transmissibility and relative displacement transmissibility when subjected to sinusoidal excitation. The results are obtained for variation of bleeder orifice diameter as well as amplitude of excitation. The mass of the system is assumed 125 Kg with static stiffness of the chamber material

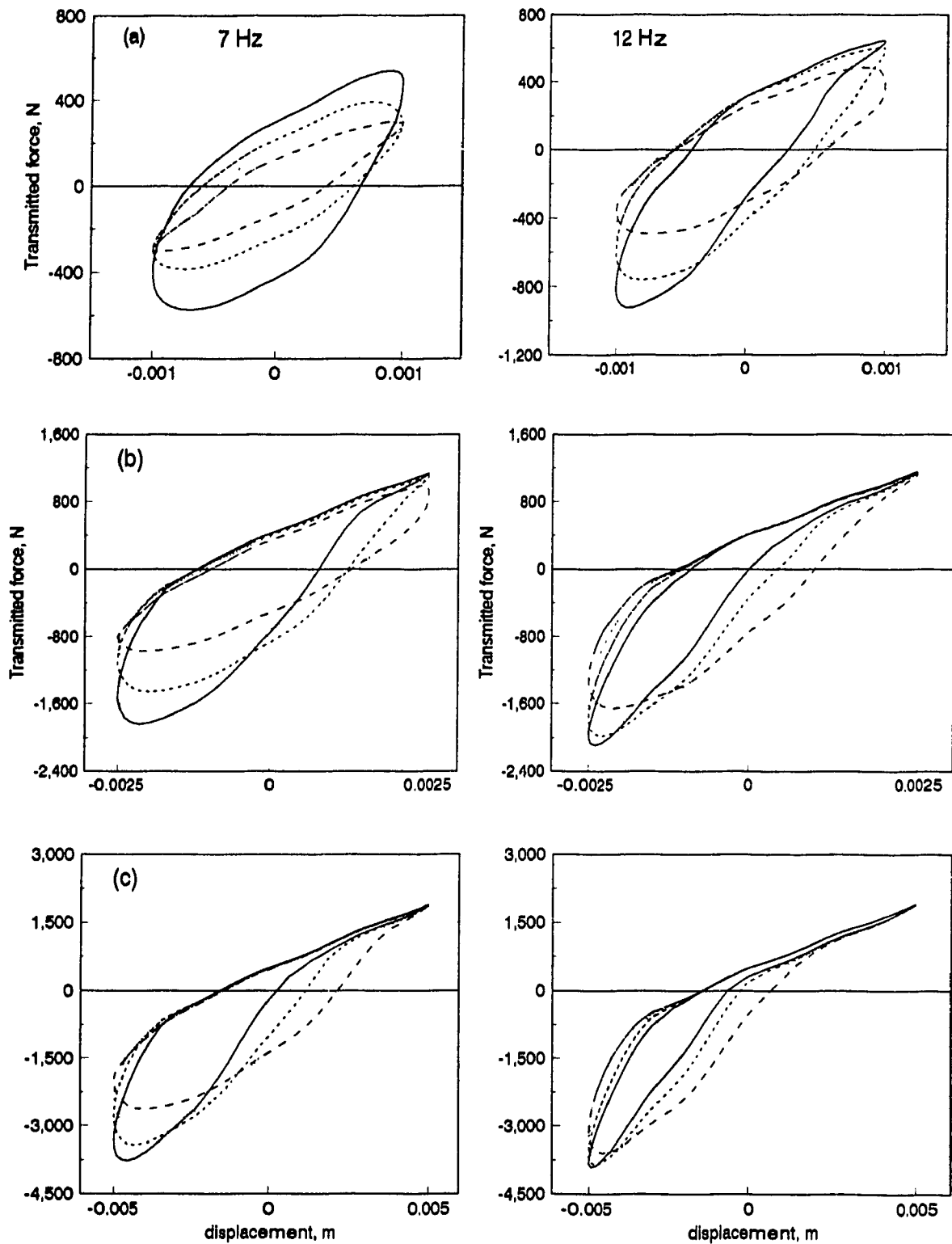


Figure 6.24 Effect of bleeder orifice diameter on the force-displacement characteristics of the damper. bleeder orifice diameter, —, 0.0mm (without), ----, 3mm; — · —, 4mm; - - - - , 5mm; (a)  $X_1=1\text{ mm}$ , (b)  $X_1=2.5\text{ mm}$ , (c)  $X_1=5\text{ mm}$ ; ( $L_o=150\text{ mm}$ ,  $D_o=7\text{ mm}$ ).

as 270 N/mm. The performance is finally evaluated for shock response in shock severity domain following the same steps as those presented for long orifice in section 6.3.2.

### 6.5.1 Performance Under Sinusoidal Excitation

Figure 6.25a shows the acceleration transmissibility of the one DOF system with a LSHDF damper. Long orifice length is taken as 150 mm with orifice dia 7 mm. Amplitude of excitation is 0.75 mm. The solid curve represents the transmissibility of the system without the short orifice. It is observed that system's response at first resonance is excellent but detrimental at second resonance which goes as high as 6.2. However, inclusion of short bleeder orifice can improve the performance dramatically with the minor loss at first resonance. At 3 mm orifice dia, transmissibility at second resonance greatly reduces to below 3 with minor increase at first response. At 4 mm orifice dia both peak transmissibility remains below 2. At 5 mm orifice dia second peaks vanishes but results in first peak transmissibility to reach above 2.

Inclusion of bleeder orifice increases the relative displacement transmissibility (Figure 6.25b) around first resonance but does not exceed a transmissibility of 2. Around frequency of second peak, relative transmissibility decreases with the increase in orifice diameter. These results clearly show that such dampers can be tuned to provide excellent isolation performance through the frequency range.

Figure 6.26 shows the same performance of the system but at excitation of 2.5 mm to demonstrate the better response of LSDHF damper at high excitation. It is found that, without the orifice, first peak is absent and the second peak goes up to 12 which reduces to 3.5 with the addition of a short orifice of diameter of 5 mm. Reduction in relative displacement transmissibility is also observed in a similar fashion.



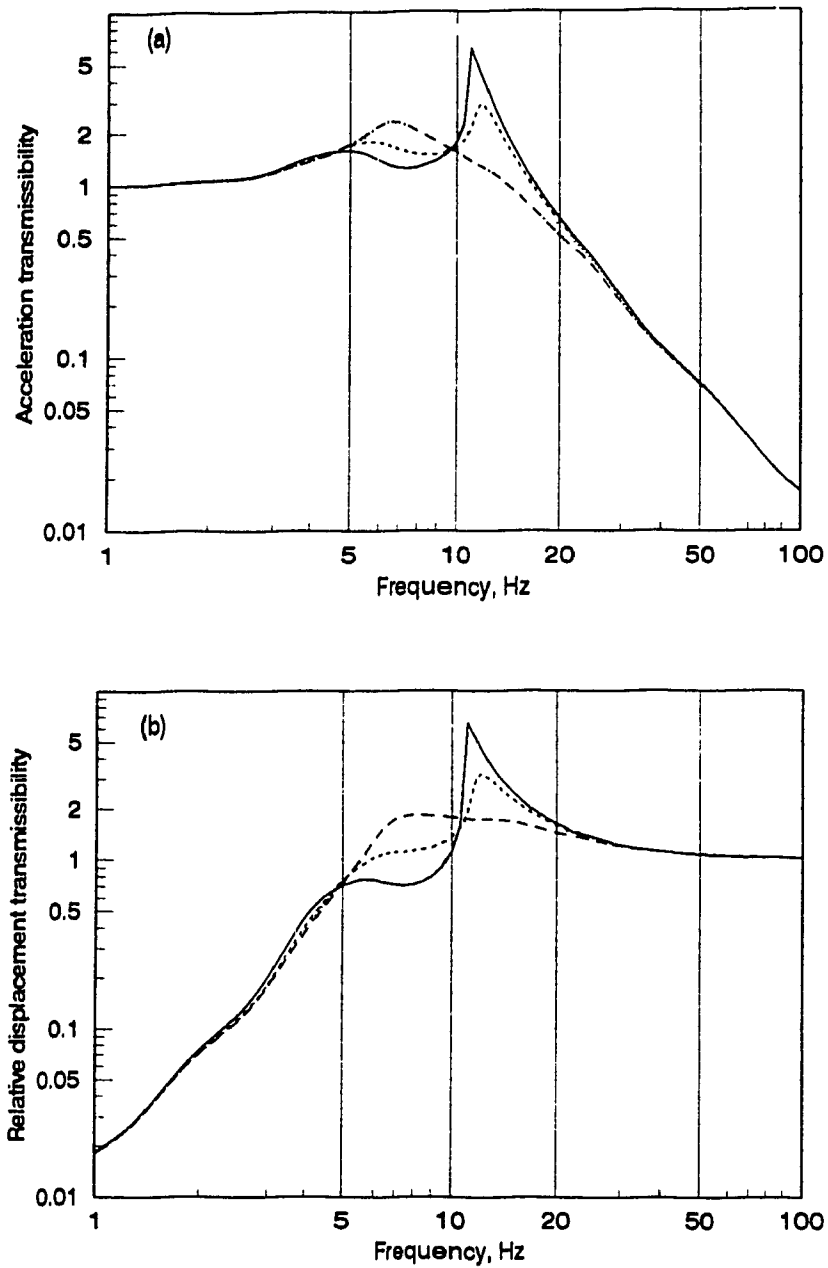


Figure 6.25 Effect of bleeder orifice diameter on the transmissibility performance of the damper. bleeder orifice diameter, —, 0.0mm (without); ----, 3mm; — · —, 4mm; · · · ·, 5mm; ( $X_1 = 0.75\text{mm}$ ,  $L_o = 150\text{mm}$ ,  $D_o = 7\text{mm}$ ).

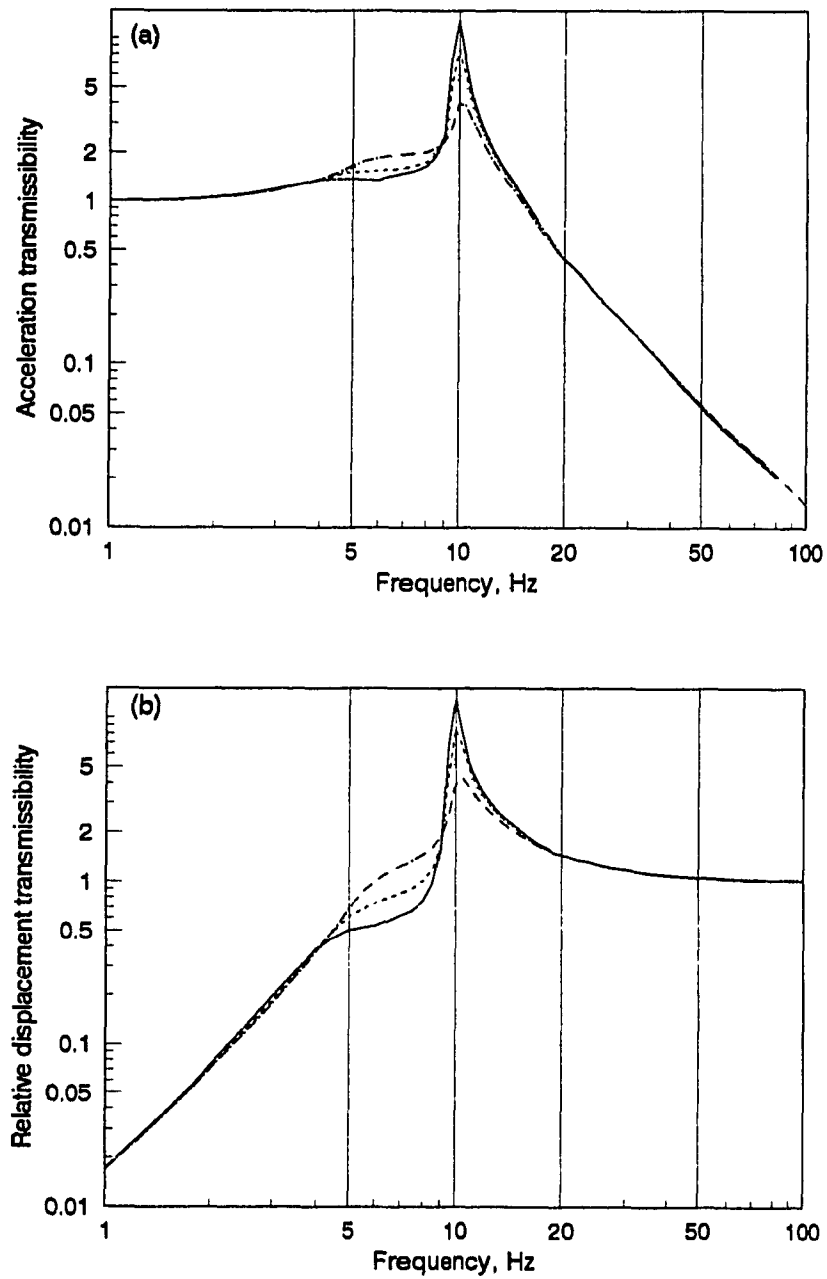


Figure 6.26 Effect of bleeder orifice diameter on the transmissibility performance of the damper. bleeder orifice diameter, —, 0.0 (without); - - - - , 3.0 mm; , 4mm - - - - , 5mm; ( $X_1=2.5\text{mm}$ ,  $L_o=150\text{mm}$ ,  $D_o=7\text{mm}$ ).

It is thus concluded that the LDHF damper with the inclusion of bleeder orifice improves the system's performance and it can accommodate higher amplitude of excitation without affecting the overall performances.

### **6.5.2 Performances Under Shock Displacement**

The flexible chambered damper currently investigated includes a short orifice in addition to the long orifice. This will certainly help to subside the rapid pressure buildup in the chamber, and lead to improved shock response. Similar to long orifice damper, the LSDHF damper is also excited with a rounded pulse displacement of amplitude 20 mm and the response is measured at the sprung mass. The shock acceleration response (SAR), shock velocity response (SVR), shock displacement response (SDR) and relative displacement response (RDR) are evaluated for a range of shock severity.

Figure 6.27 shows the SAR, SVR, SDR and RDR characteristics of the LSDHF damper having long orifice of 100 mm length and short orifice diameter 4 mm. The long orifice diameter is varied as 6 mm, 7 mm and 8 mm. Compared to Figure 6.20 which is for LDHF damper, the SAR characteristics is much improved for all range of shock severity except for very low shock severity. It is already established that very low severity input acts like a static load, therefore, the inclusion of a short orifice does improve shock responses. The increase in long orifice diameter improves the SAR even more for all range of shock severity.

The SVR characteristics of the LSDHF damper as shown in Figure 6.27b. Unlike SAR, the SVR characteristics is mostly similar to that of a LDHF damper. At low shock severity SVR is slightly higher and at high severity SVR is slightly better than that of a long orifice damper. The increase in long orifice diameter of the damper marginally improves SVR performance for the shock inputs higher than 0.50.

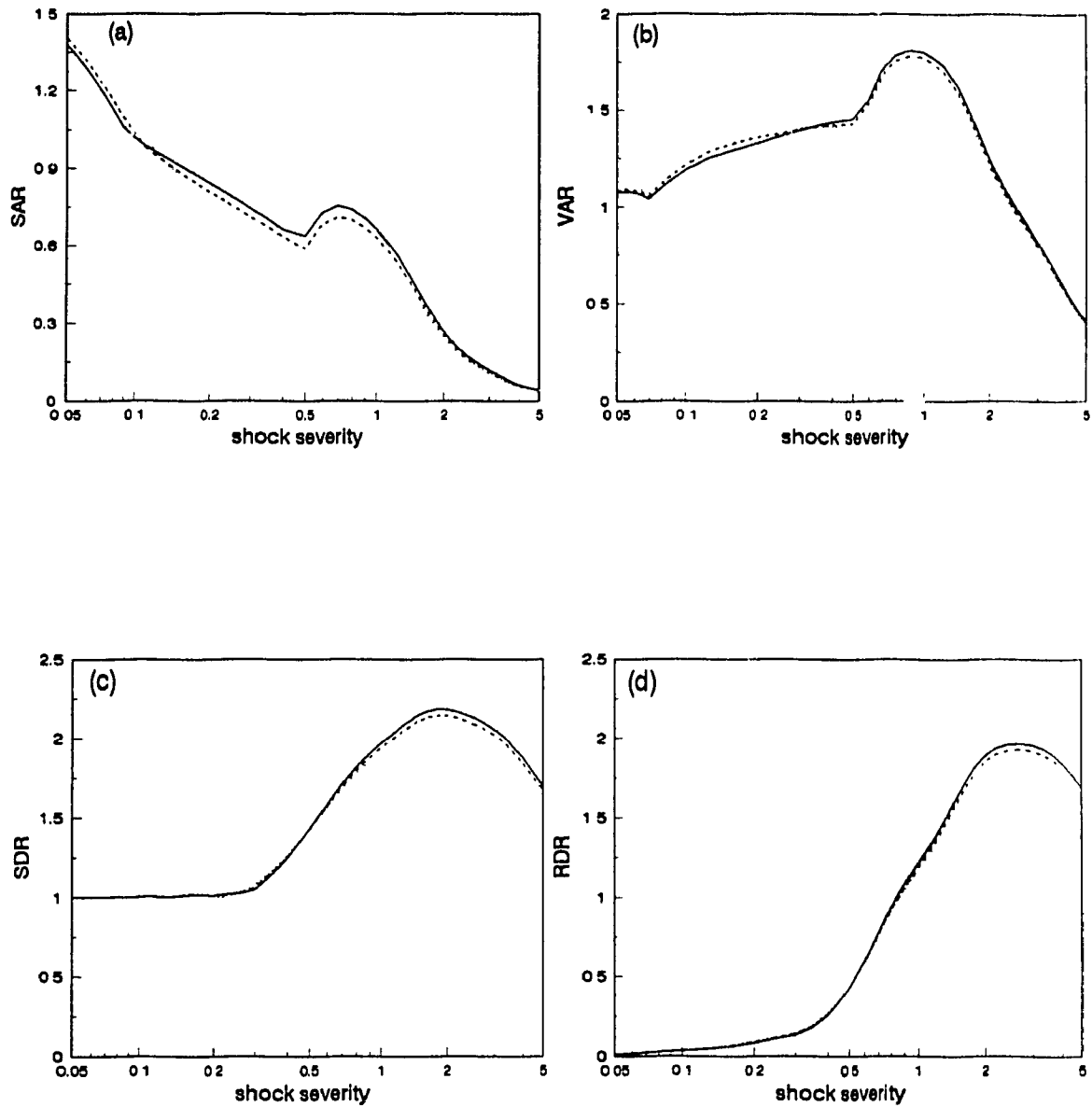


Figure 6.27 Shock responses as a function of shock severity with the variation of long orifice diameter; —, 6mm; ----, 7mm; ···, 8mm; (a) SAR, (b) VAR, (c) SDR, (d) RDR. ( $Y_s = 20\text{mm}$ ,  $L_o = 150\text{mm}$ ,  $D_{ob} = 4\text{mm}$ ).

Shock displacement response and shock relative displacement responses of the damper are shown in Figure 6.27c and 6.27d. The responses are mostly similar to that of a long orifice damper except the peak responses are lower. Again increase in long orifice diameter ameliorates the shock response. The diameter of short orifice may have influence on the shock performance which is examined next.

*Effect of short orifice diameter:* Figure 6.28 shows the shock performances of LSDHF damper in terms of SAR and SVR with the variation of short orifice diameter. The damper parameters are: long orifice length 100 mm, diameter 8 mm. The short orifice diameter is varied as 3 mm, 4.5 mm and 6 mm. It is observed that the increase in short orifice diameter significantly improves the SAR characteristics of the damper in the dynamic range. The larger the orifice diameter, the better the shock responses. SVR characteristics in dynamic range also improves with the increase in short orifice diameter. In both cases, again, SAR and SVR increase for very low shock severity.

It is evident that addition of a short orifice with a long orifice and an increase in the diameter of the short orifice leads to better dynamic response in terms of second peak and shock response. The design of such damper should, however, also consider the increase in first peak which results from the larger diameter of the short orifice.

## **6.6 Conclusion**

This chapter presented a detailed analysis of long orifice hydraulic damper with flexible chambers. The nonlinear model that includes fluid oscillation effect is used to study its dynamic characteristics and response under vibration and shock. The results clearly showed that negligence of oscillation effect grossly overestimates the orifice flow. Furthermore, oscillation effect leads to a reduction in flow rate with higher frequencies which can not be predicted otherwise. In

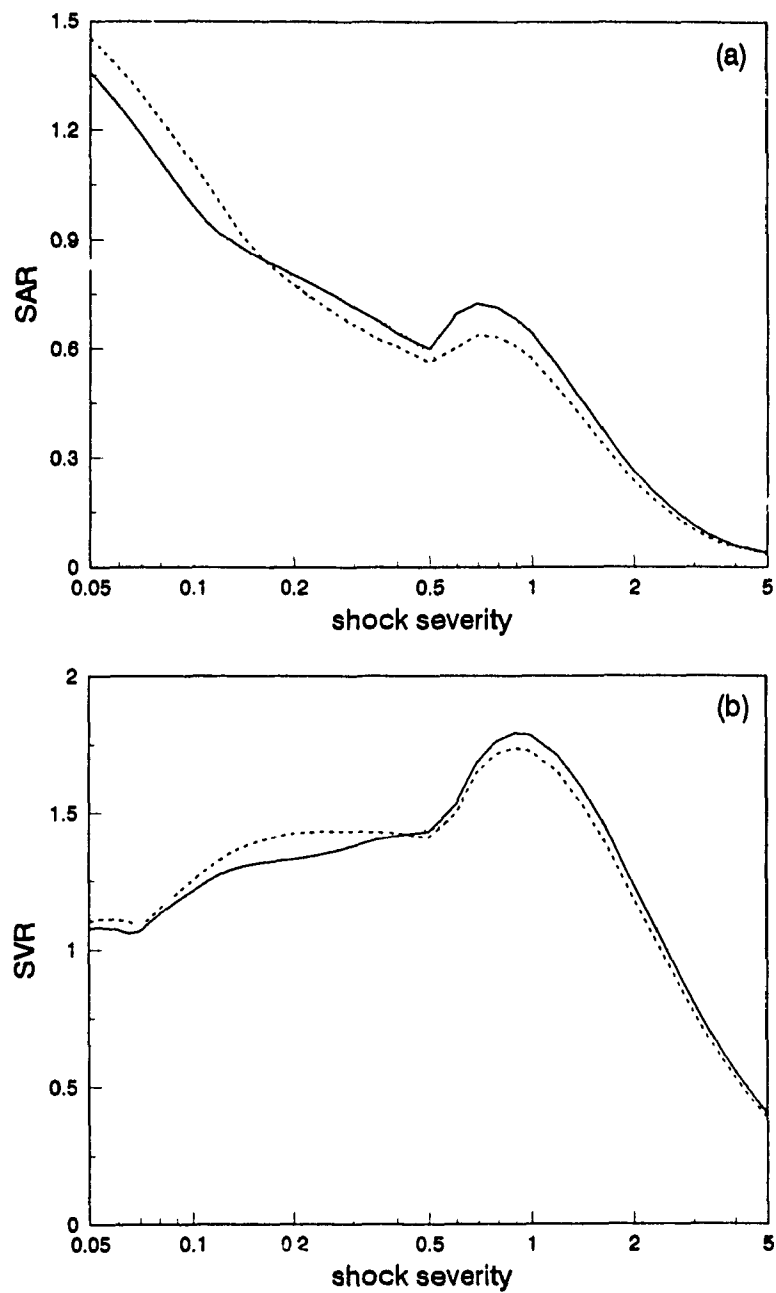


Figure 6.28 Shock responses as a function of shock severity with the variation of bleeder orifice diameter; —, 3mm; ---, 4.5mm; ···, 6mm; (a) SAR, (b) VAR. ( $Y_s = 20\text{mm}$ ,  $L_o = 150\text{mm}$ ,  $D_o = 8\text{mm}$ ).

comparison to short orifice, long orifice produces a rapid and large increase in dynamic stiffness with increasing frequency. Long orifice also produces larger and sharper loss angle peak. The parametric study shows both orifice diameter and length have significant influence on the dynamic characteristics mainly in terms of peak loss angle and frequency of its occurrence. A ratio of diameter to length of orifice will make a good parameter for tuning of such damper.

The performance of long orifice damper exhibits two distinct peaks: one for system resonance, and one for fluid resonance. The results show that such damper can be tuned to provide superior isolation performance near resonance compared to a short orifice damper. However, the second peak tends to deteriorate rapidly for larger amplitude of excitation. The overall shock response for long orifice damper is also found inferior to that of short orifice damper.

In attempts to improve, the extended model of long orifice damper which include a short orifice is also analyzed in this chapter. The results show that such addition and tuned parameter can produce satisfactory performance at relatively higher amplitude of excitation. Further, the shock performance in the dynamic range can be improved significantly by introducing large diameter short orifice. Short orifice of large diameter in this case is found to improve both shock response and transmissibility of second peak. A compromise is, however, required as it leads to an increase in the first resonance peak.

## **CHAPTER 7**

# **PERFORMANCE OF LONG ORIFICE DAMPER WITH SPRING LOADED VALVE**

### **7.1 Introduction**

The performance of hydraulic dampers with flexible chambers and short orifice was presented in chapter 5. Chapter 6 described the performance for long orifice with and without bleeder orifice. As it was found, these dampers although perform well for low amplitudes, have severe limitation in application for high amplitude or in shock. Comparatively, long orifice provides better performance in a low frequency range, hence a fixed bleeder orifice was added in attempts to improve performance as discussed in chapter 6. As found, a constant bleeder orifice tends to reduce damping at system's resonance as it is active all the time. This could be overcome by introducing spring loaded valve for the orifices.

A proposed model for this concept of hydraulic damper with flexible chamber, long orifice and orifices with spring loaded valve (LDHVF) was developed as presented in chapter 3. The LDHVF damper includes a long orifice, two forward short orifices and a reverse bleeder orifice. All orifices are equipped with spring loaded valves possessing variable spring constant. The objective of this chapter is to carry out and present a detailed analysis of this damper both in terms of dynamic characteristics and performance under vibration and shock. Similar steps as those of chapters 4, 5 and 6 are followed.



The following section presents a thorough investigation of damper characteristics in time domain to study the influence of spring loaded valve on the internal variables of the damper. This section further presents the dynamic characteristics in frequency domain. In all cases an amplitude of excitation equal to 5 mm is used, which is considered large for such dampers. The evaluation of characteristics is followed by a performance analysis under large amplitude vibration and shock.

## **7.2 Characteristics of the Damper**

The characteristics of the LDHVF damper are evaluated in terms of orifice flow through all four orifices, top chamber pressure and transmitted force. The motion of the disk of the valve with time is also observed. The opening and the closing of the valve governs the orifice flow through orifice 1, 2 and 3. Results are presented in time domain, at steady state. In frequency domain, characteristics of the damper is observed in terms of dynamic stiffness and loss angle. Parametric study is also carried out to study the effects of short orifice diameter. The spring constants for valves 1, 2 and 3 which determine the preset pressure limit for valves, are also varied to see their effect on the performance. The nominal parameters used are same as those presented for long orifice in chapter 6. Here the long orifice parameters include length of 150 mm and diameter of 8 mm which are kept constant.

### **7.2.1 Time Domain Analysis**

As the LDHVF has a number of orifices and some of which work at a preset pressure, it is necessary to study the characteristics of the damper in time domain. The time domain results are recorded after steady state has been reached. The orifice flow through long orifice, short orifices, bleeder orifice and transmitted

force as well as top chamber pressure are studied in detail. The motion of the spring loaded valves are also observed.

#### 7.2.1.1 Orifice flow

Figure 7.1 shows the steady state long orifice flow and bleeder orifice flow (acts only during reverse stroke) in time domain for an excitation amplitude of 5 mm at 10 Hz. Results are plotted for three different diameters for both of short orifices, taken as 4 mm, 6 mm and 8 mm to observe its effect on long orifice flow and bleeder orifice flow. Bleeder orifice dia is taken as 6 mm, where the preset pressure for valve 1 is taken as 50 KPa and for valve 2, it is 100 KPa. It is seen from the Figure 7.1a that inclusion of other orifices creates a major change in long orifice flow. Orifice flow during reverse stroke (bleeder orifice open) becomes flat after reaching certain flow rate level. This is due to the fact that part of the fluid easily passes through bleeder orifice as there is no fluid intertance. Bleeder orifice dia is constant, therefore, no changes in the long orifice flow is observed during reverse stroke.

(a) Effect of short orifice diameter : During forward stroke, long orifice is active and two short orifices at different operating pressure are active as well. As expected, increase in short orifice area decreases the long orifice flow as seen by the Figure 7.1a. For the same simulation, Figure 7.2a represents the flow for orifice 1 which opens and closes at 50 KPa and Figure 7.2b for orifice 2 which operates at 100 KPa. These results show the trend for short orifice flow for the three different diameters used. As the duration of 50 KPa pressure state in the damper is more than the duration of 100 KPa, orifice 1 remains opens longer than orifice 2. Consequently, for the same diameter total flow through orifice 1 is more than orifice 2. It is also observed that the higher the orifice diameter, the shorter the duration, specially for the high pressure orifice (orifice 2).

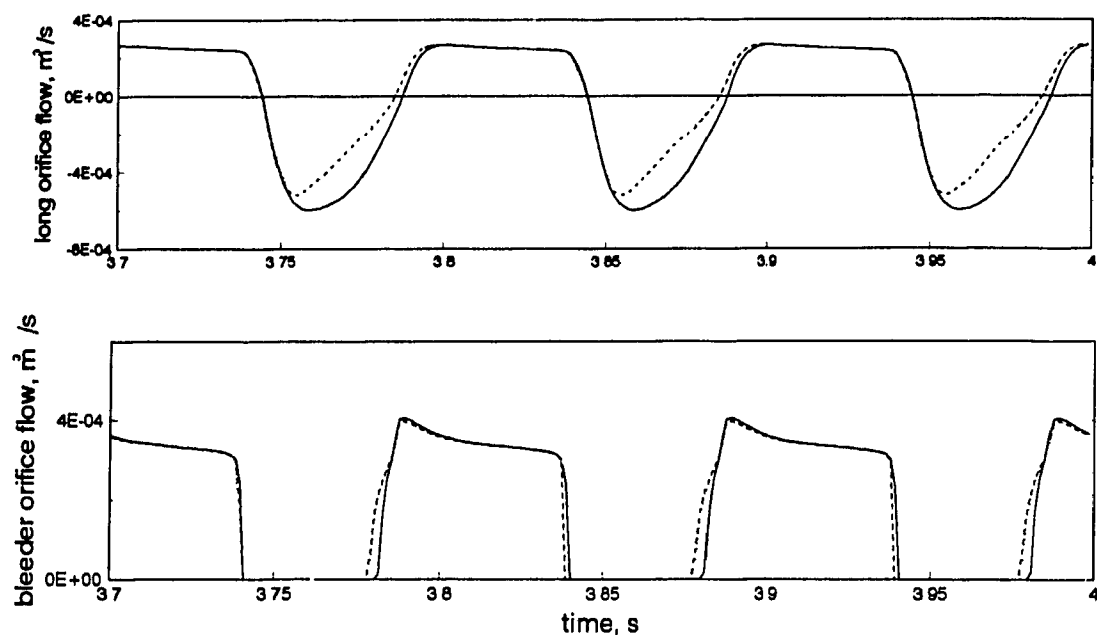


Figure 7.1 Long orifice flow and bleeder orifice flow of the LDVHF damper with the variation of valve short orifice —, 4mm; ----, 6mm; ·····, 8mm; ( $X_1 = 5\text{mm}$ ,  $L_o = 150\text{mm}$ ,  $D_o = 8\text{mm}$ ,  $D_{ob} = 8\text{mm}$ ).

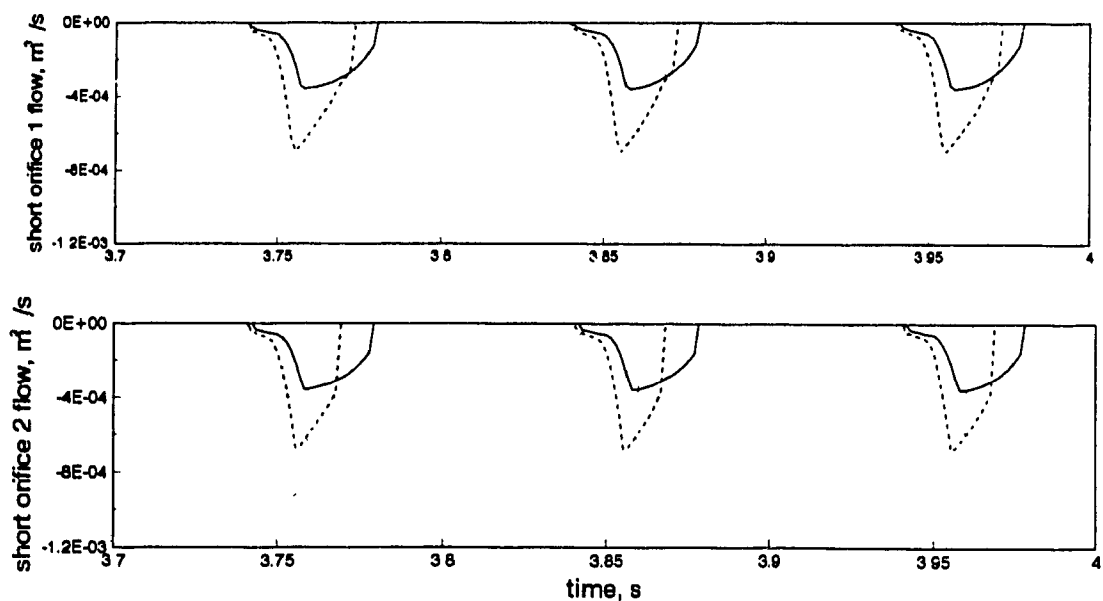


Figure 7.2 Valve short orifice flows of the LDVHF damper with the variation of its diameter; —, 4mm; ----, 6mm; ·····, 8mm; ( $X_1 = 5\text{mm}$ ,  $L_o = 150\text{mm}$ ,  $D_o = 8\text{mm}$ ,  $D_{ob} = 6\text{mm}$ ).

(b) Effect of bleeder orifice diameter: Keeping all other parameters constant, the bleeder orifice diameter is next varied as 6 mm, 8 mm and 10 mm. These results not presented to avoid duplication exhibit similar trend as that shown in Figure 7.1 for 6 mm. These results only indicate that as bleeder orifice diameter is increased the bleeder orifice flow increases where the duration of flow is reduced. At the same time the duration of reverse flow through long orifice is reduced for the same peak rate of flow. It has negligible influence on short orifice flow as well as forward flow of long orifice.

#### 7.2.1.2 Top Chamber Pressure and Transmitted Force

For the same simulation presented in Figure 7.1 and 7.2, this section presents the steady state time history of top chamber pressure and transmitted force. Figure 7.3 shows these results for three values of orifice diameter when bleeder orifice diameter is 6 mm. The solid line represents short orifice flow for orifice diameter of 4 mm. The pressure rise would have been higher, had there been no orifices except the long orifice.

(a) Effect of short orifice diameter: The result (Figure 7.3a) clearly demonstrates that for orifice diameter of 6 mm (dashed line) and 8 mm (dotted line), the opening of the valve causes rapid decrease of the top chamber pressure. For larger diameter, the pressure falls during forward stroke and remains just above 200 KPa prior to start of reverse stroke, during which the top chamber pressure falls near to zero. Since the pressure ratio falls below 0.35, there is cavitation during this part of the cycle for high amplitudes. The simulation, accordingly utilizes reduced value of discharge coefficient [31] in the cavitation period. The decrease in pressure with increase in orifice area is also reflected in the negative part of the transmitted force (Figure 7.3b). Transmitted force decreases to almost 50% for the change in orifice diameter from 4 mm to 6 mm. At 8 mm

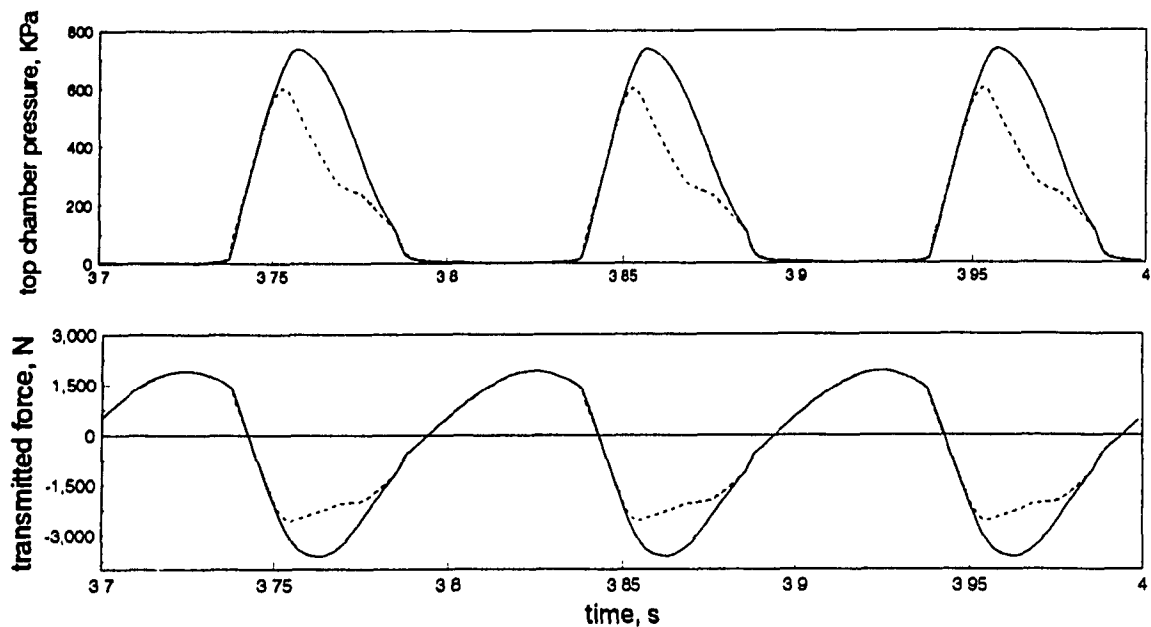


Figure 7.3 Top chamber pressure and transmitted force (in time domain) of the LDVHF damper. Valve short orifice diameter —, 4mm ; ---, 6mm; . . . , 8mm; ( $X_1=5\text{mm}$ ,  $L_o=150\text{mm}$ ,  $D_o=8\text{mm}$ ,  $D_{ob}=6\text{mm}$ ).

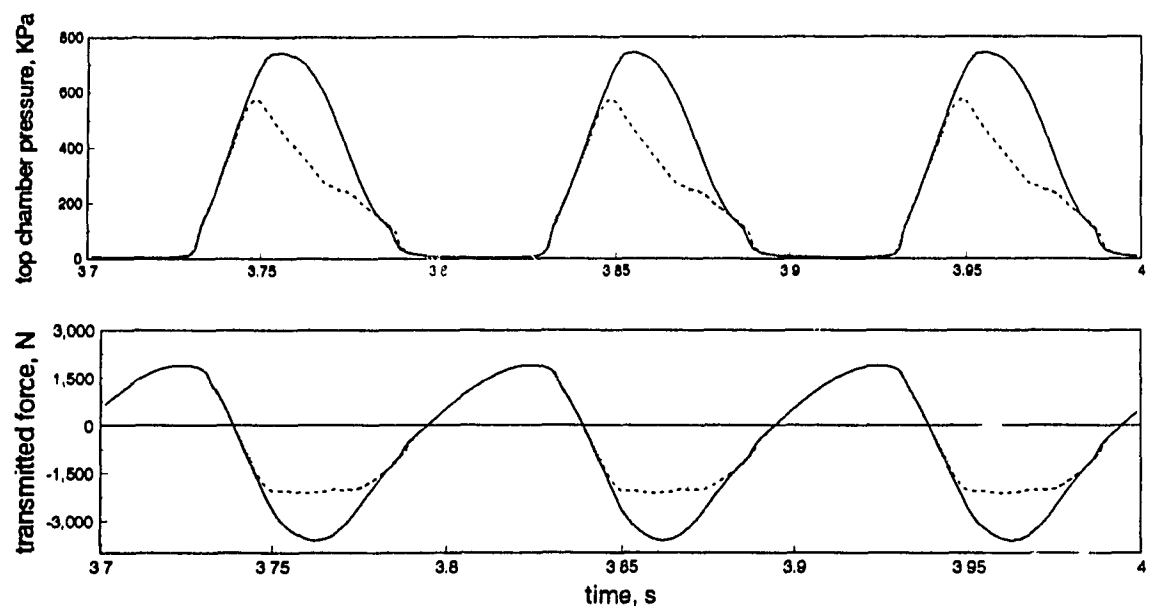


Figure 7.4 Top chamber pressure and transmitted force (in time domain) of the LDVHF damper. Valve short orifice diameter —, 4mm ; ---, 6mm; . . . , 8mm; ( $X_1=5\text{mm}$ ,  $L_o=150\text{mm}$ ,  $D_o=8\text{mm}$ ,  $D_{ob}=8\text{mm}$ ).

orifice diameter, transmitted force is even lower with the occurrence of another peak. For each change in orifice diameter, bleeder orifice diameter is kept constant, therefore, the positive part of the transmitted force remains unchanged.

(b) Effect of bleeder orifice diameter: The simulation result presented in Figure 7.3 for bleeder orifice of 6 mm is repeated for bleeder orifice of 8 mm and 10 mm as shown in Figure 7.4 and 7.5 respectively. These results show that the bleeder orifice diameter has minor effect on the peak pressure for short orifice diameter of 4 mm. But with the increase in bleeder orifice and short orifice diameter, top chamber pressure reduces. It is also observed that increase in bleeder diameter increases the high pressure state per cycle and decreases the low pressure state (vacuum) gradually. This change in top chamber pressure affects the force transmitted by the damper. At 4 mm valve orifice diameter, no appreciable change is noticed. But for valve orifice diameter 6 mm or higher, transmitted force decreases.

### 7.2.1.3 Motion of the Valve

The results obtained in terms of the valve motion for the three values of orifice diameter are shown in Figure 7.6. It shows the displacement of the valve for orifice 1 (low pressure, Figure 7.6a) and for orifice 2 (high pressure, Figure 7.6b) obtained with the variation of orifice diameter as 4 mm, 6 mm and 8 mm. The corresponding maximum valve displacement for orifices would be 1 mm, 1.5 mm and 2 mm respectively. As the results show, the valves for all diameters of orifice first open partially prior to opening to its maximum limit. But when the pressure drops they close instantaneously. For valve 1, with the increase in diameter, duration of 'full open' state of the valve decreases to some extent. Larger orifice reduces the pressure of the damper, so the valve closes early. The high pressure valve (orifice 2) stays 'full open' for even shorter period as seen in Figure 7.6b.

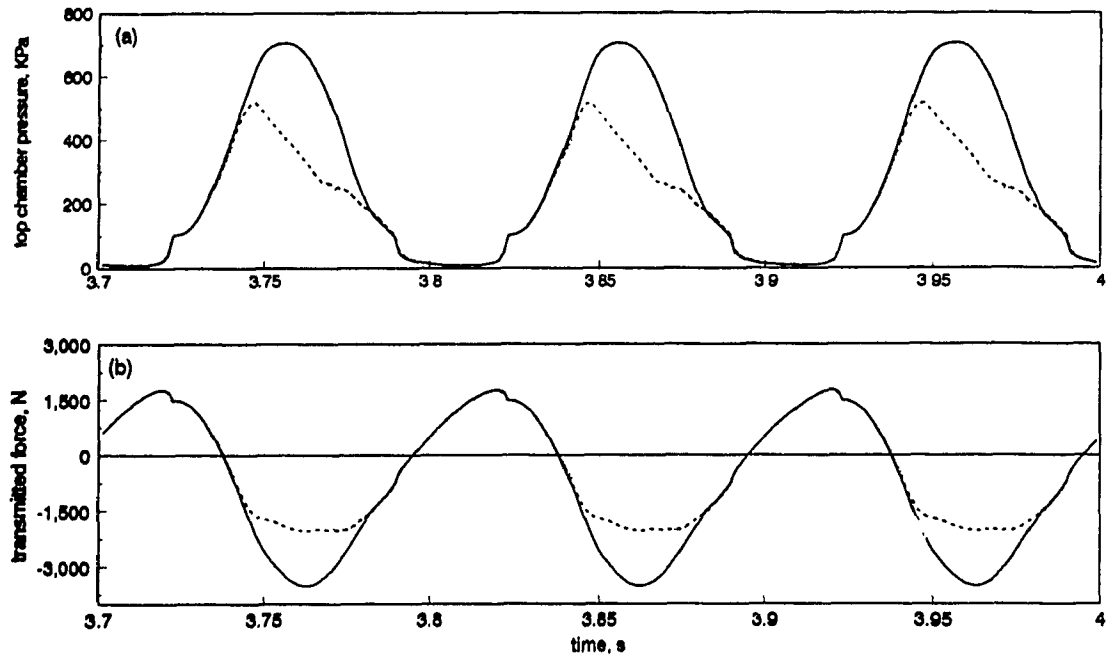


Figure 7.5 Top chamber pressure and transmitted force (in time domain) of the LDVHF damper. Valve short orifice diameter —, 4mm ; ----, 6mm; . . . , 8mm; ( $X_1 = 5\text{mm}$ ,  $L_o = 150\text{mm}$ ,  $D_o = 8\text{mm}$ ,  $D_{ob} = 10\text{mm}$ ).

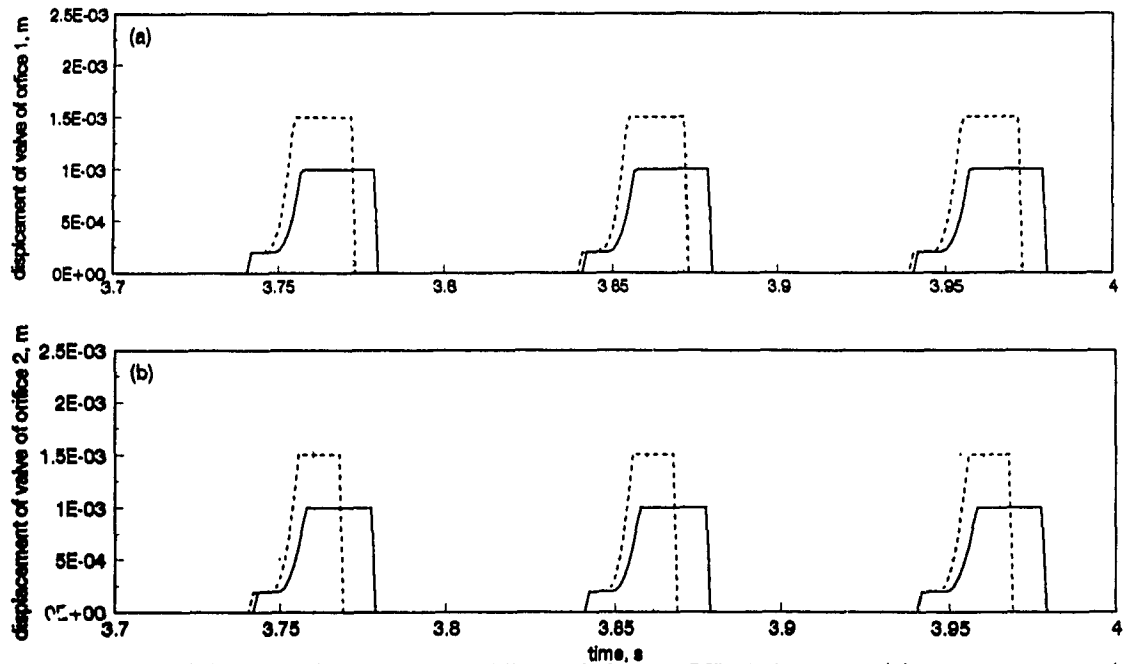


Figure 7.6 Motion of the valve orifice of the LDVHF damper. (a) orifice 1 and (b) orifice 2. Valve short orifice diameter —, 4mm ; ----, 6mm; . . . , 8mm; ( $X_1 = 5\text{mm}$ ,  $L_o = 150\text{mm}$ ,  $D_o = 8\text{mm}$ ,  $D_{ob} = 6\text{mm}$ ).

Here the duration of open state also reduces sharply for increase in orifice diameter.

### **7.2.2 Frequency Domain Analysis**

The characteristics of the LDHVF damper, so far discussed, is represented in time domain only. In this article, the behavior of the damper is presented in frequency domain for a range of 1 to 100 Hz. Only the dynamic stiffness and loss angle are chosen as the properties of the damper to analyze frequency domain characteristics. The damper characteristics are determined for different valve orifice and bleeder orifice diameters for a 5 mm excitation applied across the damper. The stiffness of the spring of the valve is also varied to see its effect.

Figure 7.7 shows the dynamic stiffness and loss angle of the LDHVF damper as a function of frequency for three different valve orifice diameters. The orifice diameters chosen are 4 mm, 6 mm and 8 mm while bleeder orifice diameter is held at 6 mm. It is found from Figure 7.7a that for all orifice diameters, dynamic stiffness is constant for up to 5 Hz (rubber stiffness) and starts to rise with the increase in frequency. Increase in the valve orifice diameter to 6 mm decreases the dynamic stiffness throughout the dynamic frequency range. The reverse effect is somewhat similar to the effect of variation of piston diameter for long orifice damper as shown in Figure 6.13. For 8 mm valve orifice diameter, the dynamic stiffness decreases even further.

The corresponding loss angle property of the damper is shown in Figure 7.7b. Peak loss angle is observed at 7 Hz for 4 mm orifice. Increase in valve orifice diameter decreases the peak value of loss angle with its occurrence at higher frequency. But at high frequency, beyond 10 Hz, loss angle increases slightly with increase in orifice diameter. In the case of a long orifice damper, increase in piston



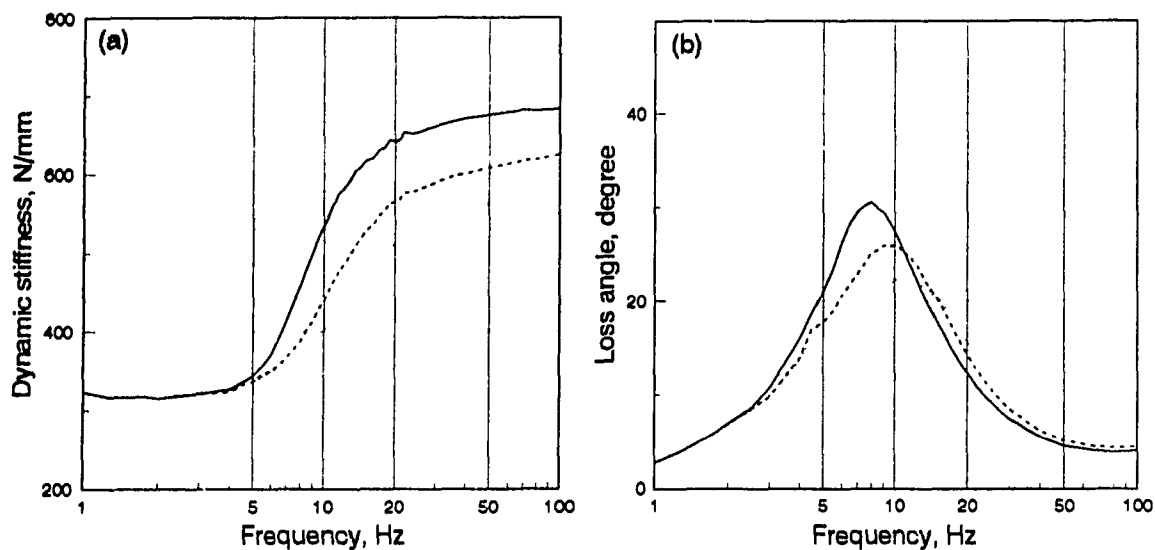


Figure 7.7 Effect of valve short orifice diameter on the (a) dynamic stiffness and (b) loss angle of the damper. Valve short orifice diameter —, 4mm; ----, 6mm; ·····, 8mm; ( $X_1=5\text{mm}$ ,  $L_o=150\text{mm}$ ,  $D_o=8\text{mm}$ ,  $D_{ob}=6\text{mm}$ ).

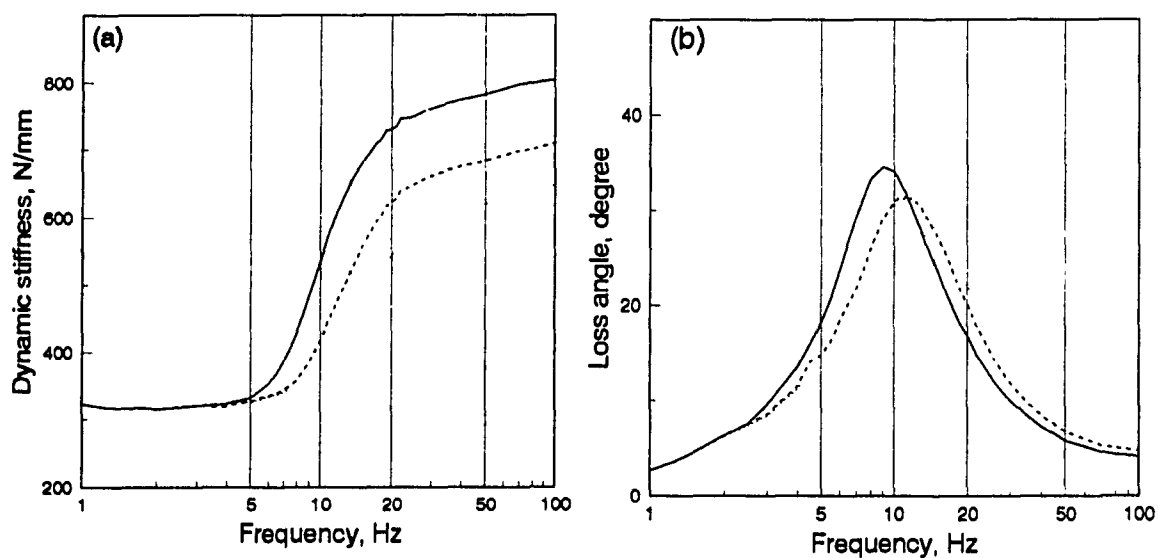


Figure 7.8 Effect of valve short orifice diameter on the (a) dynamic stiffness and (b) loss angle of the damper. Valve short orifice diameter —, 4mm; ----, 6mm; ·····, 8mm; ( $X_1=5\text{mm}$ ,  $L_o=150\text{mm}$ ,  $D_o=8\text{mm}$ ,  $D_{ob}=8\text{mm}$ ).

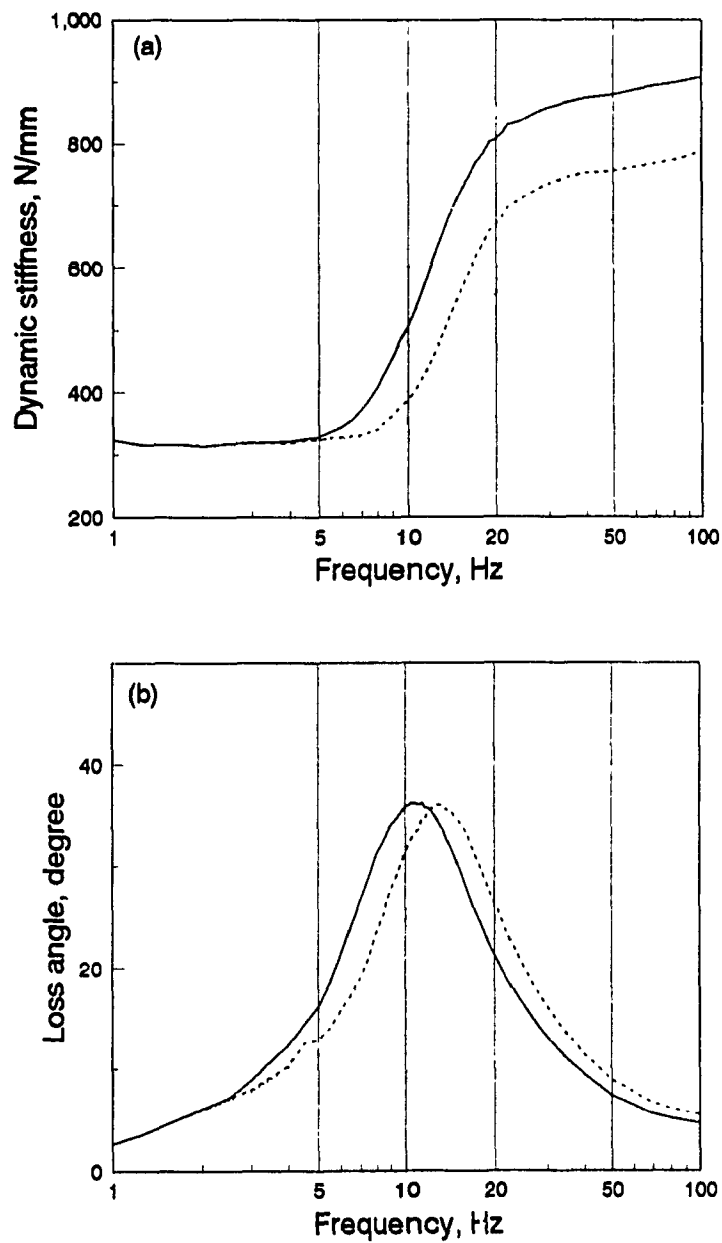


Figure 7.9 Effect of valve short orifice diameter on the (a) dynamic stiffness and (b) loss angle of the damper. Valve short orifice diameter —, 4mm ; — — —, 6mm; ·····, 8mm; ( $X_1=5\text{mm}$ ,  $L_o=150\text{mm}$ ,  $D_o=8\text{mm}$  and  $D_{ob}=10\text{mm}$ ).

diameter increases the peak value of loss angle with its occurrence at lower frequency.

The results of above simulation are repeated for bleeder orifice diameter of 8 mm and 10 mm are presented in Figures 7.3 and 7.9. As the results indicate, bleeder orifice diameter has significant influence on the dynamic characteristics for frequencies beyond 10 Hz. The variation in chamber pressure observed in time domain (Figure 7.3-7.5) was insignificant as the curves were plotted for 10 Hz only. Increase in bleeder orifice diameter increases the dynamic stiffness and loss angle of the damper, whereas increase in short orifice diameter reduces the dynamic characteristics of the damper. The larger bleeder orifice diameter increases the top chamber pressure creating higher dynamic stiffness. For a 4 mm orifice, increase in bleeder orifice from 6 mm to 8 mm leads to a increase in maximum dynamic stiffness from 700 N/mm to over 800 N/mm. Similarly a 10 mm bleeder orifice produces stiffness of over 900 N/mm. The trend in change in dynamic stiffness for increase in short orifice size remains same for all sizes of bleeder orifice.

Peak loss angle and corresponding frequency as shown in this figure increases as bleeder orifice diameter is increased. For larger bleeder orifice size, the effect of orifice diameter on the peak reduces to some extent. This also leads to significant increase in the loss angle for higher frequencies.

### **7.3 Performance Analysis of the Damper**

The performance analysis of the LDHVF damper is carried out by implementing the damper to a one DOF system. Similar to the previous studies, the sprung mass is chosen as 125 Kg. The base of the system is excited sinusoidally for the range of frequency of 1 to 100 Hz with an amplitude of excitation 2.5 mm. This excitation, instead of 5 mm, is used due to the fact that such hydraulic damper can not provide

satisfactory response for such high amplitude even with the valve orifices proposed. For a simple hydraulic damper, however, 2.5 mm is considered large amplitude. The response of the system is measured at the unsprung mass. The damper parameters chosen are: long orifice length 150 mm, long orifice diameter 8 mm, piston diameter 75 mm, bleeder orifice diameter is varied from 5 mm to 7 mm. Orifice valve diameter is varied as 4 mm, 6 mm and 8 mm. Response characteristics are determined in terms of acceleration transmissibility and relative displacement transmissibility.

### **7.3.1 Performances Under Sinusoidal Excitation**

Figure 7.10 shows the transmissibility performances of the LDVHF damper for three different valve orifice diameters, 4 mm, 6 mm and 8 mm. It was also found in chapter 6 that long orifice hydraulic dampers with or without short orifice or decoupler normally exhibits two peaks. One frequency occurs around 7 Hz and the other around 12-15 Hz, depending on the parameter of the damper. For the results obtained here, it is observed in the Figure 7.10 that for valve orifice diameter 4 mm, peak acceleration transmissibility due to first resonance disappears due to the presence of spring loaded valves. The damper shows the transmissibility for second resonance only slightly above 3. Still, maximum relative displacement does not exceed 4 as shown in Figure 7.10b. For valve orifice diameter 6 mm, only one resonance frequency is visible which is around 9.5 Hz, peak transmissibility at that frequency is below 3. High frequency transmissibility beyond 10 Hz is better compared to the damper of valve orifice diameter 4 mm. But the damper does not perform satisfactorily for a valve orifice diameter of 8 mm, where transmissibility goes very high at the natural frequency.

For a LDHVF damper with a bleeder orifice of 8 mm, transmissibility curves are shown in Figure 7.11. For all valve orifice diameters, both the acceleration and

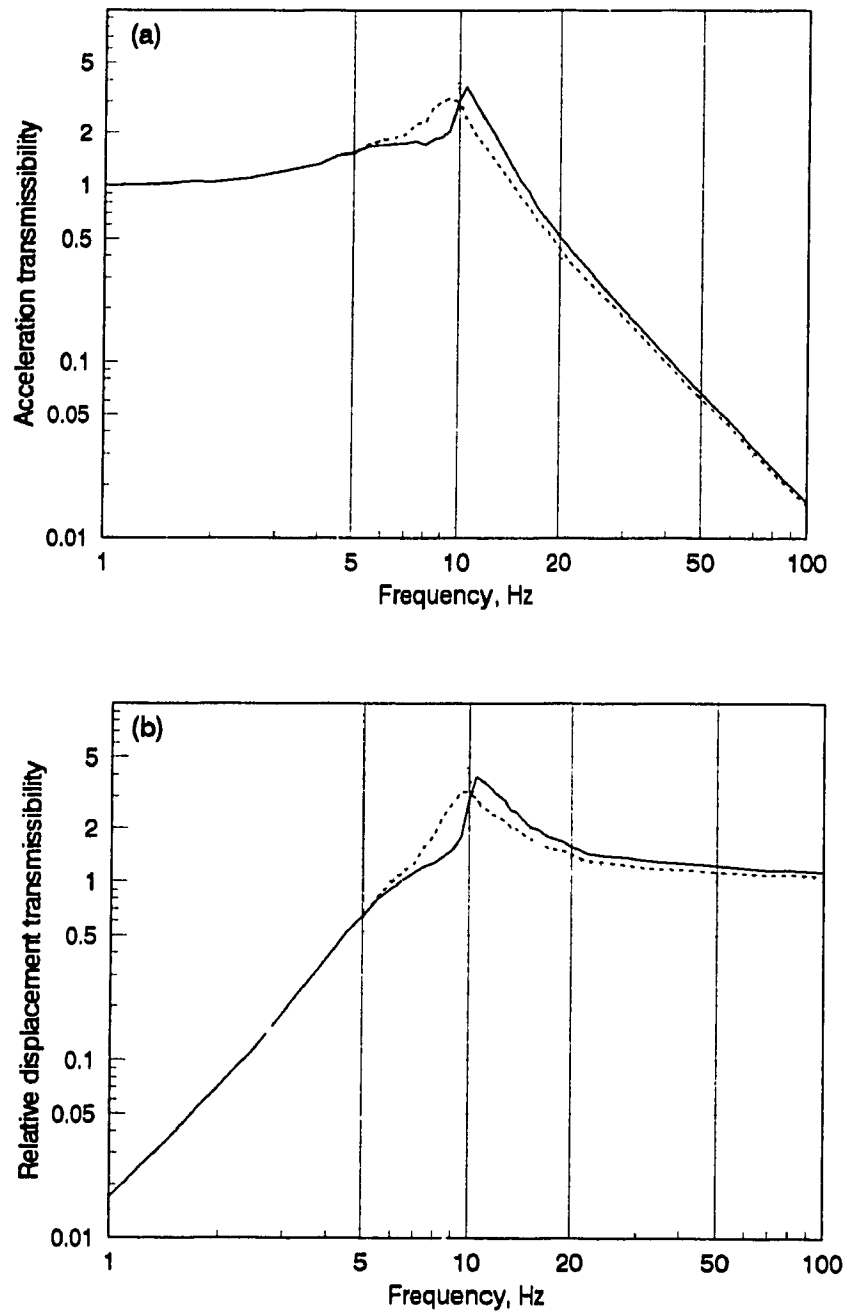


Figure 7.10 Effect of valve orifice diameter on (a) acceleration transmissibility and (b) relative displacement transmissibility. Valve short orifice diameter —, 4mm; ----, 6mm; ·····, 8mm; ( $X_1=2.5\text{mm}$ ,  $L_o=150\text{mm}$ ,  $D_o=8\text{mm}$  and  $D_{ob}=5\text{mm}$ ).

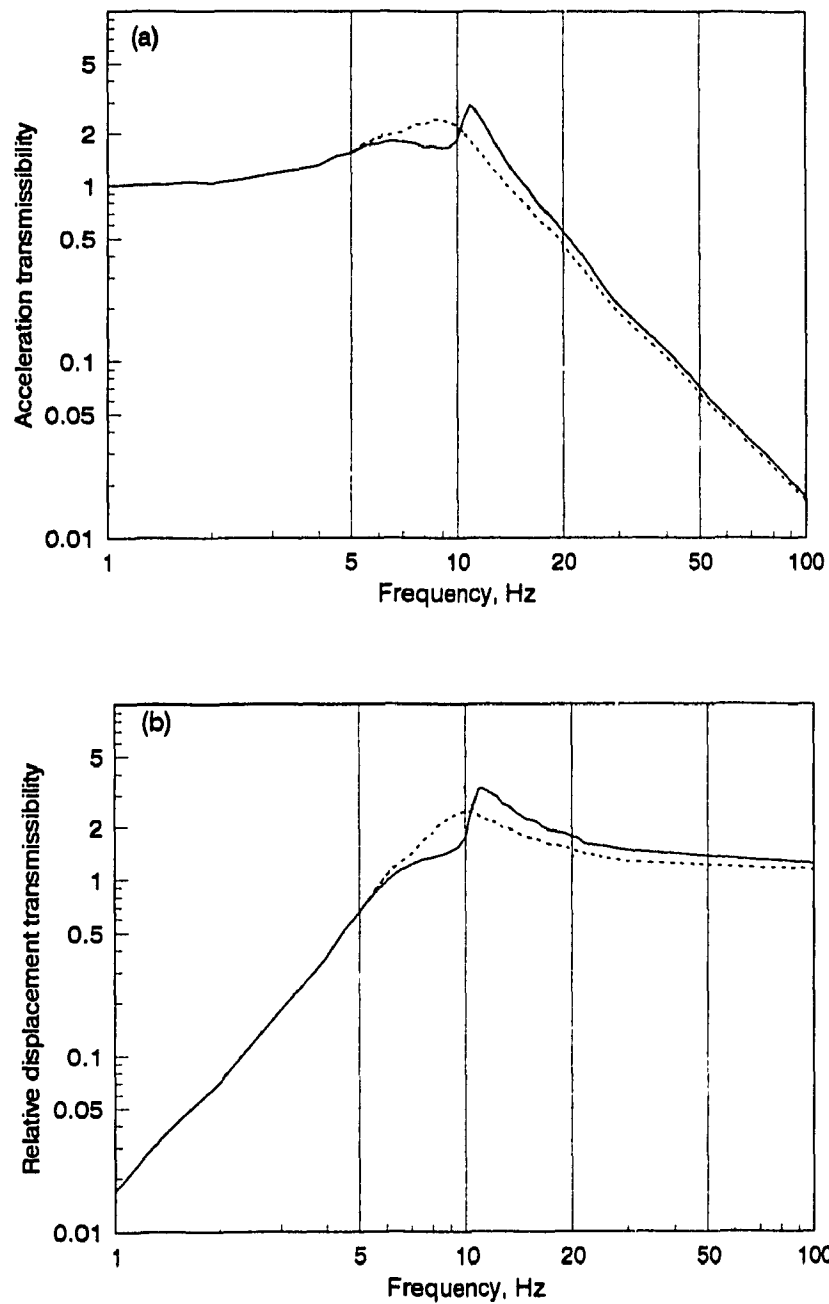


Figure 7.11 Effect of valve orifice diameter on (a) acceleration transmissibility and (b) relative displacement transmissibility. Valve short orifice diameter —, 4mm; ---, 6mm; ···, 8mm; ( $X_1=2.5\text{mm}$ ,  $L_o=150\text{mm}$ ,  $D_o=8\text{mm}$  and  $D_{ob}=6\text{mm}$ ).

relative displacement transmissibilities response are much better than that of the damper with the bleeder orifice of 5 mm. At valve orifice diameter of 4 mm, first resonance transmissibility is well below 2 and the second resonance transmissibility is also reduced without any increase in high frequency transmissibility. For valve orifice diameter of 6 mm, transmissibility for the whole range of frequency is much improved, at resonance it is just above 2 and the high frequency transmissibility is also satisfactory. The corresponding relative displacement transmissibility (Figure 7.11b) also show minimum peak response. Acceleration transmissibility for the damper with bleeder orifice diameter of 7 mm is shown in Figure 7.12a. The corresponding relative displacement transmissibility is shown in Figure 7.12b. As these results show, this combination of parameters with 6 mm valve orifice can produce superior response. Any further increase in bleeder orifice diameter will lead to larger peak at 7 Hz. These results clearly demonstrate that a combination damper such as long orifice with spring loaded orifices can be tuned effectively to provide highly satisfactory isolation performance for amplitudes as large as 3 mm.

Figure 7.13 shows a comparative performance characteristics for all the four hydraulic dampers, so far investigated, in terms of acceleration transmissibility and relative displacement transmissibility for an amplitude of excitation of 1 mm. Results are taken for the damper parameters which are not optimal but produce reasonably good performance. The parameters are: for SDHF, orifice diameter 8 mm; LDHF, long orifice dia 9 mm and length 200 mm; LSDHF, long orifice dia 7 mm, length 150 mm and short orifice dia 3 mm; LDHVF, long orifice dia 7 mm, length 150 mm, short orifice dia 4 mm and bleeder orifice dia 7 mm. It is found from the Figure 7.13a that SDHF is very satisfactory for high frequency vibration isolation but at resonance, performance is very poor. Overall performance of LSDHF is better compared to LDHF damper, both are excellent compared to

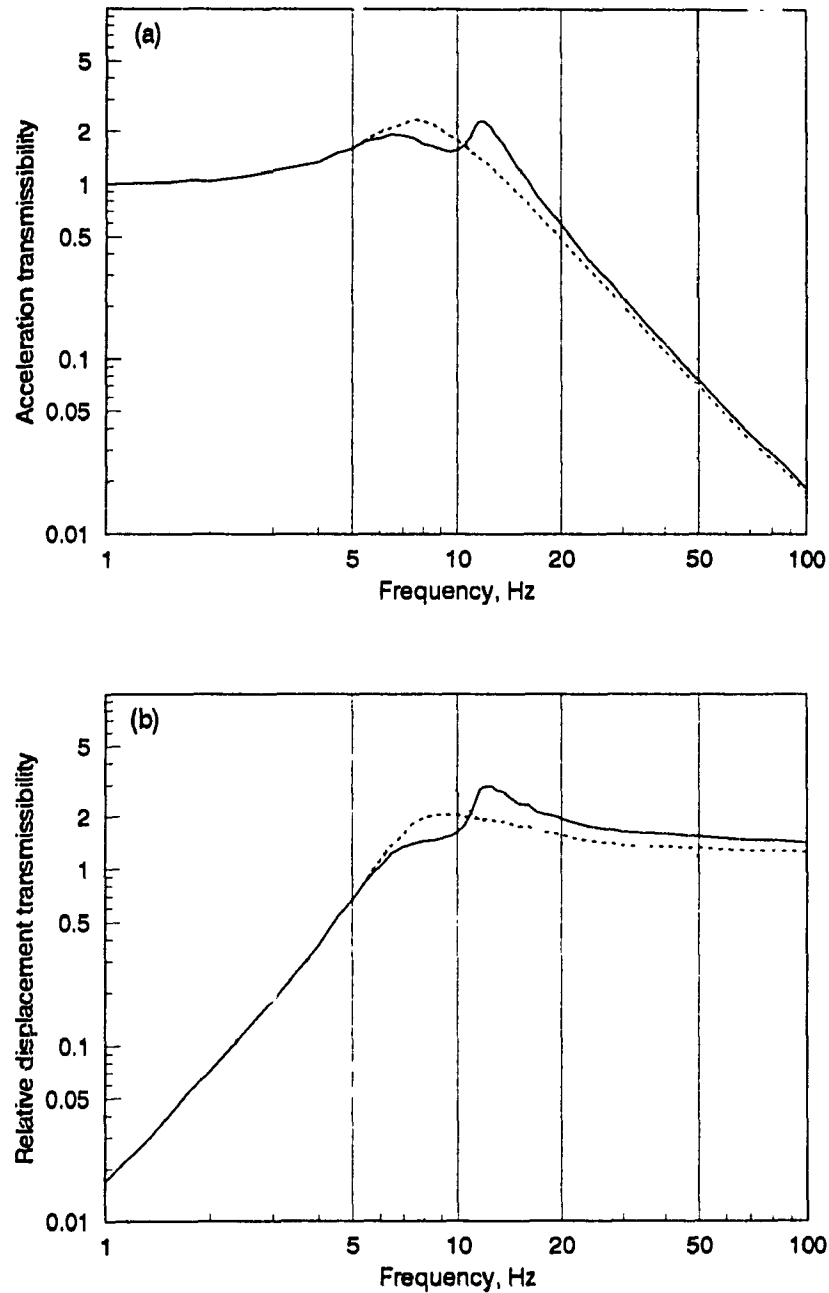


Figure 7.12 Effect of valve orifice diameter on (a) acceleration transmissibility and (b) relative displacement transmissibility. Valve short orifice diameter, 4mm;-----, 6mm; , 8mm; ( $X_1=2.5\text{mm}$ ,  $L_o=150\text{mm}$ ,  $D_o=8\text{mm}$  and  $D_{ob}=7\text{mm}$ ).



SDHF around resonance frequency. The LDHVF damper for the amplitude of excitation of 1 mm is able to eliminate the second resonance without affecting the first resonance transmissibility. However, there is a minor increase in high frequency transmissibility compared to LDHF or LSDHF damper. Relative displacement transmissibility also minimum around resonance frequency compared to that of other dampers as shown in Figure 7.13b. The LDHVF damper is, thus, superior compared to all other DHF damper and is applicable for all range of frequency.

Similar conclusion may be drawn for the dampers when subjected to the excitation amplitude of 2.5 mm as shown in Figure 7.14. At this amplitude, the LDHF damper is mostly undesirable. Again the performance of the LDHVF damper is satisfactory although there is a rise in relative displacement at high frequency.

### **7.3.2 Performances Under Shock Displacement**

The long orifice hydraulic damper with spring loaded valve is implemented to a single DOF system and the base of the system is excited by the shock displacement. A rounded pulse displacement of amplitude 20 to 50 mm is considered adequate to demonstrate the LDHVF damper performances. The characteristics of the shock displacement and performance indices are discussed in chapter 4. The shock severity parameter is also considered here in the range 0.05 to 5, which covers a satisfactory range of shock severity. The mass and the spring stiffness are kept same as other models to compare the shock response of the damper with other types of dampers. A time domain analysis is also carried out to see the duration as well magnitude of the shock response in terms of acceleration ratio, velocity ratio, displacement ratio and relative displacement ratio.

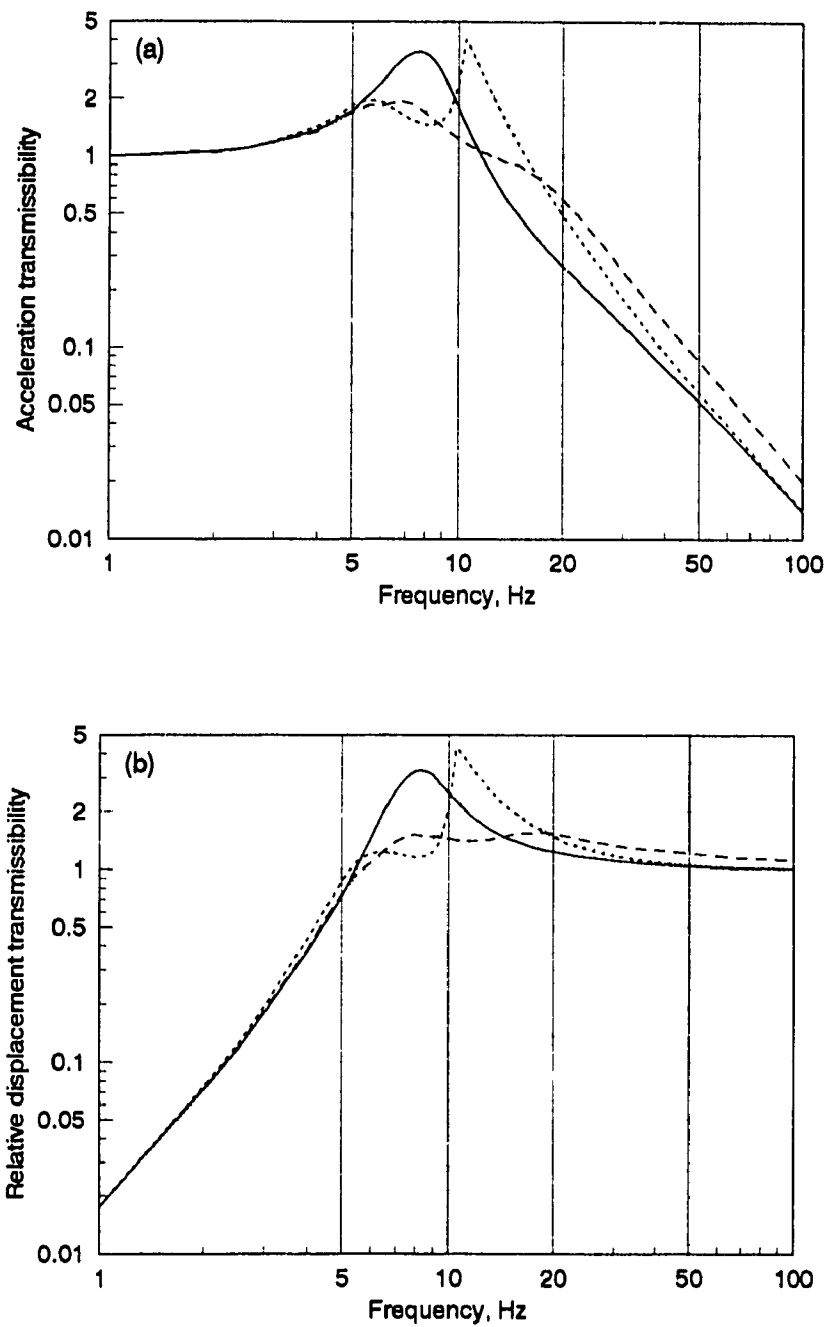


Figure 7.13 Comparison of performance of hydraulic dampers.  $X_1 = 1\text{mm}$ ; —, SDHF; ----, LDHF; ·····, LSDHF; - · - ·, LDHVF.

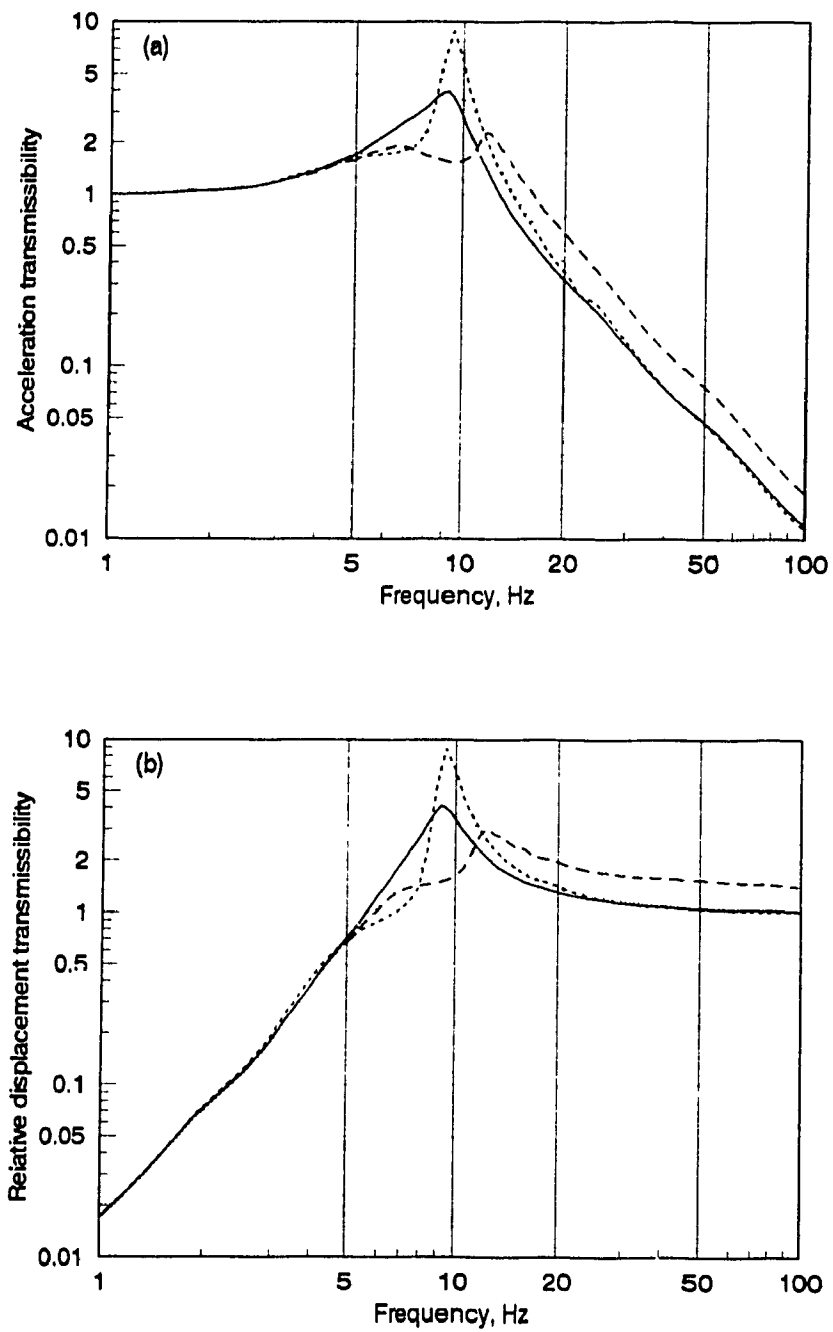


Figure 7.14 Comparison of performance of hydraulic dampers.  $X_1 = 2.5\text{mm}$ ; —, SDHF; ----, LDHF; - · - · -, LSDHF; — — —, LDHVF.

### 7.3.2.1 Time Domain Analysis

The shock response time history in terms of acceleration ratio, velocity ratio, displacement ratio and relative displacement ratio for four different shock severity in the range of 0.1 to 1 are presented in Figure 7.15. These results are obtained for a shock displacement of amplitude 20 mm. Damper parameters for this simulation include: long orifice length 150 mm, long orifice diameter 8 mm, short valve orifice diameter 6 mm, preset pressures for valve 1 is 50 KPa and for valve 2 is 150 KPa. Piston diameter is considered as 75 mm.

It is very interesting to observe (Figure 7.15) that the acceleration ratio obtained by the damper is very satisfactory compared to other three types of hydraulic dampers with flexible chambers presented in chapter 5 and 6. Its performance is almost similar to the performance of the dual-phase shock absorber (Figure 4.20-4.21). The trend indicates that the peak shock acceleration decreases with the increase in shock severity, and for all shock severity (Figure 7.15a), acceleration ratio dies out right after one cycle of oscillation. The other three types of flexible dampers were found to take equivalent to three to four cycle of oscillation to die out completely. The peak acceleration in this case is also lower compared to that of the other flexible dampers.

The velocity ratio characteristics of the sprung mass for the above simulation is shown in Figure 7.15b. The LDHVF damper again shows better performance in terms of velocity ratio characteristics in comparison to other damper studied. At high shock severity ( $v = 1$ ), the velocity ratio, in this case, diminishes within two oscillations whereas other dampers take at least four oscillations to vanish. The peak velocity ratio corresponding to each shock severity is also lower in comparison to other dampers.

The displacement ratio and the relative displacement ratio characteristics of the LDHVF damper are shown in Figure 7.15c and 7.15d for four values shock

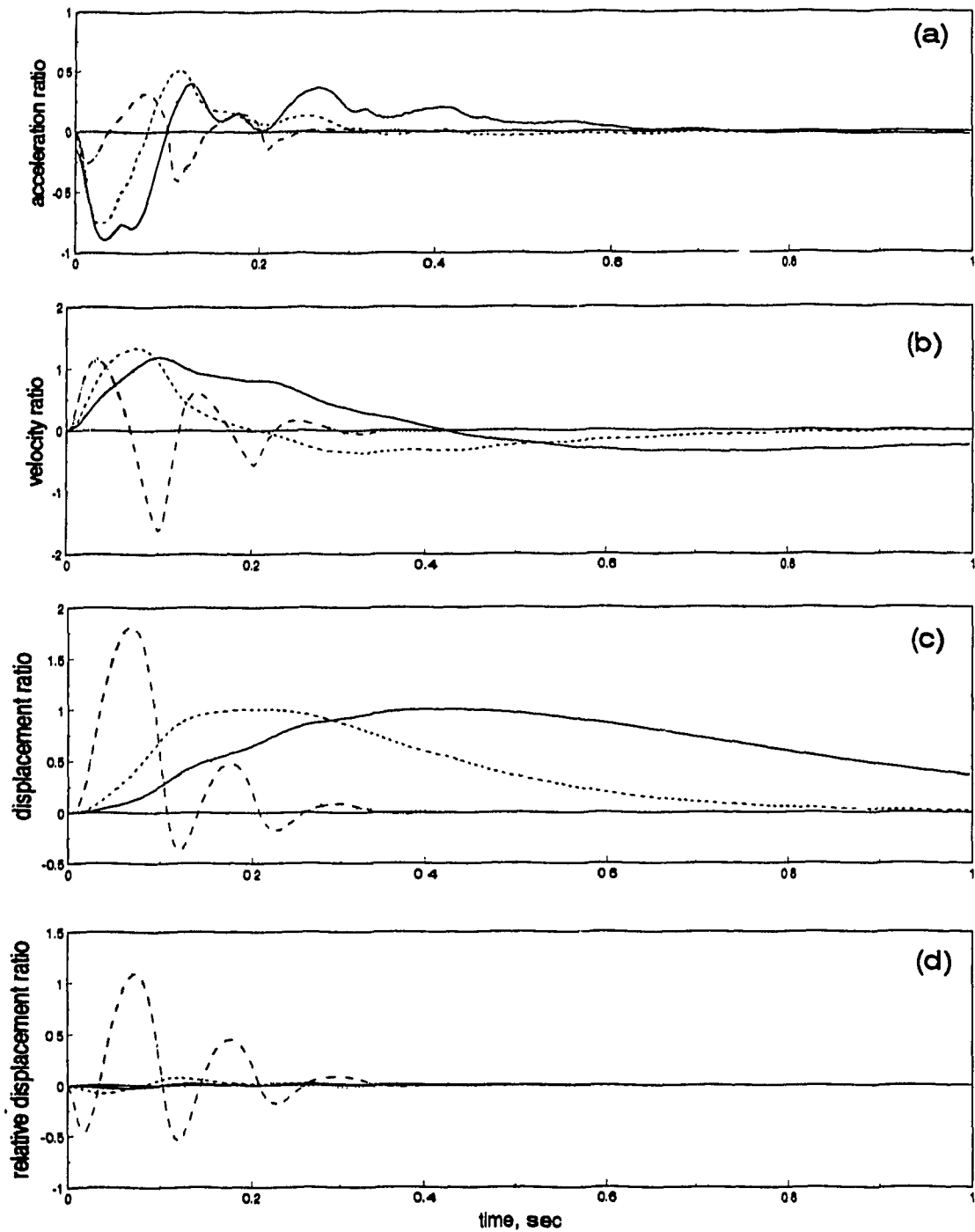


Figure 7.15 Shock responses in time domain. Shock severity, —, 0.1; ---, 0.2; . . . , 0.5; - · - · - , 1.0; (a) acceleration ratio, (b) velocity ratio, (c) displacement ratio and (d) relative displacement ratio.

severity parameter. Similar to previous performance, these performance also show improvement over other dampers considered. Even at high shock severity ( $v = 1$ ), the damper absorbs both displacement and relative displacement within two oscillations. The performance of LDHVF in terms of relative displacement ratio shows a significant improvement over other hydraulic dampers utilizing only short or long orifice.

The proposed damper with one long orifice and three short orifices with spring loaded valve constitutes a very large number of parameters. Parameters suspected to have significant influence on the performance is investigated in this study. A systematic optimization of all parameters for minimization of response will surely lead the damper to a even superior isolator for application to both vibration and shock of relatively large amplitudes.

### 7.3.2.2 Performance Analysis in Shock Severity Domain

The LDHVF damper is excited at the base with rounded pulse displacement of shock severity 0.05 to 5.0. The response of the sprung mass is obtained in terms of shock acceleration ratio (SAR), shock velocity ratio (SVR), shock displacement ratio (SDR) and shock relative displacement ratio (RDR). The damper parameters are; long orifice length 150 mm, diameter 8 mm. short orifice diameter for return 6 mm. Amplitude of excitation is 20 mm. The valve orifice diameter is varied as 4 mm, 5 mm and 6 mm to investigate the effect of valve orifice diameter on responses. The resulting responses are presented in Figure 7.16.

It is observed from the Figure 7.16a that SAR response of the LDHVF damper decreases with the increase in shock severity in a similar fashion as those obtained earlier. Any significant effect of valve orifice diameter occurs after shock severity reaches 0.5 beyond which increase in valve orifice diameter reduces the SAR. This decrease in SAR is more prominent within the severity of 0.6 to 1.5. The SAR

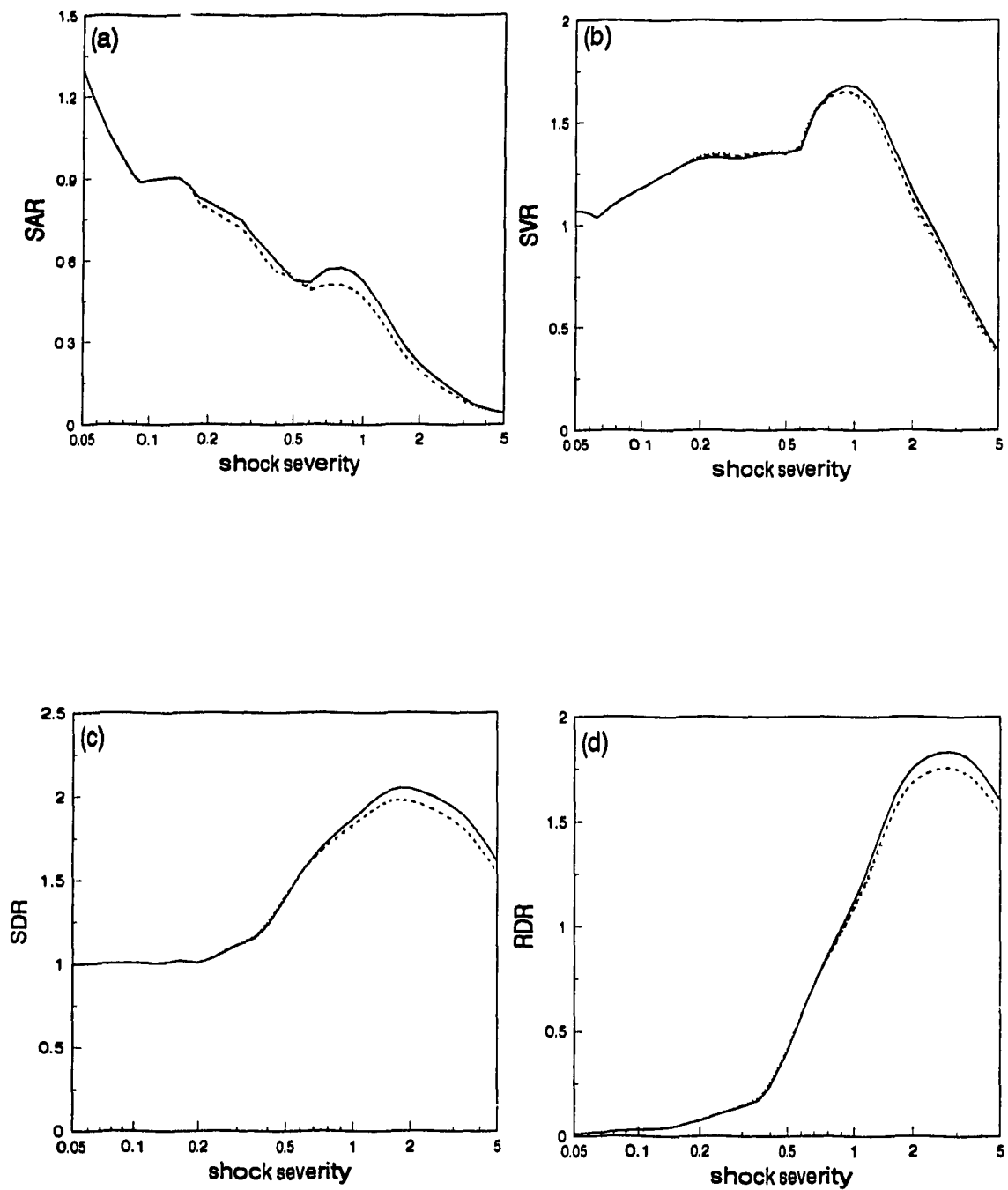


**Figure 7.16** Shock responses as a function of shock severity with the variation of valve orifice diameter; —, 4mm; ----, 5mm; ···, 6mm; (a) SAR, (b) SVR, (c) SDR and (d) RDR.

performance throughout the whole range of shock severity is much better (lower) than the performance produced by the other flexible dampers.

Figure 7.16b shows the SVR characteristics of the LDHVF damper with the variation of shock severity. Again shock severity below 0.5 has no noticeable effect on the SVR where duration of rounded pulse is greater than natural period of the system. The SVR after shock severity 0.5 is prominent and at  $\nu = 1$ , it is maximum. The SVR decreases rapidly with the increase in shock severity. Compared to other flexible dampers, SVR is low throughout the shock severity range. It is also found that the increase in valve orifice diameter marginally decreases SVR response.

Figures 7.16c and 7.16d show the shock displacement response (SDR) and shock relative displacement response (RDR) for the LDHVF damper. For shock severity below 0.5 is the static region where SDR is close to unity and RDR is close to zero. For shock severity beyond 0.5, where period for natural frequency is higher than the duration of pulse, SDR as well as RDR increase and reach maximum around  $\nu=2$  and then decrease with increase in  $\nu$ . Increase in valve orifice diameter decreases SDR and RDR at higher shock severity.

To visualize the superior performance of the damper even for shock isolation, the shock response for all hydraulic dampers are combined and presented in terms of SAR and SVR as shown in the Figure 7.17. Without finding the optimal parameters of the dampers as it is beyond the scope of the thesis, the response characteristics of the dampers presented are best obtained from their parametric studies. It is observed clearly that except for very low severity below 0.2 which is the static region, the LDHVF damper shows minimum acceleration and velocity response for the whole range of shock severity. At  $\nu=0.9$ , LDHVF reduces the SAR to 40% compared to LDHF dampers.



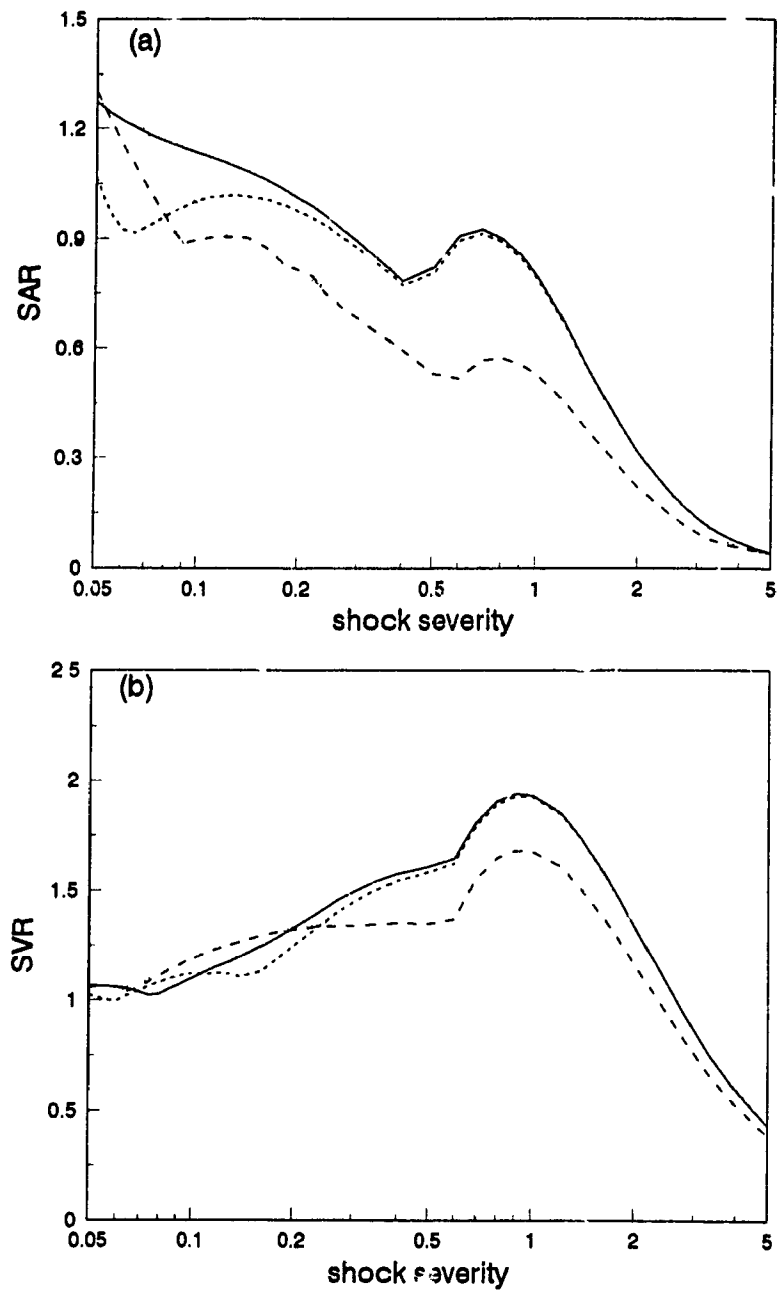


Figure 7.17 Shock response as a function of shock severity for hydraulic dampers. —, SDHF; ---, LDHF; - - - , LSDHF; ·····, LDHVF; (a) SAR, (b) SVR.

It is, thus, concluded that the proposed LDHVF dampers are most suitable for isolating low or high amplitude of vibration as well as shock of different severity.

#### 7.4 Summary

From the results obtained for short and long orifice dampers, it was concluded that long orifice produced better performance for isolation of vibration, but both system with flexible chambers only work well under very low amplitude of excitation. Furthermore, such dampers perform very poorly under shock excitation. A long orifice damper was, therefore, proposed with spring loaded valve (LDHVF), in attempts to improve both vibration and shock isolation performance at higher amplitudes of excitations.

A detailed time history of the LDHVF damper studied here show that both valve orifice and bleeder orifice influences the flow rate and transmitted force characteristics. The valve orifice reduces the top chamber pressure for part of the cycle and bleeder orifice reduces the reverse flow period. For the influence on dynamic characteristics, increase in valve orifice size is found to reduce both dynamic stiffness and peak loss angle where increase in bleeder orifice has the opposite effect. From the isolation performance in frequency domain, it is found that the LDHVF damper can be tuned to provide satisfactory performance even at excitations as large as 3 mm throughout the frequency range. Such dampers without orifice valves were found to perform poorly for excitation over 1 mm. Response of a system with LDHVF shows superior performance compared to all flexible chambered damper considered in this investigation. LDHVF with optimal parameters has the potential to supersede all other similar dampers for isolation of vibration and shock of relatively large amplitudes.

## **CHAPTER 8**

### **CONCLUSIONS AND RECOMMENDATIONS FOR FUTURE WORK**

#### **8.1 General**

A detailed and fundamental study on a class of passive hydraulic dampers is carried out. Based on a thorough review of hydraulic dampers, two groups, namely: dual-phase and flexible chamber hydraulic dampers are selected for their potential in application as isolators. Among the dual-phase dampers, it is found that for each low-high and high-low velocity sensitive dual-phase damper, there exists an equivalent high-low and low-high displacement sensitive system. Due to the potential for realization via passive means, displacement sensitive dual-phase system is selected for this study. Although such system has been investigated previously, it is found that the damping force characteristics used, do not satisfy the fundamental definition of it. Models are, therefore, thoroughly redeveloped utilizing integral formulation of damping force characterization. The results are compared with those of previous analytical and experimental studies. The "correct" model is then utilized for thorough investigation of its damping characteristics and performance under vibration and shock. In general, it is found that a low-high displacement sensitive damper has high potential for isolation of vibration, where a high-low type is superior for isolation of shock.

The hydraulic damper with flexible chambers has, although, gained popularity in mount application, only long orifice type has received more attention and has been found suitable for only low amplitude vibrations. A complete model of the system that includes nonlinear compliance of the chambers and fluid oscillation effect, has not been investigated. The study, therefore, focuses on a systematic development of the damper model with: nonlinear compliance for chambers; short orifice that includes turbulent flow and effect of geometry; long orifice that include fluid oscillation effect; and orifices with spring loaded valves and valve motion. The study in general shows that nonlinearity of the compliance makes the damper model, a realistic one. The effect of fluid oscillation is found to be highly significant both on the damper characteristics and its performance. In general, peak orifice flow is grossly overestimated when oscillation is not considered. The effect is even more significant at higher frequency. Although performance of long orifice damper is found to be better, both short and long orifice dampers are not suitable for large amplitude excitation (more than 1 mm) and shock.

An extended model that includes a long orifice as well as a short one is, therefore, investigated. It is found that a constant short orifice of appropriate diameter, that is active at all time, can improve the vibration transmissibility performance to a great extent. However, it can not satisfy the conflicting requirement between isolation of vibration and shock. This study, therefore, proposes an innovative concept of long orifice with a set of spring loaded valves designated for forward and reverse (bleed) flows. Such damper is shown to be perform adequately for both large amplitudes and shock. Further study is, however, needed to optimize such damper that posses very large number of possible variables.

This chapter presents the highlights of the study for each damping concept considered, the various conclusions drawn for each concept and a list of recommendations for future study.

## **8.2 Highlights of the Study**

As discussed above, the thesis is devoted to the analytical investigation of hydraulic dampers with an objective to improve vibration and shock simultaneously. Five different kinds of hydraulic dampers have been taken into consideration for accurate modeling and evaluation of characteristics and performance. This section presents the highlights of the present investigations. Only the aspects that highlight contributions made through this study are discussed under the headings of the damper type.

### **Displacement Sensitive Dual-phase Damper**

It is identified that high-low velocity sensitive and low-high displacement sensitive, as well as low-high velocity sensitive and high-low displacement sensitive dampers are essentially the same.

Comprehensive models of displacement sensitive dampers are developed through integral formulation of damper force characteristics based on the fundamental definition. It is shown that such formulation can not be carried out in a straight forward manner. In this case, a point by point transformation of displacement sensitivity to velocity sensitivity must be carried out prior to formulation of damping force.

A well established local equivalent linearization technique is applied to the displacement sensitive dual-phase damper for the first time to demonstrate its effectiveness in obtaining frequency response.

Through simulation, it is shown that the present "correct" model leads to significantly different characteristics for the damper as well as its performance in vibration isolation when compared to previous investigations. Experimental results also support simulation.

A thorough study of the dual-phase damper is carried out using the correct model to investigate their performance potentials both under vibration and shock. The results of extensive parametric study are also presented.

#### Short Orifice Hydraulic Damper with Flexible Chamber

Comprehensive investigation of short orifice damper with flexible chamber is not commonly available in literature. To the best knowledge of the author, their performance both under vibration and shock has not yet reported.

In this study, a comprehensive model of short orifice hydraulic damper with flexible chamber is developed. It includes experimentally measured chamber compliance, and effect of orifice geometry. The discharge coefficient for orifices is taken as a function of orifice geometry, length to diameter ratio and Reynolds number based on the work of Shapiro, et al [53].

The damper characteristics are evaluated and presented in terms of internal variables both in time and frequency domain for an in-depth understanding. Detailed performance is evaluated both in terms of transmissibility response and

shock response. An extensive parametric study is also carried out to demonstrate its performance potentials.

It is shown that such dampers have the potential to perform well but only under low amplitude vibration. The performance is highly limited for response under high amplitude excitation and shock.

#### Long Orifice Hydraulic Damper with Flexible Chamber

Although long orifice hydraulic damper has been investigated in the past, the most comprehensive study, to date, neglects the effect of fluid oscillation within the orifice.

For a complete and systematic investigation of dampers with flexible chamber, a comprehensive model with long orifice is also developed. The model includes nonlinear chamber compliance, orifice geometry along with oscillatory flow through the long orifice.

Through an extensive evaluation of damper characteristics in both time and frequency domain, it is shown that oscillation effect has significant influence on the flow rate and dynamic characteristics. A parametric study is carried out to show that long orifice damper can produce a highly desirable loss angle characteristics with higher peak compared to short orifice only around resonance, with low loss angle at high frequencies.

A detailed performance analysis is presented for both vibration and shock utilizing the developed model. This damper although exhibits two peaks, is shown to perform even better than short orifice for low amplitude vibration in a wide

frequency range. The shock isolation performance in this case is, however, worse than that of the short orifice damper. Furthermore, this damper is shown to exhibit very large second peak when subjected to large amplitude of excitation.

#### Long and Short Orifice Hydraulic Damper with Flexible Chamber

Due to conflicting performance requirement between vibration response and shock, a short orifice is added to the long orifice damper. This new concept is modeled utilizing all the details used in the previous models.

Systematic evaluation of damping characteristics and performance are carried out along with an extensive parametric study. It is found that the addition of short orifice reduces the peak damping to a certain extent, but leads to a better performance than long orifice alone for shock response. The shock response of this damper is very similar to that of a simple short orifice system.

This study provides a useful insight on the internal variables of the damper when a combination of long and short orifice is used. It is found that a short orifice that is in operation at all time can only yield marginal improvement over long orifice alone. Furthermore, potential of such damper in application to high amplitude of excitation remains poor.

#### Long Orifice Hydraulic Damper with Spring Loaded Valves

Based on the useful insight and experience of all previous simulations, an innovative and new concept is proposed. Here a set of short orifices with spring loaded valves are added to a damper with long orifice. The valves that operate in forward stroke (compression) are equipped with different preset pressure limit.



The thorough model for flow including valve motion is developed and studied for influence of short orifice parameters on the internal variables and dynamic characteristics. An iterative process is adopted for the simulation that considers variable flows during opening of the valves. This model includes a very large number of variables. Beside all the parameters associated with long orifice system with flexible chamber, this model may further include combination of the orifice size, length, valve preset pressure and valve stiffness.

For a limited parametric study, it is shown that both forward orifice and bleeder orifice have influence on the dynamic characteristics and performance. It is shown that such damper can be tuned to provide satisfactory performance even at excitations as large as 3 mm ( all previously studied similar dampers perform poorly even at 1 mm) over the entire frequency range. A comparative study also shows superiority of such damper in isolation of shock. Further study is recommended for its potentials in many applications.

### **8.3 Conclusions of the Investigation**

Specific observations and conclusions drawn from the dissertation research are summarized for each type of damper, as follows:

#### **Dual-phase Damper**

- The integral formulation approach of damping force characterization is the correct method to determine the damping force of a variable damper such as dual-phase. The traditional approach may lead to over or underestimation of the damping force, depending on low-high or high-low system.

- Equivalent linearization method using energy similarity is proved to be a powerful tool in analyzing displacement sensitive nonlinear damper in the convenient frequency domain. It is found that the numerical integration and equivalent linearization provides the same results within an error of less than 1 percent.
- A low-high displacement sensitive dual-phase damper has the characteristics similar to a high-low velocity sensitive dual-phase dampers. Similarly, a high-low displacement sensitive damper has the similar property to that of an equivalent low-high velocity sensitive damper.
- A low-high dual-phase damper provides higher dynamics stiffness and loss angle characteristics compared to a high-low dual-phase damper.
- The ratio ( $\beta$ ) between low and high damping of dual-phase system has more influence on the transmissibility response of a low-high system.
- A low-high damper has superior potential for performance over a wide frequency range which, however, must be designed for a given vibration excitation environment to realize its best potentials.
- In shock isolation, the ratio  $\beta$  has more influence on the high-low damper. It can be tuned for superior shock performance over a low-high damper.

#### Short Orifice Hydraulic Damper with Flexible Chamber

- The damper possesses highly nonlinear characteristics.

- Short orifice diameter and piston diameter has very strong influence on the dynamic characteristics of the damper. Increase in orifice diameter reduces dynamic stiffness and increases the frequency corresponding to peak loss angle. Increase in piston diameter increases the dynamic stiffness and loss angle peak.
- The geometry of the opening of the short orifice does not affect the dynamic characteristics of the damper significantly. Variation of chamber compliance has similar effect as that of piston diameter.
- Short orifice damper can be designed to provide better high frequency performance in comparison to a long orifice (Figure 5.22 and 6.21).
- Performance of short orifice is better than long orifice under shock excitation, which is, however, not satisfactory (compared to the dual-phase). This performance is highly influenced by orifice diameter).
- Application is limited to very low amplitude excitation

#### Long orifice Hydraulic Damper with Flexible Chamber

- Negligence of fluid oscillation effect grossly overestimates the orifice flow rate specially at high frequency. With increasing frequency, the flow rate first increases and then decreases, a trend that can not be predicted without oscillation effect.
- Long orifice leads to higher and sharp loss angle peak compared to short orifice which makes it suitable for isolation near resonance.

- Due to the appearance of a second peak, its performance for higher frequency vibration is inferior compared to a short orifice damper.
- Most sensitive parameters are orifice diameter and length, where increase in length increases peak loss angle and increase in diameter increases frequency corresponding to peak loss angle. A ratio of length to diameter will, therefore, make a good parameter for tuning.
- The damper can be tuned for good performance near resonance and reasonable performance over the entire frequency range, only for low amplitude of excitations. The second peak is highly sensitive to the amplitude.
- Overall shock response is poor compared to short orifice damper.

#### Long and Short orifice Hydraulic Damper with Flexible Chamber

- Total orifice flow increase compared to a long orifice hydraulic damper because of the presence of one short orifice. Addition of short orifice reduces the peak loss angle but increases the corresponding frequency closer to second peak.
- The damper performs better at higher amplitude of excitation without deteriorating other performances.
- It significantly improves the performance of the damper at second resonance without harming the first resonance transmissibility by any significant amount.

Therefore, it is advantageous to use a long orifice hydraulic damper with the inclusion of a short orifice.

- Compared to a long orifice, a short and long orifice damper performs better under shock excitation.
- Similar to other dampers with flexible chamber, the performance under high amplitude of excitation is limited.

#### Long orifice Hydraulic Damper with Spring Loaded Valves

- A long orifice hydraulic damper with spring loaded valve has the best characteristics compared to all other hydraulic dampers. It can be effectively tuned to isolate vibration in a wide range of frequency and to isolate shock displacement.
- Increase in short orifice area decreases the dynamic stiffness throughout the whole range of frequency.
- The most sensitive parameters of the damper are long orifice diameter, bleeder orifice diameter, short orifice diameter and spring constants of the valve spring.
- The damper may isolate sinusoidal vibration for higher range of amplitude without harming transmissibility performances.
- Provides best shock isolation performance among all the flexible chambered dampers considered.

## REFERENCES

- [1] Bernuchon, M. 1984 *SAE Technical Paper Series* 840259 A New Generation of Engine Mounts.
- [2] Corcoran, P. E. and Ticks, G. H. 1984 *SAE Technical Paper Series* 840407 Hydraulic Engine Mount Characteristics.
- [3] Clark, M. 1985 *SAE Technical Paper Series* 851650 Hydraulic Engine Mount Isolation.
- [4] Flower, W. C. 1985 *SAE Paper #* 850975. Understanding Hydraulic Mounts for Improved Vehicle Noise, Vibration and Ride Qualities.
- [5] Taylor, H. J. Jr., 1986 *SAE paper #* 862052. The New Generation of Engine Mounts.
- [6] Marjoram, R. H. 1985 *SAE paper #* 852349. Pressurized Hydraulic Mounts for Improved Isolation of Vehicle Cabs.
- [7] Su, H., Rakheja, S. and Sankar, T. S. 1989 *Mechanical Systems and Signal Processing*, Vol. 3, No. 1, 71-85 Vibration and Shock Isolation Performance of a Pressure Limited Hydraulic Damper.
- [8] Venkatesan, C. and Krishnan, R. 1975 *Journal of Aircraft* 112(10), 847-849. Dual-phase Damping in a Landing Gear Touch-Down.
- [9] Hagino, Y., Furuishi, Y., Makigawa, Y., Kumagai, N. and Yoshikawa, M. 1986 *SAE Technical Paper Series* 860552. Active Control for Body Vibration of F.W.D. Car.
- [10] Anderson, R. J. and Fan, Y. 1990 *SAE Technical Paper Series* 902282. Dynamic Testing and Modeling of a Bus Shock Absorber.
- [11] Hall, P. B. and Gill, K. F. 1986 *Proceedings of the Institution of Mechanical Engineers* Vol. 200, No. D2, 115-123. Performance of a Telescopic Dual-Tube Automotive Damper and the Implications for Vehicle Ride Prediction.

- [12] Ushijima, T. and Dan, T. 1936 *SAE Technical Paper Series* 860550. Nonlinear B.B.A. for Predicting Vibration of Vehicle with Hydraulic Engine Mount.
- [13] Sugino, M. and Abe, E. 1986 *SAE Technical Paper Series* 861412. Optimum Application for Hydroelastic Engine Mount.
- [14] Kadomatsu, K. 1989 *SAE Technical Paper Series* 891138 Hydraulic Engine Mounts for Shock Isolation at Acceleration on the FWD Cars.
- [15] Ushijima, T., Takano, K., and Kajima, H. 1988 *SAE paper # 880073*. High Performance Hydraulic Mount for Improving Vehicle Noise and Vibration.
- [16] Singh, R., Kim, G. and Ravindra, P. V. 1992 *Journal of Sound and Vibration* 158(2) 219-243. Linear Analysis of Automotive Hydro-Mechanical Mount with Emphasis on Decoupler Characteristics.
- [17] Kim, G. and Singh, R. 1993 *Journal of Dynamic System, Measurement, and Control* Vol. 115, No. 3. Nonlinear Analysis of Automotive Hydraulic Engine Mount.
- [18] Straw, R. L. 1984 *SAE Technical Paper Series* 840781 The Development of Isolation Mounts.
- [19] Helms, H. 1989 *International Journal of Vehicle Design* Vol. 10, No. 6, 609-624. Investigation of Vibration, Oscillation and Noise in the Car Test.
- [20] Popov, G. and Sankar, S. 1993 *Journal of Sound and Vibration* 40(3), 409-413. Modeling and Analysis of Nonlinear Orifice Type Damping in Vibration Isolators.
- [21] Rakheja, S. and Sankar, S. 1987 *The shock and Vibration Bulletin*, No. 57, Part 3. A publication of The Shock and Vibration Information Center, USA. Response of a Sequential Damper to A Shock Inputs.
- [22] Kim, G. 1992 *Ph.D. Thesis, The Ohio State University*. Study of Passive and Adaptive Hydraulic Engine Mounts.
- [23] Seto, K., Sawatari, K., Nagamatsu, A., Ishihama, M. and Doi, K., 1991 *SAE Technical Paper Series*, 911055. Optimum Design Method for Hydraulic Engine Mounts.

- [24] Graf, P. L., Shoureshi, R., Starkey, J., Novotny, D. and Severson, R. W. 1988 *SAE Technical Paper Series* 880074. Active Frame Vibration Control of Automotive Vehicles with Hydraulic Engine Mounts.
- [25] Su, H. 1990 *Ph.D. Thesis, Mechanical Engineering Department, Concordia University, Montreal, Canada*. An Investigation of Vibration Isolation Systems using Active, Semi-active and tunable Passive Mechanism with Application to Vehicle Suspensions.
- [26] Lang H. H. 1977 *Ph.D. Thesis Mechanical Engineering Department, University of Michigan, USA*. A Study of the Characteristics of Automotive Hydraulic Dampers at High Stroking Frequencies.
- [27] Singh, R. and Kim, G. 1993 *Advanced Automotive Technologies*, ASME DSC- Vol. 52, 247-255. A Broadband Adaptive Hydraulic Mount System.
- [28] Sankar, S. 1978 *The Shock and Vibration Bulletin*, No. 48, Part 4, A publication of The Shock and Vibration Information Center, USA. Stability and Frequency Response of Hydro-mechanical Shakers in Vibration Rigs.
- [29] Hundal, M. S. 1977 *Journal of Sound and Vibration* 50(2), 195-202. Impact Absorber with Two-stage, Variable Area Orifice Hydraulic Damper.
- [30] Venkatesh, S. 1989 *M. Eng. Thesis, Concordia University, Montreal*. Vibration Isolation using Hydraulic Mounts with Dual-phase Damping.
- [31] Fomichev, V. M., Olenin, O. M., Birukov, O. I., and Kotlov, A. V. *Vestnik Mashinostroyeniya* No 11, Nov. 1975, pp. 7-11. Non-dimensional Hydraulic Characteristics of Cylindrical Orifices as Function of Cavitation (number) and Reynolds Number.
- [32] Nikajima, Z., Matsuoka, C., and Okuya, S. 1990 *SAE paper # 901729*. The Development of Hydraulic Strut Mount.
- [33] Popov, G. and Sankar, S. 1993 *Journal of Sound and Vibration* 40(3), 409-413. Modeling and Analysis of Nonlinear Orifice Type Damping in Vibration Isolators.
- [34] Bouchellon, S., Shoureshi, R., Knurek, T. and Schilke, P. 1989 *SAE Technical Paper Series* 891160. Optimal Tuning of Adaptive Hydraulic Engine Mounts.



- [35] Vliet, M. V. 1983 *Ph.D. Thesis Mechanical Engineering Department, Concordia University*. Computer Aided Analysis and Design of Off-Road Motorcycle Suspensions.
- [36] Venkatesan, C. and Krishnan, R. 1975 *Journal of Sound and Vibration* 40(3), 409-413. Harmonic Response of a Shock Mount Employing Dual-phase Damping.
- [37] Sankar, S., Ahmed, A. K. W. and S. Venkatesh 1994 *Journal of Sound and Vibration* 169(1), 55-69. Analytical and Experimental Evaluation of Displacement Dependent Dual-phase Dampers.
- [38] Guntur, R. R. and Sankar, S. 1982 *Journal of Sound and Vibration* 4(2), 253-267. Performance of Different Kinds of Dual-phase Damper Shock Mounts.
- [39] Graf, P. L. and Shoureshi, R. 1988 *ASME Journal of Dynamic Systems, Measurement and Control*, Vol. 10, No. 12, 422-429. Modeling and Implementation of Semi-Active Hydraulic Engine Mounts.
- [40] West, J. P. 1987 *Automotive Engineer* 12, 17-19. Hydraulically-damped Engine Mounting
- [41] Duclos, T. G. 1987 *SAE Technical Paper Series* 870963. An Externally Tunable Hydraulic Mount Which Uses Electro-rheological Fluid.
- [42] Mizuguchi, M., Suda, T., Chikamori, S. and Kobayashi, K. 1984 *SAE Technical Paper Series* 840258. Chassis Electronic Control Systems for the Mitsubishi 1984 galant.
- [43] Snowdon, J. C. 1970 *The Shock and Vibration Bulletin* 4, 21-41. Isolation from Mechanical Shock with a Mounting System having Nonlinear Dual-phase Damping.
- [44] Galvin, D. D. 1994 *Mechanical Engineering*, March Edition 99-102. Electronic Mounts Reduce Engine Vibrations.
- [45] Ruzicka, J. E. and Derby, T. F., 1971 *ASME, Journal of Engineering for Industry* 627-635. Vibration Isolation with Nonlinear Damping.

- [46] Rakheja, S. and Ahmed, A. K. W. 1991 *Engineering Computations* Vol. 8, 333-344. Simulation of Non-linear Variable Damper using Energy Similarity.
- [47] Rakheja, S. and Sankar, S. 1986 *Engineering Computations* Vol. 3, 11-17. Local Equivalent Constant Representation of Nonlinear Damping Mechanisms.
- [48] Rakheja, S., Vliet, M. V. and Sankar, S. 1985 *Journal of Sound and Vibration*, 100(4), 511-526. A Discrete Harmonic Linearization Technique for Simulation of Nonlinear Mechanical System.
- [49] Ahmed, A. K. W. and Rakheja, S. 1992 *Journal of Sound and Vibration* 53(3), 537-542. An Equivalent Linearization Technique for the Frequency Response Analysis of Asymmetric Dampers.
- [50] Lance, G. N. 1960 *Numerical Methods for High Speed Computers*. New York: Iliffe & Sons Ltd.
- [51] Streeter, V. L. and Wylie, E. B. 1979 *Fluid Mechanics*, 7th Edition, McGraw-Hill, New York.
- [52] Merritt, H. E. 1967 *Hydraulic Control System*. John Wiley & Sons, New York, NY.
- [53] Shapiro, A.H., Siegel, R. and Kline, S.J. 1954. *2nd US Natl Cong. Appl. Mech.* Friction Factor in the Laminar Entry of a Smooth Tube.
- [54] Doebelin, E. O. 1980 *System Modeling and Response: Theoretical and Experimental Approaches*. John Wiley & Sons, New York.
- [55] Doebelin, E. O. 1972 *System Dynamics: Modeling and Response*. Columbus, Merrill.
- [56] Harris, J. and Stevenson, A. 1987 *International Journal of Vehicle Design*, Vol. 8, Nos. 4-6, 553-577. on the Role of Nonlinearity in the Dynamic Behaviour of Rubber Components.
- [57] James, M. L., Smith, G. M., Welford, J. C. and Whaley, W. P. 1989 *Vibration of Mechanical and Structural Systems*. Harper & Row, New York.

- [58] Snowdon, J. C., 1968 *Vibration and Shock in Damped Mechanical Systems*, John Wiley and Sons, New York, N. Y.
- [59] Harris, C. M. and Crede, C. E. 1977 *Shock and Vibration Handbook*. McGraw-Hill Book Company, New York, N. Y.
- [60] Haque, M. M., Ahmed, A. K. W. and Sankar, S. 1995 *Journal of Sound and Vibration* 187(1), 95-109. Simulation of Displacement Sensitive Non-linear Dampers Via Integral Formulation of Damping Force Characterization.
- [61] Haque, M. M., Ahemd, A.K.W. and Sankar, S. 1994 *Proceedings of the 24th Canadian Society of Mechanical Engineering (CSME) Conference*, Montreal, Canada. June 27-29. Nonlinear Analysis of Hydraulic Damper with Flexible Chambers.